CARBOTHERMIC REDUCTION OF SULPHIDE MINERALS.

A thesis submitted to the University of London
for the degree of Doctor of Philosophy.

by

Animesh Jha.
John Percy Research Group
Royal School of Mines
Imperial College of Science and Technology
London SW7 2BP.

August, 1984.

ABSTRACT.

The carbothermic reduction of copper sulphide minerals is thermodynamically impossible without the presence of an exchange medium e.g. CaO, MgO etc at any temperature attainable in practice. The exchange medium provides a mechanism for the exchange of S^{-2} ion of metal sulphide with O^{-2} ions and hence in the process ties the sulphur, without generating SO_2. As a result of the exchange reaction, metal oxides are generated which can be easily reduced using any reducing agent. In the present investigation, the reduction mechanism of Copper Sulphides (CuS and $Cu_{2-x}S$) has been studied using lime and carbon.

In this study, it has been shown that during the reduction of sulphides, a pseudo ternary Cu_2S-Cu_2O-CaS liquid forms as a result of the exchange reaction and this liquid is saturated with CaS. The rate governing step in the overall process is the carbon gasification reaction. However, when small quantities of carbon or very unreactive carbon is used cessation of the reduction occurs temporarily. This phenomenon is explained in terms of the relative rates of the exchange reduction reactions and conditions for rapid reduction are specified.

Finally, the efficiency and economy of the process related to industrial application are briefly discussed.

From May 1983, the project was extended to study iron sulphide mineral. The synthetic pyrrhotite was treated with lime and carbon over a range of 800°C to 1000°C in a flowing stream of argon. During the reduction of iron sulphide, the existance of a quarternary liquid was found which belongs to the Fe-Ca-S-O system. The presence of this liquid above 850°C accelerates the rate of reduction. Apart from the existence of a quarternary liquid, two oxysulphide compounds were discovered

which belong to FeS-CaO and FeO-CaS pseudo-binary sections. The exact composition and their crystal structures are still under investigation but one compound has composition near FeO.CaS and is related to a tetragonal cell with an 'a' dimension similar to CaS and 'c' dimension expected for one layer of 'O' and 'Fe' replacing 'Ca' and 'S'.

From our investigation it has been found that FeS can be reduced to iron in the presence of lime and coal within 45 minutes at 950°C. The rate of reduction is essentially governed by the rate of reduction of the quarternary liquid at higher temperatures or of the quarternary compound at lower temperatures. This part of the investigation is important to understand the feasibility of the selective extraction of iron and copper from complex copper-iron sulphide minerals. It also suggests that naturally occuring pyrite or pyrrhotite minerals which are normally used for sulphuric acid manufacture, can be treated for the production of metallic iron.

Chalcopyrite is the complex copper-iron sulphide mineral being investigated on this project. During the reduction, it was found that the quarternary compounds FeO.CaS and FeS.CaO also exist in this system. Depending upon the temperature and oxygen potential copper or iron can be nucleated first and it seems possible from the present investigation that both iron and copper can be preferentially separated. It has also been found out that the reaction proceeds with a liquid phase intermediary which belongs to the Cu-Fe-Ca-S-O systems. From the X-ray diffraction analysis it has been confirmed that a pentanary compound exists and it governs the rate of reduction.

A complete metallization of copper and iron can be achieved with coal at 950°C within an hour. Unlike copper and iron sulphides it has been found that indirect reduction of chalcopyrite is much slower than either Cu_2S or FeS.

The possibility of extraction of nickel from synthetic nickel sulphide has also been investigated. It appears that the reduction is assisted because of the presence of liquid Ni_3S_2 above 800°C. In this matter, the oxygen dissolves to form an oxysulphide liquid which is saturated with CaS. The rate of reduction was found to be extremely fast in case of coal than in the case of graphite but a higher lime to sulphide and coal to sulphide ratio was necessary to obtain 100 pct metallization.

ACKNOWLEDGEMENTS

The author expresses his profound gratitude to Professor Paul Grieveson and Professor J.H.E.Jeffes for supervision,suggestions and encouragements which he received through out this work.

He is also indebted to INLAKS FOUNDATIONand RTZ Company for providing the finacial assistance,without their help thiswork would have been impossible to accomplish.

The author sincerely wishes to thank Mr. A.Willis, Mr. L.E.Leake and Mr. Gordon Higgs for providing their technical assistance during this project.

Lastly he expresses his thanks to Miss C.A.Miller and Mr. Keneth S. Coley who helped him to prepare this thesis. The author sincerely thanks Mr. Noel Machinguwata for his contribution to the 8th chapter of this thesis.

CONTENTS.

Chapter 1.		Page No.
1a	Importance of present investigation	1
1b	The thermodynamic principles.	5
1c	Thermodynamic calculation for carbothermic reduction.	7
1d	Literature Reviews.	
1d(i)	The carbothermic reduction of metal sulphide.	12
1d(ii)	The hydrogen reduction of metal sulphide.	17

Chapter 2.		
Phase relationships and their importance during the carbothermic reduction.		
2a	Copper - Sulphur system	29
2b	Iron - Sulphur system	29
2c	Nickel - Sulphur system	32
2d	Copper - Iron - Sulphur system	32
2e	Copper - Sulphur - Oxygen system	37
2f	Iron - Sulphur - Oxygen system	40
2g	Copper - Iron - Sulphur - Oxygen system	43
2h	Calcium - Sulphur - Oxygen system	46
2i	Calcium - Sulphur - Copper - Oxygen system	46
2j	Calcium - Iron - Sulphur - Oxygen system	47

Chapter 3.		
	Thermal stability of sulphides.	54

Chapter 4. — Page No.

Experimental Techniques.

4A(i) Kinetic studies in a flowing gas system 58

4A(ii) Kinetic studies with controlled atmosphere conditions. 62

4B Synthesis of sulphides 65

Chapter 5.

Carbothermic Reduction of Sulphide Minerals.

5A Carbothermic reduction of copper sulphide 68

5A(i) Results 68

5A(ii) Discussions of the results of copper sulphide reduction 93

5A(ii)a The direct reduction 93

5A(ii)b The indirect reduction 121

5A(ii)c The reduction under reduced pressure 124

5A(ii)d Relation between the length of plateau temperature and composition 125

5B Carbothermic Reduction of Iron Sulphide Minerals.

(i) Results 126

(ii) Discussions 150

(a) Phase relationships and mechanism of reaction 150

(b) The kinetics of direct reduction of iron sulphide 162

(c) The kinetics of indirect reduction of iron sulphide 165

(d) Cementite formation 167

5C Carbothermic Reduction of Complex Iron Copper Sulphide Minerals

(i) Results 169

(ii) Discussions 189.

Chapter 6.		Page No.
Calcination of Sulphate.		
6.A	Introduction	198
6.B	Experimental Technique	206
6.C	Results	206
6.D	Discussions	231.

Chapter 7.

Whisker Growth.

7.1	Introduction	248
7.2	Existing Models of Whisker Growth	250
7.3	Conditions for Whisker Growth	255
7.4	Anistropy of Surface Energy	257
7.5	Experimental Procedure	263
7.6	Results	265
7.7	Discussions	288

Chapter 8.

Reduction of Nickel Sulphide.

Results and discussions	314
Appendix 8A	338
Appendix 8B	340
Appendix 8C	340

Appendix 1.

Phase Combinations in Fe-Ca-S-O and Fe-Ca-Cu-S-O systems	343
Appendix 2.	351.

List of Figures.

Chapter 1.		Page No.
Fig (1.1)	Schematic diagram for conventional copper making	1
Fig (1.2)	Free energy - temperature diagram for metal sulphides	9
Fig (1.3)	Free energy temperature diagram for metal oxides	10
Fig (1.4)	Free energy - temperature diagram for the carbothermic reduction of sulphides	11
Fig (1.5)	Reduction of bornite with H_2	20
Fig (1.6)	Reduction of chalcopyrite with H_2	20
Fig (1.7)	Variation of reduction rate of Cu_2S with stoichiometry	20

Chapter 2.		
Fig (2.1)	Cu-S phase diagram	30
Fig (2.2)	Fe-S phase diagram	31
Fig (2.3)	Ni-S phase diagram	33
Fig (2.4)	Cu-Fe-S phase diagram	34
Fig (2.5)	Cu_2S-FeS psuedo binary diagram	38
Fig (2.6)	Univariants in Cu-S-O system	38
Fig (2.7)	Variation of 'O' solubility in liquid matte (Cu_2S)	38
Fig (2.8)	P-T- composition diagram for Cu-S-O system	42
Fig (2.9)	FeO-FeS pseudo binary diagram	42
Fig (2.10)	Fe-S-O ternary section	42
Fig (2.11)	Univariants in Ca-S-O system	44
Fig (2.12)	Univariants in Cu-Fe-S-O-system	44
Fig (2.13)	Pct CaS conversion vs temperature relationship.	49
Fig (2.14)	Phase relationships in CaO-FeS-CaS-FeO system	49
Fig (2.15)	FeO-CaS pseudo binary diagram	49
Fig (2.16)	Univariants in Cu-Ca-S-O and Cu-Fe-S-O-Ca systems	50

Chapter 4.

		Page No.
Fig (4.1)	Schematic diagram of apparatus for carbothermic reduction of sulphides	59
Fig (4.2)	Schematic diagram of apparatus for carbothermic reduction of sulphides under controlled atmosphere.	63.

Chapter 5.

Chapter 5A Reduction of Copper Sulphides.

Fig (5A.1)	Rate of reduction of CuS with graphite	71
Fig (5A.2)	Rate of reduction of Cu_2S with graphite	72
Fig (5A.3)	Rate of reduction of CuS: Cu_2O mixture	81
Fig (5A.4)	Rate of reduction of Cu_2S CuO mixture	82
Fig (5A.5)	Cu-S-O phase diagram at 1000°C	84
Fig (5A.6)	RTln p_{O_2} vs $^1/_T$ relationship for Cu-S-O liquid	85
Fig (5A.7)	Rate of reduction of CuS with Coal	94
Fig (5A.8)	Rate of reduction of Cu_2S with coal	95
Fig (5A.9)	Rate of reduction of CuS with CO	96
Fig 5A.10)	Rate of reduction of Cu_2S with CO	96
Fig (5A.11)	Rate of reduction of CuS with increased lime	98
Fig (5A.12)	Rate of reduction of Cu_2S with increased lime	100
Fig (5A.13)	Rate of reduction of Cu_2S in controlled atmosphere	102
Fig (5A.14)	Rate of reduction of Cu_2S in controlled atmosphere.	103
Fig (5A.15)	Cu_2S - Cu_2O pseudo binary section	105
Fig (5A.16)	d (RTln a_{O_2}) /dt vs temperature relationship for Cu-S-O liquid	105

Page No.

Fig (5A.17)	Rate of reduction of CuS with increased lime and graphite.	110
Fig (5A.18)	Rate of reduction of Cu_2S with increased lime and graphite.	111
Fig (5A.19)	Rate of reduction of Cu_2S with coal and with catalytic graphite.	114
Fig (5A.20)	Rate of reduction of CuS under dual treatment condition with CO.	116
Fig (5A.21)	Rate of reduction of CuS-CuO mixtures in graphite crucible.	118.

Chapter 5B.

Reduction of Iron Sulphide.

Fig (5B.1)	Rate of reduction of pyrrhotite ($Fe_{1-x}S$)	132
Fig (5B.2)	Rate of reduction of ($Fe_{1-x}S$) with coal	134
Fig (5B.3)	Rate of reduction of ($Fe_{1-x}S$) in presence of increased lime	140
Fig (5B.4)	Rate of reduction of ($Fe_{1-x}S$ in presence of increased lime and graphite.	142
Fig (5B.5)	Rate of reduction of ($Fe_{1-x}S$) with CO	143
Fig (5B.6)	Rate of reduction of ($Fe_{1-x}S$) with CO at 950°C	145
Fig (5B.7)	Rate of reduction of ($Fe_{1-x}S$) under controlled atmosphere	151
Fig (5B.8)	Rate of reduction of (FeS:CaO) heat-treated mixtures	155
Fig (5B.9)	Rate of reduction of ($Fe_{1-x}S$) with catalytic graphite.	157

Page No.

Fig (5B.10) FeS-CaO-FeO-CaS quarternary section. 160

Chapter 5C.

Reduction of Complex Copper - Iron Sulphides.

Fig (5C.1) Rate of reduction bornite and chalcopyrite with graphite 177

Fig (5C.2) Rate of reduction chalcopyrite with graphite at different temperatures. 178

Fig (5C.3) Rate of reduction of chalcopyrite with coal at different temperatures. 179

Fig (5C.4) Rate of reduction of chalcopyrite with CO at different temperatures 187

Fig (5C.5) Phase relationships in Cu-Fe-S-Ca-O system during the reduction of complex sulphides. 191

Chapter 6.

Calcination of $CaSO_4$

Fig (6.1) Variation of rate of SO_2 evolution with temperature 204

Fig (6.2) Ca-S-O predominance diagram 204

Fig (6.3) Pct vol. of SO_2 vs $^{p}CO_2/p_{CO}$ relationship. 205.

Fig (6.4) Schematic diagram for sulphate decomposition 205

Fig (6.5) Rate of reduction of $CaSO_4$ with graphite 209

Fig (6.6) Conversion of 'S' as 'CaS' and SO_2 during the reduction of $CaSO_4$ 211

Fig (6.7) Rate of calcination of sulphate with CaS 215

Fig (6.8) Rate of calcination of sulphate at 1000°C. 216.

Page No.

Fig (6.9)	Schematic diagram of the product layer in case of CaS-$CaSO_4$ mixture calcination.	219
Fig (6.10)	Schematic diagram for the production layer formed during the calcination of CaS-$CaSO_4$ composite.	219
Fig (6.11)	Calcination CaS-$CaSO_4$ composite at 1000°C in presence of lime	225
Fig (6.12)	Data on the solubility of CaS and $CaSO_4$ in CaO	235
Fig (6.13)	Rate of calcination of CaS-$CaSO_4$ in pure argon.	235
Fig (6.14)	Relationship between rate of calcination and geometric factor	239

Chapter 7.

Growth of Whiskers.

Fig (7.1)	The steps involved during whisker growth.	261
(7.2)	Variation of surface energy with θ	261
(7.3)	Equilibrium shapes of fcc metal in controlled atmosphere.	262
(7.4)	Variation of equilibrium shape with plot	262
(7.5)	Design of crucible used for the experiment.	264
(7.6)	Cu-S-O ternary with composition co-ordinates	281
(7.7)	Relationship between the length of whikser and the time.	286
(7.8)	Variation of chemical potential around the curved surface.	299
(7.9)	Variation of surface and volume diffusion with temperature	301
(7.10)	Design of Wagner's experiment	305.

Page No.

Chapter 8.

Reduction of Nickel Sulphide.

Fig (8.1)	Rate of reduction of NiS with graphite in presence of lime	322
(8.2)	Rate of reduction of NiS with coal in presence of lime	323
(8.3)	Phase relationship in NiS-CaO-CaS system at 950°C	324
(8.4)	Rate of SO_2 evolution during the heat-treatment of NiS in presence of lime and NiO	325
(8.5)	Rate of reduction of NiS with graphite in presence of increased lime.	326
(8.6)	Rate of NiS in presence of increased lime and coal.	327.

LIST OF PHOTOGRAPHIC PLATES.

Chapter 5.		Page No.
Chapter 5A	Reduction of Copper Sulphides	
5A.1	Reduction of CuS with lime and graphite at 1000°C	75
5A.2	Reduction of Cu_2S with lime and graphite.	86
5A.3	Formation of copper and 'O' rich matte during the heat-treatment of Cu_2S:Cu_2O = 1:3 at 1000°C in flowing argon.	87
5A.4	Heat treatment of Cu_2S and Cu_2O mixtures at 1000°C	88
5A.5	Heat treatment at CuS and CuO at 1000°C in argon	89
5A.6	Heat treatment of CuS:CuO = 3:1 mixture with lime and reduced in graphite crucible at 1000°C	117

Chapter 5B. Page No.

Reduction of Iron Sulphides.

5B.1	Reduction of iron sulphide with lime (S:O:C = 1:2:2)	136
5B.2	Reduction with iron sulhide with lime of carbon monoxide	146
5B.3	FeS:CaO = 1:1 at 950°C with CO	147
5B.4	Reduction of iron sulphide with lime	152
5B.5	Scanning electron micrograph of FeS:CaO = 1:1 pellet reduced with CO at 950°C	153
5B.6	Energy dispersive X-ray (K) analysis of FeS:CaO = 1:2 mixture heat treated at 900°C in argon atmosphere.	154.

Chapter 5C.		Page No.
Reduction of Complex Copper Iron Sulphides		
5C.1	Energy dispersive X-ray (K) analysis of Cu FeS:CaO:C = 1:2:2 reduced at 1000°C in argon atmosphere.	181
5C.2	Energy dispersive X-ray (K) analysis of CuFeS:CaO:C = 1:2:2 reduced at 1000°C in argon atmosphere	182
5C.3	(a) Decomposition of chalcopyrite into two sulphides at 800°C in argon. Sample etched with acidified $K_2 Cr_2O_7$	183.
	(b) Formation of copper during the heat treatment of $CuFeS_2$ with lime T = 900°C Atm. Argon.	
5C.4	Reduction of chalcopyrite with lime at graphite (25:0:C = 1:2:2)	184.
5C.5	Reduction of $CuFeS_2$:CaO = 1:2 at 1000°C with CO.	187.

Chapter 6.	Calcination of $CaSO_4$	Page No.
6.1	Calcination of calcium sulphate	221

****

Chapter 7.

Growth of Whiskers.

7.1	Growth of bi-partite whiskers during the reduction of copper oxide - copper sulphide pellet preheat treated in argon at 1000°C	272
7.2	Scanning electron micrograph of the trip of bi-partite whiskers	273
7.3	Heat treatment of Cu_2S-Cu_2O composite in argon atmosphere at 1000°C	274
7.4	Growth of copper whiskers from the surface of Cu_2S during the heat treatment of Cu_2S-Cu_2O at 1000°C (Argon)	275
7.5	Faceting of the surface of Cu_2S during the heat-treatment of Cu_2S-Cu_2O composite at 1000°C in argon.	276
7.6	Morphological changes occurred on the surface of Cu_2S-Cu_2O composite at 1000°C in argon.	277

Page No.

7.7 Growth of Cu_2S crystals during the dual treatment of CuS:CaO mixture in CO and growth of pure Cu in case CuS-CaO red — 278

7.8 Photograph of Cu_2O-Cu_2S composite pellets with whiskers. — 279

7.9 Whisker growth during HI of Cu_2S - Cu_2O composite at 750°C in CO_2

****

Chapter 8.

Reduction of Nickel Sulphide.

8.1 Energy dispersive X-ray analysis of NiS: CaO = 1:1 pellet reduced with graphite. — 327

8.2 Energy dispersive X-ray analysis of NiS:CaO = 1:1 pellet reduced with coal at 950°C — 328

Appendix 1.

		Page No.
A1.1	Scanning electron micrograph at heat treated FeO:CaS = 2:1 mixture in argon at 1000°C	345
A1.2	EDX elemental analysis and scanning electron micrograph of FeO:CaS = 2.5:1 mixture heat treated in argon atmosphere 1000°C	346

****

Appendix 2

A2.1	Calcination of $CaSO_4$ in presence of Cu_2S at 1000°C in argon atmosphere.	352

1. INTRODUCTION.

1a. The Importance of this Investigation.

The conventional methods for the production of non ferrous metals from mineral sulphides are based on two main pyrometallurgical principles. In one case, the mineral sulphides are dead roasted (i.e. a complete elimination of sulphur from the sulphides by converting them to metallic oxides) and then treated in a blast furnace to reduce the metal oxides to metal. Alternatively if the sulphide concentrates are rich and fine, they are directly charged into the Flash Smelting Furnace to produce matte. Little progress has been made in the former method for many years whereas the latter has been transformed to a very efficient metal making process e.g. the continuous copper smelting. If a matte phase is the product of the concentrate it is then converted to produce metal. During the converting of matte, controlled oxidation is carried out to eliminate all the sulphur. These processes are shown in the form of a schematic diagram, see fig 1.1. Although continuous copper smelting and flash smelting furnaces are widely used, these conventional methods pose a major threat to the environment, because of the large volume of dilute sulphur dioxide gas emission at each stage of the process. The long processing time, the vast quantity of the energy required and the complexity of the processes are the major drawbacks. Table 1.1. briefly summarises the energy balance of some of the existing processes (1.1).

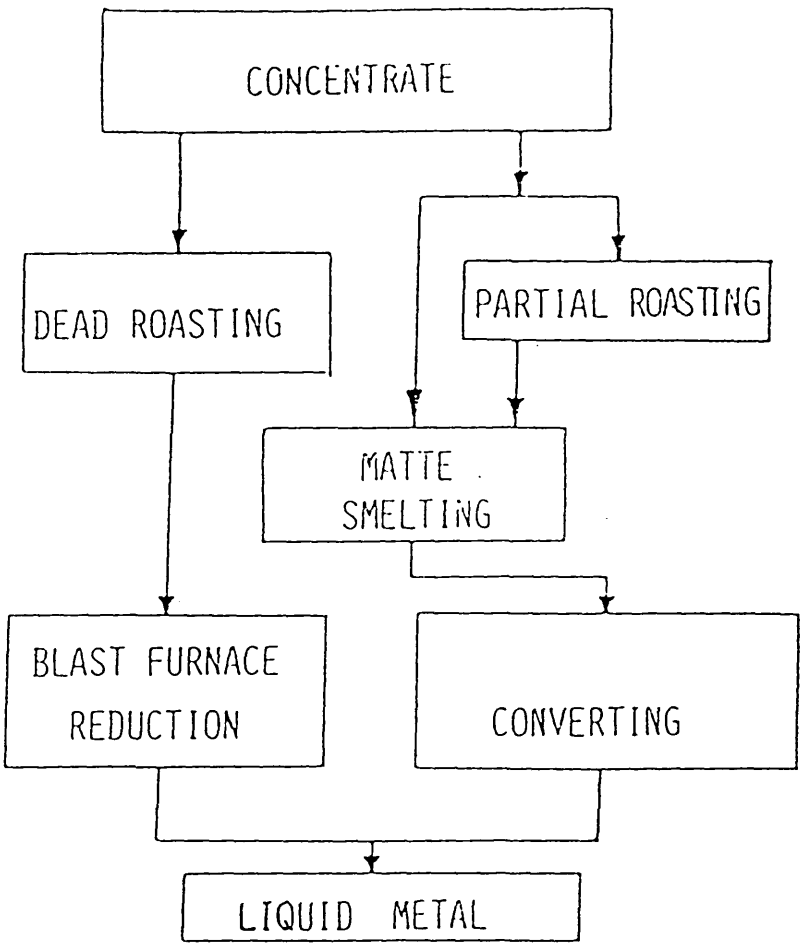


Fig.(1.1) The Existing Process Routes of Non-ferrous Metal Production.

TABLE 1.1. Simplified Heat Balances for Reverberatory, Outokumpu Flash and INCO Oxygen Flash Smelting. The Charge is Dry in all Cases (1.1).

Basis: reverberatory furnace

Flash Furnace: 1 tonne dry charge (incl. fluxes) av. comp. 30% Cu, 23% Fe, 27%S, 10% oxides

Produces: 0.6 tonnes of matte (50% Cu); 0.35 tonnes of slag. All units - 10^6

ITEM.	Reverberatory Furnace	Outokumpu flash furnace (air at 550°C)	INCO oxygen (95% O_2 flas
Heat Input and Production			
Sensible heat in converted slag	1.7	-	-
Sensible heat in air for sulphide oxidation	0.2 (220°C)	1.0 (550°C)	-
Heat of matte and SO_2 production $CuFeS_2$ + O_2 matte + SO_2 (25°C)	1.8	1.8	1.8
$FeS + \frac{3}{2} O_2 = FeO + SO_2$ (25°C)	-	1.8	1.8
$FeS + \frac{5}{2} O_2 = \frac{1}{3} Fe_3O_4 + SO_2$ (25°C)	-	1.6	1.6
$FeO + SiO_2 = FeO.SiO_2$ (25°C)	-	0.1	0.1
Total heat input	3.7	6.3	5.3

/contd..

Table 1.1. Contd.

Item	Reverbertary furnace	Outokumpu flash furnace (air at 550°C)	INCO Oxyge 95% O_2 fla
Heat Output.			
Sensible heat in matte (1150°C)	1.9(40%Cu)	1.5(50%Cu)	1.5(50%Cu)
Sensible heat in slag (1200°C)	1.9	1.3	1.3
Sensible heat in SO_2 (1250°C)	0.4	0.7	0.7
Sensible heat in N_2 from the air used for sulphide and iron oxidation	1.0	2.5	0.1
Heat losses (convection, radiation)	2.3	2.1	1.7
Total heat output	7.5	8.1	5.3
Net deficit to be made up by external energy	3.8	1.8	5.3
Fuel energy required	8.1×10^5Kcal (at 47% efficiency)	4.5×10^5Kcal (at 40% efficiency)	0.0
No converter slag fuel burners	220°C air preheat		No air preheat in

It is for these reasons, a new method has been considered which may eliminate these problems. A single step production route has been developed in which the mineral sulphides are directly reduced to metal in the presence of a reducing agent. In this work, the reducibility of sulphides with graphite and coal will be the main subject.

1.b. The Thermodynamic Principles.

The single step production of metal from mineral sulphides can be represented by the following chemical equilibrium.

$$2\ MS\ (s) + C\ (gr) = M\ (s) + CS_2\ (g) \qquad (1.1)$$

This essentially outlines the principle of carbothermic reduction of sulphide minerals. The feasiblity of this chemical reaction can only be appreciated by applying thermodynamic principles. Chemical reactions are not thermodynamically feasible when the Standard Gibbs Free Energy change ΔG^{o} is positive at reasonably high temperatures which makes the equilibrium constant (k) very small. The reason for this thermodynamic non-feasibility can be explained in terms of the sulphur potential of the system. In the present situation, the formation of the gaseous product CS_2 needs a higher sulphur potential than the sulphur potential of the metal sulphide MS, because CS_2 gas decomposes rapidly at high temperatures into its basic constituents. Thus, it is essential to reduce the sulphur potential of the product by providing a thermodynamic sink. This sink can be achieved by a variety of methods i.e. if the gas phase is immediately removed from the system, the reaction would never achieve equilibrium. On the other hand, a method may be used to tie the sulphur within the system so that the sulphur potential in the r.h.s. is lower than the l.h.s. Although these two types of sinks are practically possible the former one is not economically viable. The latter may be achieved by the use of any basic oxide e.g. CaO, MgO, BaO etc.

The provision of the basic oxides as a sulphur sink splits the chemical equilibrium (1) into two steps - the exchange reaction during which S^{-2} ions of MS is exchanged with O^{-2} ions of basic oxides XO, and a reduction step during the metal oxides are reduced to metal. These two steps are represented as follows:-

a) The Exchange Reaction:-

$$MS\ (s) + XO\ (s) = MO\ (s) + XS\ (s) \qquad (1.2).$$

The Reduction Reaction:-

b) $$MO\ (s) + C\ (g\ ) = M\ (s) + CO\ (g) \qquad (1.3)$$

In the present investigation, lime has been used as the exchange medium. The choice of lime as an exchange medium and carbon as a reducing agent has been exercised for the following reasons:-

i. Calcium oxide forms a very stable sulphide CaS during the exchange reaction and provides an 'insitu' sink for sulphur which does not allow sulphur to escape as SO_2 or CS_2 into the atmosphere.

ii. Both lime and carbon are extremely cheap and are available in plentiful amounts.

iii Carbon is also the most efficient reducing agent as it produces carbon monoxide gas which can either be used as a fuel or as a reducing gas.

iv. The use of vacuum is uneconomical because of the high running and maintenance cost of the vacuum system.

v. Also a vacuum system would not prevent environmental pollution as CS_2 gas is more toxic than SO_2.

In the present investigation, the reduction mechanism of synthetic copper sulphide and iron sulphide has been studied and applied to understand the reduction mechanism of synthetic chalcopyrite minerals. The present investigation also deals with the optimum conditions for the reduction of these minerals.

1.C. Thermodynamic Calculations for the Carbothermic Reduction of Sulphides.

It is understood that the carbothermic reduction of mineral sulphides are not thermodynamically possible in the absence of the exchange medium. From the free energy temperature diagram for sulphides of metals, the reasons for the progress of the reaction in the forward direction can be appreciated by a large difference in the chemical potential of sulphur between MS and XS see fig. (1.2). In addition to a knowledge of the sulphide free energy temperature diagram it is necessary that these metal oxides (MO) can be easily reduced to metal carbon, see fig (1.3). On the basis of the available thermodynamic data a free energy temperature diagram has been constructed for the exchange reaction, the reduction reaction and the combined reaction, see fig (1.4). The relative stability of the metal sulphides and the metal oxides are evident from this graph which at any temperature gives the value of partial pressure of carbon monoxide generated as a result of the carbothermic reduction.

From fig (1.4) it is evident that the standard free energy change for the exchange reaction is almost independent of the temperature and it shows that at any temperature, the reaction is not thermodynamically feasible, but under conditions where the activity of the product is lowered the reaction will always move to the right. The free energy (ΔG^{o}) vs temperature relationships shown in fig (1.4) are drawn for the following sulphides.

All units in calories per mole.

a) Cu_2S (s) + CaO (s) = Cu_2O (s) + CaS (s)

$\Delta G^{o}_{(a)} = 16120 - 12.56T + 6.22T \log T$

b) Cu_2O (s) + C (gr) = 2Cu (s) + CO (g) (1.4)

$\Delta G^{o}_{(b)} = 13100 - 37.83T$

c) Cu_2S (s) + C (gr) = 2Cu (s) + CaS (s) + CO (g)

$\Delta G^{o}_{(c)} = 29220 - 50.39T + 6.22T \log T$

a) NiS (s) + CaO (s) = NiO (s) + CaS (s)

$\Delta G^{o}_{(a)} = 740 + 2.8T$

b) NiO (s) + C (gr) = Ni (s) + CO (g) (1.5)

$\Delta G^{o}_{(b)} = 29310 - 41.32T$

c) NiS (s) + CaO (s) + C (gr) = Ni (s) + CaS (s) + CO (g)

$\Delta G^{o}_{(c)} = 30050 - 38.52T$

a) FeS (s) + CaO (s) = FeO (s) + CaS (s)

$\Delta G^{o}_{(a)} = -5470 + 2.18T$

b) FeO (s) + C (gr) = Fe (s) + CO (g) (1.6)

$\Delta G^{o}_{(b)} = 36610 - 36.57T$

c) FeS (s) + CaO (s) + C (gr) = Fe (s) + CaS (s) + CO (g)

$\Delta G^{o}_{(c)} = 31140 - 34.39T$

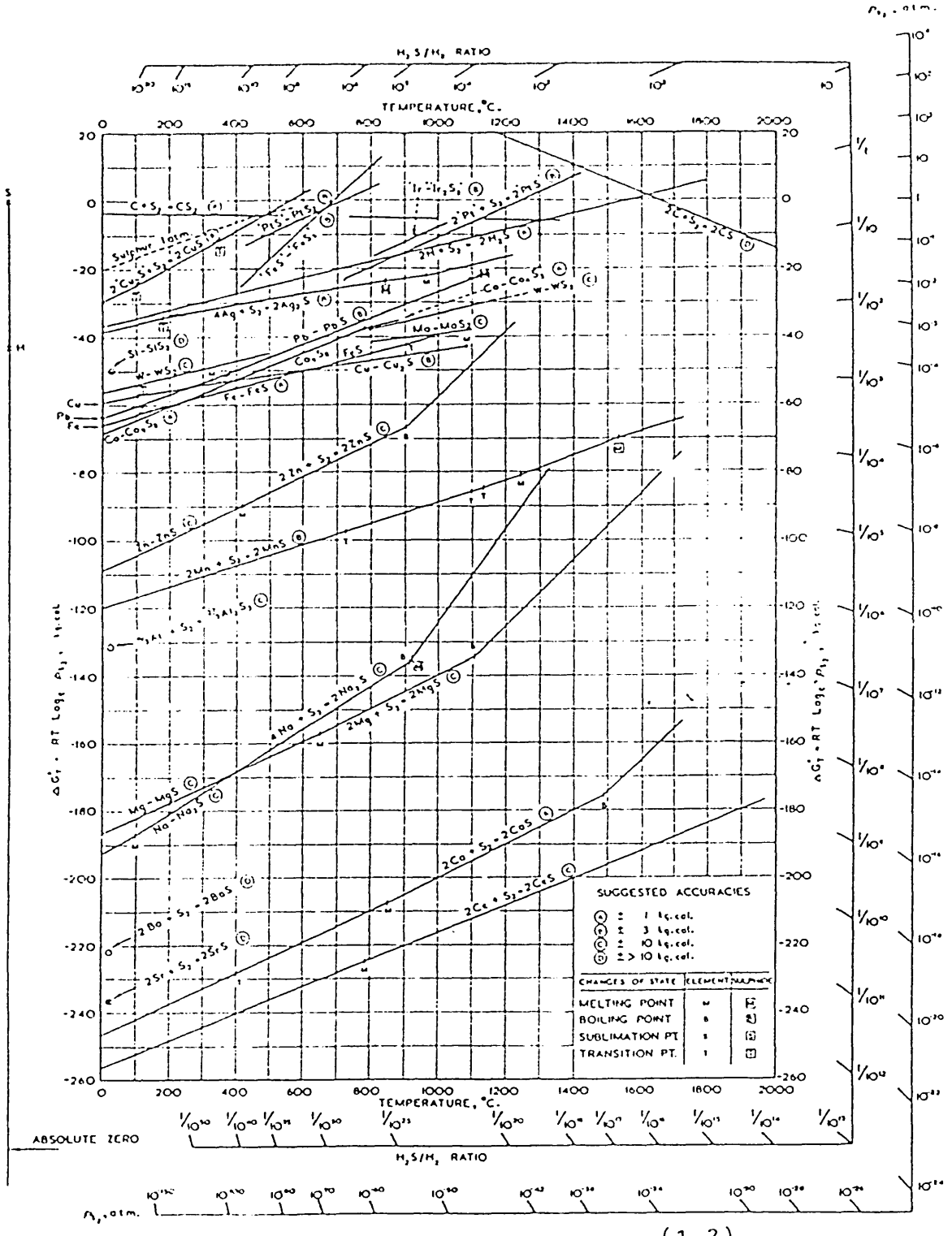


Fig (1.2) Free-energy diagram for sulphides of metals (1.2)

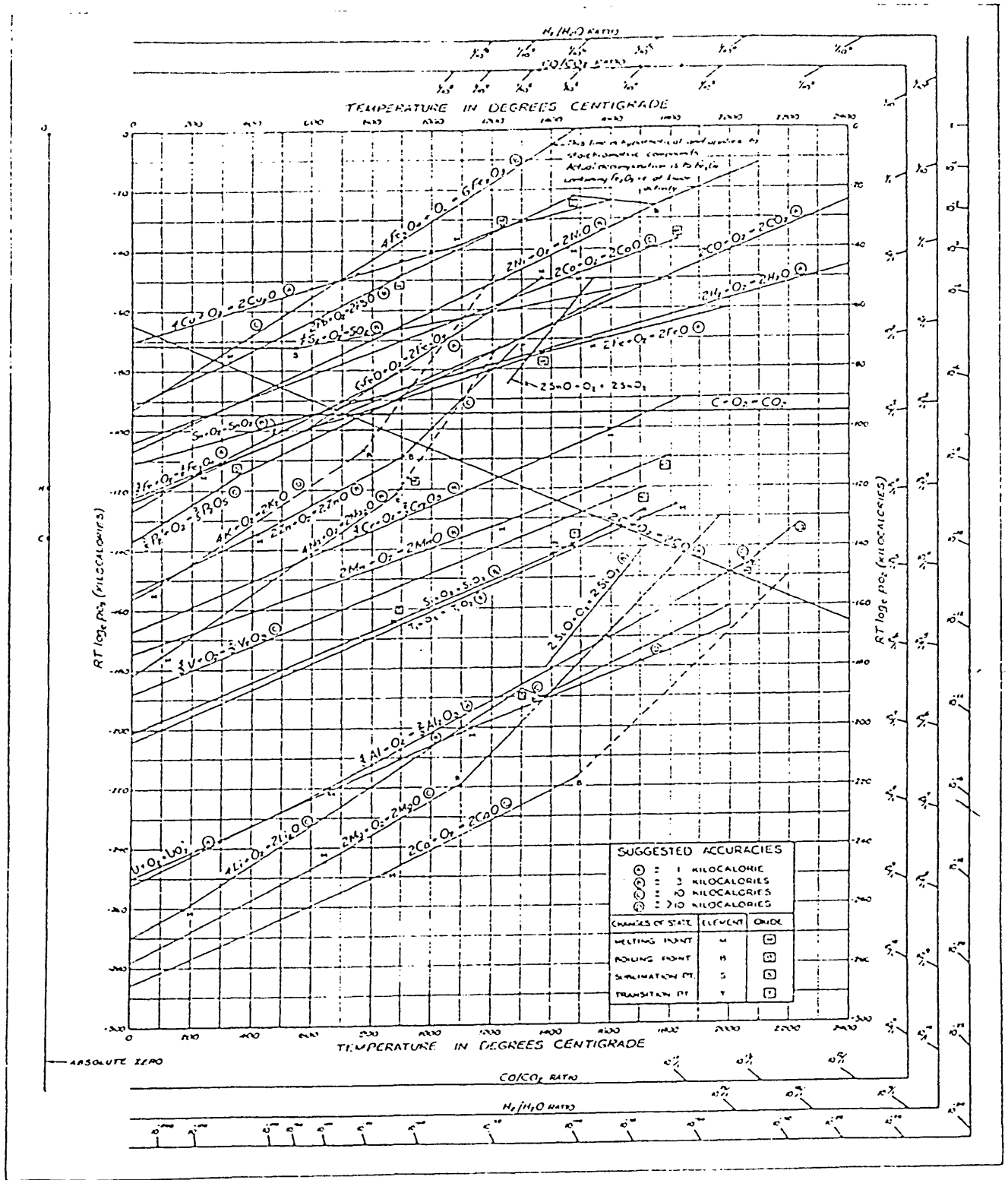
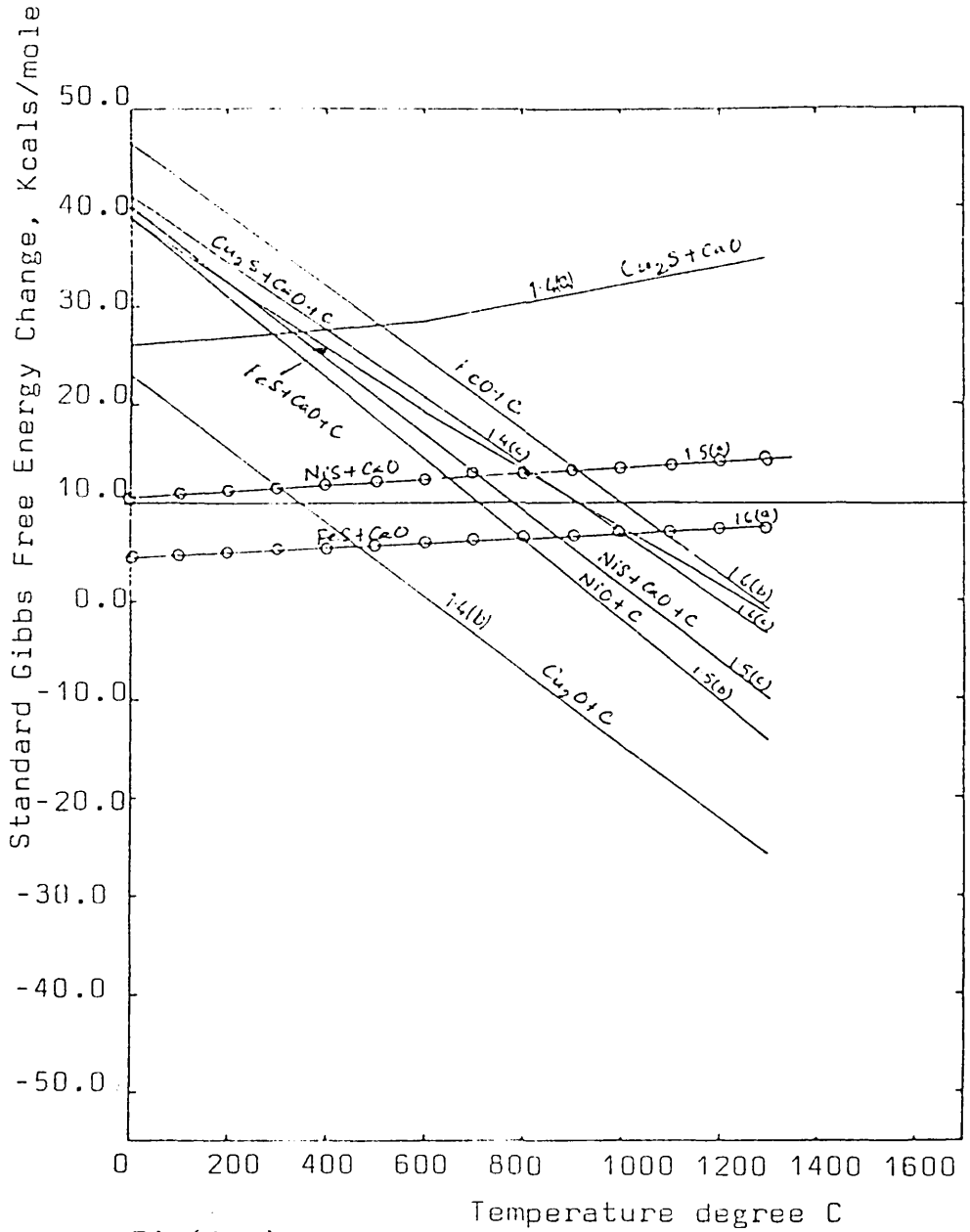


Fig (1.3) Oxygen potentials in oxide systems (1.3) F. D. Richardson, 1961



Fig(1.4) Free Energy- Temperature diagram for the carbothermic reduction of metal sulphides.

1.0. Literature Review.

1.0(i) The Carbothermic Reduction of Metal Sulphides

Most of the earlier studies on the carbothermic reduction of metal sulphides has been carried out by the Russians and the Japanese (1.5-1.12) on the recovery of lead from Galena ore.

Both the lean and the rich ores were treated with sodium carbonate (soda ash) with a small amount of NaCl and Na_2SO_4 in the presence of carbon. The mixture was heated over a range of temperature 900 - 1250°C to study the recovery of the metal. Some workers (1.8-1.10) have used a mixture of iron and Na_2CO_3 or a mixture of pyrites and Na_2CO_3 to desulphurise the galena ore in the presence of carbon. It has been claimed that iron forms as an intermediate product, when pyrite is used, and this metallic iron reacts with galena ore to give metallic lead. It has been claimed by Pendar (1.13) that volatilization losses do not occur on account of the presence of chlorides.

Considering the situation, where pyrites was added during the carbothermic smelting of the galena the possibel initial reaction is:-

(1.7) $FeS\ (s) + Na_2CO_3\ (s) + 2\ C\ (gr) = Fe\ (s) + Na_2S + 3\ CO\ (g$

(1.8) $FeS\ (s) + Na_2O\ (s) + 2C\ (gr) = Fe(s) + Na_2S\ (s) + CO\ (g)$

As a result of these two equilibria, metallic iron is produced. Since these two equilibria operate under the condition of sulphur potential fixed by FeS-Fe; in parallel, the equilibrium fixed by PbS-Pb would also operate to give metallic lead. Hence these two reactions would compete with each other under the given set of conditions. Once metallic iron is generated, the desulphurisation rate of galena would occur due to the following equilibrium.

(1.9) $PbS\ (s) + Fe\ (s) = Pb\ (l) + FeS\ (s)$

$$\Delta G^{0} = 1670 - 6.565T$$

These reactions explain the reason for the use of pyrites or metallic iron during the desulphurisation of galena. The equilibria (1.7) to (1.9) are considered such that the reactants and the products are at unit activity. The relative magnitude of the equilibrium constants for these equilibria would change if mutual dissolution of the reactants and the products takes place.

Pendar (1.13) has quoted that the addition of NaCl during the carbothermic smelting of galena with soda ash prevents volatilization losses. Thermodynamically, the partial pressure of lead vapour is almost insignificant in the range 900-1250^{o}C, At 1250^{o}C P_{Pb} = 47.31mm = 0.062atm which is small. The other notable weight loss due to volatilisation could only be the evaporation of metallic sodium at this temperature which would form as a result of the following reaction:-

(1.10) Na_2S (s) + Pb (l) = PbS (s) + 2 Na (g).

The addition of NaCl to the mixture would act as a sink for sodium vapour, as most of the alkali metals have been found to be soluble in their halides (1.14). The most important aspect of the addition of alkali halides is the generation of a liquid phase which accelerates the exchange reaction kinetics by increasing the surface area of the reaction.

The work on the carbothermic reduction of zinc sulphide has been once again dominated by Russian workers (1.16,1.17) using different types of exchange medium e.g. CaO, $CaCO_3$ and CaC_2. According to Skopov (1.16) the reaction

(1.11) ZnS (s) + CaO (s) + C (gr) = CaS (s) + Zn (g) + CO (g).

$$\Delta G^{o} = 58720 - 58.33T + 4.6T \log T \quad (1.4)$$

proceeds at 570 - 600°C and accelerates above a temperature of 860°C and finally undergoes completion at 1250°C. A 20pct stoichiometric excess of both CaO and carbon (acetylene black) enchances the reaction rate but decreases the recovery of zinc from the reaction mixture into the gaseous phase. A further increase of CaO and carbon ie an excess of 20 to 60pct results in a decrease in the reaction rate. The apparent activation energy of the reaction at 800-1050°C is 29-35 Kcal per mole. The reduction of zinc with $CaCO_3$ proceeds with the preliminary dissolution of $CaCO_3$. The addition of 1pct Na_2CO_3 accelerates the reaction at 800°C due to the appearance of a liquid phase enabling better contact between the reacting components. The same system has been investigated by Y.K. Rao (1.17) and quite a different value for the activation energy has been quoted. According to this work in the range of 920° to 1080°C the apparent activation energy was found to be (50.1 + 4.0) Kcal/mole. The effect of catalysts has also been investigated. With the use of a sodium catalyst during the reaction, the apparent activation energy was (42.5 + 4.5) Kcal/mole for Na_2CO_3 and (36.0 + 4.0) Kcal/mole for Na_2SO_4 catalyst. Both workers (1.16,1.17) have mentioned the appearance of a liquid phase when Na_2CO_3 and Na_2SO_4 were used as catalysts. Neither of these works explain the mechanism of the reduction and particularly the electrochemical mechanism of RaO (1.17) leads to a concept which is very confusing.

Lapin (1.18) et al have observed that ZnS mineral when heated with lime, forms a liquid phase with the formation of compounds belonging to Zn-Ca-S-O system which appear in the columnar and accicular form on solidification. They have proposed a mechanism of dissolution process identical to reaction (1.2). The oxysulphides obtained differ in the physical properties. This matter will be dealt with in greater length later.

In the presence of such quaternary liquid and quaternary compounds the reduction mechanism can be quite different. It is speculated that such liquid and compounds are quite prevalent in the temperature range 800-900^{o}C, and in this liquid it is quite likely that sulphates, carbonates and fluorides of sodium might be soluble. These alkali metal compounds were added in very small quantities such that in the liquid phase their behaviour would probably be Henrian and in this dilute solution of these alkali metal compounds their electro-chemical contribution to the carbothermic reduction of ZnS would be purely decided by their activity about which no information is available. There is no supporting evidence for the existence of any intermediate phases e.g. Na_2S, Na_2O etc. Therefore, it is evident that there is little contribution of these alkali halides to the electro-chemical mechanism suggested by Rao, rather their influence can be seen as a catalyst to enhance the Boudouard Chemical Reaction and in providing liquid by depressing the melting point which eventually accelarates the exchange reaction of O^{-2} ion and S^{-2} ion. Later in the thesis a separate section is devoted to illustrate the catalytic effect of alkali-metal compounds and the possible mechansim involved during the carbon gasification by CO_2.

In the absence of a detailed information on the reduction mechanism of zinc sulphide, and with the supporting evidence of RaO (1.17) and Skopov (1.16), the assumption that the Boudouard Reaction is the rate controlling step may be reasonable. If this is so, the difference in the apparent activation energy (Ea) observed by these two workers could be related to the following reasons:-

a) Two different types of carbon were used. Acetylene black was used by Skopov and Carbon black of fixed carbon 99.5 pct an average particle diameter 0.256μm, and surface area of 12.9m^2/gm by Rao.

b) The problem of analysis of the data, which was found by Rao in determining the slopes of the rate curve, as any error in slopes would drastically change the value of (Ea).

Even in the presence of catalysts the activation energies reported by Rao are not in agreement with those of Skopov. It is therefore recommended that a more systematic study of the reduction mechanism of zinc sulphide is necessary.

Panfilov's (1.15) investigations were based on the use of calcium carbide and the suggested mechanism for the various metal sulphides is given below:-

(1.12) $MS\ (s) + CaC_2(s) = CaS\ (s) + M\ (s) + 2\ C\ (gr)$.

The value of standard free energy change ΔG^o for cuprous sulphide has been calculated according to equilibrium (1.12) using the standard state of calcium vapour.

Therefore for cuprous sulphide the equilibrium (1.12) reduces to:

(1.13) $Cu_2S\ (s) + CaC_2\ (s) = CaS\ (s) + 2\ Cu\ (s) + 2\ C\ (gr)$

$$\Delta G^o_{13} = -82975 + 4.68T + 6.22T \log T.$$

From the standard free energy change for the equilibrium (1.13) it is evident that the reaction is extremely exothermic and it is expected that a large quqntity of heat might be generated at the reaction front. At $T = 873^oK$, the value of equilibrium constant $K_{13} = 5.6596 \times 10^{+15}$. For this reason initiation of reaction was observed at 878^oK. However, once the reaction proceeds in the solid state CaC_2 and MS will be seperated by a solid layer of CaS and metal respectively such that any further reaction should, in principle, be governed by some diffusion mechanism. It has been observed by Panfilov that a maximum of 71.8 pct reduction was recorded at 1200^oC after 60 minutes. Any further reaction at 1200^oC would continue to proceed because of the liquefaction of Cu_2S which could maintain contact with CaC_2. Once, the liquid matte is isolated, the reaction would not proceed any further. There is a considerable doubt whether the reaction proceeds because of the decomposition of CaC_2 in the presence of metal sulphides to calcium and carbon. The calcium would evaporate and react with metal sulphide to form CaS. The thermodynamic

data shows that the vapour pressure of calcium over pure solid and liquid calcium is very small at these temperatures. Thus only logical explanation for the continuation of the reaction at low temperature is the exothermic heat generated at the reaction front which probably causes incipient melting of sulphide to maintain contact with CaC_2.

1. 0 (ii) Hydrogen Reduction of Metal Sulphides in the Presence of Alkaline Oxides.

Several workers (1.19-1.22) have studied the hydrogen reduction of metal sulphides in the presence of basic oxides. All these workers have carried out the reduction of metal sulphides both in the presence of the basic oxides and in their absence. The thermodynamic feasibility of reduction of metal sulphides has been summarized in Table 1.2.

Table 1.2 Equilibrium Constants for the Hydrogen Reduction of Metal Sulphides (1.19).

$$CaO\ (s) + H_2S\ (g) = CaS\ (s) + H_2O\ (g) \qquad (a)$$

$$Cu_2S + H_2\ (g) = 2\ Cu\ (s) + H_2S\ (g) \qquad (b)$$

$$Ni_xS\ (s) + H_2\ (g) = x\ Ni\ (s) + H_2S\ (g) \qquad (c)$$

$$Co_yS(s) + H_2\ (g) = y\ Co\ (s) + H_2S\ (g) \qquad (d)$$

$$Fe_z\ S\ (s) + H_2\ (g) = z\ Fe\ (s) + H_2S\ (g) \qquad (e).$$

The equilibrium constants for the combined reactions (a) and (b), (a) and (c), (a) and (d) and (a) and (e), equal to the gas ratio P_{H_2O}/P_{H_2} over the system at equilibrium are:-

T°K	Ka	Kb	Ka × Kb	Kc	Ka × Kc	Kd	Ka × Kd	Ke	Kc × Ka
800	1.22×10^{3}	7.13×10^{-4}	0.68	7.05×10^{-4}	0.59	5.20×10^{-4}	0.33	2.10×10^{-4}	2.56
900	4.08×10^{3}	1.19×10^{-3}	4.86	1.19×10^{-3}	4.86	2.20×10^{-3}	8.98	5.60×10^{-4}	2.28
1000	1.70×10^{3}	1.74×10^{-3}	2.96	2.10×10^{-3}	3.57	6.65×10^{-3}	11.31	1.21×10^{-3}	2.05
1100	9.41×10^{2}	2.14×10^{-3}	1.94	2.90×10^{-3}	2.41	1.31×10^{-2}	11.08	2.30×10^{-3}	1.95
1200	4.56×10^{2}	2.95×10^{-3}	1.35	3.60×10^{-3}	1.65	1.72×10^{-2}	7.87	4.00×10^{-3}	1.83
1300	2.76×10^{2}	3.56×10^{-3}	0.98	4.15×10^{-3}	1.15	2.00×10^{-2}	5.52	6.00×10^{-3}	1.66
1400	1.79×10^{2}	4.15×10^{-3}	0.74	4.60×10^{-3}	0.824	2.22×10^{-2}	3.96	7.30×10^{-3}	1.31
1500	1.23×10^{2}	4.72×10^{-3}	0.58	4.95×10^{-3}	0.608	2.30×10^{-2}	2.83	8.20×10^{-3}	1.01

The values of the equilibrium constant products show that the hydrogen reduction of metal sulphides is thermodynamically less feasible compared to carbothermic reduction at higher temperatures.

(1.14) $H_2(g) + \frac{1}{2} O_2 (g) = H_2O (g)$ $\Delta G^{o}_{14} = -58900 + 13.1T.$

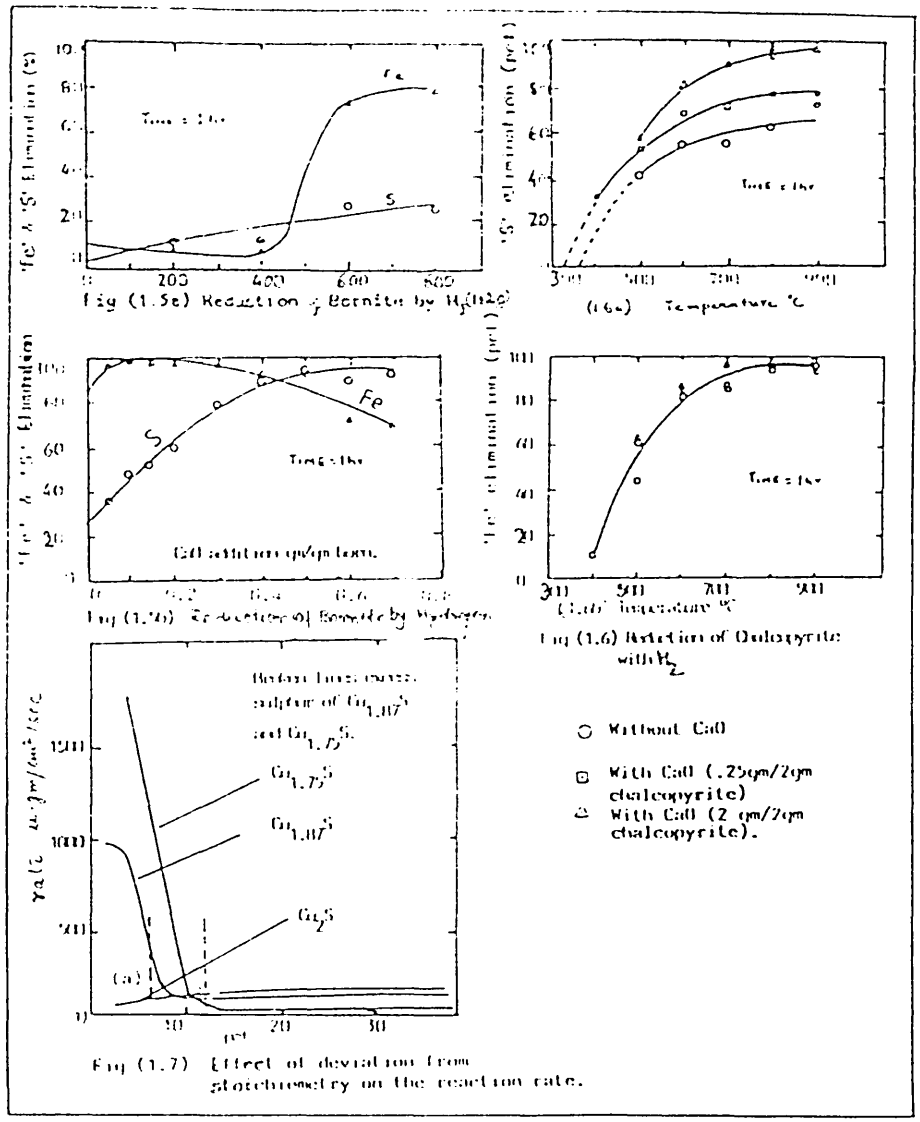
The work of Cech and Tiemann's (1.19) has been mainly devoted to a study of the mechanism of the filamentary growth of metal fibres from metal sulphides during the reduction with hydrogen. A separate chapter will be devoted later to elaborate the knowledge of the mechanism of whisker and filamentary growth. Habashi and Dugdale (1.20) studied the reduction kinetics of copper and iron base sulphide minerals and their morphological observations were in agreement with those of Cech and Tiemann.

Habashi and Dugdale (1.20) have also shown in the absence of CaO, approximately 80pct of iron and 26pct of sulphur can be removed by H_2 reduction at 800°C from bornite see fig (1.5a). When the reduction of bornite mineral was carried out with lime at 800°C, in presence of hydrogen, the removal of iron was found to decrease when more than 0.2gm of

CaO for each gram of bornite were used. In addition, surprisingly, at 800°C the removal of sulphur without lime was found to be about 33pct. The discrepancy in the two results of 'S' removal is not explained see fig 1.5(b). Stoichiometrically, for complete reduction of bornite to iron and copper, 0.45 gm of CaO is necessary for each gram of bornite. Theoretically, the sulphur equivalent for FeS in bornite is 6.38pct and needs 11.17pct of lime to remove sulphur and iron as experimentally observed in their work. Their observations show that an increase in lime decreases the iron elimination has not been properly explained. The reason for the decrease in elimination with increasing lime will be presented in a later chapter where the phase correlations in Fe-Ca-So system will be discussed. Habashi and Dugdale have also found that the metallization of copper is possible by heating cuprous sulphide with lime over a range of temperatures (400 + 800°C) in 1 hours. They have also observed the presence of cupric oxide CuO over this temperature range; a matter which is rather disputable.

Their observations (1.20) on the reduction of chalcopyrite mineral leaves some doubts about the independent nature of iron elimination in the presence and in the absence of lime with H_2 as reactant; see fig (1.6b) where sulphur elimination has been considerably affected by the presence of lime, see fig (1.6a). As the heat treatment of the chalcopyrite at any temperature above 500°C results in decomposition to bornite, pyrrhotite and gaseous sulphur.

Therefore, essentially it is the mineral bornite which is reduced in the presence of lime and hydrogen and yet their results on chalcopyrite were found to disagree with those for bornite (compare fig (1.5) and fig (1.6). These discrepancies need clarification which would be dealt with later in this thesis with the results and discussions on the reduction of chalcopyrite mineral.


Fe
S
Time = 1hr
Fig (1.5a) Reduction of Bornite by H2(H2S)
(1.6a) Temperature °C
Fig (1.6) Reduction of Chalcopyrite with H2
Without CaO
With CaO (.25gm/2gm chalcopyrite)
With CaO (2 gm/2gm chalcopyrite).
Fig (1.7) Effect of deviation from stoichiometry on the reaction rate.

Ford (1.21) and Prasad (1.22) have basically devoted their time to understanding the kinetics of the hydrogen reduction of metal sulphides with lime. The detailed information on the rate of reduction of cobalt sulphides can be seen in ref. 1.23 where a reaction rate model is developed. Most of the literature available on the hydrogen reduction of metal sulphides have been surveyed by Prasad (1.22) and he has summarized the rate data for the H_2S reaction with lime and the kinetic studies on the direct reduction of metal sulphides carried out by several authors. These two sets of rate data are summarized in Table 1.3 and Table 1.4.

Makinen (1.24) has studied the effect of the non-stoichiometry of cuprous sulphide on the reduction rate. According to him, a small deviation in the stoichiometry affects only the initial rate where as large deviations affect both the initial and the final stage of the reduction, see fig (1.7). However, the rate of reduction of these non-stoichiometric sulphides was affected only slightly by the temperature. Assuming that the deviation from stoichiometry leads to the equivalent amount of cationic vacancies in the sulphide lattice under the given set of conditions, the chemical diffusivity (D_c) of the cation Cu^{+1} should be related to the self-diffusivity (D^*) and the stoichiometric deviation (δ) by the following relation:

$$D_c = \frac{3}{\delta} D^* \qquad (1.15).$$

Using the stoichiometric deviation data on $Cu_{1.75}S$ and $Cu_{1.87}S$, it is evident that chemical diffusivity of Cu^{+1} in $Cu_{1.75}S$ is half the value observed for $Cu_{1.87}S$. If the activation energy for the ionic diffusion is considered, the reaction rate in $Cu_{1.87}S$ should be twice as fast as $Cu_{1.75}S$. Also, cationic vacancies should have shown a considerable dependence on the temperature, yet it has been claimed that the temperature effects are very small. It is evident that the

Table 1.3 Summary of studies on H_2 reduction of metal suphides.

Investigators	Scavenger	Reactant Gas	Temperature range of Study (°C)	Rate Equation	Activation Energy, K. cals per mole	Main Conclusions
Gavrilova & Altschuler[17], [18], [19]	CaO	0.2-0.45% H_2S (bal. N_2)	500-1100	—	3.3-4.5	Diffusion-controlled reaction.
	CaO, MgO, 1:1 CaO+MgO, Kaolin	only H_2S	—	—	—	Order of absorbing power CaO> CaO+MgO> Kaolin>MgO
Habashi & Mikhail[18]	CaO	only H_2S	470-800	Parabolic	16.0	Gaseous diffusion through product layer.
Habashi & Dugdale[16]	CaO, BaO and MgO in the H_2 reduction of Cu_2S	H_2S formed *in situ*	800	—	—	BaO as good as CaO in enhancing the reduction rate; MgO is not effective.
Vestal & Johnston[20]	Calcined dolomite	0.1% H_2S (bal. He)	—	—	38.0	First order reaction.
Pell[21] & Pell & Co-workers[21], [22]	Calcined dolomite	—	475-950	—	—	Homogeneous first order reaction w.r.t. CaO; MgO behaved as an inert filler.
Gavrilova[24]	MnO	0.27% H_2S	550-800	Linear	—	First order reaction; 99% desulphurisation at 40-50% reagent efficiency.

Table 1.4: Kinetic Studies on Direct Hydrogen Reduction of Sulphides (1.27).

Sulphide (Investigators)	Temperature (^{o}C) range of study (observed critical hydrogen flow rate cc min^{-1})	Observed Energy rate equation	Activation energy Kcals per g at %	Rate Determining step (s).
CuS discs (Tanaka et al)	450-750 (2100)	Linear up to over 45% conversion	(i) 42.8 (<450^{o}C) (ii) 4.7 (450-750^{o}C)	(i) <450^{o}C: H_2 chemisorption at the interface (ii) >450^{o}C: H_2S diffusion through product layer.
CuS discs & powder (Makinen)	500-1000 (823)	(i) Linear up to 60% conversion (600-780^{o}C) (ii) Parabolic (800-1000^{o})	(a) 33.4 (500-580^{o}C) (b) 15.5 (580-780^{o}C) (c) 4.8 (>780^{o}C) for disc samples	(i) <580^{o}C: Chemical reaction control. (H_2 absorption at reaction interface). (ii) 580-780^{o}C: H_2S diffusion through product Cu whisker (iii)>780^{o}C: H_2S diffusion through product Cu crusts.
AgS discs (Tanaka & Shibayama)	300-500	-	22.7	-
NiS powder (Tanaka & Abe)	500-625 (600)	Linear	21.9	Sparse absorption of H_2 on the reaction interface.

/Contd

Table 1.4 Contd..

Sulphide (Investigators)	Temperature (^{o}C) range of study (observed critical hydrogen flow rate cc min^{-1})	Observed Energy rate equation	Activation Energy Kcals per g at %	Rate Determing step (s)
FeS (Maekawa & Tanaka)	-	Linear up to 40% conversion	18.3	Chemical control
FeS discs (Kapur et al)	650-900 (1500 twice crit. value)	Linear	31.6	Chemical control
Pyrrhotite Spheroids (Kor)	600-900 (21 STP)	-	-	Mass transfer control (counter current H_2 - H_2S diffusion through porous iron product & gas bound layer)
Fe Ni S Synthetic Pellets (Shah & Ruzzi)	550-750 (400-600)	Linear after 0.5 hr	5.9	H_2S diffusion through boundary layer.
MoS_2 powder bed 0.2-3.36mm deep. (Sinadinovic & Durkovic.	900-1100 (1000)	-	-	Rate drops steeply with the depth from 0.1-1.0mm range
Molten Sulphides of Cu,Pb Fe & Ni (Byerley et al)	1080-1340 (High)	-	20.6 for FeS 23.8 for CoS 20.1 for Ni_3S_2 26.5 for Cu_2S	Metal catalysed reaction of atomically dissolved hydrogen with sulphur.

Table 1.4 Contd..

Sulphide (Investigators)	Temperature (^{o}C) range of study (observed critical hydrogen flow rate cc min^{-1})	Observed Energy rate equation	Activation energy Kcals per g at %	Rate Determining step (s).
BiS powder (Chida & Ford)	475-630 (1000)	Linear	38.8	Chemical control unreacted core model applicable up to 530^{o}C above which Co whiskers are formed.
CoS (Pennatier et al)	496-586	-	32.0	Nucleation process control rate.
	603-734	-	24.0	Chemical Control.
CoS pellest & powder (Fahim & Ford)	600-800 (2500 for pellets 1000 for powder)	Linear	2.71 for pellets (600-800^{o}C) & 27.8 for powder (600-737^{o}C)	Chemical control in the region 600-737^{o}C; Above 780^{o}C pellet swelling & rupture due to Co whisker formation.
Co & Ni sulphides (Chizhikov et al)	-	Linear	-	Formation on non-compact product layer on the sulphides.

extent of non-stoichiometry also determines the cupric to cuprous ratio in the sulphide during the hydrogen reduction of these non-stoichiometric sulphides, where the activity of CuS in the compound is low, decomposition would occur by the evolution of S_2 gas. This could be the reason why at a larger concentration of excess sulphur, the rates are faster and logically as the Cu^{+2}/ Cu^{+1} ratio decreases, the rate of reaction should match the rate of reduction of pure Cu_2S. This is not quite comprehensible from the data of fig (1.7)[1.24], as sulphur is removed from the system, the composition of sulphide should approach Cu_2S, which should reduce at a constant rate. Also point (a) in fig (1.7) represents the compound $Cu_{1.97}S$, not Cu_2S.

From the aforementioned reviews on the carbothermic and the hydrogen reduction of metal sulphides, it is evident that little is known about the possible phase correlations during the course of reduction and it is difficult to determine absolute reaction rates.

****

REFERENCES

Chapter 1.

1.1 A.K. Biswas and W.G. Davenport - The Extraction Metallurgy of Copper. PErgamon Int. Library. Int. Series. Mat Sci. & Tech. vol 20. 1976

1.2 F.D. Richardson & J.H.E.Jeffes J.I.S.I. Inst. 160 261 (1948) 163 397, (1949)

1.3 Physical Chemistry of Melts in Metallurgy, vol 2, 1974. Academic Press.

1.4 O.Kubacheswki, C.B. Alcock. E.K.K. Evans - Metallurgical Thermochemistry, Pergamon Press. 1967.

1.5 K.V. Suskov et al - Chemical Abstract 53 (1959) 2059.

1.6 K.V. Suskov et all-- Chemical Abstract 64 (1966) 6162

1.7 G. ELenkov et al - Chemical Abstract 56 (1962) 6964

1.8 O. Hitoshi et al - Chemical Abstract 56 (1962) 4437.

1.9 I.T. Matsukawa et al - Chemical Abstract 53 (1959) 2025.

1.10 Mishisha and Hori - Chemical Abstract 65 (1966) 14913.

1.11 Odeen et al - Chemical Abstract 48 (1954) 8159.

1.12 Chesti and Sirkar - Indian J.I. of Tech. vol. 9 1971, 339-43.

1.13 Pendar - Chemical Abstract 51 (1957) 5677.

1.14 F.D.Richardson - Physical Chemistry of Melts in Metallurgy vol.1. pp 67-8 Academic Press 1974.

1.15 Panfilov et al - Izv. Vyssh. Ucheb. Zaved. tsvet Metally. vol. 12. no.4. 1969, pp 22-4 Chem Abs. vol. 72. 1970. 23655.

1.16 Skopov et al - Izv. Vyssh. Ucheb. Zaved tsvet. Metally. vol. 4, 1976 pp 33-7

1.17 Y.K. Rao & H. Abrahamcowitz - IMM Trans. C. Sept 1978 pp 180.

1.18 Lapin et al Irvest. Akad. Nauk SSSR. Metally 1975(6) 64. Chem. Abs. 1976 84 108977X.

1.19 R.E. Cech & T.D. Tiemann - Trans AIME. Vol 245. 1965. pp - 1727

1.20 F. Habashi & R. Dugdale - Met Trans vol. 4 1973 pp 1865.

1.21 J.D. Ford & F.A. Fahim - Met. Trans vol 613 1975 pp 461.

1.22 P.M. Prasad & T.R. Mankhand - Trans. Ind. Inst. Met vol 32. No. 3 June 1979. pp 253-85

1.23 J.D. Ford & F.A. Fahim - Cond. J. Chem. Engg. 55 (1977) 313

1.24 J. Makinen - Doctor. Tech. Thesis Helsinki University of Technology, Helsinki (1975).

****

2. Phase Relationships Important During the Carbothermic Reduction of Metal Sulphides.

2.a Copper-Sulphur (Cu-S) System.:-

The copper-sulphur phase diagram has been investigated by Kullerd (2.1) and is shown in fig (2.1a) which shows the existence of two eutectics between Cu and Cu_2S at 1067^oC and another eutectic at 813^oC between CuS and S. The liquid at 813^oC between CuS sulphur exists under a partial pressure of sulphur P_{S_2} > 1.00atm. A more elaborate phase diagram has been worked out by Elliott (2.2) which shows the related sulphur partial pressures in equilibrium with the condensed phase, see fig(2.1b). Little appears to be known about the equilibrium partial pressure of sulphur across the non-stoichiometric range of Cu_2S.

2.b Iron-Sulphur (Fe-S) system.

The iron-sulphur equilibrium diagram has been constructed by Kullerd (2.3) and it is in complete agreement with Chang and Sharma's (2.4) recent solution model to describe the thermodynamic behaviour of Fe-S liquid. The model assumes the existence FeS species in addition to Fe and S in the liquid. With two solution parameters for each of the binaries Fe-'FeS' and 'FeS'-S this model accounts for the compositional dependence of the thermodynamic properties of Fe-S liquid from pure Fe to pure S over a wide range of temperature. Using this model for the liquid phase and a defect thermodynamic model for the pyrrohtite phase, the Fe-S phase diagram is calculated and is in excellent agreement with the experimental data accounting for the range of

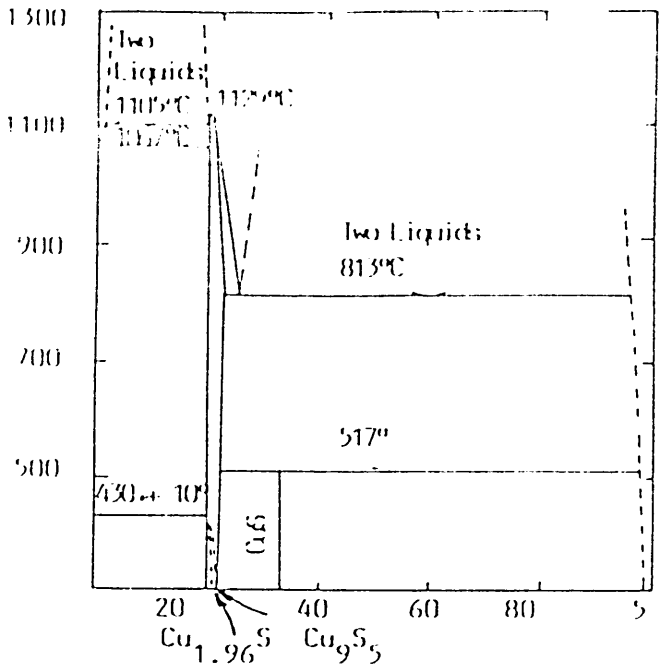


Fig (2.1a) Cu-S Phase diagram (2.1).

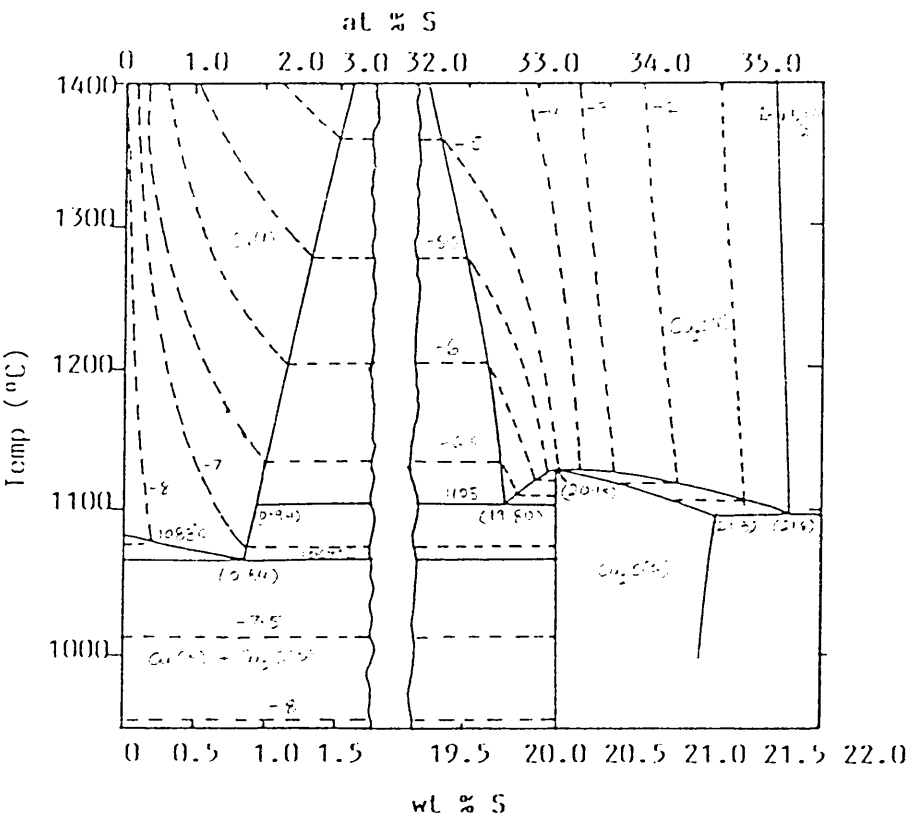


Fig (2.1b) Phase relationships in Cu-S system with sulphur partial pressure and temperature (2.2).

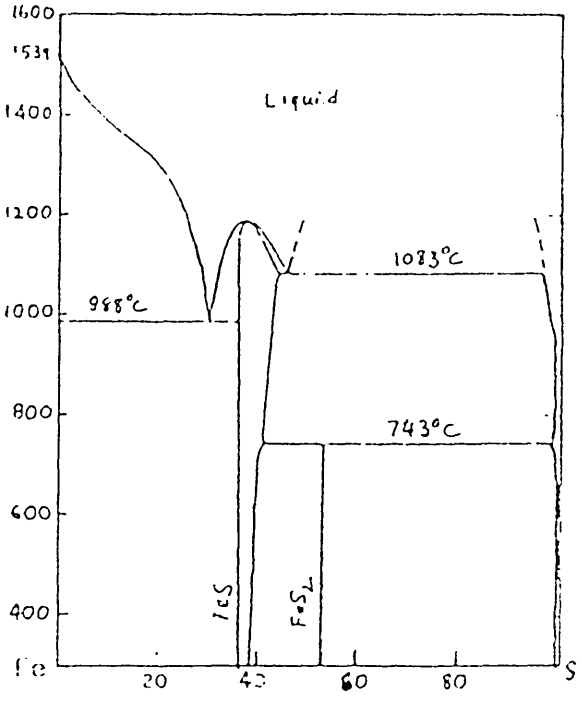


Fig (2.2a) Fe-S phase diagram (2.3)

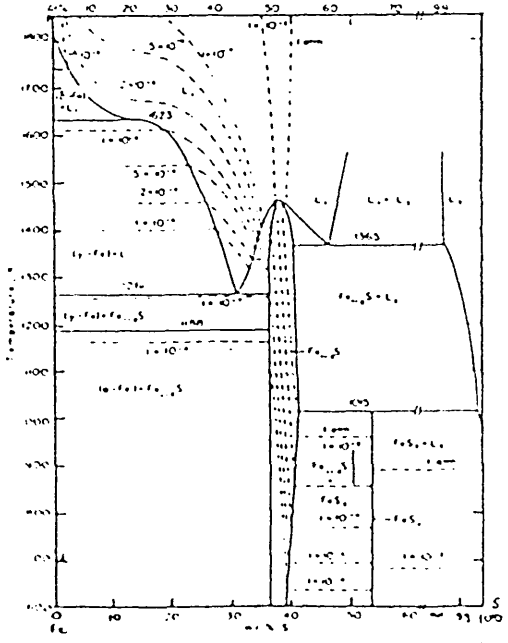


Fig (2.2b) - The calculated Fe-S phase diagram with isobar values of $S_2(g)$ up to 1 atm, 1 atm = 1.01325×10^5 Pa. (2.4)

homogenity of pyrrohtite at all temperatures, see fig (2.2a) and (2.2b) [2.6]

2.c. Nickel-Sulphur (Ni-S) system

Kullerd (2.5) and Chang (2.6) have studied the nickel-sulphur system but the latter's work is more up to date with the related sulphur partial pressures in equilibrium with the condensed phases see fig (2.3a) and(2.3b). Chang's work reviews all the studies carried out.

2.d. Copper-Sulphur-Iron (Cu-Fe-S) system.

Related to the pyrometallurgy of the copper-iron matte, most of the thermodynamic analyses on this system have been carried out above 1100^{o}C. This system has been studied by Releaux (2.7). Schlegal and Schiiller (2.8) and more recently Krivsky and Schumann (2.9) in the temperature range of 1150^{o} to 1350^{o}C. In the present investigation all the experiments were carried out below the melting point of copper, hence the thermodynamic information available for this system above 1083^{o}C is of little interest.

The Cu-Fe-S system is extremely complicated in the low temperature range, which is important for the carbothermic reduction of chalocopyrite and bornite minerals and the following phase diagrams are referred, fig (2.4). In this system, it has also been shown that there is a wide range of solid-solubility between Cu_2S and FeS with two compounds see fig (2.5) [2.11]

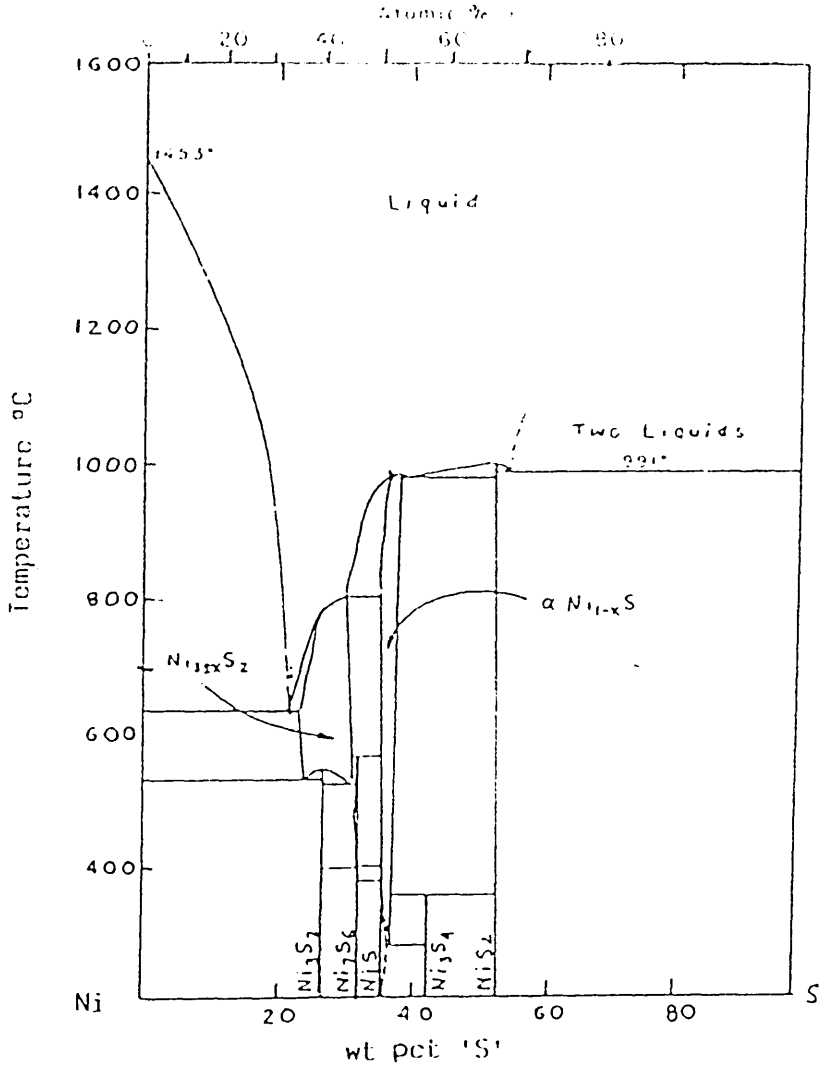


Fig (2.3a) Ni-S phase diagram (2.5).

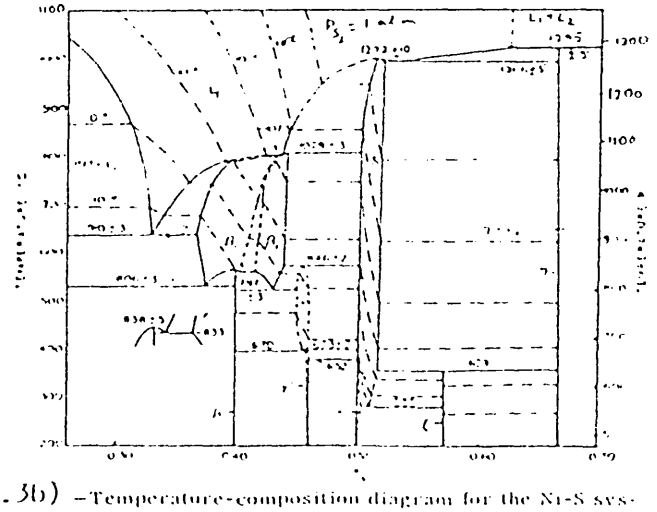


Fig (2.3b) –Temperature-composition diagram for the Ni-S system with isobars of $S_2(g)$. Estimated phase boundaries are shown as dashed lines and the isobar lines are shown as dash-dotted lines. 1 atm = 1.01325×10^5 Pa. (2.6).

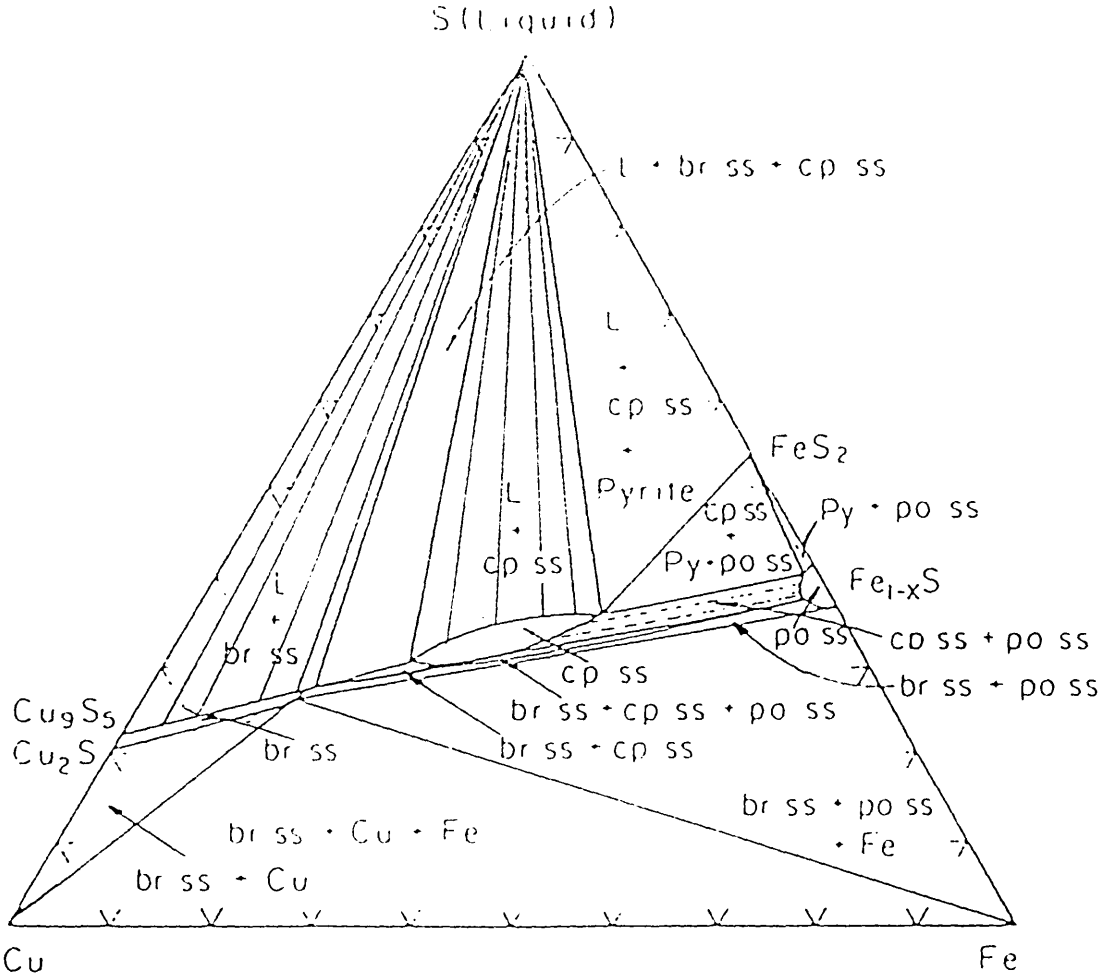


FIG. 2.4(a).—System Cu-Fe-S at 700°C. Vapor is present in all assemblages. br ss = bornite solid solution, cp ss = chalcopyrite ss, po ss = pyrrhotite ss and L = liquid. (2-10)

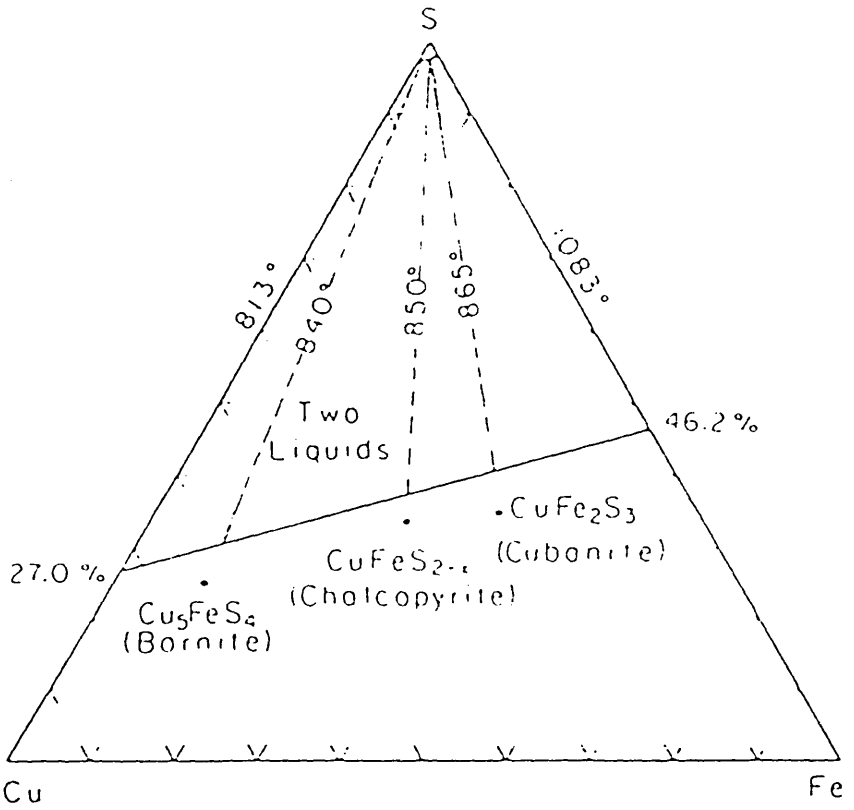


FIG.2.4(b) --System Cu-Fe-S showing conodes in liquid immiscibility region (2-10)

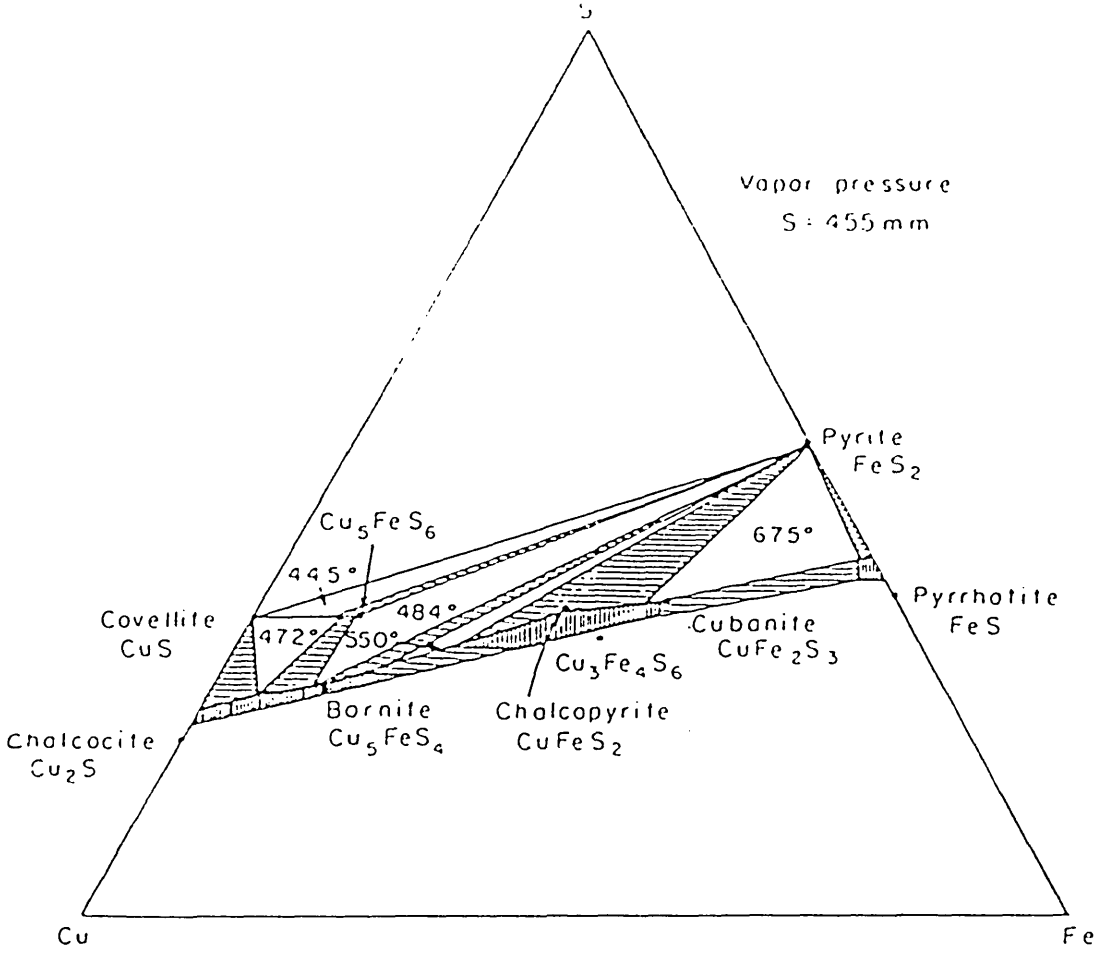


Fig. 2.4(c)-System Cu-Fe-S under constant sulfur vapor pressure of 455 mm Hg.(2.10)

2.e. Copper-Sulphur-Oxygen (Cu-S-O) System.

Most of the investigations in this system have been devoted to the phase relationships related to roasting which is carried out between 500-800°C or smelting and refining. Rosenqvist (2.12) has established a relationship between oxygen potential and the temperature on the basis of available literature data. A plot between log p_{O_2} and $1/T$ is shown in fig (2.6) which shows various univariant and invariant phase field over a range of 350° to 1000°C. Elliot has reviewed various work in the temperature range of 750° to 1300°C and has established a correlation between the activity coefficient of Cu_2O in Cu_2S at infinite dilution which is valid for the temperature range of 1100° to 1300°C.

$$\log \gamma^{\circ}_{Cu_2O} = \frac{1708}{T} - 1.271 \qquad (2.1)$$

According to Elliott (2.2) the Cu_2S-Cu_2O system is close to ideal in its behaviour. In this review, Elliott has not mentioned the existence of any liquid phase between 750° to 1050°C.

The solubility of oxygen and sulphur in liquid copper in equilibrium with liquid Cu_2S and the solubility of oxygen in liquid Cu_2S in equilibrium in the liquid metallic copper has been investigated by Schmiedl (2.13). The variation of solubility with the pressure of SO_2 at different temperatures is shown in fig (2.7). From his measurements it is apparent that no detectable level of 'O' was observed in the liquid Cu_2S below P_{So_2} = 0.276 atm at which an oxygen solubility of 0.86 wt pct was measured. According to Schmiedl (2.13) the empirical relationship for the solubility of oxygen is:

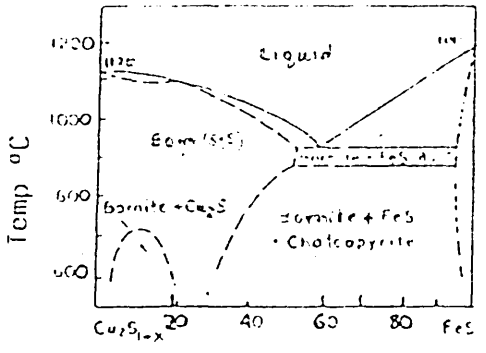


Fig (2.5) Cu_2S-FeS phase diagram (2.11)

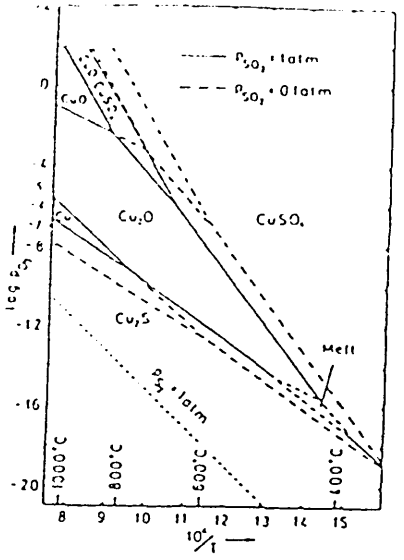


Fig (2.6) Oxygen potentials in the system Cu-S-O at 1 and 0.1 atm of SO_2. (2.12)

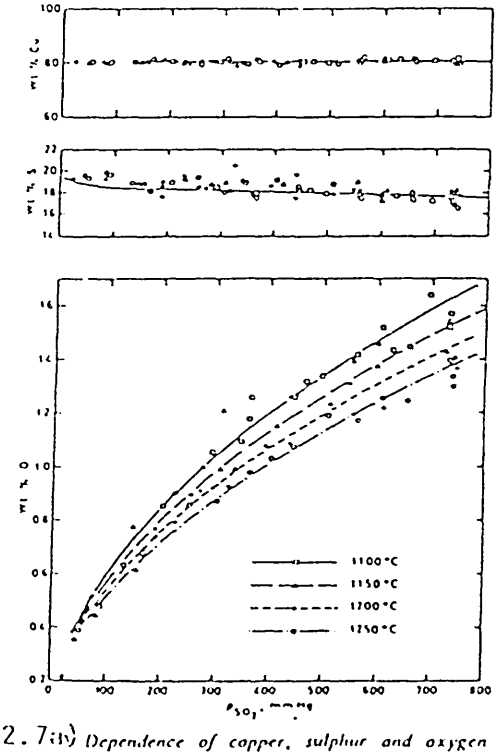


Fig (2.7a) *Dependence of copper, sulphur and oxygen contents in sulphide melt on p_{SO_2} at 1100, 1150, 1200 and* (2.13)

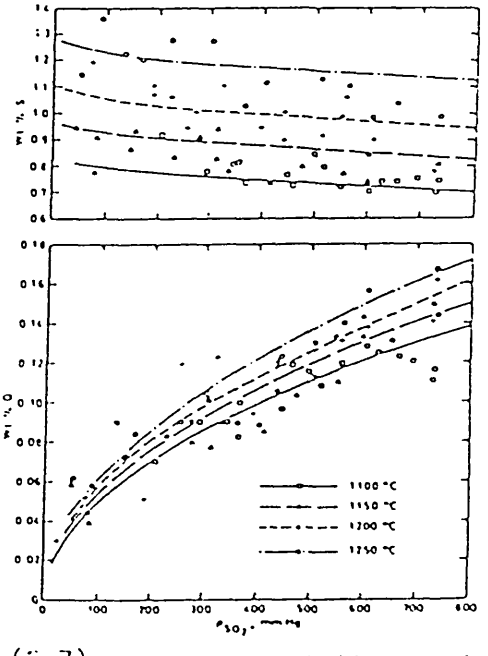


Fig (2.7) *Dependence of oxygen and sulphur content in copper on p_{SO_2} at 1100, 1150, 1200 and 1250°C* (2.13)

Metal Phase.

(a) wt% 'O' = $10^{(-1.37684 - (1277.67/T))} \times p_{So_2}^{\frac{1}{2}}$

(2.2) (b) wt% 'Cu' = $10^{(1.97893 + (23.8886/T))}$

(c) wt% 'S' = 100 - wt % O - wt % Cu

Sulphide Phase.

(a) Wt% O = $10^{(-1.95989 + (1013.2/T))} \times p_{So_2}^{\frac{1}{2}}$

(2.3) (b) Wt% Cu = $79.695 + 0.26042 \times 10^{-12} T^4$

(c) Wt% S = 100 - wt % O - wt % Cu

Although all these workers (2.2, 2.12, 2.13) have indirectly referred to Kauxmann and Benecke's (2.14) work to establish phase relationships and to measure and calculate thermodynamic properties, none of them reported the existence of any oxysulphide liquid below 1100°C, which is quite evident from their predicted diagram.

The pressure-temperature-composition diagram shown in fig (2.8) shows that there is a eutectic between Cu_2S and Cu_2O at NCu_2S = 0.6 and T = 840°C. The eutectic temperature calculated theoretically also explains the observation by Schimiedl of a significant minimum oxygen solubility in liquid Cu_2S at 1100°C. This can be explained in terms of an invariant phase field in the three component (Cu-S-O) system. At T = 1100°C, from the Cu_2S- Cu_2O pseudo binary section it is evident that up to NCu_2O = 5.40 mole pct, the only phase combination possible is (L + Cu_2S). In this invariant phase field the activity of oxygen or Cu_2O is constant. From the equilibrium

phase relationship

(2.4) $Cu_2S\ (s) + 2\ Cu_2O\ (s) = 6Cu\ (l) + SO_2\ (g)$

$$\Delta G^{o}_{T} = 40930 - 79.637T + 14.067T \log T$$

(2.5) $$a_{Cu_2O} = \left[\frac{P_{SO_2}}{K}\right]^{\frac{1}{2}}$$

where a_i - activity of i^{th} species

K - equilibrium constant.

At the unit activity of metal and metal sulphide and at $T = 1100^{o}C$, $a_{Cu_2O} = 0.1251$ and $\gamma_{Cu_2O} = 2.32$; which indicates the melt behaves more like a regular solution with a repulsive interaction. The nature of interaction also shows that there is a possibility of eutectic transformation. From Kauxmann and Benecke's prediction and Schmiedl's measurement using equation (2.4) it is evident that at $T = 1100^{o}C$, the equilibrium $P_{SO_2} = 0.27$ atm at which the liquid phase exists. Therefore it can be inferred that higher equilibrium partial pressures of SO_2 would be expected at lower temperatures.

2.F. Iron-Sulphur-Oxygen (Fe-S-O) System.

Vogel and Fulling (2.15) investigated the FeO-FeS diagram but their observations indicated that the oxide component approximated Fe_3O_4 rather than FeO which shows that the system is not truely binary. Although in their observations, the eutectic was observed at $920^{o}C$, there was a great deal of doubt about the precise location of the critical point ie the miscibility gap which was reported close to the

Fe-S edge at 1320°C. This was disputed by Hilty and Craft (2.16), who has investigated the ternary system and essentially is an improvement of the diagram constructed by Vogel et al. Darken and Gurry (2.17) constructed the FeS-FeO binary see fig (2.9) and reported the eutectic temperature at 908°C. Turkdogan and Kor's (2.18) work is more analytical and covers the entire range of temperatures with all possible univariants and invariants. Their work was based on the theorem developed by Roozeboom and Schreinemakers on the relation of the invariant curves intersecting at an invariant point in a pressure vs temperature (P-T) plot for ternary system. Darken modified this theorem after Morey and Williamson's extension on the multicomponent system, and he gave a constructive illustration of this theorem to ternary systems. Bog and Rosenqvist (2.19) on the other hand studied the activity relationship in the entire molten range where the melts were equilibrated with (H_2 + H_2S + H_2O) to determine the $^{a}s = {}^{P}H_2S/P_{H_2}$ and $^{a}O = {}^{P}H_2O/ P_{H_2}$.

On the basis of Turkdogan and Kor's work it can be concluded that by applying Darken's modification of the Morey-Williamson theorem on univariant curves intersecting at an invariant point the elthalpy of formation of liquid oxysulphide is estimated for Fe-S-O system e.g. -43.5 Kcal per gm of Fe at the eutectic invariant 915°C and -36.4 Kcal per gm atom Fe at the peritectic invariant 942°C. The ternary sections and the relevant phase fields on the basis of above calculations are shown in fig (2.10)

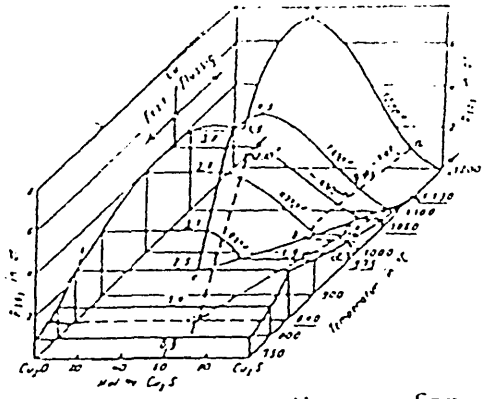


Fig (2.8) P-I composition diagram for Cu-S-O system (2.14)

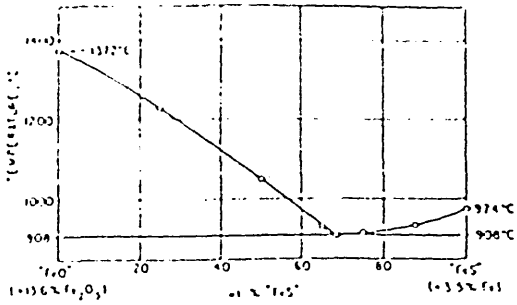


Fig (2.9) Melting diagram of system iron oxide—iron sulfide in equilibrium with metallic iron. (2.17)

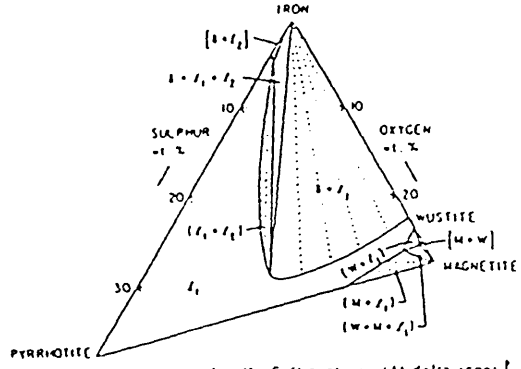


Fig (2.10a) 1400°C isotherm for Fe-S-O system. (δ) delta iron; (IV) wustite; (M) magnetite; (l_1) liquid oxysulfide; (l_2) liquid metal.

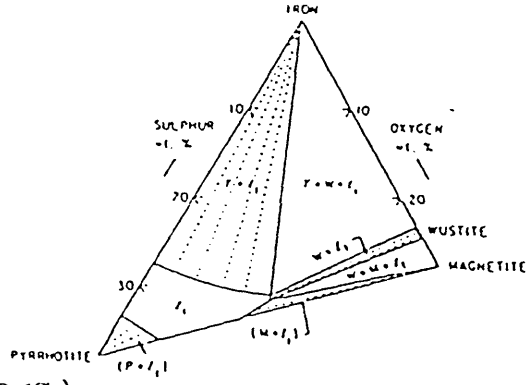


Fig (2.10b) 1100°C isotherm for Fe-S-O system. (γ) gamma iron; (IV) wustite; (M) magnetite; (P) pyrrhotite; (l_1) liquid (1) (2.18)

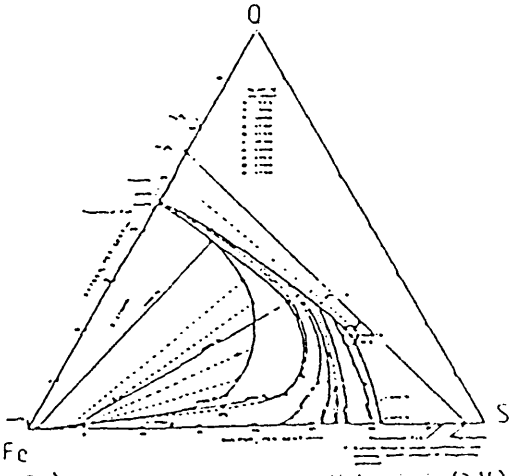


Fig (2.10c) Fe-O-S diagram according to this investigation (2.16)

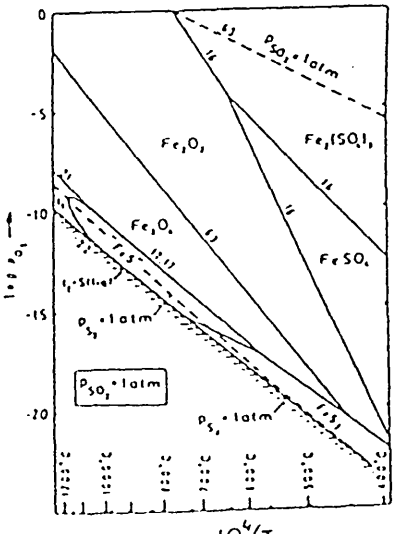


Fig (2.10d) Oxygen potentials in the Fe-S-O system at 1 atm of SO_2 (2.17).

2.G. Copper-Iron- Sulphur-Oxygen (Cu-Fe-S-O) system.

Related to matte smelting of complex copper-iron sulphide and to the roasting of complex copper-iron sulphide concentrate the phase predominance diagrams have been constructed by several workers. (2.2, 2.12, 2.13, 2.20, 2.21) but once again the existence of any possible quaternary liquid phase in the temperature range of 750°C to 1000°C has been overlooked. Although Rosenqvist (2.12) in his review paper has mentioned the occurence of incipient melting above 900°C in certain parts of system but this has been ignored in order to present a simplified phase relationships over a wide range of temperature (see fig (2.12)).

Invoking the existence of a eutectic and a peritectic invariant in Fe-S-O system at 915°C and 942°C (2.18) and a eutectic invariant in Cu-S-O system at 840°C (2.14), it is possible according to the Clausius - Clapeyron Relationship to estimate correctly the quaternary liquid or any other possible invariants. This can also be estimated by Darken's Modified Morey - Williamson theorem for multicomponent univariants. Recently, Wagner (2.22) has devised an analytical method based on the Gibbs-Duhem Relationship and on the basis of experimentally determined data, to calculate the activity of various components in the Cu-Fe-S-O mattes. Although his model has been focussed to determine the activity of components in the matte phase along 1100°C, it can be applied to lower temperatures leading to the determination of the liquidus surface.

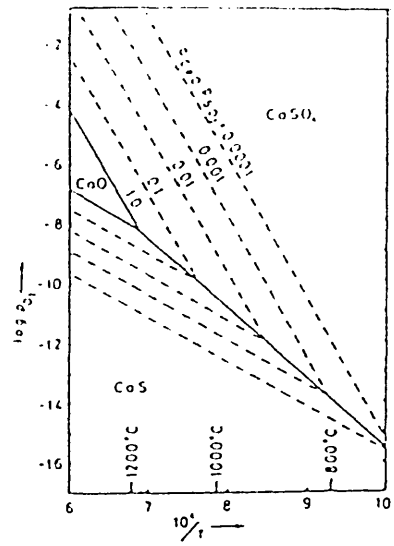


Fig (2.11) -Oxygen potential in the system Ca-S-O as function of temperature. (2.12)

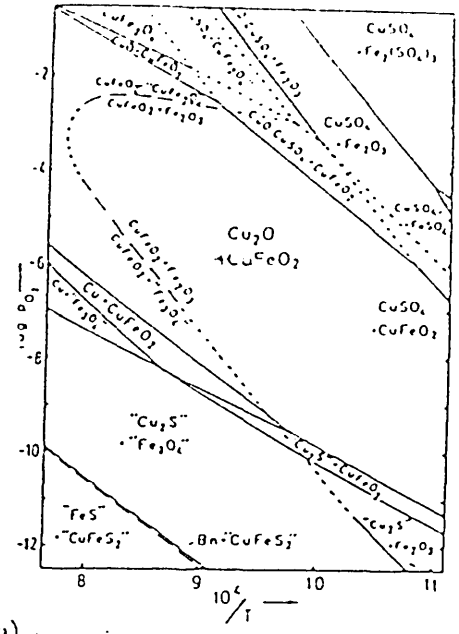


Fig (2.12a) -Effect of temperature on the oxygen potential for 1 atm of SO_2 for all three-phase combinations in the system Fe-S-O. ——— $N_{Fe} < 0.5$. ------ $N_{Fe} > 0.5$. ..... (2.12)

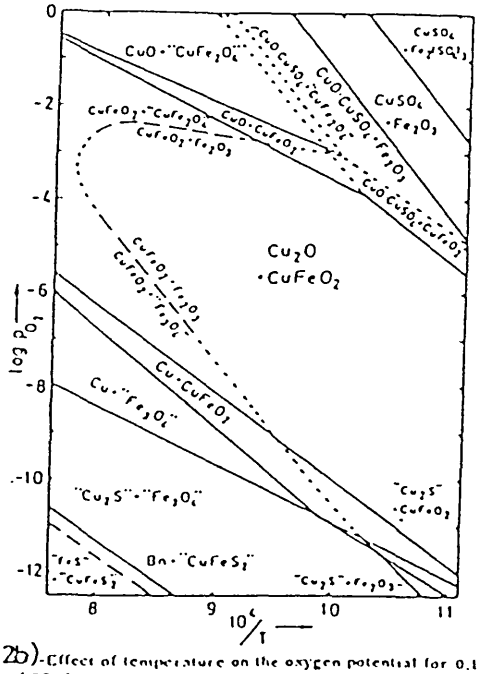


Fig (2.12b) -Effect of temperature on the oxygen potential for 0.1 atm of SO_2 for three-phase combinations in the system Cu-Fe-S-O. (2.12)

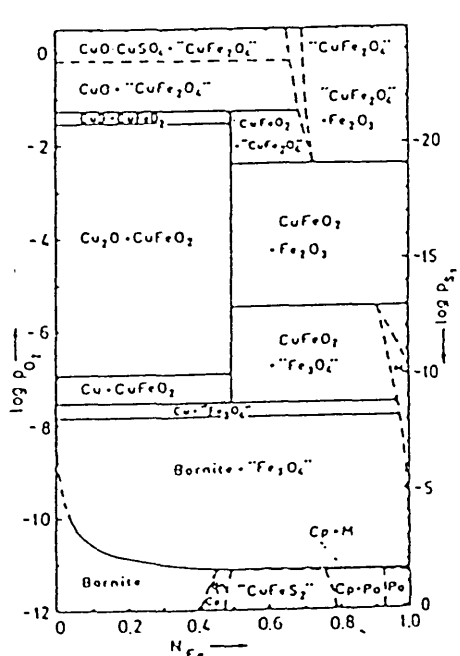


Fig (2.12c) -Oxygen potential in system Cu-Fe-S-O as function of N_{Fe} for 1 atm of SO_2 and 927°C. Symbols as in Fig. ---------- estimated. (2.12)

Related to the roasting of sulphide minerals, some excellent observations have been made by Henderson (2.23) and Thornhill and Pidgeon (2.24). Using the optical microscope, and X-ray diffraction, they have shown during complex sulphide roasting there is a segregation of copper to the centre and iron to the outer region of the particle known as Kernel Roasting. It has been summarized as a phenomena with combined thermodynamic and kinetic effects. Wustite and magnetite are formed first in the early stages of the oxidation of chalcopyrite. Since copper sulphides and oxides have negligible solubilities in iron oxide there is a preferential diffusion of iron in the oxide phase and copper in the sulphide phase away from the chalcopyrite-wustite interface. This counter current diffusion results in the accumulation of copper at the centre of particle forming chalcocite (Cu_2S) or digenite (Cu_9S_5) while iron oxide free of copper accumulates on the periphery of the particle..

Thornhill and Pidgeon (2.24) have presented their results based on X-ray diffraction analysis where they have explained the breaking of chalcopyrite, bornite and pentlandite minerals into parent high temperature sulphides. The development of Widmanstatten structure, localized zones of shrinkage, apparently conforming to certain crystallographic planes resulting in the formation of gaps between primary and secondary oxide layer and in some cases between oxide and sulphides. However, there is no justification given which explains the presence of any preferential crystallographic planes.

On the other hand, Henderson (2.23) in his work has shown in micro-graphs the presence of an intermediary liquid phase prevalent under the conditions of oxidation. In the case of the roasting of fused copper sulphides containing (79.5 pct Cu, 0.12pct Fe and 20.4pct S), a inner layer of Cu_2O was

enveloped by a layer of CuO. At the Cu_2S-Cu_2O interface, metallic copper was observed at 890°C and larger quantities were observed at 965°C. There is no information given on the morphology of the copper but according to Kauxmann and Benecke (2.14), copper should have formed from a liquid phase in equilibrium with SO_2 which might isolate the oxide from any further contact, as well as preventing the entry of the oxidizing gas to come into direct contact with sulphide. The abrupt increase in the growth of the oxide layer is due to the channel formation and the exposing of fresh surfaces to the oxidizing gas. The mechanism of segregation roasting will be dealt with at greater length.

2.H. Calcium-Sulphur-Oxygen (Ca-S-O) System.

The univariant equilibria in this system have been investigated by Rosenqvist (2.12) and Glasson and O'Neill (2.25) and they have shown with decreasing partial pressure of SO_2, the predominance area of lime increases, see fig (2.11). This system will be discussed in greater length in a seperate section in which the mechanism of inert and reduction calcination of calcium sulphate will be considered.

2.I. Calcium-Copper-Sulphur-Oxygen (Ca-Cu-S-O) System.

The existence of various univariant equilibria with temperature has been summarized by Rosenqvist (2.12) see fig (2.12). From this, it is evident that conditions can be created to produce desirable products by treating metal sulphid with lime, which could be suitable for processes based on aqueous or pyrometallurgy.

2.J. Iron-Calcium-Sulphur-Oxygen (Fe-Ca-S-O) System.

Most of the investigations carried out in this system falls in the temperature range of iron and steel making. Vert and Kamentsev (2.26) studied the FeS-CaO system according to the following chemical equilibrium given by equation (1.6a)

$$FeS\ (s) + CaO\ (s) = FeO\ (s) + CaS\ (s) \qquad (1.6a)$$

and observed changes over a range of temperature 400-1225^{o}C. The products of the reaction above 840^{o}C formed a melt. A plot between percentage CaS formed and the temperature has been drawn from which the extent of CaS formation at any temperature can be determined and hence phase correlation can be studied, see fig (2.13). The frequent changes in the percentage of CaS shows that the exchange reaction represented by equation (1.6a) is not the main equilibrium prevailing in the system, but it shows the formation and decomposition of a number of compounds. The formation of CaS begins at 400^{o}C and it rises with temperature reaching 25pct at 550^{o}C. At 630^{o}C, a shallow minimum is observed after which the quantity of CaS in the mixture increases again up to 715^{o}C which is the maximum yield recorded. Any further increase in the temperature results into a sharp decrease in the amount of CaS. At 840^{o}C, a melt forms which has also been observed by Lapin (1.18). Lapin's investigation based on microscopic analysis suggests that columnar and accicular phases were found during the cooling which belong to compounds in the Fe-Ca-S-O system. It has also been proved that the presence of CaO lowers the temperature of primary recrystallization of $Fe_{1-x}S$ and expands the solidification range from 820^{o}C to the solidus. A maximum drop in the primary recrystallization temperature was observed at 35 pct CaO which rises rapidly up to 1050^{o}C between 35 - 50 pct CaO.

The investigation of Yarigin et al (2.27) in this system relates to the structural studies of the compounds, and they have reported that these oxysulphide compounds may have crystal lattice of low symmetry either orthorhombic or monoclinic.

Rosenqvist (2.12) on the other hand has reviewed the work of various authors and has produced a reciprocal system considering FeO-CaS-FeS-CaO and has divided the diagram into three three-phase areas and a two phase area where CaS coexists with FeO containing a varying range of CaO, see fig (2.14). It is evident that the oxysulphides would occur only at a very low oxygen potential and their presence would introduce more three phase fields.

The diagram becomes more complicated at intermediate and higher oxygen potentials where various types of calcium ferrites appear. A eutectic in the ternary section CaS-FeO-FeS exists at 880^{o}C in the presence of iron which does not agree with other workers (1.6,2.26,2.27). Various invariant equilibria prevailing at different temperatures and at different P_{O_2} have been shown in reference (2.12) which does not include either oxysulphides in the system nor the liquid phase.

Tromel et al (2.28) have reported the existence of two oxysulphide phases in the quaternary, and it has also been established that these oxysulphides decompose peritecticly. Various phase combinations in the quaternary at 900^{o}C are shown in fig (2.15) and on the basis of their observations a pseudo binary FeO-CaS diagram has been constructed, from which it can be appreciated that these two compounds melt incongruently.

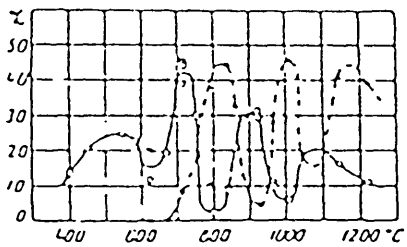
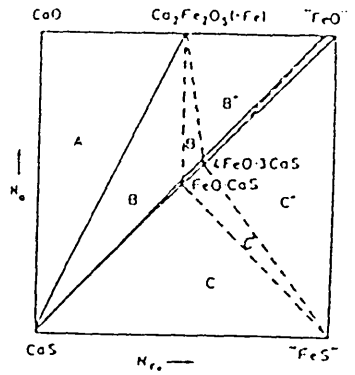


Fig (2.13) Formation of CaS by the reaction of CaO with FeS. -O- yield of CaS (O atmosphere of nitrogen, Q-air), ----●----- CaO bound (2.26)



Phase combinations in the system CaO-"FeO"-CaS-1 600 to 900°C and iron saturation (2.12)

Fig (2.14a)

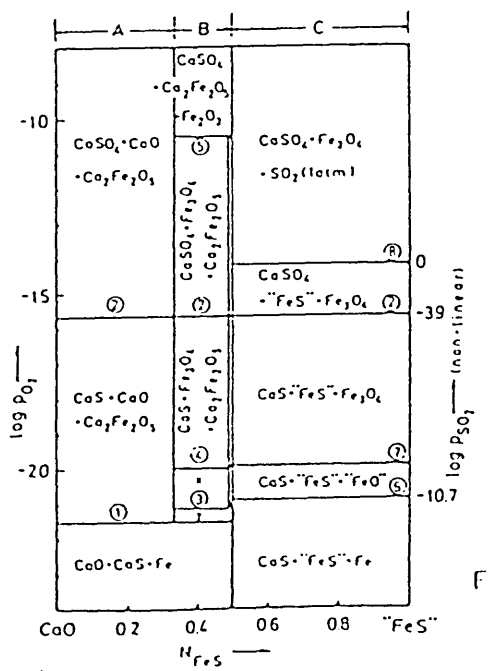


Fig (2.14b) Phase combinations as function of oxygen potential in the system CaO-"FeS" at 727°C. A = CaS + $Ca_2Fe_2O_5$ + "FeO", B = CaS + $Ca_2Fe_2O_5$ + Fe. (2.12)

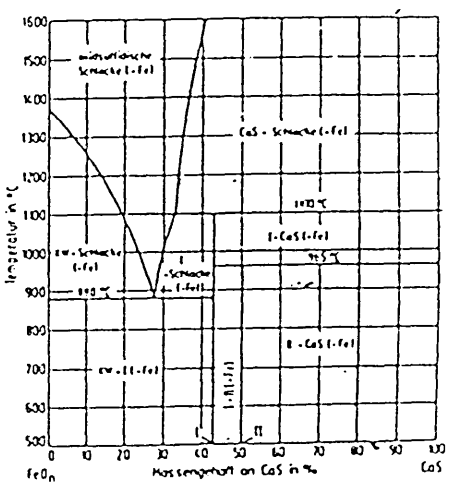


Fig (2.15) Schematic derivation of the system FeO_n-CaS ("quasi-binary" section through the system FeO_n-CaO-CaS-FeS for iron saturation) (2.28)

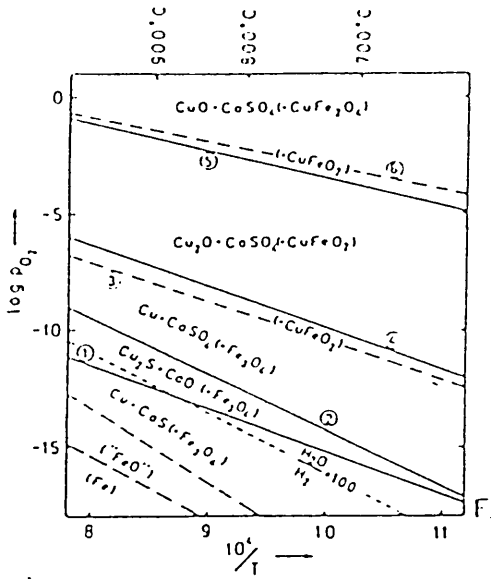


Fig (2.16a) Oxygen potential for univariant equilibria in the system Ca-Cu-S-O (solid lines) and Cu-Fe-O (dashed lines) as function of temperature. (2.12)

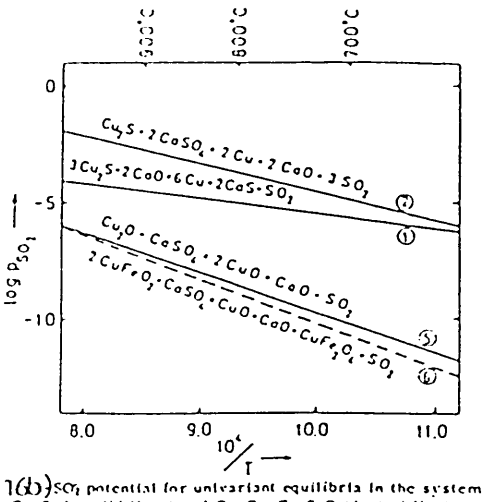


Fig (2.16b) SO_2 potential for univariant equilibria in the system Ca-Cu-S-O (solid lines) and Ca-Cu-Fe-S-O (dashed line) as function of temperature. Calcium ferrites disregarded. (2.12)

No literature is available on the pentnary Ca-Cu-Fe-S-O system from which any possible phase combinations can be discussed; except by the superimposition of various ternary and quarternary univariant equilibria established after Rosenqvist (2.12), some positive inferences can be drawn in relation to the prevailing oxygen partial pressures and temperature, see fig (2.16).

Chapter 2.

2.1 G. Kullerd, Phase diagram for ceramists Fig 3945 vol 1969.

2.2 J.F. Elliot, Met Trans. vol 7B March 1976 pp 17.

2.3 G. Kullerd, Phase diagram for ceramists fig 3948 vol 1969.

2.4 R.C. Sharma and Y.A. Chang, Met Trans vol 10B 1979 pp 103.

2.5 G. Kullerd, Phase diagram for ceramists fig 3951 vol 1969

2.6 Y.A. Chang et al, Met Trans vol 9B pp 531

2.7 O. Releaux. Met Erz 1927 vol 24 pp 99-111

2.8 H. Schlegel and A. Schuller, Metallik, 1952 vol 43 pp 421-28

2.9 W.A. Krivsky and R. Schumann, Trans TMS AIME 1957 vol 209 pp 981-8

2.10 G. Kullerd, Phase diagram for ceramists vol 1969 Fig 8961-3

2.11 Kipylov and Novoselov, Russian JI Inorg. Chem (Eng Trans) 1039 1964

2.12 T. Rosenqvist, Met Trans vol. 9B Sept 1978 pp 337-351

2.13 J. Schimedl, The Physical Chemistry of Process Metallurgy The Richardson Conference IMM Publication pp 127.

2.14 U. Kauxmann and T. Benecke, Erz Metall. Bond XIX (1966) pp 251-21

2.15 Vogel and Fulling, Das System Eisen - Eisensulfid (FeS) wustite (FeO) fEstskriftam. J. Arvid Hedvall (1948)

2.16 D.C. Hilty and W. Crafts, Trans AIME Dec 1952 J.I. of metals pp 1307

2.17 L.S. Darken and R.W. Gurry, Met Trans 1971 vol. 2 pp 1569

2.18 E.T. Turkdogan and G.J.W. Kor, Met Trans 1971 vol.2 pp 1561.

2.19 S. Bog and T. Rosenqvist, The Physical Chemistry of Metallic Solutions and Intermetallic Compounds Vol. II NPL Symp. no 9, 1958 pp 6B p2

2.20 A.Yazawa, Met Trans 10B 1979 pp 307

2.21 A. Yazawa, Canadian Met Qtly vol 13 No. 3 1974.

2.22 C. Wagner, Met Trans 7B Sept 1976 pp 339

2.23 T.A. Henderson, Inst. Min Metall Trans 67 437 (1957-58) 68 193 (1958-59)

2.24 P.G. Thornhill and L.M. Pidgeon, Trans AIME 209, 989 (1957).

2.25 D.R. Glasson and P. O'Neill, The Industrial use of Thermochemical Data. Edt. T.I. Barry, NPL. Published by Burlington House, London.

2.26 Zh.L. Vest and M.V. Kamentsev, J.I. of Inorg. Chemistry USSR. Russian Zh Neog Kluin Vol 11 No 31956 pp 489-498.

2.27 V.I. Yarygin et al. Izv Akad. Nauk SSSR Met 1977 (2) 104-7 (RuS)

2.28 G. Tromel - Arch Eisenhuettenw 1976 vol. 47 pp 471-6

3. Thermal Stability of Sulphides.

Most of mineral sulphides exhibit physical or chemical changes with temperature. The stability of sulphides at any temperature can be studied either from the phase diagram or the Ellingham diagram. The thermodynamic stabilities of sulphides such as Cu, Ni and Fe are well known and can be understood in great detail from the metal - metal sulphide Ellingham diagram.

These sulphides are very non-stoichiometric and across the range of stoichiometry, there are large differences in sulphur potential in equilibrium with the sulphide.

In this section, the stability of complex copper-iron sulphides will be reviewed and the focus will be mainly on chalcopyrite and related minerals. Chalcopyrite mineral when heat treated in a closed system undergoes two phase transformations at $550^{o}C$ and $657^{o}C$ due to a loss of sulphur as a vapour phase. The transformation at $550^{o}C$ is related with the breakdown of the tetragonal network (α chalcopyrite) and formation of a cubic structure β chalcopyrite.

$$CuFeS_2\ (\alpha) \xrightarrow{550^{\circ}C} CuFeS_{2-x}\ (\beta) + xS \qquad (3.1)$$

Habashi (3.1) has reviewed the changes occuring during the heat-treatment of chalcopyrite, and has reported an enthalpy change of 3.83 Kcal per mole with a weight loss of less than 1 pct. This irreversible transformation is very sensitive to the

amount of 'S' present in the ß phase and hence the stability range of the ß phase depends on the value of x varying from 0.144 to 0.260. There appears to be some anamolies concerning the crystal structure of non-stoichiometric chalcopyrite. Mooihoekite ($Cu_9Fe_9S_{16}$) is a non-stoichiometric sulphide where x = 0.222 which has been reported by several workers (3.2, 3.3) to have a tetragonal structure, whereas Pearson (3.4) indicates that the ß phase has a cubic structure. From the review of crystallographic data, it appears that Pearson's data deserves more credibility. Considering the range of stoichiometry for the ß phase the Moohoekite composition falls into this composition range and the weight loss for this change is 3.87 pct a value which does not agree with Habashi's review on the weight loss associated with the change.

The second transition found at 657^{o}C was taken to be the Neel Temperature (3.1) ie an antiferromagnetic transition temperature. The chalcopyrite mineral on heating in an open system loses sulphur and converts into bornite mineral.

$$5\ CuFeS_2(s) = Cu_5FeS_4(s) + 4\ FeS(s) + S_2(g) \qquad (3.2)$$

According to most work it has been shown that bornite is the most stable phase. The low temperature form of bornite has a tetragonal cell a = 10.94^{o}A, c = 21.88^{o}A which appears to be a stacking arragement of two cubic cells of bornite as c/a = 2.0. The change in the lattice parameter with the annealing temperature of bornite has been reported by Pearson (3.4).

Various sulphides close to the bornite composition have been reported in reference 3.2. Habashi (3.1) has reviewed the thermochemical properties of these two sulphides and has reported the vapour pressure of sulphur over chalcopyrite and bornite mineral as chalcopyrite.

Chalcopyrite

$$\log p = \frac{179973.3}{T} + 21.9 \quad \text{in mm of Hg} \qquad (23)$$

Bornite

$$\log p = \frac{-8072.9}{T} + 8.84 \quad \text{in mm of Hg} \qquad (24)$$

but these equations do not agree with the thermochemical data compiled in the INCRA Monograph II (3.5). The vapour pressures in the invariant fields of Cu-Fe-S system are given in ref 3.2. The growth of metallic copper and metallic iron during heat treatments of bornite and chalcopyrite has been reported by Leavenworth et al (3.6)

****

Chapter 3.

3.1 F. Habashi Chalcopyrite Its Chemistry and Metallurgy McGraw Hill Int. Book Comp. 1978.

3.2 INCRA Series on Metallurgy of Copper Phase Diagrams for Cu-S-Fe system.National Standard Reference Data System. U.S.A.

3.3 ASTM X-ray Card Index 14-32 Bornite Mineral.

3.4 W.B. Pearson Hand Book of Lattice Spacing and Structure of Metals Vol. 2 Int. Ser Mono. Met Phy. and Phy. Metally. Edt. G.V. Raynor.

3.5 INCRA Monograph II Printed in U.S.A. Same as ref (3.2)

3.6 Leavenworth et al U.S. Bureau of Mines Dept. Invest. 7833 (1974).

4. Experimental Techniques.

4A(i) Kinetic Studies in a Flowing Gas Stream.

Kinetic studies of the carbothermic reduction of sulphides were carried out employing a thermogravimetric analysis technique. A schematic diagram of the apparatus used for the rate of reaction study is shown in fig (4.1). The sulphides were mixed with freshly calcined lime and spec pure graphite or coal containing only about 13pct volatile matter in an agate mortar and pestle in their respective stoichiometric amounts and mixed overnight on a roll mixer. The mixed powder was pelletized in a steel die by applying constant load into a cylindrical geometry. The pellet was suspended from the extension lead of a load cell (A) inside an alumina crucible or on a platinum pan (B). The load cell was based on the principle of a strain transducer which had a d.c. output of 2mv per gram on its pan. The d.c. out put was fed to the chart recorder (C) which was calibrated against the load cell out put. In this way any weight change in the pellet could be monitored continuously. The alumina crucible (B) was protected from oxygen pick-up during the heating of the pellet using a double wall borosilicate glass reaction tube (R) which was connected with a cone and socket joint to the load cell assembly. The load cell assembly was mounted on a water cooled platform (D) to avoid excessive heating by radiation. A continuous flow or argon was

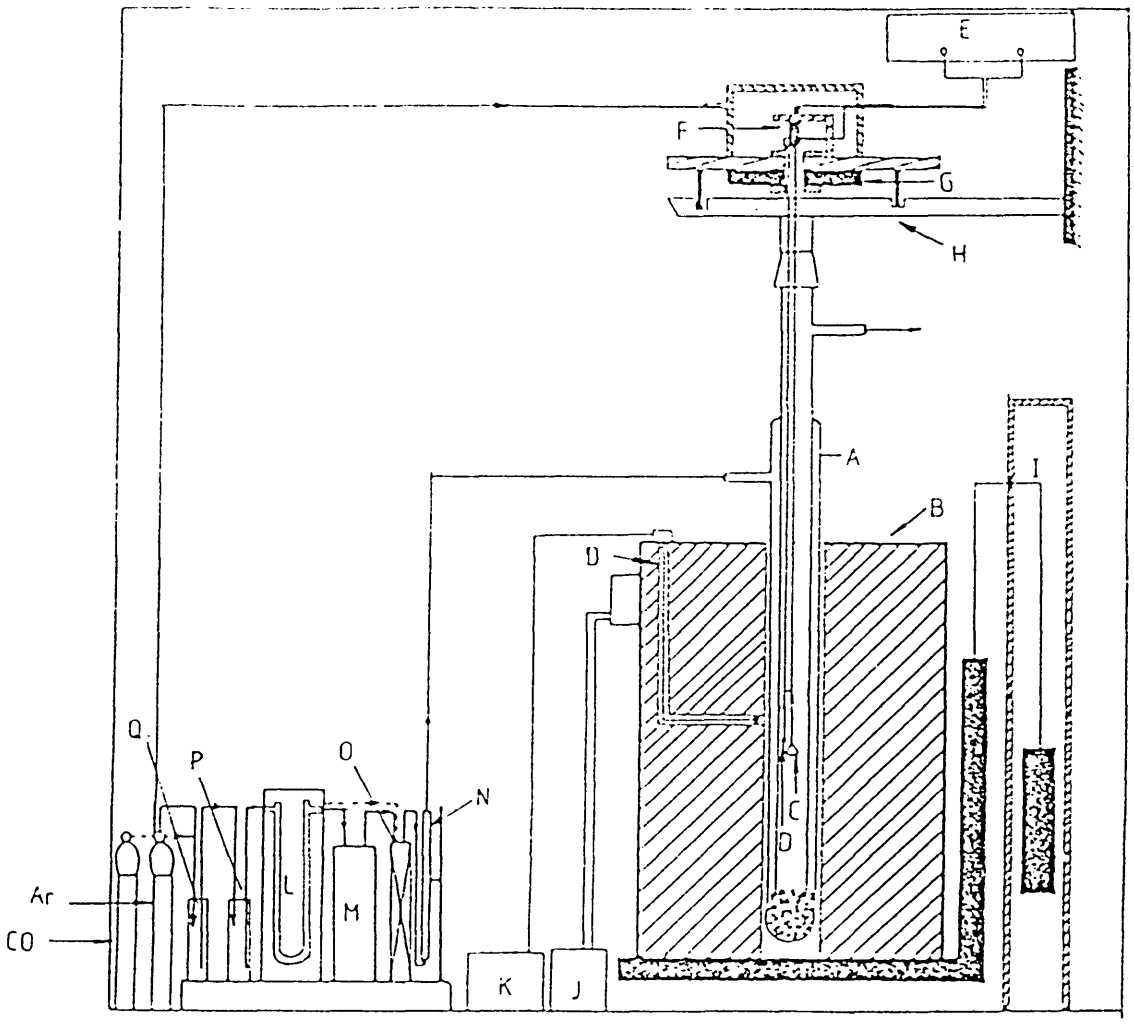


Figure 1. Schematic Diagram of the apparatus for the Carbothermic Reduction of Sulphides.

A - Silica Reactor Tube
B - Resistance Heating Fce
C - Pan
D - Pt-Pt-13.5% Rh Th.couple.
E - Chart Recorder
F - Load Cell
G - Water Cooled Platform
H - Suspended Support
I - Counter Balance Platform.
J - Power Supply
K - Eurotherm
L - Flowmeter
M - Oxygen Removing FCE
N - Rotameter
O - Mixing Tower
P - Soda Asbestos Tower
Q - Magnesium Percholorate Tower.

also maintained through the load cell assembly in order to avoid the entry of hot rising currents of argon and the product gas into the load cell assembly. All these protective measures were taken in order to harness the best operation of load cell and to avoid disruption in its operation because of the temperature changes.

The silica reaction tube was flushed with a stream of argon. The flow of argon was maintained during the heating of the pellet in order to sweep the product gas away from the reaction tube so that the reverse reaction would not influence the progress of the reaction. The stream of argon before entering the reactor tube was decarburised using soda asbestos (E) dehydrated in the column containing magnesium perchlorate (F) and finally deoxidized using a hot bed of titanium at 950^{o}C (G). The flow was maintained at a constant rate of 150ml/per minute using a di-butyl pthalate manometer (M). A similar technique was used for carbon monoxide. In order to maintain a constant pressure drop between gas cylinder (H) and the reactor tube, in the gas flow train, a tube filled with glass shots was connected in series (I). This technique is often used for mixing gases.

A kanthal wound resistance furnace (J) was used which was seated on a platform operated on a counter balance and a pulley arrangement (P). The furnace temperature and the temperature of the pellet inside the reaction tube was measured using a Pt-Pt-13.5pct Rh thermocouple (K). The power supplied to the furnace was controlled by a eurotherm (L) and an ammeter. The furnace had a constant temperature zone of 4cms between 750^{o}C to 1100^{o}C. The error involved in the measurement of the temperature was $\pm$ 10^{o}C. In order to monitor the isolated conditions maintained during the reaction the millivolt output from the furnace was fed to the second channel of the chart recorder.

To start the reaction, the furnace was raised in order to bring the sample into the constant temperature zone. Any weight change occuring during the reaction was monitored on the chart recorder. The error involved in the measurement was ± 0.001 gm. The completion of the reaction was anticipated when the pen of the chart recorder did not show any change over a fairly long duration of time. An approximate estimate of possible weight change was also made by considering the expected chemical mass balance in any particular reaction and once this stage was achieved the furnace was lowered and the sample was allowed to cool in a flowing stream of argon while the outside of the reaction tube was cooled by air. The weight of the pellet before and after the reaction was measured using an analytical balance and it was always found that the two results of the weight changes were in very good agreement.

After the reduction a representative part of the sample was used for X-ray diffraction analysis in order to identify the phases. A Guinier Focussing Camera was used for the diffraction analysis. The other half of the pellet was used for optical and the electron microscopic examination to investigate the morphological and structural changes. Most of the optical microscopic studies were carried out using the Reichert Microscope employing both the bright and dark fields. In order to understand the intimate details of the phase changes, polarized light was frequently used. The morphological studies related to the phase changes were carried out on the T200 Scanning Electron Microscope where both the back scattered and the secondary electron emission techniques were used. The instrument was also capable of Energy Dispersive X-ray (EDX) analysis which was used as a tool for qualitative and semiquantitative analysis. The latter was performed by calibrating the peak heights of the elements with their relative amounts in their respective compounds.

All elements with atomic numbers greater than sodium in the Element Periodic Table could be analysed using EDX technique with the T200 microscope.

Elemental mapping and Electron Microprobe analyses were carried out on the JEOL Scanning Microscope 35 particularly for the pyrrhotite and chalcopyrite minerals. Using Elemental Mapping Techniques, the distribution of a particular element on a specific area could be determined and using EPMA technique the precise composition was established. This microscope alike T200, had limitations in the analysis of lighter elements of the periodic table. Therefore, no estimates were made on the relative amount of oxygen and carbon in the system. The amount of oxygen was computed by difference knowing the percentage of the heavier elements.

Using mass balance analysis, the phase analysis based on X-ray diffraction and the microscopic analysis it was possible to derive the path of the reaction during the reduction of metal sulphide.

4.A.

(ii) Kinetic Studies with Controlled Atmospheric Conditions.

The apparatus used for the kinetic studies of the carbothermic reduction of sulphides is shown in figure (4.2) where a manostat was used to control the atmospheric pressure in the silica reaction tube. Inside the silica reaction tube, an arrangement of the saffil insulators and an alumina tube was made to heat the pellet in a graphite crucible. The isotherm was measured using Pt-Pt-30pct Rh thermocouple contacted at the bottom of the crucible. The whole system was made leak proof. The cylindrical pellet was dropped in the graphite crucible using a magnet and a push rod. The reaction

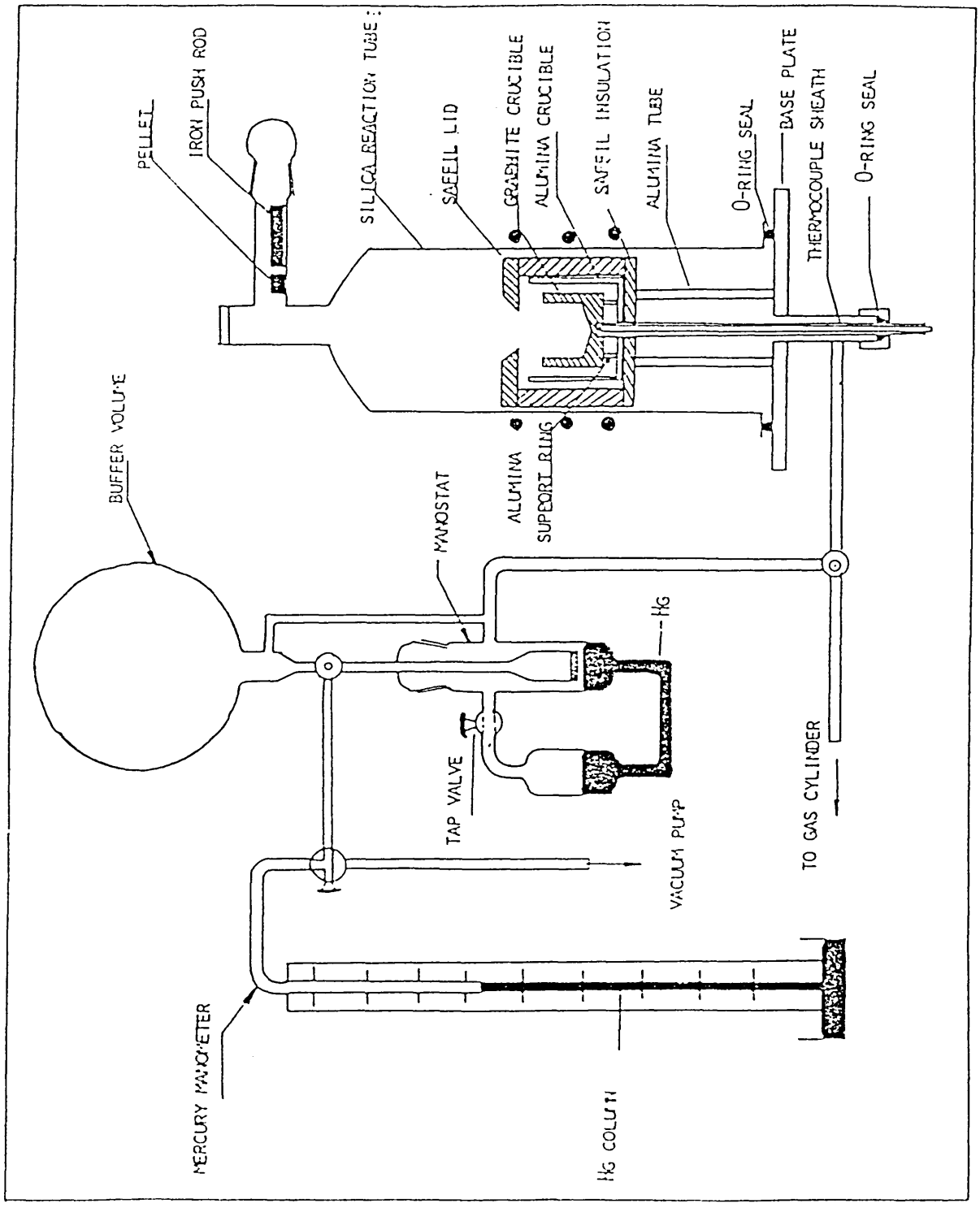


Fig (4.2) Experimental set up for the controlled atmosphere reduction of sulphides.

tube was heated with radio frequency coil, since a graphite susceptor was used, the sample and the crucible temperature could be controlled very efficiently using a potentiometer.

The reaction tube was evacuated before the experiment and then a desired pressure was maintained after introducing the gas. The pressure in the reaction tube was measured using a mercury manometer. Once the pressure of half an atmosphere was maintained, the system was isolated from the gas cylinder. During the course of reduction any gas generated in the closed system would increase the pressure and thus using a Cartesian manostat a constant pressure was maintained as any extra gas was allowed to leave the system. It is evident from the nature of the experiment that at the end of the experiment, the total pressure would comprise the partial pressures of the starting gas and the product gas.

Using this design, the system can be studied under the influence of some back reaction. The progress of the reaction was monitored with the mercury manometer where the pressure change was recorded. The volume of gas evolved was known from the pressure changes and to understand the kinetics of reaction at a certain time interval the pressure change was complete, the power of the radio frequency induction furnace was turned down and the sample was allowed to cool inside the reaction tube. At the beginning and at the end of reduction sample weight was measured using analytical balance. The weight change according to the pressure change, was in very good agreement with that determined by weighing. The sample after reduction was studied using X-ray diffraction and microscopic analysis discussed earlier in the section 4.A. (i)

4.B. Synthesis of Sulphides.

Technical grade cupric sulphide containing 25 pct amorphous sulphur was first washed with carbon disulphide solution. The washing was carried out in a batch until all the sulphur was removed. To reuse the carbon disulphide, the solution loaded with sulphur was boiled on the waterbath at $50^{o}C$ and the vapor of carbon disulphide was passed through a condenser to collect the liquid. The sulphur produced in the process was very crystalline and it was used for the synthesis of other sulphides. A known weight of washed cupric sulphide was taken and it was oxidized in air. The residue was treated with a known strength of dil. H_2SO_4. The residue was digested and it was then diluted to 200ml. About 5ml of this solution was further diluted to 50ml and this solution was used for atomic absorption spectrometric analysis from which the amount of copper was estimated. Part of the residue was used for X-ray diffraction anaysis from which it was confirmed the burnt residue was cupric oxide and the amount of copper analysed was in agreement with the amount of copper in washed cupric sulphide. The whole sequence of analysis showed that the washing treatment yielded a pure cupric sulphide free of amorphous sulphur. To verify this further, the washed sample was rapidly heat treated in an inert atmosphere and the weight loss was recorded. The weight loss recorded gave a value of 99.5 pct of that expected for the conversion of cupric sulphide to cuprous sulphide. The phase analysis after the heat-treatment showed the sulphide was pure $Cu_{2-x}S$ where $x = 0.03$ to 0.17 Cuprous sulphide was made by distilling off the sulphur of cupric sulphide in an inert atmosphere .

For the synthesis of pyrrhotite, carbonyl iron of 99.9 pct purity was first dried in a flowing stream of hydrogen at 400°C and then the stoichiometric amount of the metal was taken and mixed with stoichiometric amount of spec pure crystalline sulphur. The cylindrical pellets of this mixture was kept in a silica tube which was evacuated and flushed with argon several times to remove oxygen and finally the tube was evacuated and sealed off. The silica tube was then placed in a muffle furnace at room temperature and the furnace was slowly heated to 250°C at a rate of 1°C per minute (ie 30°C per half an hour) to ensure that the sample had reacted. The reaction between iron and sulphur is very exothermic and hence a careful heat treatment cycle was required to avoid any explosion. Afterwards the temperature was raised at a rate of 100°C per hour up to 1000°C. The sample was left for homogenization for about 15 hours and the temperature was lowered to 500°C by switching the power off. The sample was then quenched in an ice bath. For the confirmation of the phase, the sample was analysed using the X-ray diffraction technique. In the sample there was only pyrrhotite ($Fe_{1-x}S$) with no troilite (FeS). To make troilite a slight excess of iron was used because from the Fe-Sulphur phase diagram, troilite is unstable in the absence of iron where the prevalent sulphide is pyrrhotite.

Nickel sulphide (NiS_{1+X}) was synthesised by reducing NiO powder in hydrogen to metallic Ni and mixing Ni powder with spec pure sulphur. The aformentioned sequence was followed to synthesise the sulphide. In order to make chalcopyrite (tetragonal) the identical process was used except the mixture was made up of Cu_2S, sulphur and metallic iron. This particular mixture was chosen in order to avoid explosions. Mixtures of metallic copper and iron with sulphur were heat-treated but resulted in explosions. Chalcopyrite can also be synthesised using CuS and FeS but a similar problem was faced. The advantage in using Cu_2S, Fe and sulphur mixture

was that the sulphur vapor pressure never increased rapidly because of the presence of metallic iron which immediately converted into FeS and at that stage there was still sulphur left which could react with the Cu_2S - FeS mixture to produce chalcopyrite. During the synthesis of chalcopyrite it was realised the quenching temperature had a great influence on the structure of chalcopyrite. Therefore to obtain tetragonal chalcopyrite, the sample was held at 900^oC for 15 hours and then the temperature was brought down to 500^oC at which it was held for 6 hours followed by a furnace cooling to room temperature . This way the tetragonal chalcopyrite was synthesised.

For all the experiments, no control of particle size was exercised. The particle size in most of the experiments of the reduction of sulphides was -104μ to +50μ. In the reduction experiments, it was realised that liquid phases formed and hence the effect of particle size had a negligible effect on the subsequent rate of reduction.

— — — — — — — —

Chapter 5.

5.A. Reduction of Copper Sulphide Minerals:

(i). Results

The reduction of sulphide minerals is based on the thermodynamic principles presented in Chapter 1. The reduction of both cupric and cuprous sulphide minerals was carried out with stoichiometric additions of lime and carbon at different temperatures. During the reduction of cupric sulphides, distillation of sulphur was observed which was attributed to the decomposition of cupric sulphide to the stable cuprous sulphide. On the basis of mass balance analysis, the rate of reduction curves were plotted and in these rate curves for cupric sulphide, an allowance is made for the distillation of pure sulphur vapour. From the weight loss data calculated on the basis of the following chemical mass balance equation the percentage reduction was calculated:

$$Cu_2S(s) + CaO(s) + C(gr) = 2Cu(s) + CaS(s) + CO(g) \quad (5.1)$$

Thus the percentage reduction 'R' $= \frac{\Delta W}{W} \times \frac{100}{y}$ (5.2)

where ΔW = weight change at any time 't'
W = initial weight of sample
y = theoretical percentage weight loss calculated from equation (5.1).

The mass balance analysis together with X-ray diffraction analysis data for the carbothermic reduction of copper sulphides with graphite are arranged in Table 5A.1. The rate of reduction curves for copper sulphides are shown in fig (5A.1) and (5A.2) from which it is evident that the rate

Table 5A.1: Summary of data on the Carbothermic Reduction of Copper Sulphides.

MIXTURE COMPOSITION	TEMPERA-TURE °C	MASS BALANCE		ATMOS-PHERE	X-ray diffraction analysis								
		Pct wt Loss	Pct Reduc-tion		$Cu_{2-x}S$	CaO	CuS	CaS	$Cu_{2-x}O$	CuO	Gr	Cu	$CaSO_4$
1) CuS:CaO:C=1:1:2	1000°C	15·65*	95·05	Argon	W	W	-	VS	-	-	W	S	-
2) Cu_2S:CaO:C=1:1:2	1000°C	8·90	75·96	Argon	M	S	-	VS	VW	-	VW	S	-
3) CuS:CaO:C=1:1:2 second stage	1000°C	9·14*	36·7	Argon	M	VS	-	S	VW	VW	W	WM	-
3a) CuS:CaO:C=1:1:2 first stage	1000°C	4·84*	-	Argon	M	VS	-	M	W	VW	WM	-	-
4) Cu_2S:CaO:C=1:1:2 Partial Red	1000°C	4.54	38.7	Argon	M	VS	-	VS	W	VW	M	WM	-
5) Cu_2S:CaO=1:1	1000°C	5·35	24·62	Argon	S	VS	-	VVW	M	VVW	-	WM	W
6) Cu_2S:CaO:C=1:1:2+	1000°C	9·00	76·85	Argon	W	W	-	VS	-	-	VVW	MS	-
7) CuS	1000°C	16·07	95·90	Argon	MS	-	-	-	-	-	-	-	-
8) CuS:CaO=1:1	1000°C	10·64*	-	Argon	M	S	-	VS	W	VW	-	-	-
9) CuS:CaO:C=1:1:2	950°C	13·82*	86·5	Argon	M	S	-	VS	VVW	-	W	M	-
10) CuS:CaO:C=1:1:2	900°C	11·42*	37·00	Argon	M	VS	-	VS	VW	-	-	W	W
11) Cu_2S:CuO=1:1	100°C	12·42	46·30	Argon	VS	-	-	-	Med	WM	-	VS	-
12) CuS:Cu_2O=1:1	1000°C	13·43*	50·05	Argon	M	-	-	-	WM	WM	-	VS	-
11b) (11)+Graphite	1000°C	1·726	-	Argon	VS	-	-	-	WM	WM	M	VS	-
12b) (12)+Graphite	1000°C	0·57	-	Argon	M	-	-	-	WM	WM	W	VS	-
11c) (11b)+CaO+Gr	1000°C	4·63	-	Argon	-	M	-	M	-	-	WM	VS	-
12c) (12b)+CaO+Gr	1000°C	6·33	-	Argon	-	M	-	S	-	-	-	VS	-
13) CuS:CaO:C = 1:1· 55:2	950°C	14·62*	72·6	Argon	W	M	-	VS	VVW	-	W	S	-
	900°C	7·52*	38·3	Argon	M	VS	-	S	W	VW	WM	WM	W
14) CuS:CaO:C = 1:2:2	900°C	4·24	20·0	Argon	M	VS	-	M	W	W	WM	VW	WM
	950°C	15·28*	94·7	Argon	VW	WM	-	VW	-	-	W	MS	-
15) CuS:CaO:C=1:1:3	1000°C	12·32	82·5	Argon	VW	W	-	VS	-	-	W	VS	-

Table 5A.1: Summary of data on the Carbothermic Reduction of Copper Sulphides. Continued....

MIXTURE COMPOSITION	TEMPERA -TURE °C	MASS BALANCE		ATMOS -PHERE	X-ray diffraction analysis								
		Pct wt Loss	Pct Reduc- tion		$Cu_{2-x}S$	CaO	CuS	CaS	$Cu_{2-x}O$	CuO	Gr	Cu	$CaSO_4$
16) CuS:CaO:C=1:2:3	1000°C	10·61	92·3	Argon	VW	M	-	VS	-	-	W	VS	-
17) CuS:CaO:C=1:2:3	850°C	4·45	38·7	Argon	M	S	-	VS	VW	VW	-	WM	-
18) Cu_2S:CaO:C=1:2:3	1000°C	8·25	90·05	Argon	VVW	M	-	VS	-	-	WM	VS	-

* Incorporates sulphur weight loss

+ Preheat treated Mixtures

VS - Very strong
MS - Medium strong
S - Strong
M - Medium
WM - Weak medium
W - Weak
VW - Very weak
VVW - Very very weak

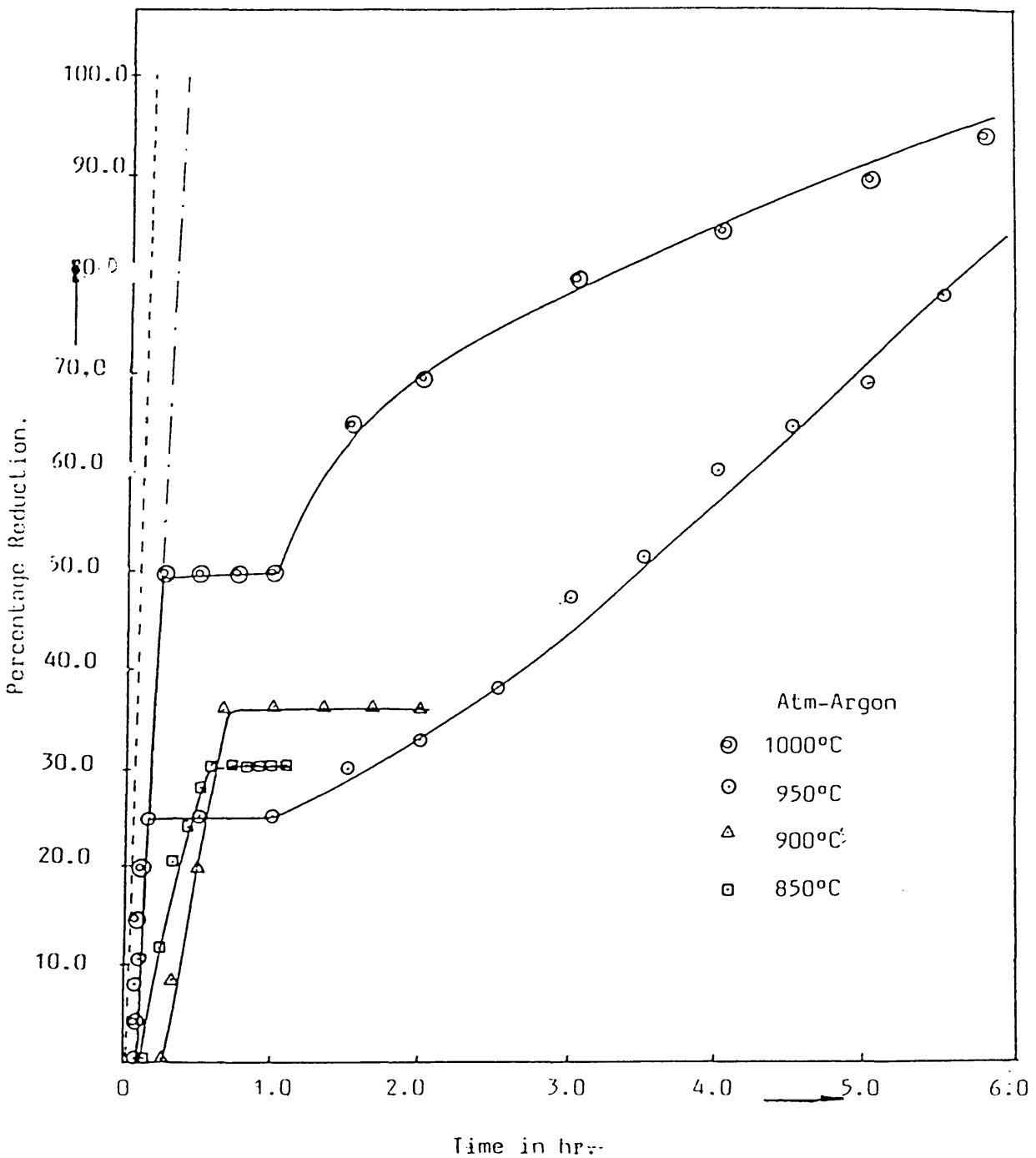


Fig (5A.1) Rate of reduction of CuS with graphite in presence of lime at different temperatures (CuS:CaO:C : = 1:1:2)
--- CuO Reduction ------Cu_2O reduction with graphite in argon atmospheres.

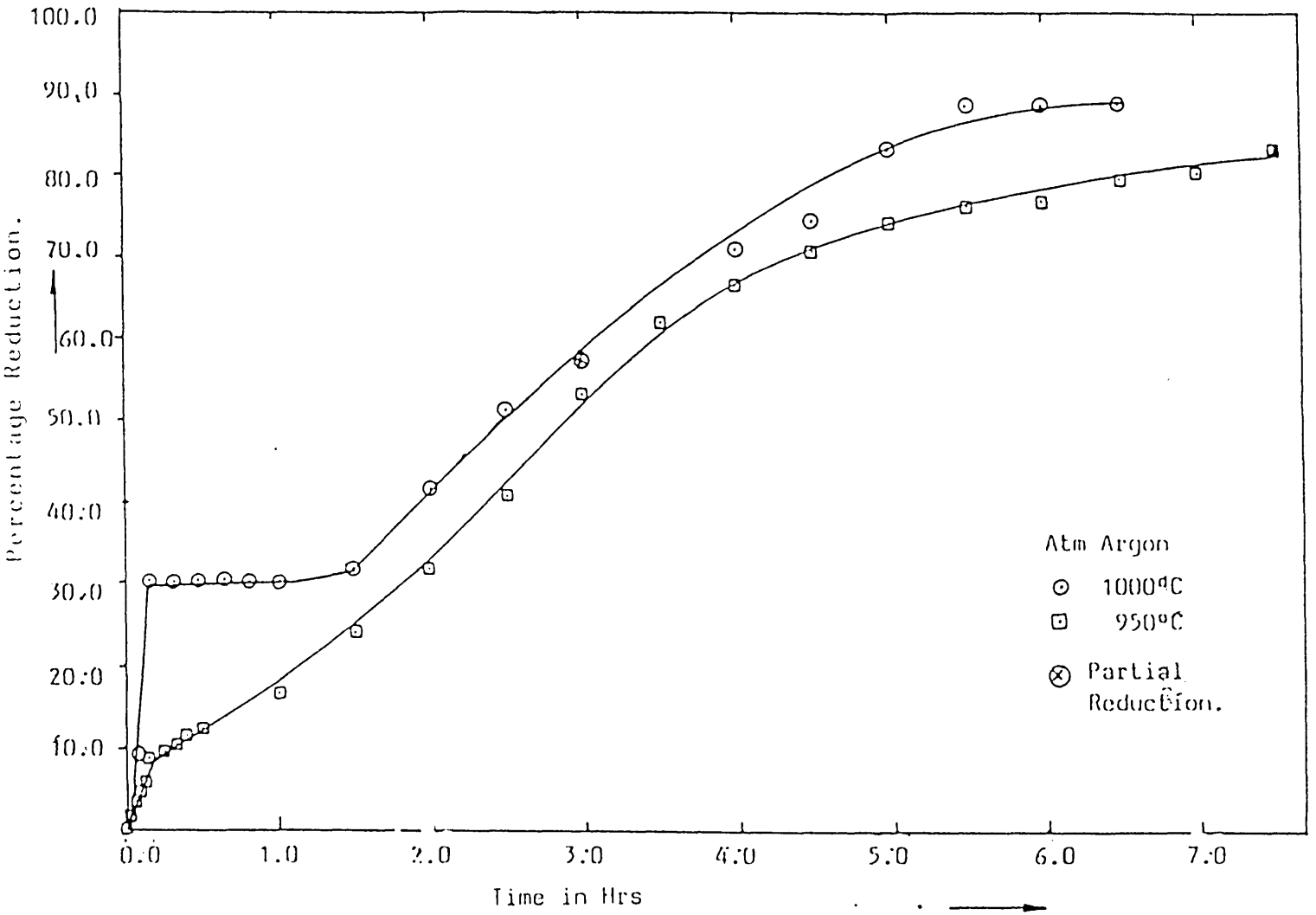


Fig (5A.2)Rate of reduction of Cu_2S with graphite in presence of lime at different temperatures (Cu_2S:CaO:C = 1:1:2).

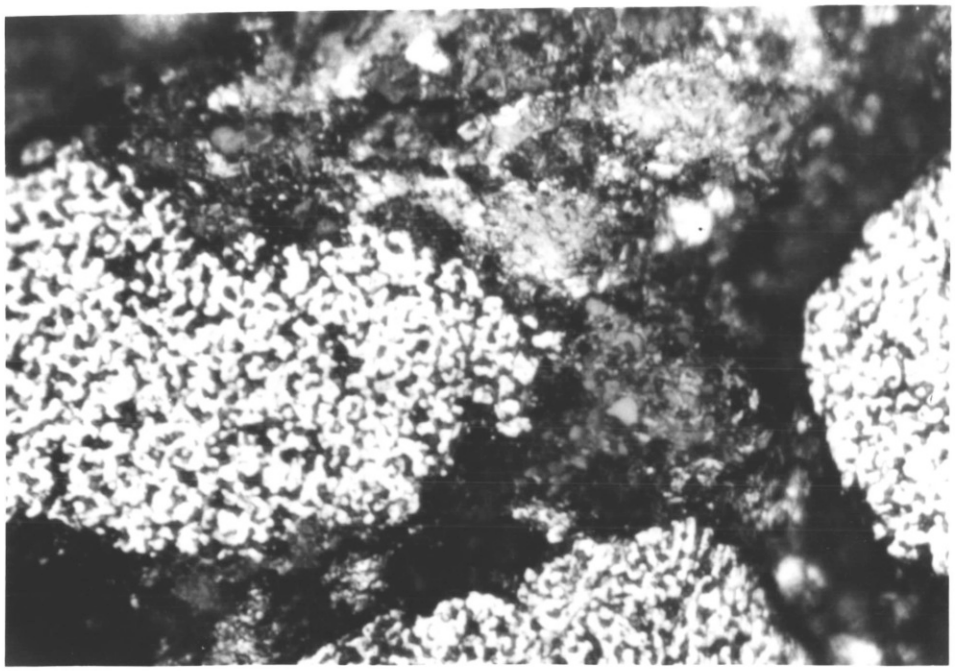
of reduction increases with temperature but the reaction appears to follow a complicated route. A momentary cessation of reaction takes place at temperatures above 950^{o}C whereas below this temperature, reaction ceases completely. To understand the mechanism of reduction of copper sulphides the reaction sequence was stopped at several stages at 1000^{o}C and the partially reduced pellets were examined using optical microscopy and X-ray diffraction. For cupric sulphides, it is evident that the relative amount of oxides of copper varies depending upon the extent of reaction but it appears that CuO formation is preferred to Cu_2O; a situation which is unexpected thermodynamically, see Table 5A.1. Further evidence of the coexistence of these two copper oxides was also found during the partial reduction of cuprous sulphide at 1000^{o}C. However, the optical microscopic analysis carried out on the partially reduced pellets of cupric sulphide clearly shows the decomposed cupric sulphide particles see plate 5A.1(a). In the subsequent stage, a liquid phase is present which is surrounded either by well grown copper nuclei or by a copper of different morphology see plate 5A.1(c). The morphology of the product phases shows the presence of a liquid whose composition and thermodynamic properties are not known at this stage. The cellular network of copper and the liquid matte shown in plates 5A.1(b) and (c) is separated by another phase which might have isolated the reactants during the course reaction.

The microscopic analyses, the presence of cupric oxide and the liquid phase demanded further investigation to diagnose the reaction mechanism. In the initial stage of this diagnosis, pure cupric sulphide was heated in a flowing argon stream at 1000^{o}C. The sulphur distillation was observed during the course of heat treatment and X-ray

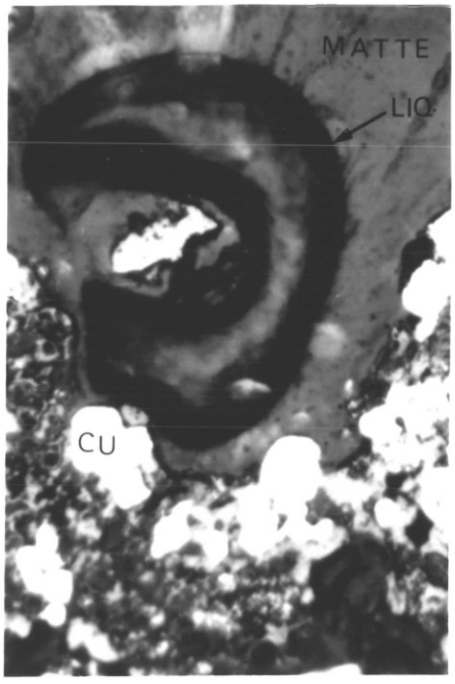
diffraction analysis of the product showed the presence of non-stoichiometric cuprous sulphide which is the only thermodynamically expected phase. Apart from this evidence of liquid phase was observed which was subsequently confirmed from the copper and sulphur phase diagram see fig (2.1a). The presence of liquid according to this phase diagram is only possible at a partial pressure of sulphur P_{S_2} > 1.0 atm, which must have prevailed during the decomposition of CuS. Thermodynamically a partial pressure of 1 atmosphere is possible at 500°C and this pressure increases exponentially with increasing temperature.

In the next stage of investigation a 1:1 stoichiometric mixtures of CuS and Cu_2S with lime were prepared and heat treated in flowing stream of argon at 1000°C. In both cases, a weight loss was observed and from the X-ray diffraction analysis, it is obvious that a relatively larger quantity of copper oxide was formed as a result of the exchange reaction. The weight loss observed in the case of Cu_2S must be associated with copper deposition which is only possible when SO_2 is liberated from the mixture. The other significant information obtained from the phase analysis is the presence of calcium sulphate and almost insignificant quantity of CaS which means that the formation of $CaSO_4$ is preferred to CaS which is only possible under sufficiently oxidizing conditions see Table 5A.2. This must have occured during the experiment and is indicated from the evidence that a sufficient quantity of Cu_2O remains at the end of 18 hours heat-treatment. A physical examination of this pellet showed that metallic copper was deposited at the gas-solid interface ie on those areas from which SO_2 could easily escape into the atmosphere.

PLATE 5A.1



(a) x 435



b x 1000



c x 1000

Plate 5A.1 Reduction of CuS with lime and graphite at 1000°C. (S:O:C = 1:1:2).

(a) Decomposition of CuS particle
(b) Liquid Matte and Copper
(c) Matte surrounded by CaS after cooling the sample

However, neither metallic copper nor $CaSO_4$ was observed during the heat tratment of cupric sulphide with lime at 1000^oC. The evidence of liquid phase formation was confirmed in both of these heat treatment experiments, which indicates that the exchange reaction does take place during the course of heat treatment and the liquefaction process commences later. It appears in the case of cupric sulphide heat treatment the liquefaction begins because of CuS decomposition. A complete disappearances of oxides and sulphate was observed when the preheat treated pellet of Cu_2S with CaO was reduced with graphite. But neither of these experiments throw any light on the presence of the higher oxide of copper in preference to Cu_2O nor does it give an explanation for the presence of sulphate.

In order to characterise the nature of the liquid formed during the course of sulphide reduction mixtures of Cu_2S - CuO and CuS - Cu_2O in 1:1 stoichiometric ratio were prepared and heat treated at 1000^oC in an argon atmosphere, see Table 5A.2. Stoichiometrically , a half mole of SO_2 would be liberated to generate copper which would correspond to 26.83pct loss in weight of the pellet. But experimental observations on the heat-treatment of these pellets, which was carried out for 3 hours, show that at the end of the reaction (as indicated by no further weight change on the chart recorder) a significant amount of oxide is left see plates (5A.3-A.5) . Also in the latter mixtures although there was no CuO at the beginning of reaction it was observed after the heat treatment see table 5.1. Neither a significant weight loss nor change in the relative intensities of the oxides of copper were observed after these preheated oxysulphide mixtures were reduced with graphite. But addition of lime and graphite resulted in the complete disappearance of both oxides and sulphide. The percentage weight loss vs time curves for these experiments are shown in fig (5A.3) and (5A.4)., and the two rate curves are identical to the rate curves for Cu_2S reduction. The most

striking features of these two heat treatment series are that there was evidence of a liquid phase and that the oxides precipitates from this liquid. Thus there is a thermodynamic barrier associated with the reduction of oxides in this liquid. These observations indicate that the liquid present during the course of reduction is a ternary liquid belonging to the Cu-S-O system.

At this stage it was considered necessary to characterise this ternary liquid. The characterisation of this liquid was carried out by heat-treating several stoichiometric mixtures of copper sulphides and copper oxides at 1000^{o}C in a flowing stream of argon for 3 hours. From the mass balance and X-ray diffraction analysis an isothermal ternary phase diagram was constructed. The mass balance analysis together with the X-ray diffraction results for the heat treatment of oxysulphide mixtures all shown in Table 5A.2 From this ternary diagram at 1000^{o}C, see fig (5A.5),it can be seen that a liquid phase exists along the Cu_2S-Cu_2O pseudo binary section and it is from this liquid that CuO is precipitated upon cooling. Therefore, during the reduction process conditions prevail, such that a liquid phase belonging to the Cu-Cu_2S-CuO ternary system forms and probably plays a very significant role during the course of reduction.

In the literature review covered in Chapter 2 under the heading Cu-S-O equilibrium relationships a several investigations (2.14-2.14) have been reviewed.. From these reviews where the occurrence of a eutectic invariant exists in which the liquid behaves more like a regular solution with repulsive interaction, a higher partial pressure of SO_2 would be expected than that for ideal behaviour. In general eutectic invariants are associated with non-ideal interactions with a positive heat of mixing. From Schmiedl's (2.13) and Kauxmann and Benecke's (2.14) work, the eutectic liquid composition exists at 840^{o}C and N_{Cu_2O} = 0.4, the composition of the invariant phase fields in the phase diagram was established. These two invariant phase fields are (L + Cu + Cu_2S) beginning at N_{n} = 8.5 mole pct and

$(L + Cu + Cu_2O)$ at N_O = 33.3 mole pct. These results determine the nature of the liquid surface within the pseudo binary section. In the ternary diagram the projection of a eutectic invariant is defined by point E. These results are also verified by integrating the Clausius - Clapeyron relationship ie

$$\ln a_i = \frac{\Delta HM_i \ (Tm_i - T)}{RT \ Tm_i} \qquad (5.3)$$

where a_i - Activity of component i in the psuedo binary section.

Tm_i - Melting point of the component i in degree Kelvin

T - Arbitrary temperature in degree Kelvin

ΔHm_i - Enthalpy of fusion of component i in Cal $gm\text{-}mole^{-1}$

R - Gas constant in Cal deg^{-1} $gm\text{-}mole^{-1}$

Using equation (5.3) and the experimentally determined enthalpy of fusion data, the computed eutectic composition is at 20 mole pct Cu_2O and 850°C which disagrees with Kauxmann and Benecke's (2.14) result. Applying Richard's Rule for the estimation of the enthalpy of fusion and using equation (5.3) gives the composition of the eutectic at 845°C and at 60 mole pct Cu_2O. Applying the Richard's Rule for the determination of enthalpy of fusion for Cu_2O it was found that the discrepancy had arisen because of a large deviation of the experimentally determine value $H_m^{Cu_2O}$ from that of the estimated value using Richard's Rule. This pseudo binary eutectic and the invariant $(L + Cu_2S + Cu)$ provide a reason for the difficulty in the measurement of a solubility of oxygen in liquid matte at 1100°C below wt pct O = 0.869 . At this temperature for the given

solubility of oxygen in the liquid in equilibrium with liquid metallic copper and Cu_2S, the pressure of SO_2= 0.27atm. This condition determines an invariant field where at a particular temperature the activities are constant. For determining the activity of oxygen in the system, Schmiedl's results were used in conjunction with the equilibrium defined by equations (2.4) and (2.5) given in Chapter 2. Although the oxygen activities calculated form Schmiedl's result only apply to the invariant (L + Cu + Cu_2S), his results can be used to draw a univariant at different partial pressures of SO_2 for different temperatures which would establish the stability range of the liquid phase existing in this ternary. Using this principle, a univariant has been drawn at P_{SO_2} = 1.0 atm. and is shown in fig (5A.6). This univariant is not shown by Rosenqvist (2.12) and exists between pure Cu_2S and pure Cu. Using the slope of the curve RT $\ln P_{O_2}$ vs $^{1}/_{T}$ in fig (5A.6) the enthalpy change for this invariant is calculated and activity of oxygen in the entire range can be calculated using Morey-Williamson's theorem modified by Darken as shown below:-

$$\left.\frac{d\,(\ln a_k)}{d\,(1/T)}\right|_p = \left(\frac{1}{R}\right) \frac{\begin{vmatrix} N_i^1 & N_i^1 & \Delta H^1 \\ N_i^2 & N_i^2 & \Delta H^2 \\ N_i^3 & N_i^3 & \Delta H^3 \end{vmatrix}}{\begin{vmatrix} N_i^1 & N_i^2 & 1 \\ N_i^2 & N_i^2 & 1 \\ N_i^3 & N_i^3 & 1 \end{vmatrix}} \qquad (5.4)$$

where N_r^p = mole fraction of component (r = i, j, k) in condensed phase (p = 1,2,3).

a_r = activity of component r

ΔH^p = enthalpy of fusion of condensed phase p

T = temperature in degree Kelvin

R = gas constant in cal deg^{-1} gm $mole^{-1}$

p = pressure in atmosphere which is constant

A detailed analysis of this equation (5.4) can be seen in chapter 2 of the Reference no 6.9. The calculation of activities in the various phase fields related to the reduction of copper sulphide will be dealt with in the next section where its importance with respect to reduction of sulphides will be highlighted.

The existence of a liquid phase during the course of reduction of copper sulphide takes place in the following sequence:-

i. the decomposition of cupric sulphide to Cu_2S
ii. the liquefaction of sulphide as a result of disproportionation.
iii (a) the exchange reaction between liquid sulphide and lime
(b) the exchange reaction between solid Cu_2S and CaO
iv. the formation of an oxysulphide liquid
v. the reduction of oxide dissolved in the oxysulphide liquid .

From the rate of reduction curves shown in fig(5A.1) and (5A.2)it is evident that the rates are dramatically different.

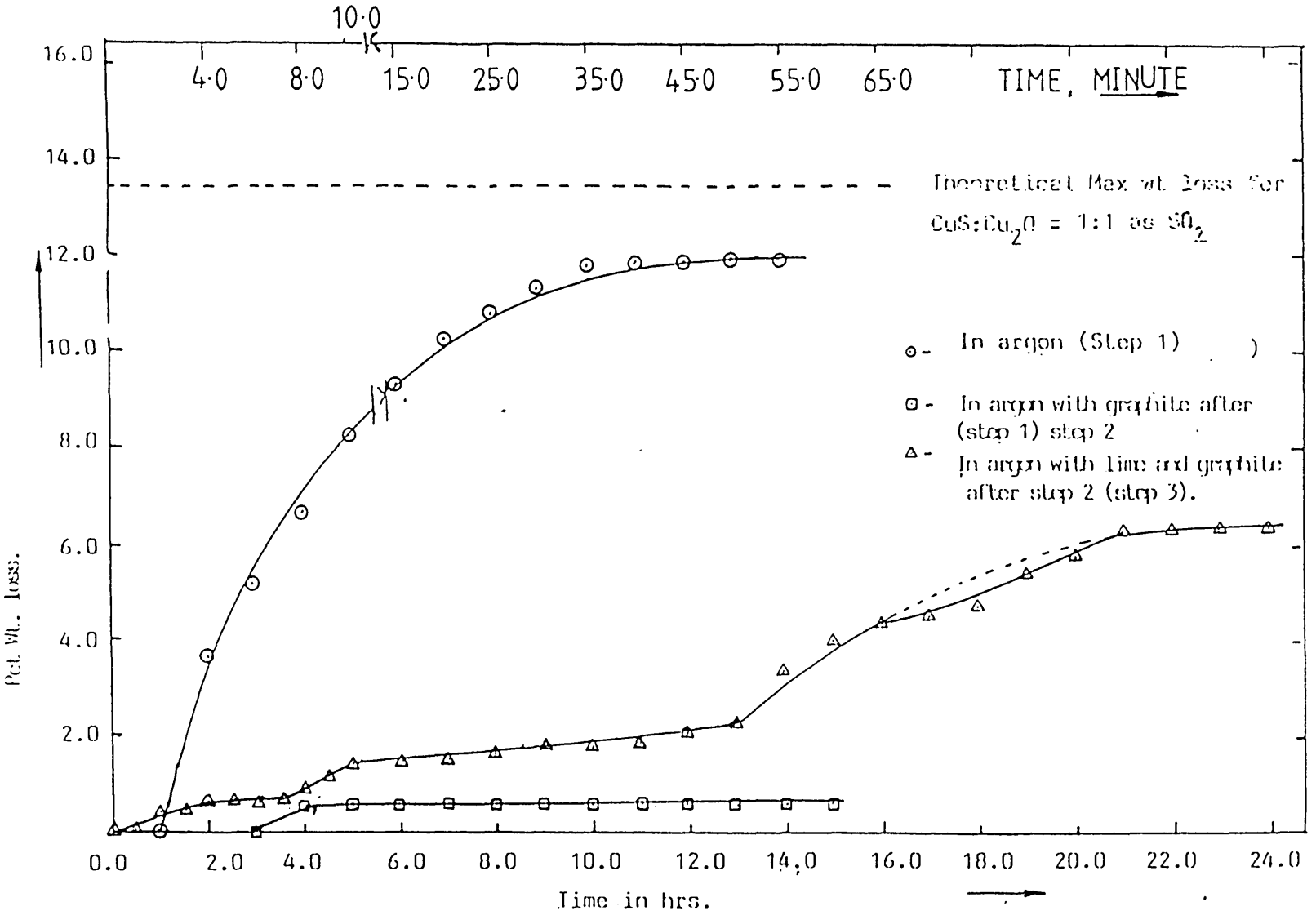


Fig (5A.3) $CuS:Cu_2O$ = 1:1 mixture heat-treated under different conditons at 1000°C in argon atmosphere (150ml/min).

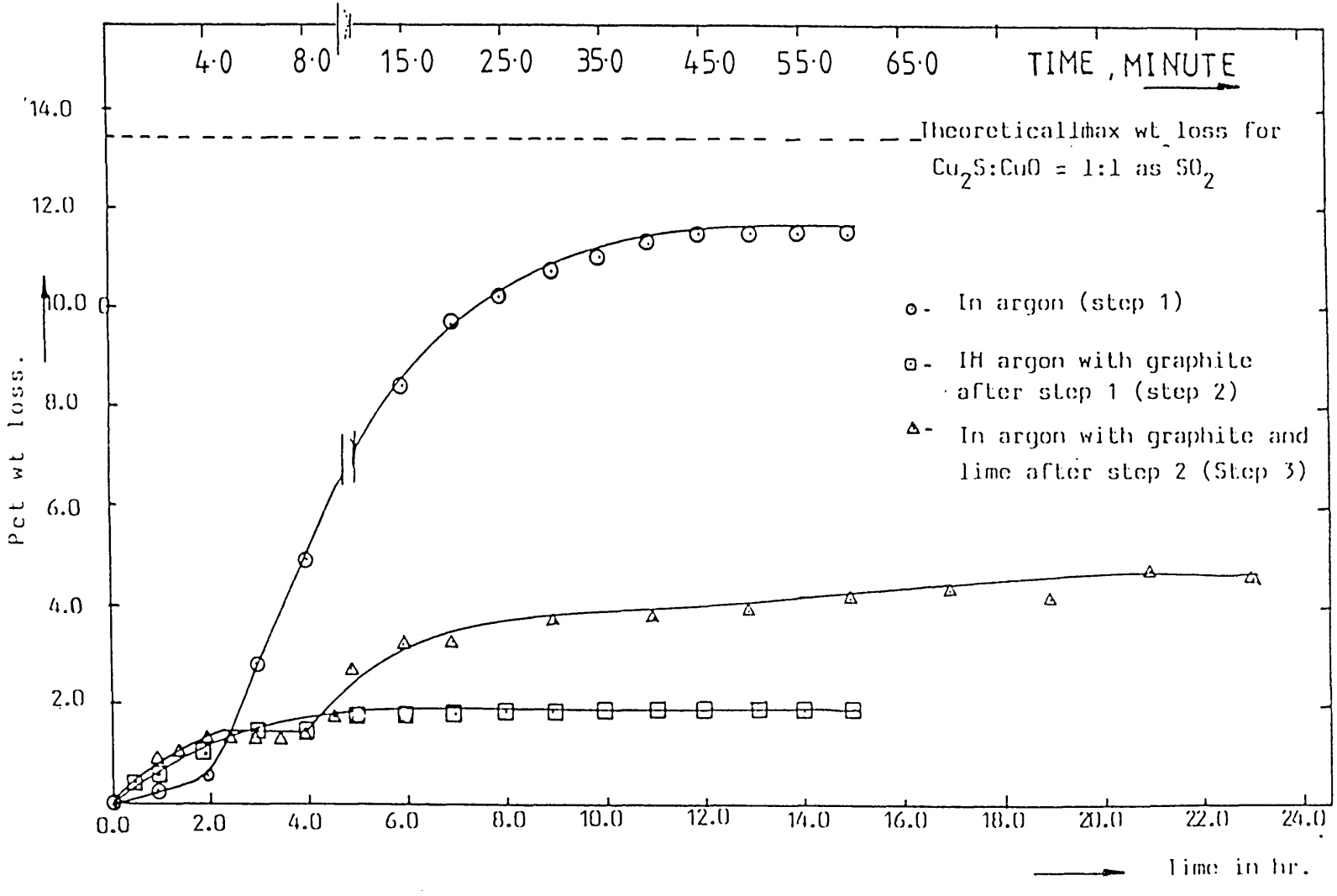
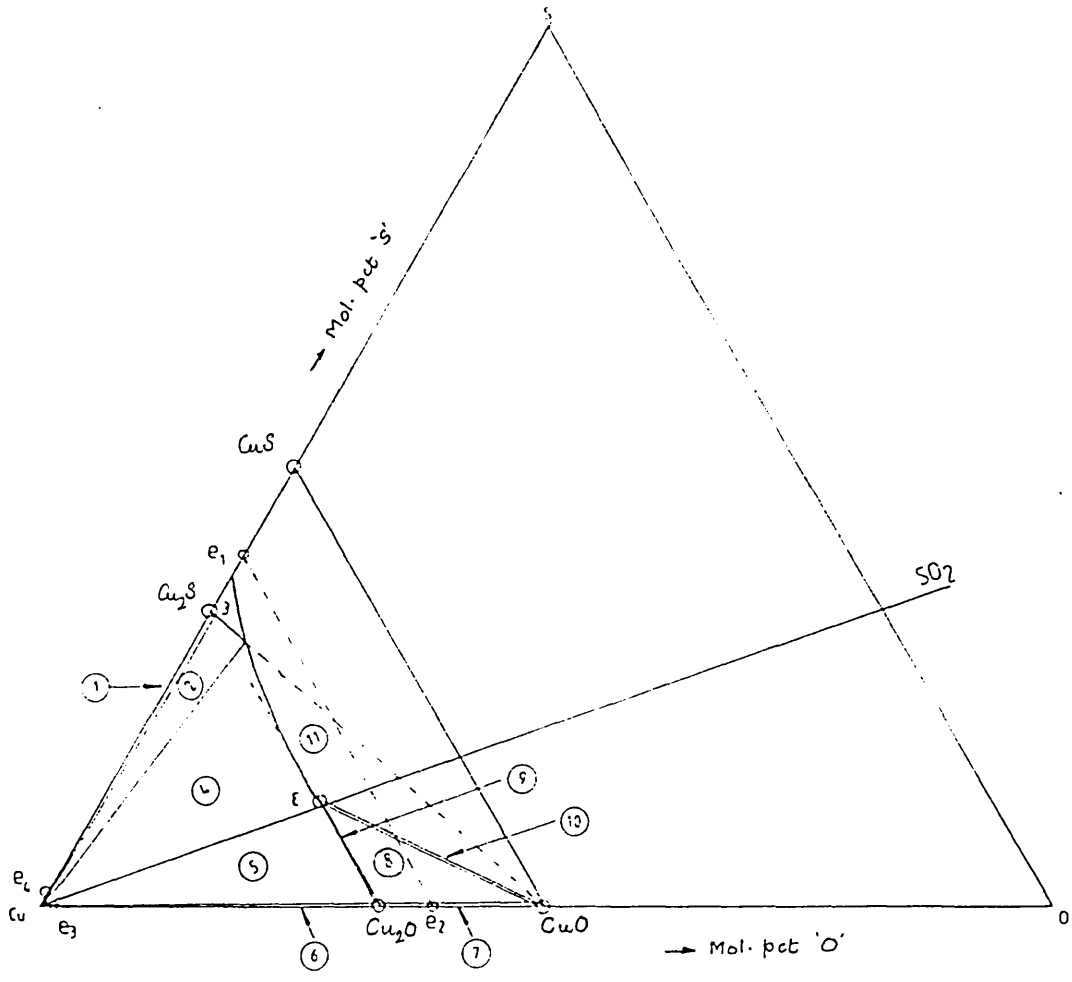


Fig (5A.4) Cu_2S:CaO = 1:1 Mixture heat-treated under different conditions at 1000°C in argon atmosphere (150ml/min).

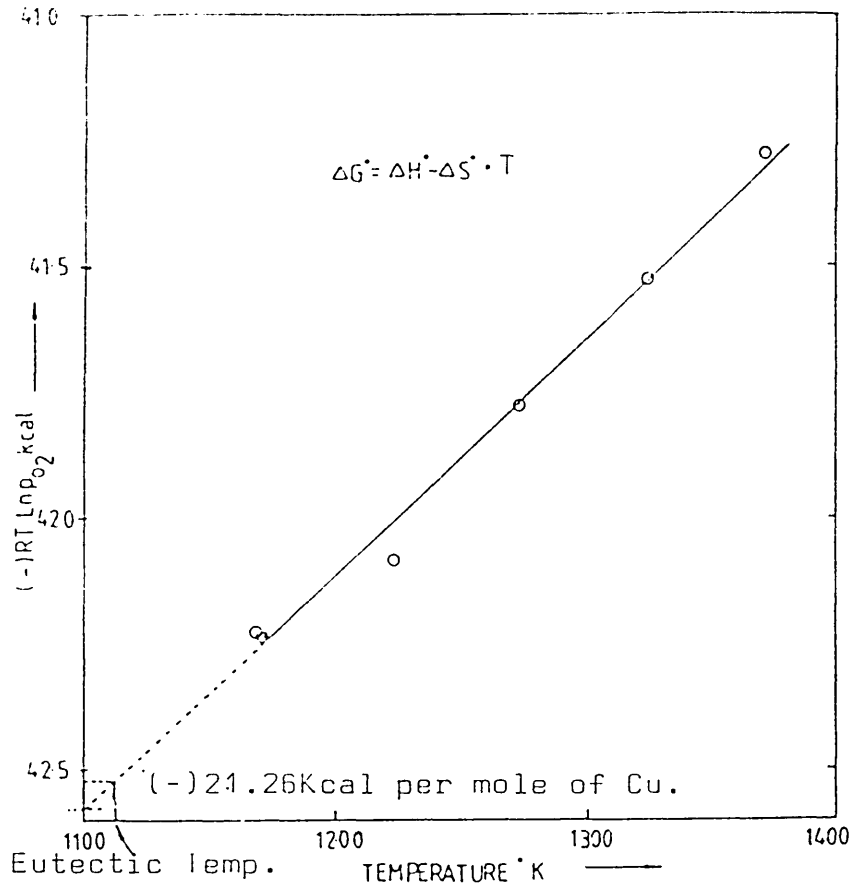
Table 5A.2 Heat-treatment of Oxysulphide Mixtures at 1000°C in Argon.

Mixture Composition	Temperature.	Mass Balance: Pct wt loss	Mass Balance: Pct Red.	Atmosphere	X-ray Diffraction Analyses. Cu	$Cu_{2-x}S$	$Cu_{2-x}O$	CuO	CuS	CaS	CaO	$CaSO_4$
CuO:CuS= = 3:1	1000°C	19.33		Argon	MS	-	VS	-	-			
CuO:CuS = 2:1	1000°C	23.01		Argon	VS	VW	-	-	-			
CuO:CuS = 1:1	1000°C	21.22		Argon	S	S	S	M				
CuO:CuS = 1:2	1000°C	15.67		Argon	W	VS	WM	VW	-			
CuO:CuS = 1:3	1000°C	15.29		Argon	-	MS	W	W	-			
$Cu_2S:Cu_2O$ = 1:2	1000°C	10.01		Argon	VS	VW	S	-	-			
$Cu_2S:Cu_2O$ = 1:1	1000°C	9.76		Argon	VS	W	W	-	-			
Cu_2S:CuO = 1:2	1000°C	17.52		Argon	VS	M	VW	-	-			
Cu_2S:CuO = 1:1	1000°C	12.01		Argon	VS	M	S	WM	-			
Cu_2S:CuO = 1:1:5	1000°C	9.26		Argon	VS	S	WM	WM	-	-	-	-
Cu_2S:CuO = 2:1	1000°C	7.43		Argon	VS	S	WM	WM	-	-	-	-
Cu_2S:CuO = 3:1	1000°C	5.73		Argon	VS	VS	WM	WM	-	-	-	-
Cu_2S:CuO = 1:1	1000°C	4.37		Argon	S	VS	WM	WM	-	-	-	-
Cu_2O:CaS = 4:1	1000°C	11.02	86.29	Argon	VS	VW	S	-	-	-	M	WM
Cu_2S:CaO = 1:1	1000°C	5.35		Argon	WM	S	M	VVW	-	VVW	VS	VW.



1. $Cu + Cu_2S$
2. $L + Cu + Cu_2S$
3. $L + Cu_2S$
4. $L + Cu$
5. $L + Cu + Cu_2O$
6. $Cu + Cu_2O$
7. $CuO + Cu_2O$
8. $L + CuO + Cu_2O$
9. $L + Cu_2O$
10. $L + CuO$
11. Liquid.

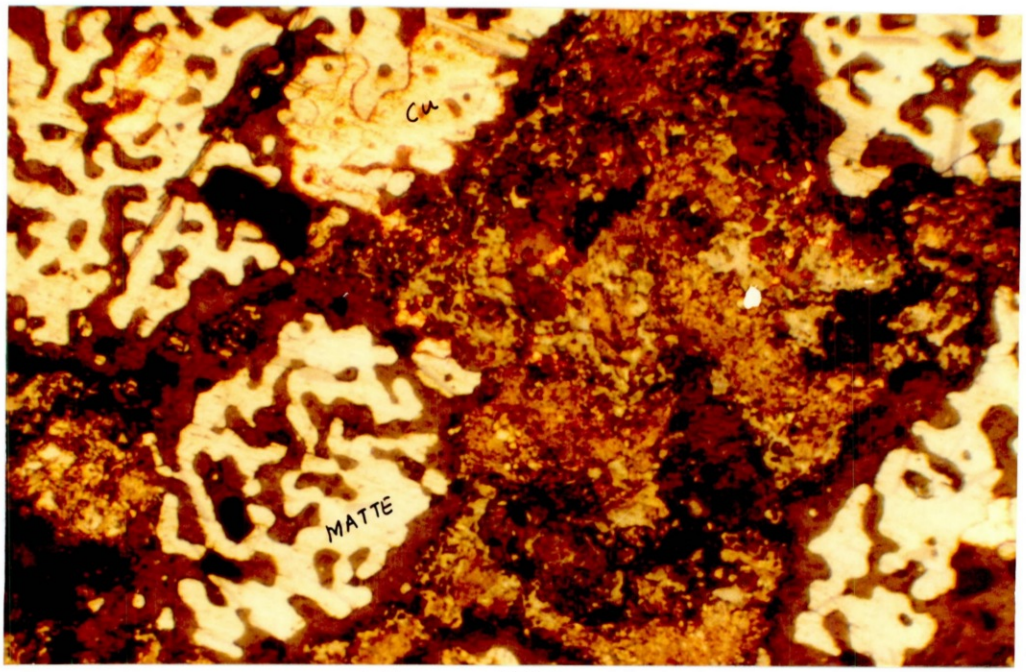
Fig (5A.5) Cu-S-O partial equilibrium ternary diagram at 1000°C. The e's are respective binary eutectics.



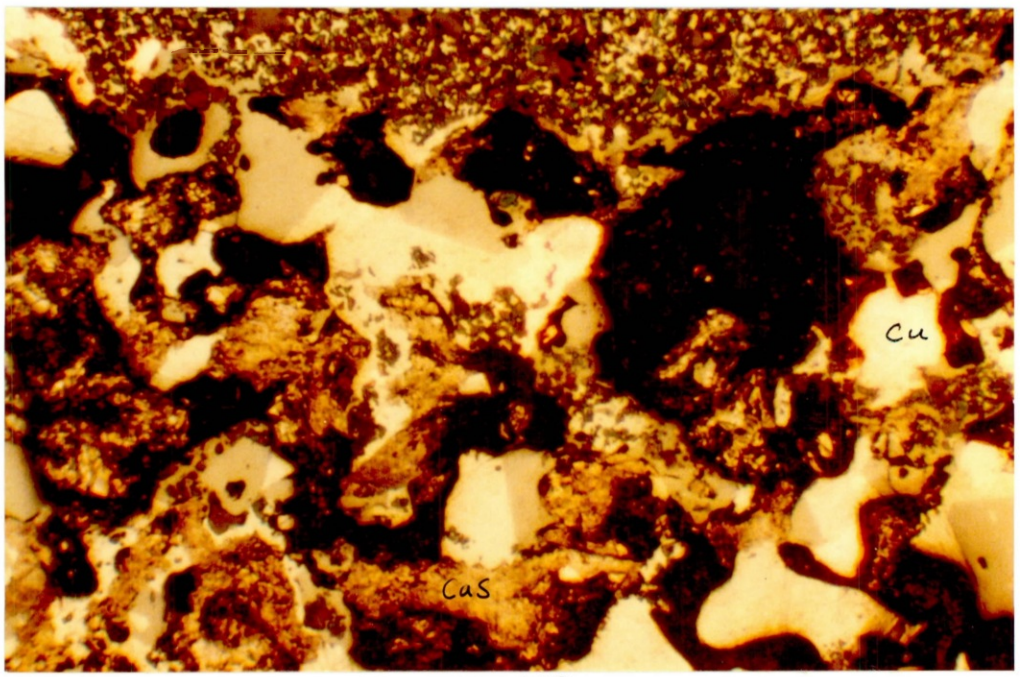
Fig(5A.6): $RT\ln P_{O_2}$ vs Temperature relationship for the oxysulphide liquid in the Cu-S-U system

$$Cu_2S(l) + 2\ Cu_2O(s) = 6Cu(l) + SO_2(g).$$

PLATE 5A.2



(a) X430



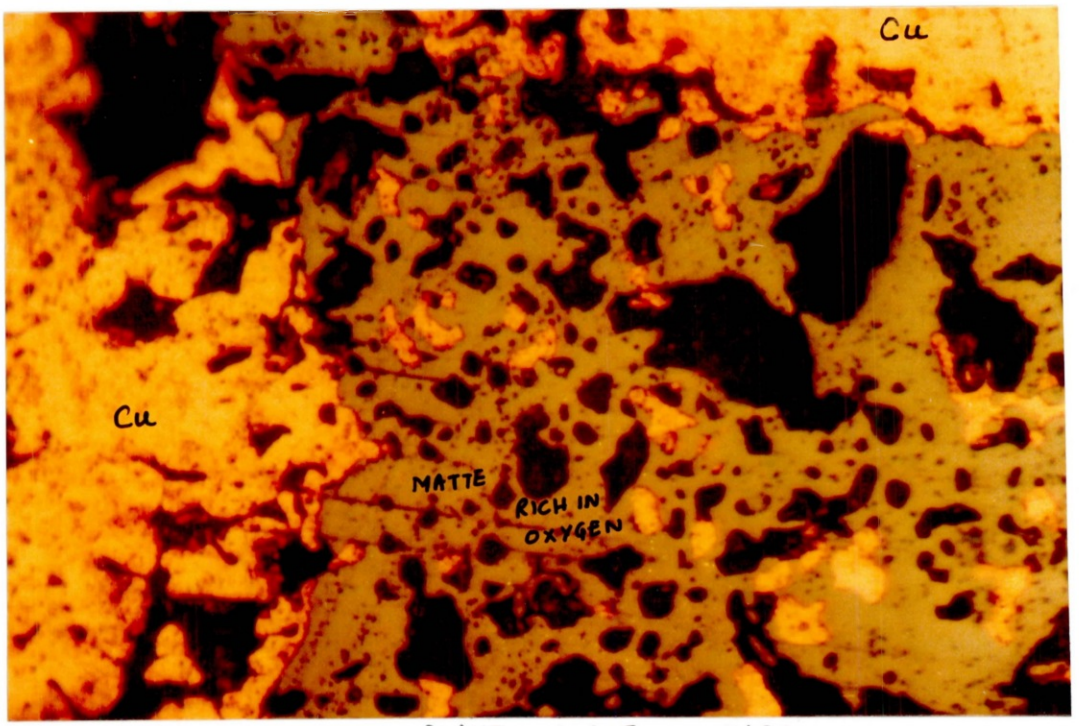
(b) X430

Plate 5A.2: Reduction of Cu_2S with lime and graphite at 1000 C(S:O:C=1:1:2)

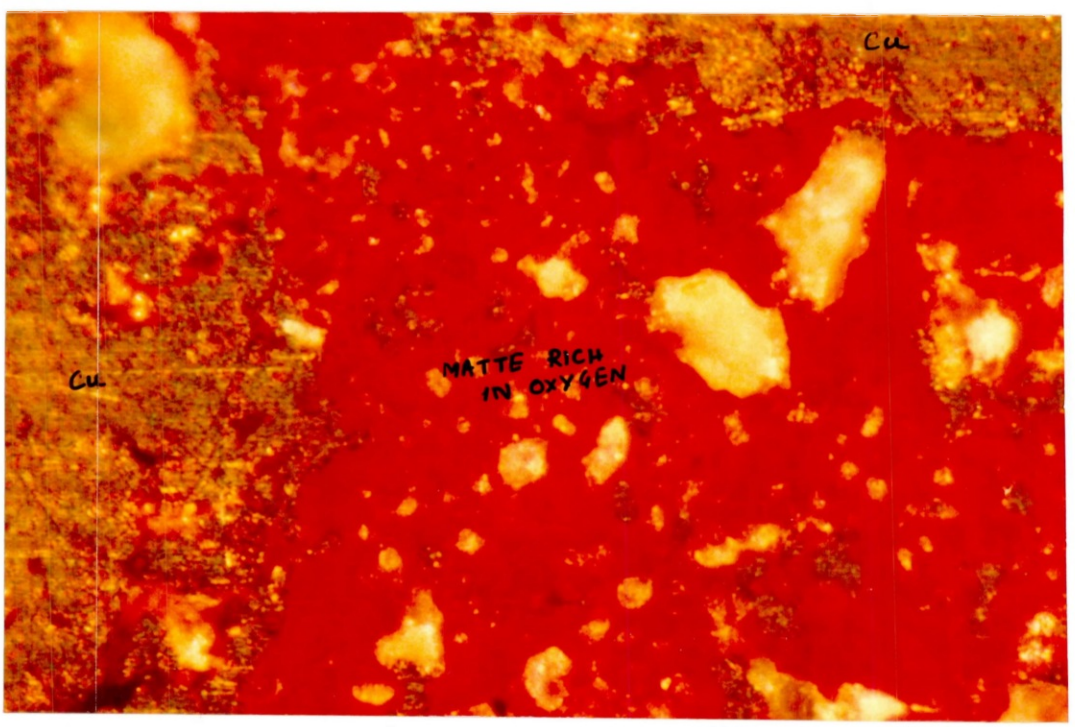
a) Eutectic liquid cooled and growth of Cu from the liquid matte.

b) CaS rejected from the liquid during cooling process.

PLATE 5A·3



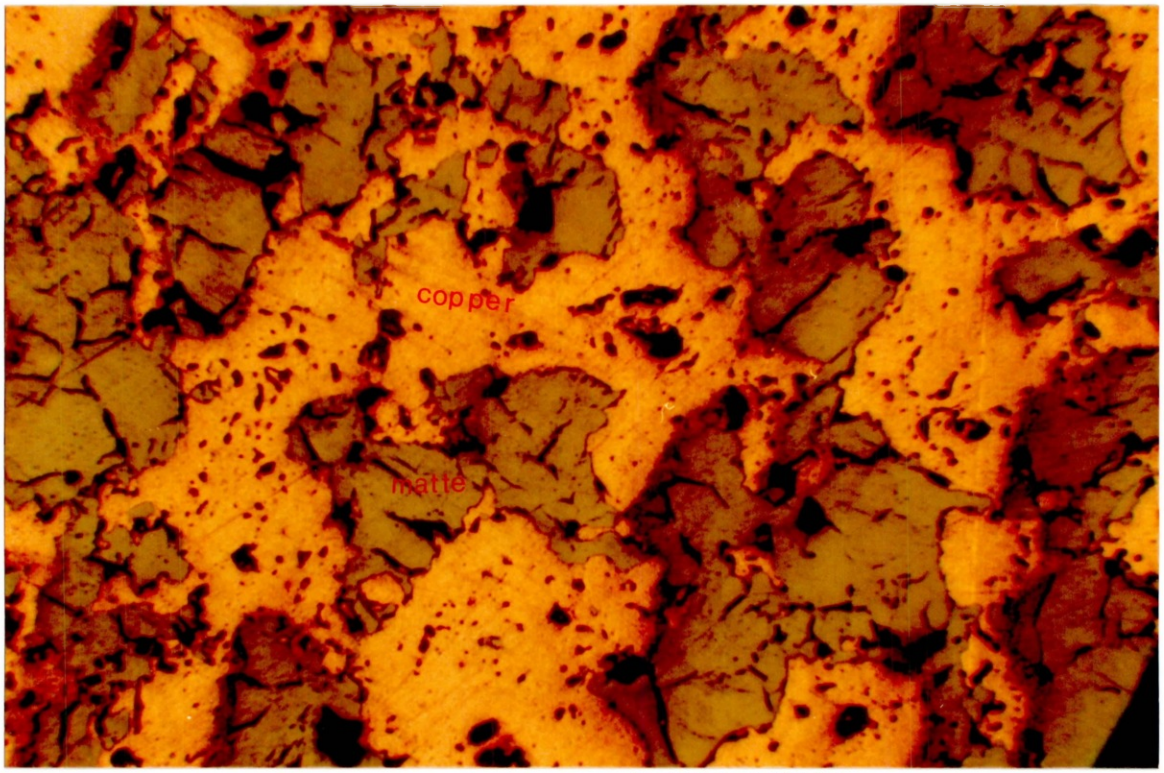
(a) PLANE LIGHT X420



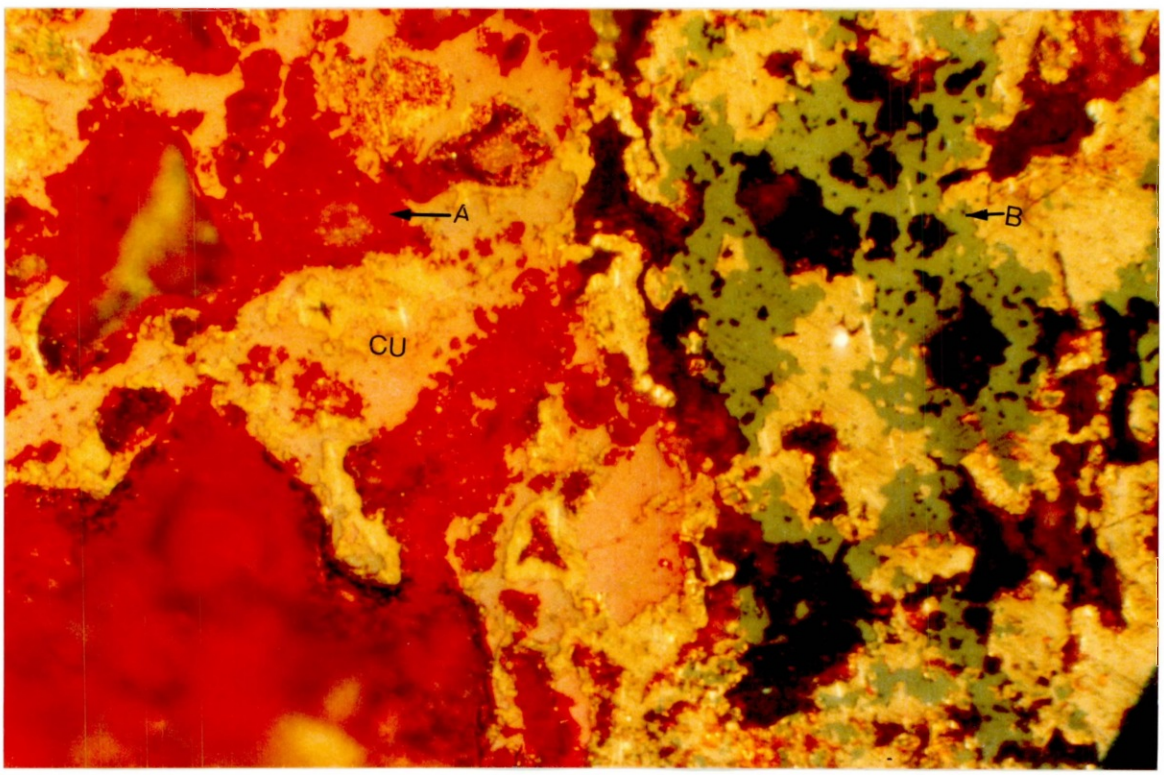
(b) POLARIZED LIGHT X420

Plate 5A.3: Formation of copper and 'O' rich matte during the heatreatment of Cu_2S:Cu_2O=1:3 at 1000°C in the flowing argon.

PLATE 5A·4



a X 420 PLANE LIGHT



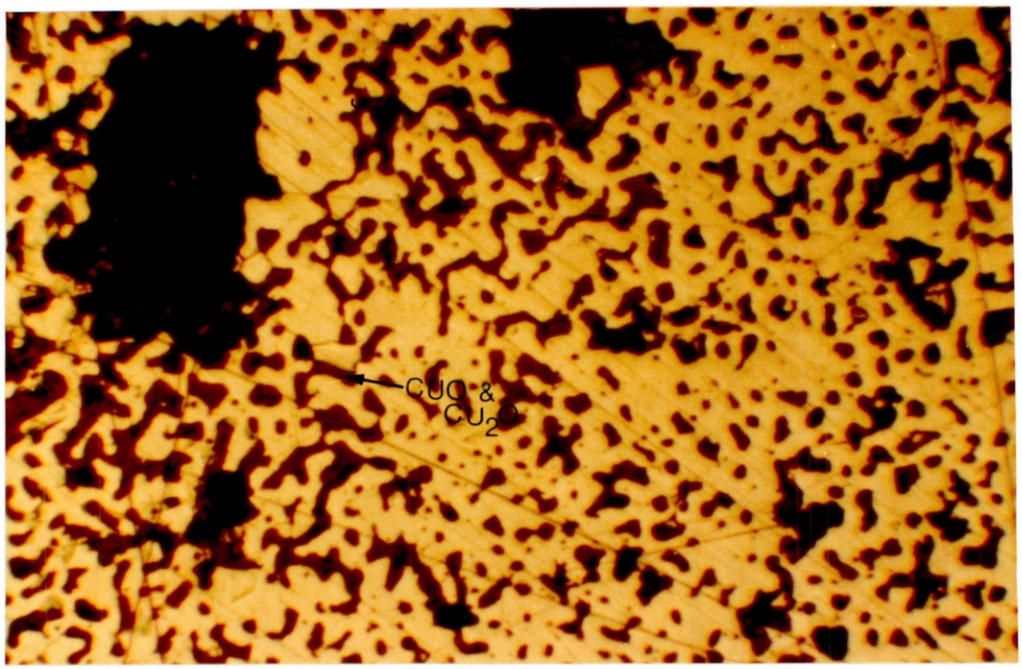
b X420 POLARIZED LIGHT

Plate 5A.4: Heat teratment of Cu_2S and Cu_2O mixtures at 1000°C.

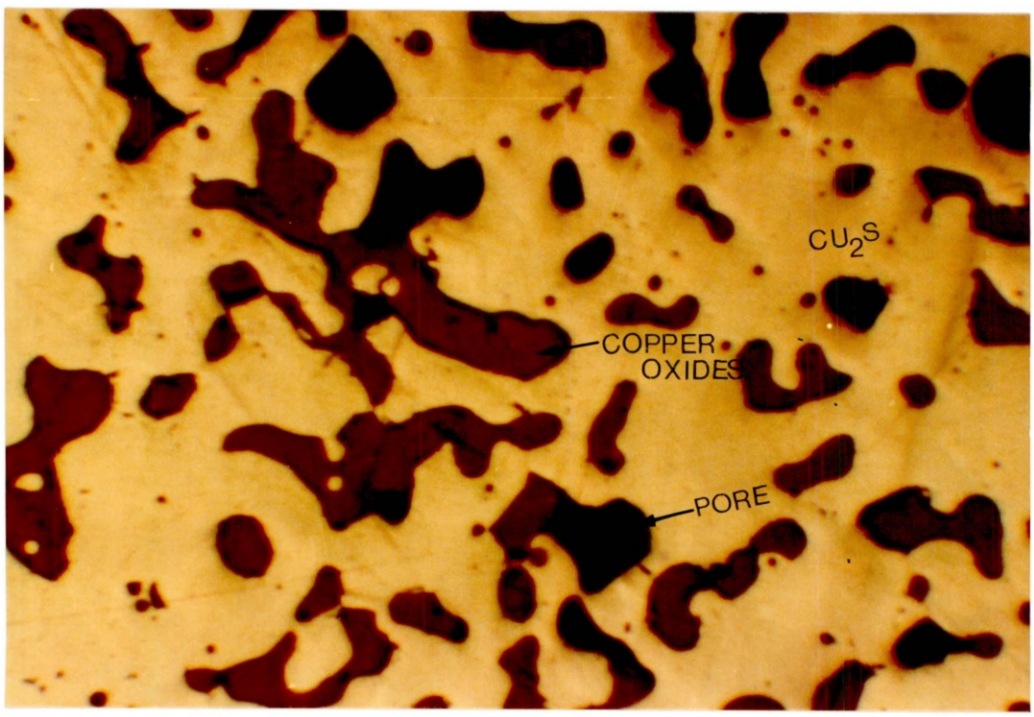
a) Matte phase and copper phase(S:O=1:1)

b) Matte phase from which Cu_2S and Cu_2O have precipated. A-Cu_2O. B-Cu_2S.

PLATE 5A.5



a X 120



b X420

Plate 5A.5: Heat treatment of CuS and CuO at 1000^{o}C in argon.

a) CuS:CuO=2:1 Copper oxide precipitation in the matrix of Cu_2S.

b) CuS:CuO=3:1 Copper oxide precipitation in the matrix of Cu_2S.

During the course of reduction, partially reduced samples were examined using X-ray diffraction analysis which confirmed the presence of oxides of copper before liquefaction or the formation of oxysulphide liquid takes place. Copper oxides were reduced with graphite in their stoichiometric ratio at 1000^{o}C in a flowing stream of argon and the rate of reduction of the pure oxides was compared with the initial slopes of the rate of reduction of copper sulphides. The rates of reduction of pure copper oxide are superimposed on the rates of reduction of sulphides in figs (5A.1) and (5A.2).

In order to investigate the effect of active carbon, reduction of both copper sulphides was carried out with partially volatilized coal at different temperatures. The plateaux were observed for shorter durations at lower temperatures in the case of CuS, whereas no plateaux were observed in the case of Cu_2S at any temperature. The results were found to increase with increasing temperature and were much faster than the rate of reduction with graphite. see fig (5A.7) and fig (5A.8). However, the initial rates of reduction of CuS with coal are identical with those for graphite but then initial rates are slightly slower in the case of Cu_2S.

During the direct reduction of sulphide, it is evident that the dominant gaseous product is carbon monoxide, which can also play a significant role in assisting the reduction reaction. To understand the role of carbon monoxide on the rates of reduction of sulphides stoichiometric mixtures of lime and sulphide (1:1) were prepared and these pellets were heated to attain an isothermal condition in inert gas. Once the isotherm was attained, the reduction was carried out by introducing dry de-carbonated carbon monoxide. The rates of reduction of CuS and Cu_2S with CO are shown in

fig (5A.9) and fig (5A.10) respectively. The rate of reduction of CuS with CO was almost independent of temperature above 800°C, but the extent of reduction achieved varied with temperature. At 800°C, the rate of reduction of CuS with CO was significantly lower than that observed at higher temperature. However, the rates of reduction of Cu_2S with CO was very different at every temperature, when compared with CuS. Suprisingly the reaction proceeded to a less extent above 950°C. At the end of the reaction, at higher temperatures liquid drainage from the pellet was observed. There was no evidence of plateaux in the case of reduction of CuS with CO but below 950°C, plateaux were observed in the case of Cu_2S reduction. Although the initial rates of reduction of Cu_2S were comparable with those of CuS, for time after the establishment of plateaux, the reaction is extremely slow and takes about 14 hours to proceed to completion.

From above observations on the rate of reduction of sulphides, it can be concluded that the exchange reaction plays a very significant role, which means that any alteration of the conditions for the exchange reaction could affect the overall reaction rate.

One way to influence the exchange reaction is to alter the reaction interfacial area.This change can be achieved simply using a higher proportion of lime in the mixture. In order to determine the effect of increased exchange reaction area on the rates of reduction,experiments with increased lime to sulphide ratios were carried out and these rate of reduction curves are shown in fig(5A.11) and fig(5A.12).

. In the case of CuS, below 1000°C long plateaux were observed after which the reaction recommenced in the case of S:O = 1:1.55 but not at 900°C with S:O = 1:2 after 2.5 hours. The rate of reduction after the plateau was much slower than in the case of S:O = 1:1. The rate of reduction of Cu_2S with enhanced lime was found to be significantly

improved at 1000°C but was slow at 950°C. From these observations, it is evident that the rates are adversely affected by increasing the amount of lime. This observation means that there must be an optimum ratio of lime and carbon to sulphide which would result in the fastest rate and the greatest extent of the reaction.

The optimum proportions of lime and graphite (carbon) to sulphide in the mixture was investigated by carrying out experiments with enhanced graphite to CaO, graphite to sulphide and lime to sulphide ratios, keeping one fixed at a particular composition. The results obtained from these experiments were remarkably different. A complete disappearance of the plateau, enhanced reduction rates and a relatively higher yield were observed at 1000°C in the case of both Cu_2S and. CuS. However, at 850°C, the extent and the rate of reaction were significantly reduced. The combination of phases under these conditions was confirmed by X-ray diffraction analysis and is presented in Table 5A.1. The existence of $CaSO_4$ under reducing conditions was observed in the case of Cu_2S :CaO:C = 1:2:2 at 900°C. The rate of reduction curves obtained under these conditons are shown in fig (5A.11) and fig (5A.12).

The reduction of copper sulphide yields a gaseous product during the course of reduction which means removal of the product gas affects the equilibrium towards the r.h.s. To see the effect of reduced pressure of CO i.e. p_{CO} = 0.5 atm. on the reduction rate, experiments with Cu_2S in different stoichiometric proportions were carried out at different temperatures. The rate of reduction curves were determined by measuring the volume of the gaseous product. The rate of reduction curves under different conditions are shown in fig (5A.15) and fig (5A.16). It is evident from

the rate curves that the reduction with graphite proceeds with several temporary arrests whereas with coal no arrest was observed. The fastest rate was observed with coal at a stoichiometric ratio of S:O = 1:2 at 1000^{o}C.

5A (ii) Discussions of the Results of Copper Sulphide Reduction.

(a) The Direct Reduction

The equilibrium phase relationships and the kinetic curves have shown that the reduction of copper sulphide proceeds through an oxysulphide liquid intermediary whose composition falls in the (L + Cu + Cu_2S) invariant phase field.

It was shown by Kauxmann and Benecke (2.14) that the eutectic invariant exists across the pseudo binary section Cu_2S-Cu_2O at 840^{o}C and at 60 mole pct Cu_2S. With the use of Schmeidl's (2.13) oxygen solubility data for the matte phase in equilibrium with liquid copper, the activity of Cu_2O in the melt has been calculated. The calculated values are tabulated below using the equations (2.3-2.5) considering equilibrium between metallic copper and Cu_2O using pure O_2 gas as a standard state.

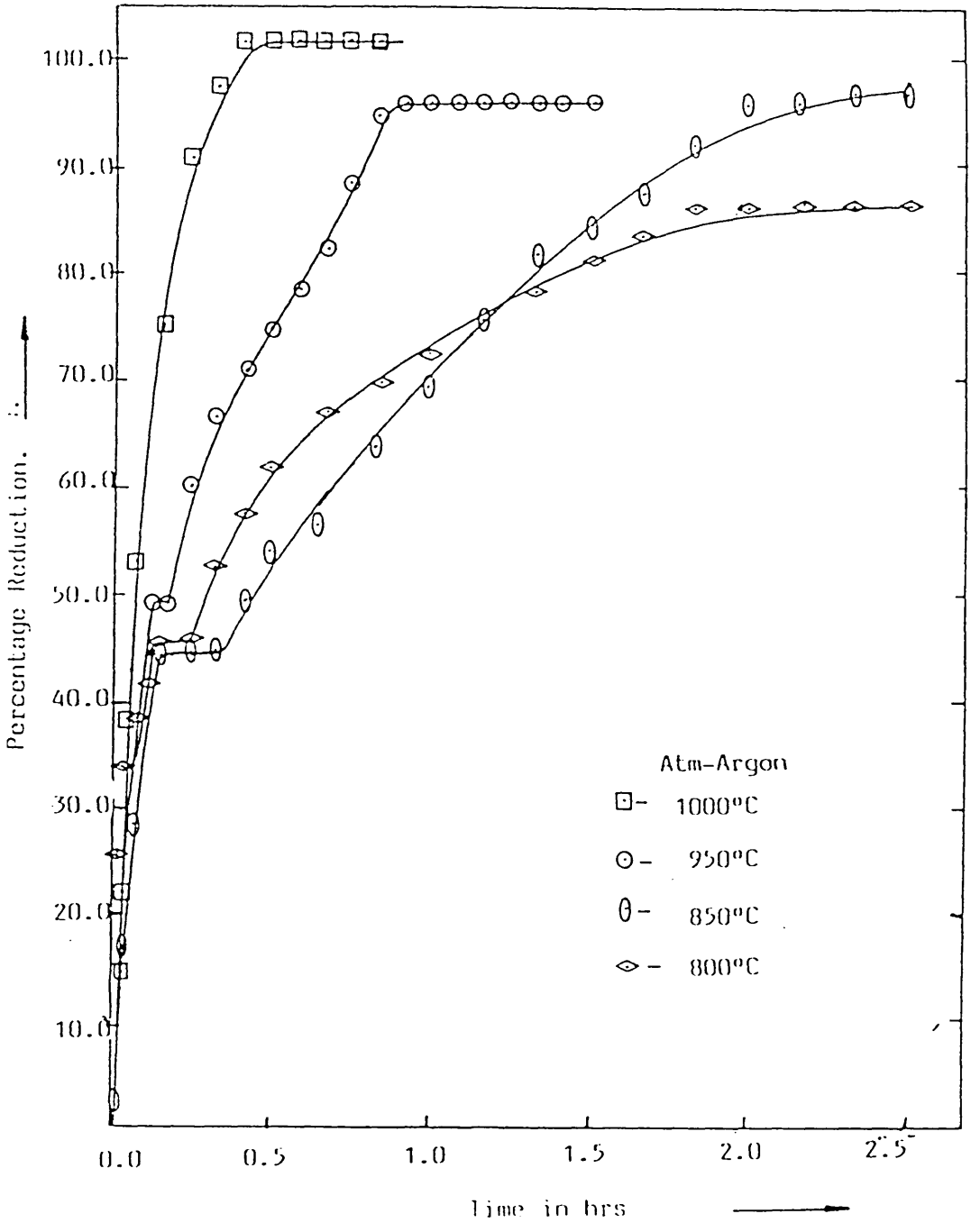


Fig (5A.7) Rate of reduction of CuS with coal in presence of lime (CuS:CaO:Coal = 1:1:2).

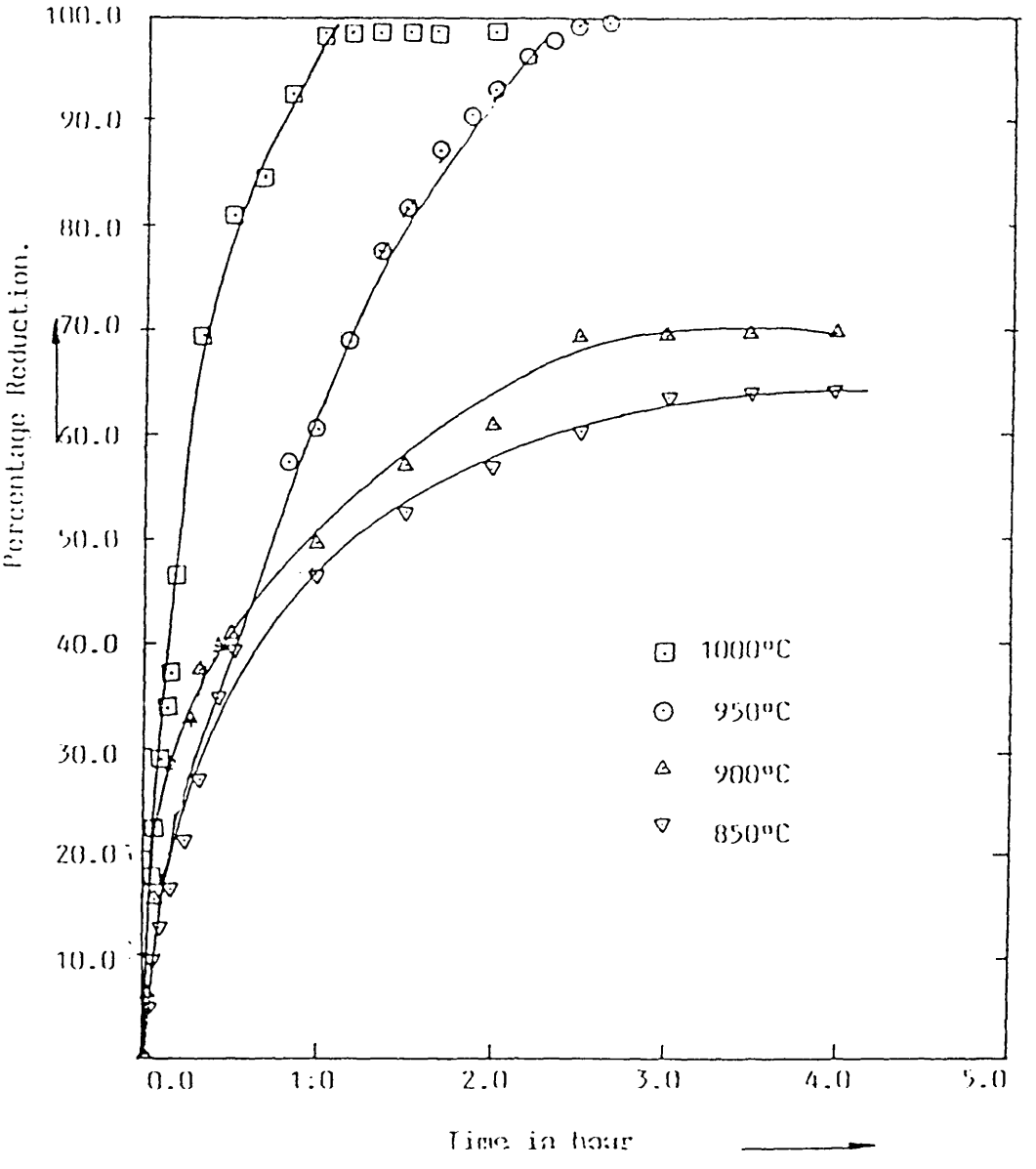
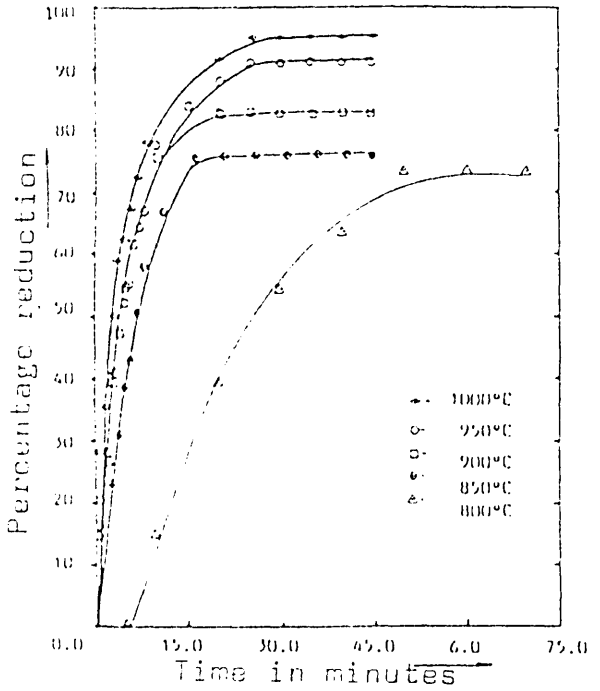


Fig (5A.8) Rate of reduction of Cu_2S with coal in presence of lime (Cu_2S:CaO:Coal = 1:1:2).



Fig(5A.9):Rate of reduction of CuS in presence of lime with CO(S:O=1:1).

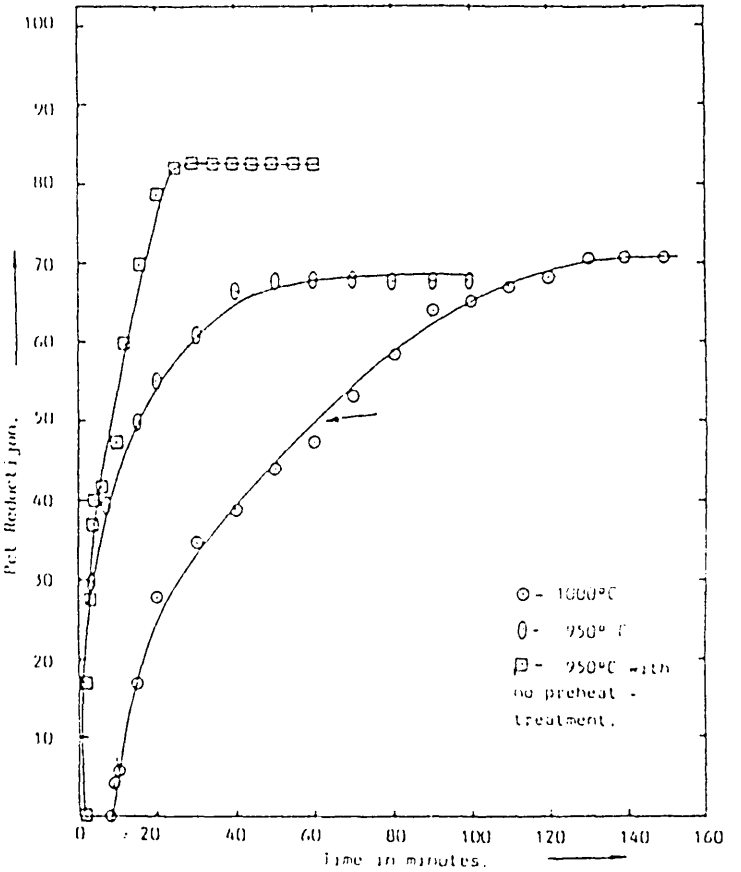
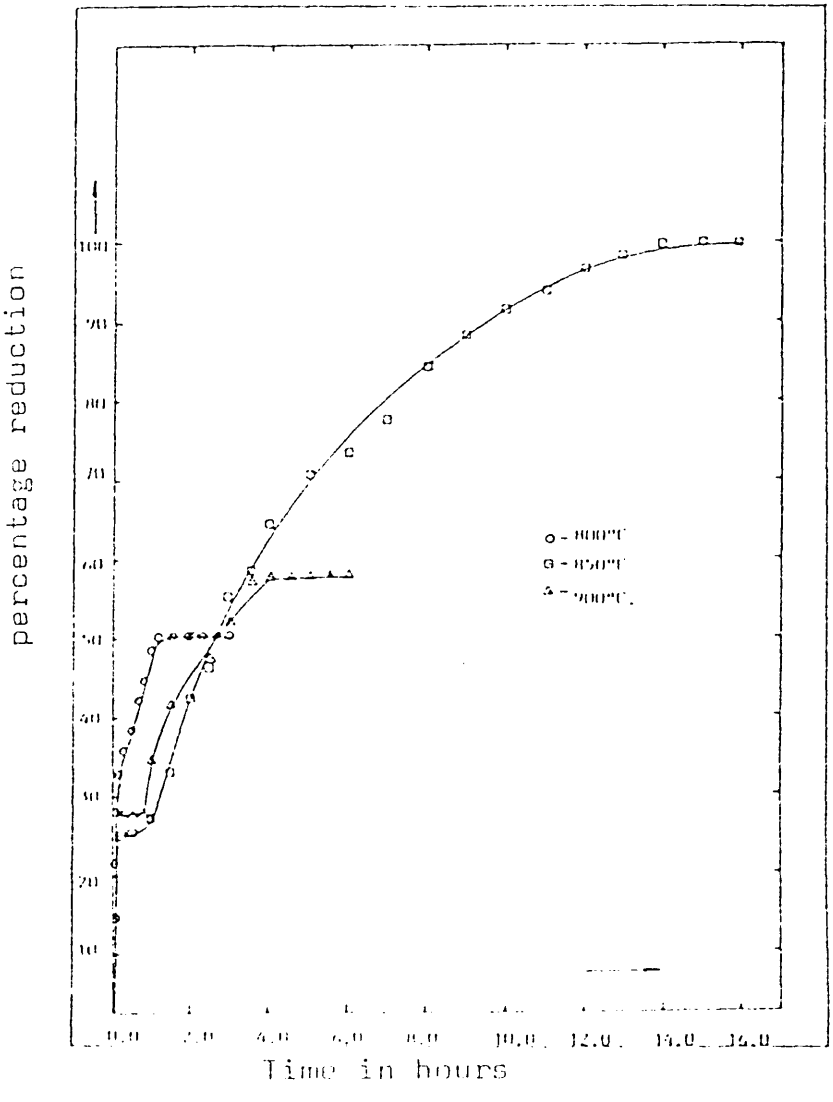
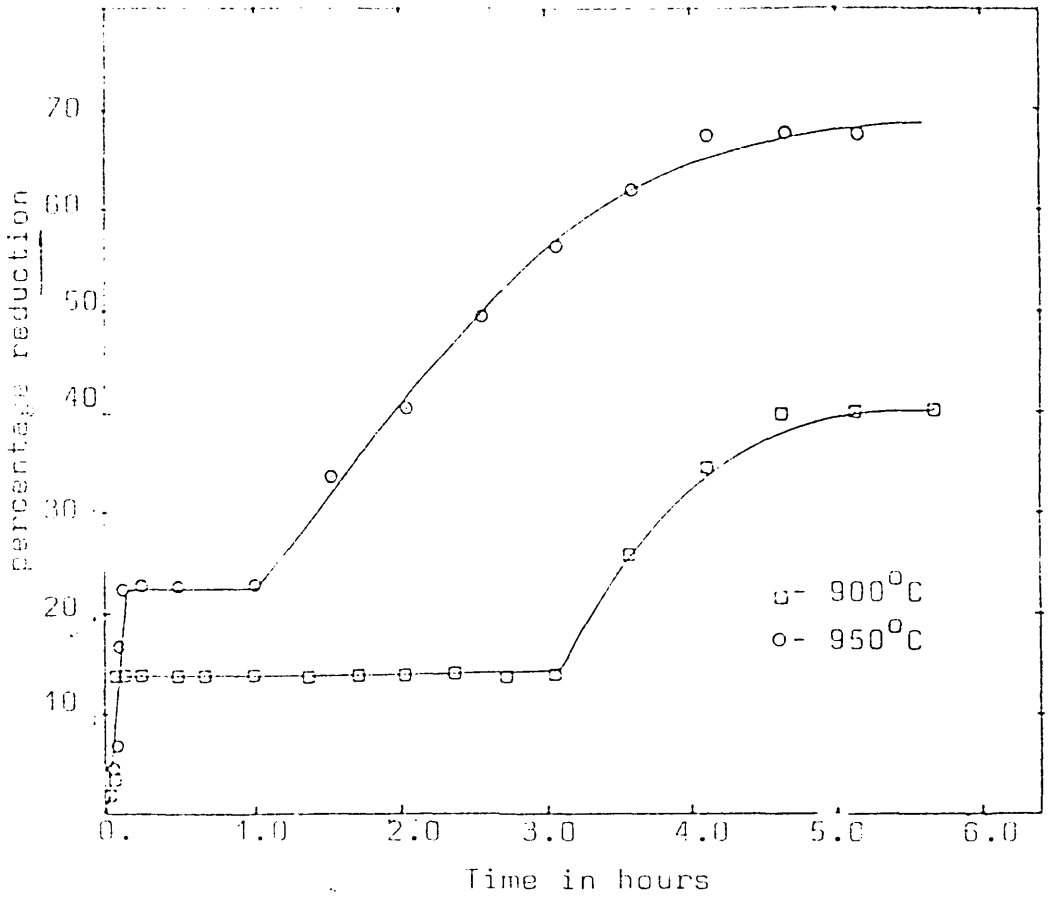


Fig (5A.10a) Rate of reduction of Cu_2S with CO in presence of CaO. Preheat-treatment before reduction was carried out in argon.



Fig(5A.10b): Rate of reduction of $Cu_{2-x}S$ in presence of lime with CO(S:O=1:1).



Fig(5A.11a): Effect of increased lime to sulphide ratio on the rates of reduction of CuS with graphite (CuS:CaO:C=1:2:2).

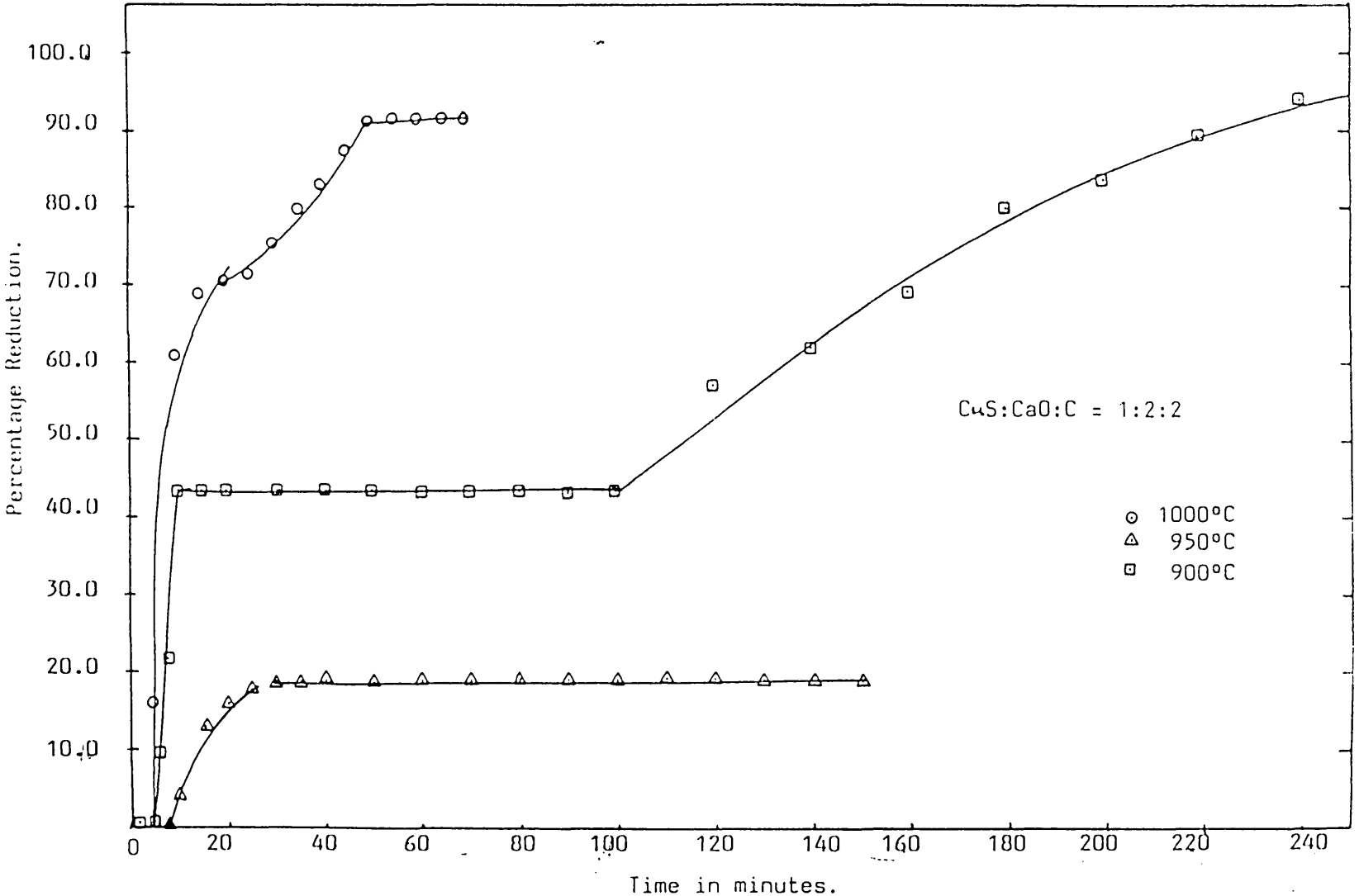


Fig (5A.11b) Effect of increased CaO amount on the rate of reduction of CuS with graphite (CuS:CaO:C = 1:2:2) Atm-Argon.

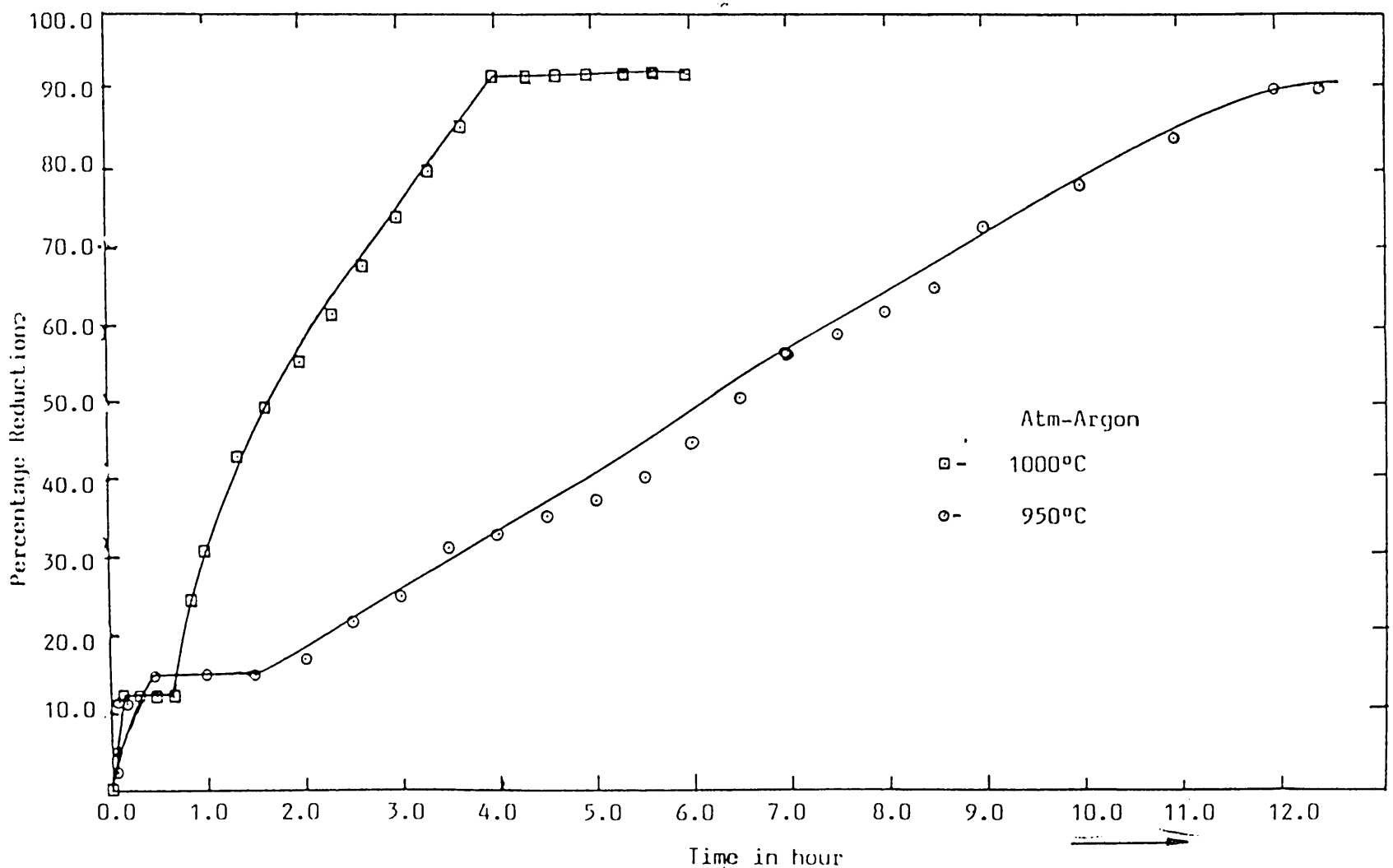
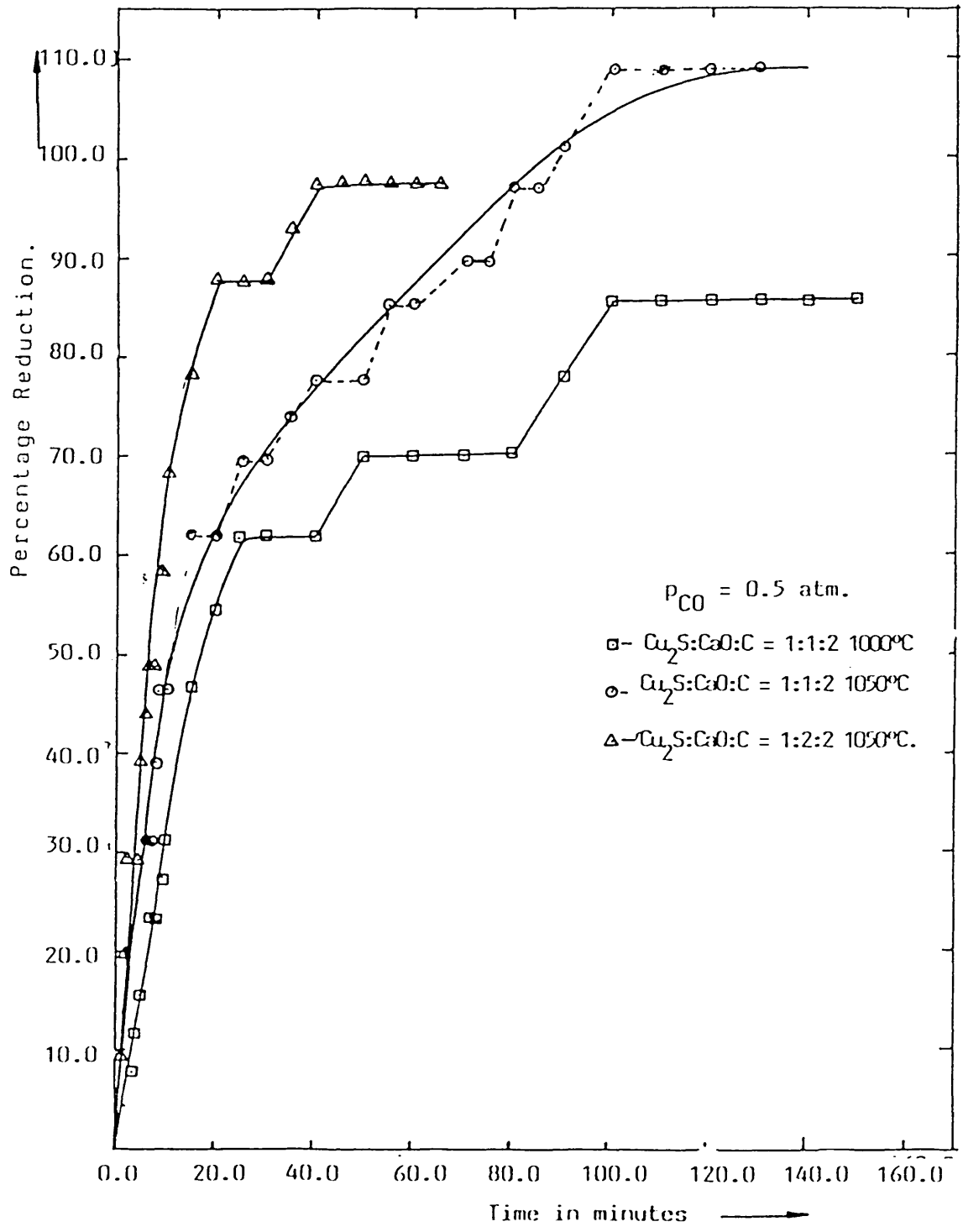


Fig (5A.12) Rate of reduction of Cu_2S with enchanced lime to sulphide ratio (Cu_2S:CaO:C 1:2:2) in argon atmosphere.

Table 5A.3 Reduction of Copper Sulphide under Reduced Pressure of Carbon Monoxide. P_{CO} = 0.5atm.

Mixture Composition	Temp °C	Mass Balance: Pct wt loss	Mass Balance: pct red.	Atmosphere	X-ray diffraction analysis. Cu_2S	CaO	Gr	CaS	Cu	Cu_2O	CuO	$CaSO_4$
Cu_2S:CaO:C = 1:1:2	1000°C	10.14	86.55	P_{CO}=0.5	W	M	WM	VS	VS	VW	VW	-
Cu_2S:CaO C = 1:1:2	1050°C	8.83	75.38	Ar	W	M	WM	VS	MS	VW	VW	-
Cu_2S:CaO:C = 1:1:2	1000°C	9.19	78.48	P_{CO}=0.5	W	M	WM	VS	VS	VVW	VVW	-
Cu_2S:CaO:C = 1:1:2	1050°C	10.81	92.39	P_{CO}=0.5	-	M	WM	VS	VS	-	-	-
Cu_2S:CaO:Gr = 1:2:2	1000°C	6.30	53.78	P_{CO}=0.5	VW	MS	WM	MS	VS	-	-	-
Cu_2S:CaO:C= 1:2:2	1050°C	7.57	79.75	P_{CO}=0.5	W	M	WM	VS	VS	VVW	VVW	-



(Fig 3A.13) Rate of reduction of Cu_2S in controlled atmosphere.

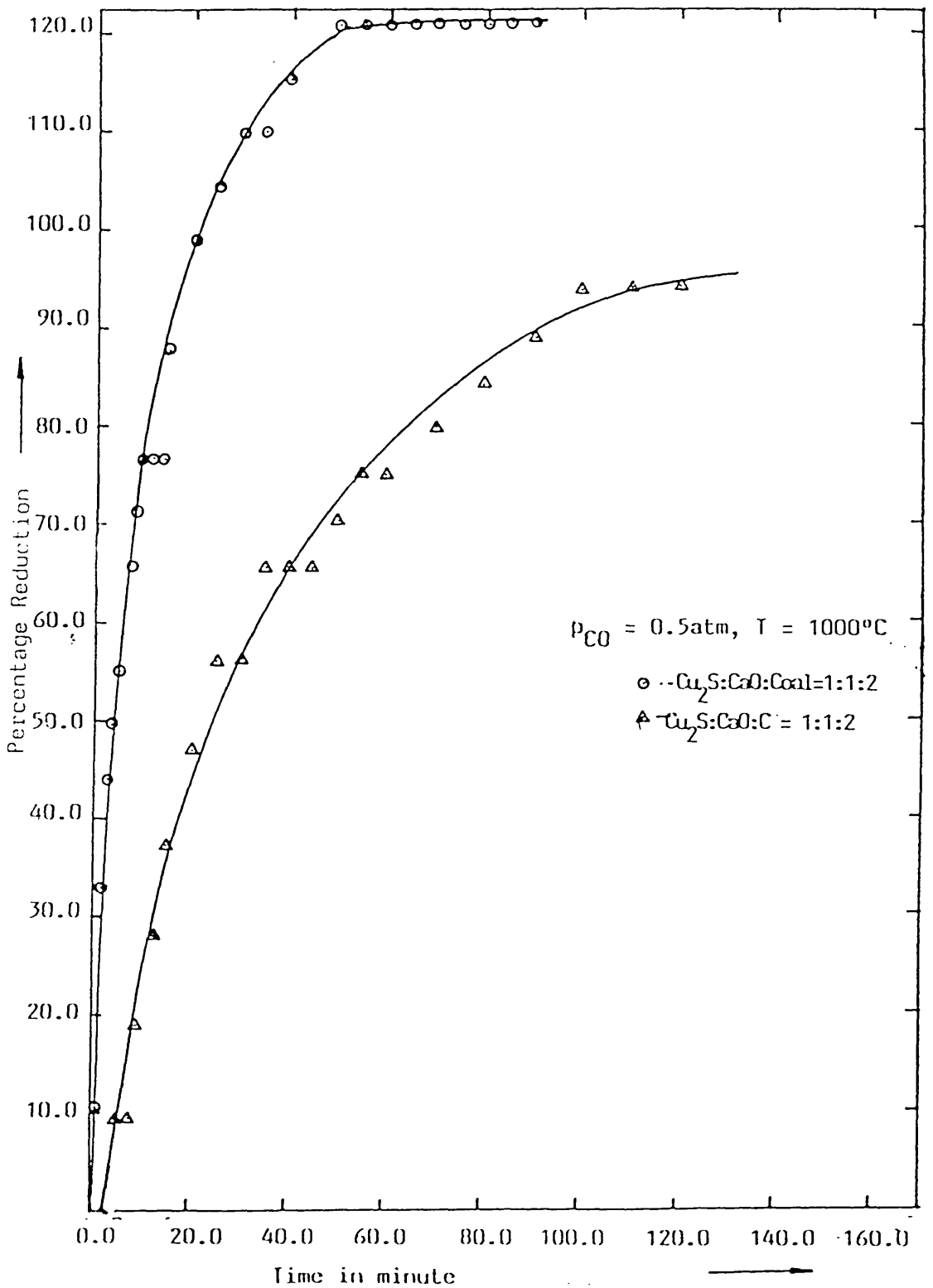


Fig (5A.14) Effect of active carbon and lime on the rates of reduction of Cu_2S under controlled atmosphere.

Table 5A.4. Thermodynamic Data on the Ternary Liquid.

Temp ^{o}K	Wt%O	N_{Cu_2O}	$K_{2.4}$	a_{Cu_2O}	Log P_{O_2}	(-)RTln P_{O_2} cal mole^{-1}
1163	2.247	0.2006	1.00	1.00	-7.969	42260.4
1173	2.209	0.1973	1.052	0.975	-7.89	42351.3
1223	2.037	0.1819	2.287	0.661	-7.52	42085.8
1273	1.889	0.1687	4.67	0.463	-7.17	41767.5
1323	1.7634	0.1574	9.067	0.332	-6.86	41531.3
1373	1.6537	0.1476	16.744	0.244	-6.57	41278.9

Plotting (-) RTln P_{O_2} vs 'T' the enthalpy of formation of this liquid was determined graphically, see fig (5A.6). On the basis of the Clausius-Clapeyron Relationship, the pseudo binary section Cu_2S - Cu_2O is shown in fig (5A.15). From the enthalpy data on Cu_2S, Cu_2O and the liquid per mole of Cu, and from equation (5.4) at the aforementioned temperatures, the relationship between the slope $\frac{d}{dT}$ (RTln a_O) and temperature shows a maximum at 850^{o}C after which it decreases rapidly approaching the Cu-S binary section asymptotically see fig (5A.16). This curve intrinsically shows the variation of the heat capacity (ΔCp) with temperature to be non-linear in nature. A non-linear variation of ΔCp with temperature was also observed by Turkdogan and Kor (2.18) in the Fe-S-O system. In fig (5A.16) the slope $\frac{d^2}{dT^2}$ (RTlna_O) is zero at the maximum ie the ΔCp for the liquid is maximum at that temperature. Thus, the existence of the oxysulphide liquid is thermodynamically justified.

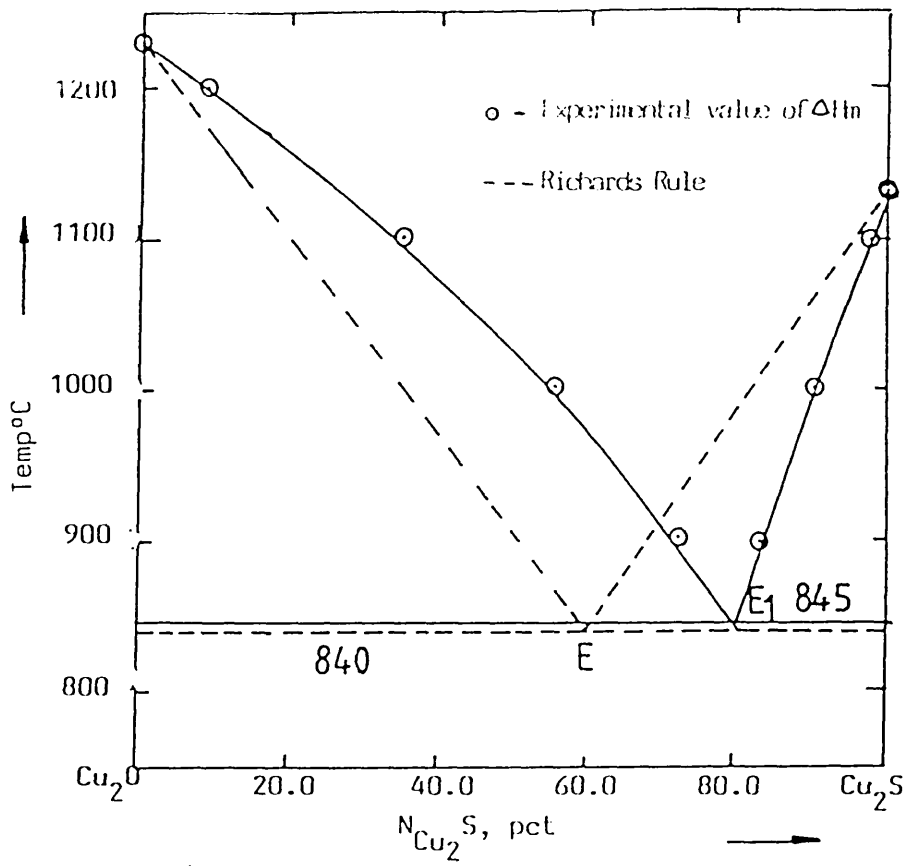


Fig (5A.15) Cu_2O-Cu_2S psuedo binary diagram.

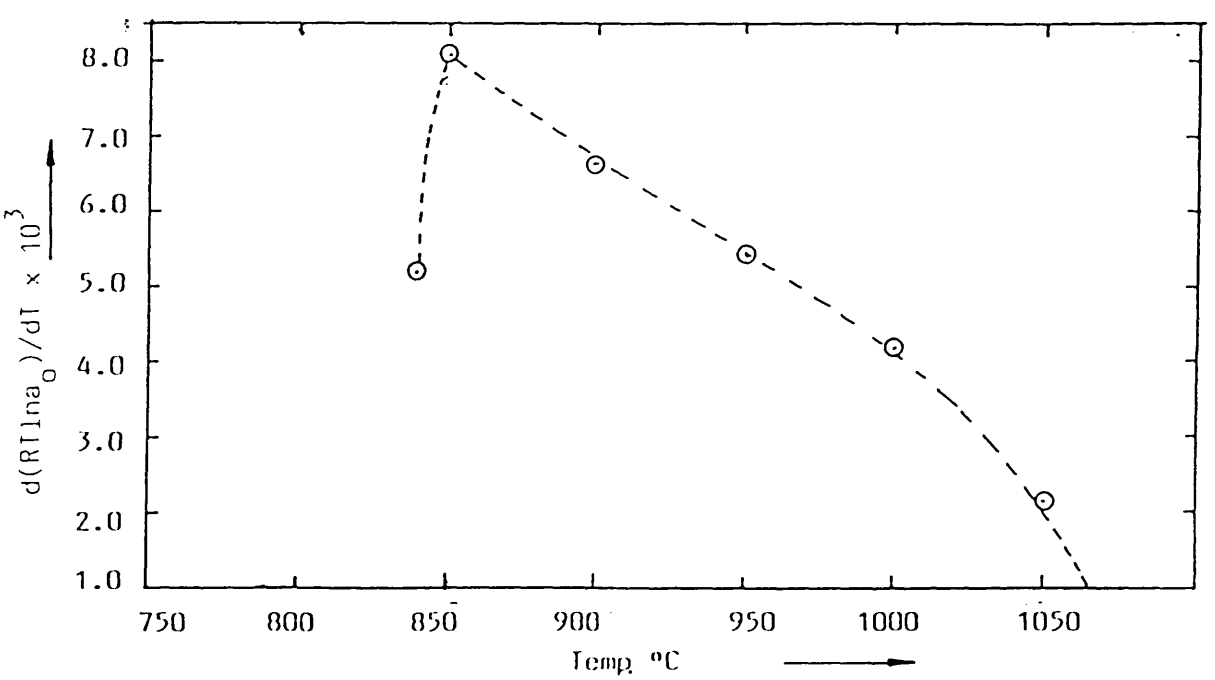


Fig (5A.16) d $(RT\ln a_O)/dT$ vs Temp relationship for the oxysulphide liquid in Cu-S-O system.

Dealing with the kinetics of the carbothermic reduction of sulphide, it is pertinent at this stage to mention that a solid layer of CaS around CaO does not exist during the course of exchange reaction. Had this been the case, the reaction might have been expected to slow down quickly after the initial stage of chemical reaction. The continuation of reaction would have reached completion via a diffusion mechanism ie the counter diffusion of S^{-2} and O^{-2} ions through the CaS lattice. The relative sizes of these anions indicate that energetically such a process would demand a much higher activation energy. It seems reasonable to accept from the rate of reduction curves that the exchange reaction is sustained during the course of reaction because of the presence of an oxysulphide liquid, which is saturated with CaS. The thermodynamics of this complex melt are not known but microscopic examinations have proved that calcium sulphide precipitates from the matte phase during the cooling process (plate 5A.1(c)). As long as the presence of this liquid is maintained the exchange reaction would not cease. It has been proved on the basis of experimental evidence that the exchange reaction copes with the reduction reaction during the course of overall reaction. Under the circumstances when the exchange reaction is faster than the reduction reaction ie when the oxygen removal from the melt is slower, there will be a build up of oxygen concentration in the CaS saturated oxysulphide liquid in the vicintiy of lime. The enrichment of oxygen in the calcium sulphide saturated oxysulphide liquid would increase the activity of oxygen up to a critical level. Once this level with respect to oxygen activity in the melt is attained, the high oxygen potential of liquid decreases by forming $CaSO_4$ by the oxidation of calcium sulphide. The formation of $CaSO_4$ results in its precipitation on the unreacted lime particles. The precipitation of $CaSO_4$ on the lime particles isolates the contact between the lime surface and the oxygen depleted oxysulphide liquid. This reaction results in the

cessation of the exchange reaction, which is the source of oxygen supply demanded by the reduction step. In addition the transport direction for the O^{-2} ions on the carbon surface is reversed away from the carbon surface towards the CaS(l) - $CaSO_4$ interface. This phenomenon is confirmed by the experimental evidence in which $CaSO_4$ is observed in the reduced pellet as confirmed by X-ray diffraction. Furthermore the relative amounts of copper oxide observed after the oxidation of CaS are consistent with this concept. The related equilibria at the plateau of the rate of reduction curve can be represented as follows:-

$$4\,(CuO)_{matte} + CaS(l) = 4Cu(s) + CaSO_4(s) \qquad (5.5)$$

$$\Delta G^{o}_{5.5} = -73250 - 6.28T$$

$$4\,(Cu_2O)_{matte} + CaS(l) = 8Cu(s) + CaSO_4(s) \qquad (5.6)$$

$$\Delta G^{o}_{5.6} = -57810 + 7.27T$$

In the above situation,the transport direction for the oxygen ions from the oxysulphide liquid to the carbon surface does not resume unless equilibrium between CaS-$CaSO_4$-CaO and the liquid phase is attained. The establishment of such an equilibrium means that the concentration of the oxide phase in the matte continuously decreases along the length of the plateau and hence the length of time of existence of a plateau decides the time to acquire an equilibrium state w.r.t. oxygen. The respective oxide activities conditions for unit activities of CaS, $CaSO_4$ and metallic copper, at $1000^{o}C$ are:-

$a_{CuO} = 3.25 \times 10^{-4}$ and $a_{Cu_2O} = 8.16 \times 10^{-3}$

Substituting the activity of Cu_2O in the equation (2.5) results in a partial pressure of SO_2 ie $p_{SO_2} = 10^{-4}$ atm and $p_{O_2} = 8.016 \times 10^{-6}$ atm under these condtions. Thus thermodynamically it is justified that under these conditions $CaSO_4$ is stable. The recommencement of the reaction takes

place because of calcination of $CaSO_4$ in the presence of CaS (a chapter has been devoted to this aspect, see chapter 6). From the available literature under the prevailing conditions, $CaSO_4$ decomposition can take place by two mechanisms:-

i). The sulphate being reduced by CaS to give lime and SO_2 according to the following equilibrium:-

$$3CaSO_4(s) + CaS(s) = 4CaO(s) + SO_2(g) \qquad (5.7)$$

Any SO_2 liberated might redissolve in the matte phase or may oxidise carbon to produce CO gas. Once CO gas is nucleated, the reduction of oxysulphide matte can proceed. The fresh lime regenerated in this way initiates the exchange reaction once again and the reduction proceeds.

ii). Any CO generated would assist both the reduction of matte and the reduction of $CaSO_4$

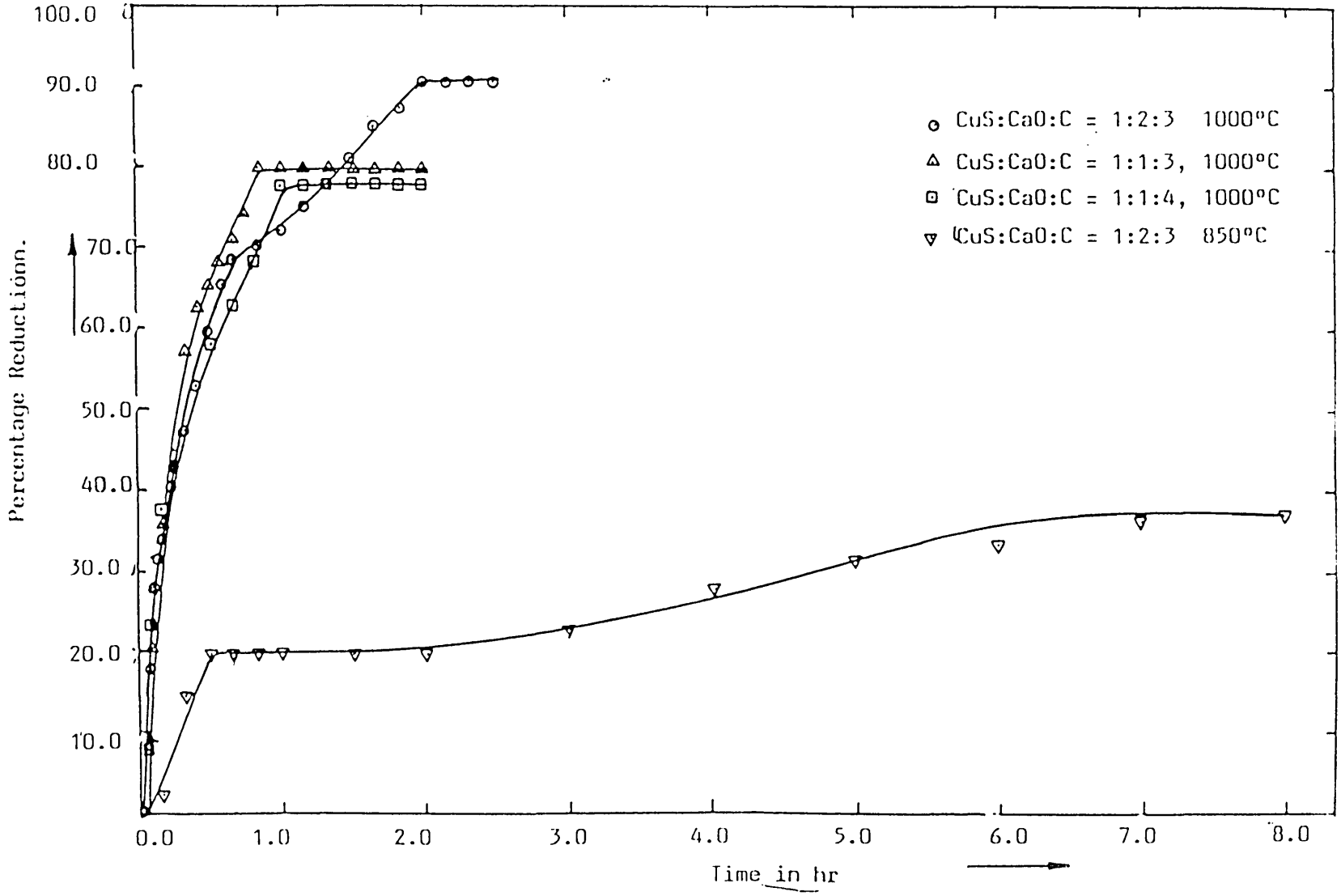
$$CaSO_4(s) + CO(g) = CaO(s) + SO_2(g) + CO_2(g) \quad (5.8)$$

Thermodynamically, the reduction of matte with CO can be justified as the standard free energy change for this reaction at such a high temperature is negative.

In the light of this hypothesis, the appearance of plateaux in the rate of reduction of sulphide with enhanced lime ratio is expected. The increase in the quantity of lime increases the surface area for the exchange reaction and in the event of a slow reduction step, thermodynamic conditions for the oxidation of calcium sulphide to calcium sulphate are expected. Thus, it is evident that any parameter which directly or indirectly influences the reduction reaction

affects the time span of existence of a plateau. One way to alter the rate of the reduction reaction is to alter the surface area for reduction reaction by increasing the carbon to sulphide ratio or using more reactive carbon. It is for this reason that plateaux were not observed in the case of reduction of sulphides with coal at temperatures above 950°C. Below this temperature, plateaux were only observed with CuS, where the quantity of CaS formed per mole of copper is increased because of sulphur distillation. Later in this thesis a correlation between the length of plateaux, the temperature and the relative amount of sulphur per mole of copper has been established.

In order to verify this hypothesis, experiments with higher carbon to sulphide and lime to sulphide ratios were carried out at 1000°C and these results are shown in figs (5A.17) and (5A.18). From these results it can be appreciated that the surface area of carbon has a greater effect on the rate of reduction and it leads to complete disappearance of the plateau. The variations in the rate of reduction curves in these figures in the case of the enhanced lime to carbon ratio is attributed to the faster exchange reaction leading to the slightly higher oxidizing conditions in the liquid oxysulphide. At 850°C, the initial rate of reduction is very fast and is essentially due to the reduction of pure copper oxide. It is also worth remembering that the volume of the liquid formed at 850°C is small and effects the continuation of the overall reaction. This is one of the reasons why at lower temperatures the extent of reaction is less than that observed at higher temperatures and supports the idea that the isolation of the oxysulphide liquid from the carbon surface becomes the critical step.



Fig(5A.17) Rate of reduction of CuS with enhanced lime to sulphide and graphite to sulphide and graphite to sulphide ratio. Atm-Argon.

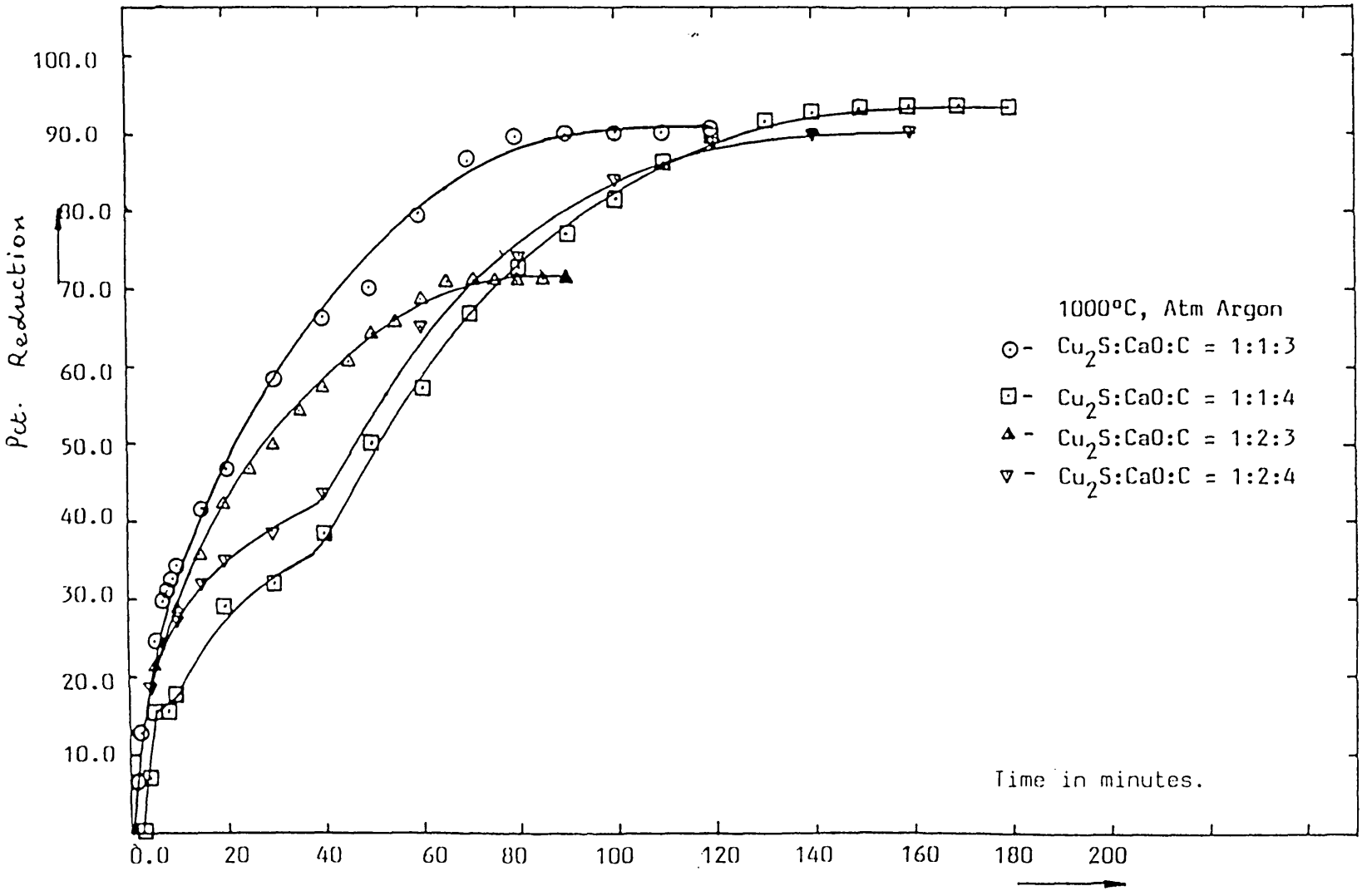


Fig (5A.10) Effect of increased graphite amount on the rate of reduction of Cu_2 in presence of CaO at 1000°C.

... reduction can also be altered by the use of coal and a catalyst. These effects have also been investigated and the results are shown in fig (5A.19). No plateaux were observed in any of these situations except at 950^{o}C where momentarily the rate of the exchange reaction has overtaken the rate of reduction reaction. The rate of reduction curves also show that a Li_2CO_3 catalyst has a greater effect than the temperature, because the rate of reduction of Cu_2S at 900^{o}C is slower than that at 850^{o}C with the catalyst addition, the latter ratio is comparable to the rate at 950^{o}C without catalyst. These investigations show two very important features:-

a). The rate of reduction after the appearance of a plateau is always slower than that observed in the situation of an equivalent weight loss. When a plateau does not appear.

b) To obtain the highest rate, a balance between temperature, the rate of exchange reaction and the rate of the reduction reaction is absolutely essential.

To prove that the rate of carbothermic reduction of sulphide is governed by the volume of liquid generated, an experiment was designed where CuS:CaO = 1:1 mixture pellet was heat-treated at 1000^{o}C in argon. At this temperature the pellet was held for half an hour to ensure that liquid was formed as a result of the exchange reaction after which the temperature was reduced to 800^{o}C and the pellet was reduced with CO. The percentage weight loss vs time curve for the entire treatment is shown in fig (5A.20) where the 1st stage indicates the rapid distillation of sulphur vapour from the pellet and the second stage relates to SO_2 loss from the pellet and to generation of metallic copper followed by an arrest. Along

the arrest for times up to 40 minutes the temperature was maintained at 1000°C and the sample temperature was reduced to 800°C within 20 minutes. From the 60th minute reduction with CO was carried out. The rate of reduction is extremely slow as the oxides are essentially precipitated in a matrix of sulphides e.g. see plate (5A.5) Thus the oxides, at 800°C are separated from the CO atmosphere and the only probable mechanism for the reduction reaction is the diffusion of O^{-2} ion towards the pellet - gas surface and the movement of Cu^{+2} ion inwards from the pellet-gas periphery. From the slope of the curve, it is apparent that the rate is extremely slow and hence the existence of a solid state diffusion mechanism is probable.

In another situation heat-treated pellets of oxide-sulphide mixtures whose microstructures are shown in plates (5A.3 and 5A.5) in a graphite crucible with and without lime at 1000°C. The microstructure of one of the reduced pellets (from which the difference in the extent of the reaction at the periphery and in the core of the pellet can be observed) is shown in plate(5A.6). The rate of reduction curve in the absence of lime with mixtures containing high 'S' content were extremely slow and can be explained in terms of the small amount of oxygen present in the mixture before reduction. In the presence of lime, the rate of reduction resembles the the rate of reduction of Cu_2S at 1000°C, but it does not reach completion. A limited amount of reaction only takes place at the contact surface and the gaseous product does not seem to make any contribution to the reduction process. It appears as soon as CO is generated at the contact surface, it immediately leaves the pellet. The rate of reduction curves are shown in figs(5.21a-21c).

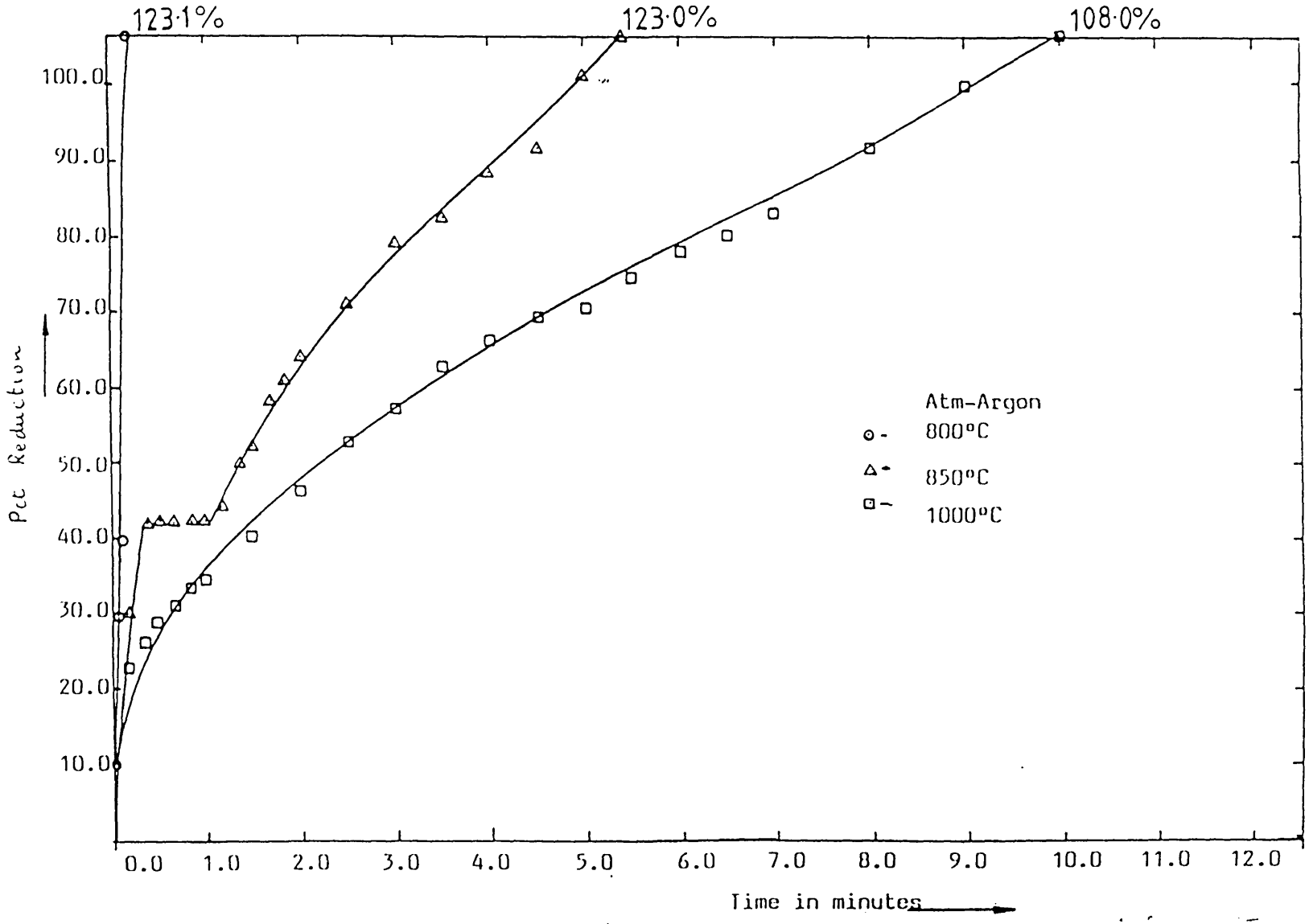


Fig (5A.19a) Effect of CaO on the rate of reduction of Cu_2S with coal.

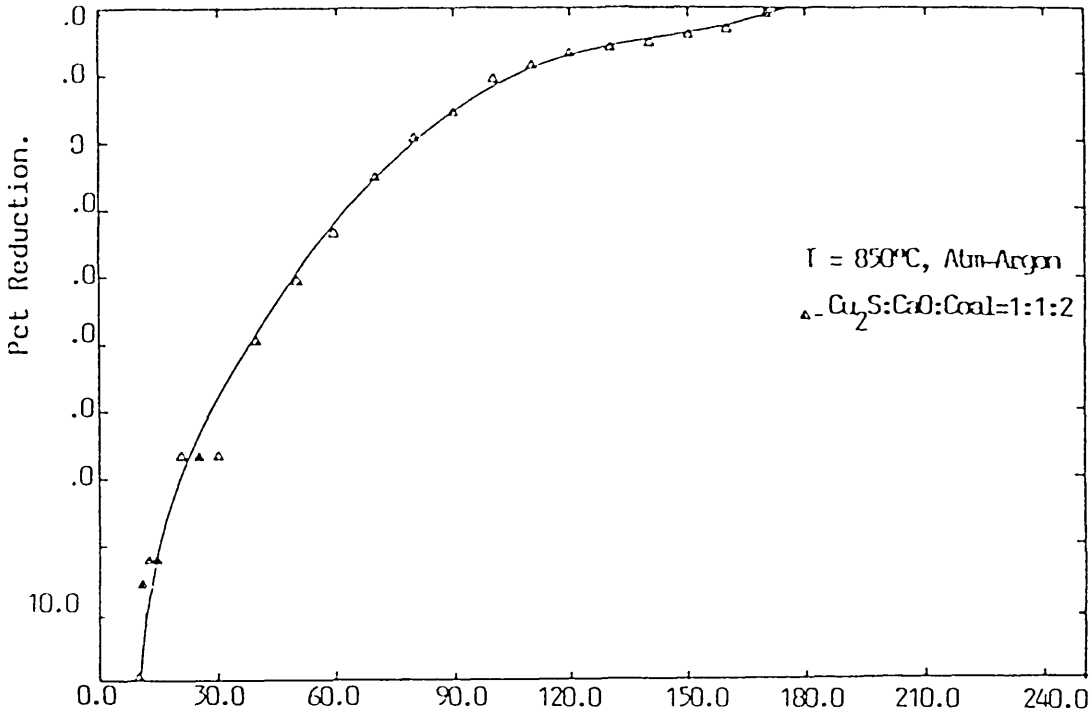


Fig (5A.19b) Effect of catalyst (Li_2CO_3) on the rate of reduction of Cu_2S with carbon in presence of CaO.

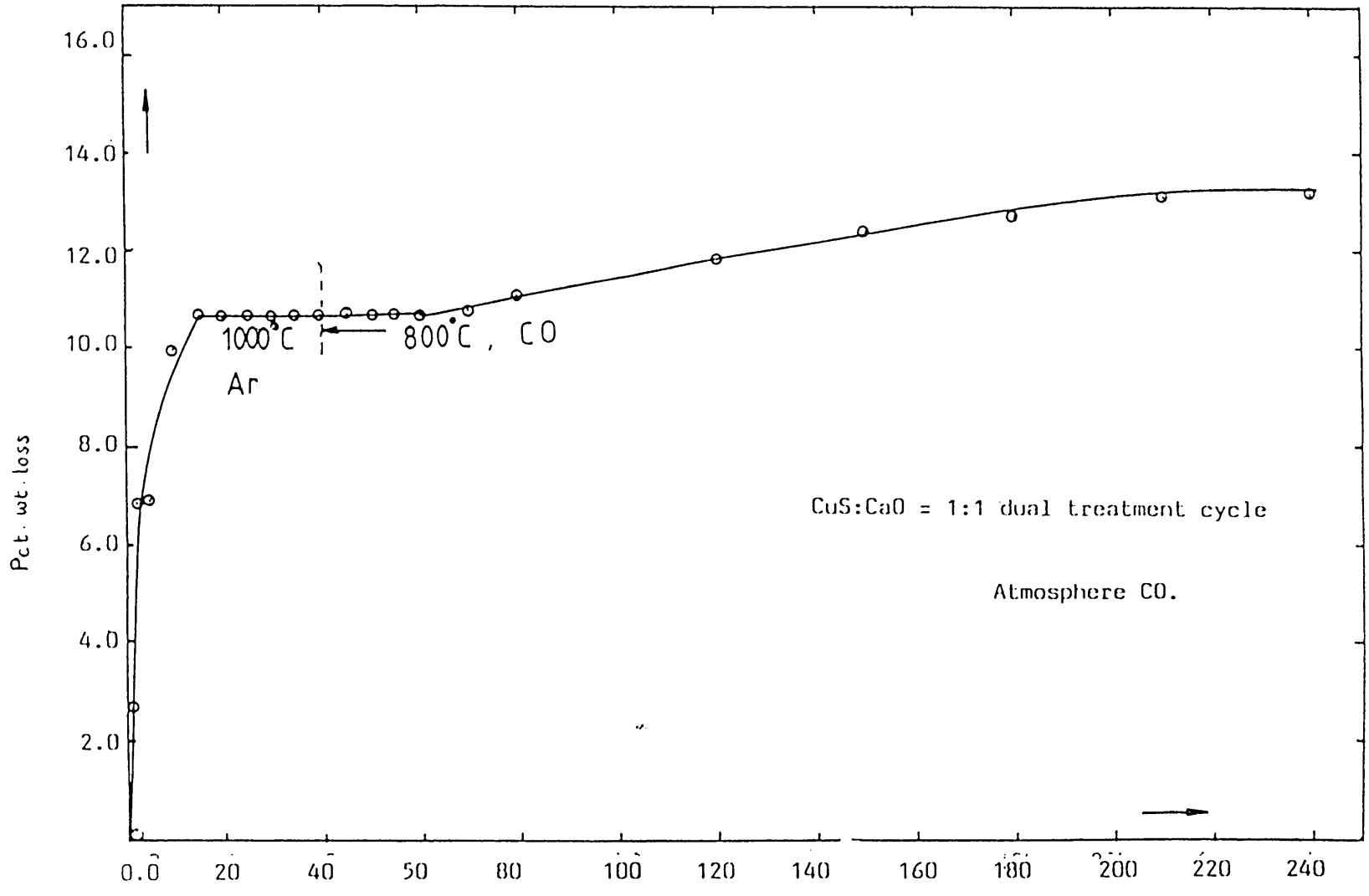
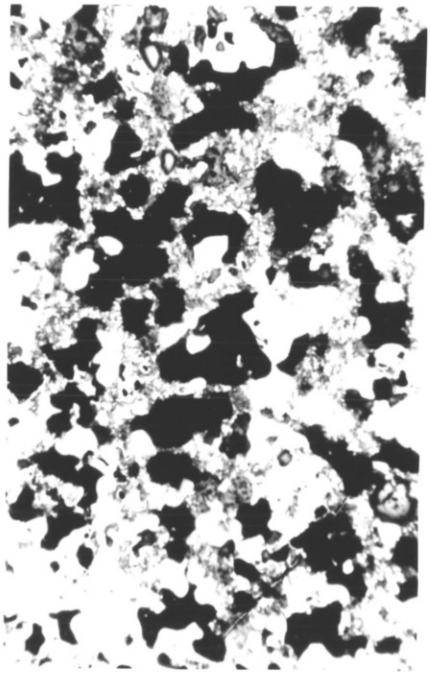


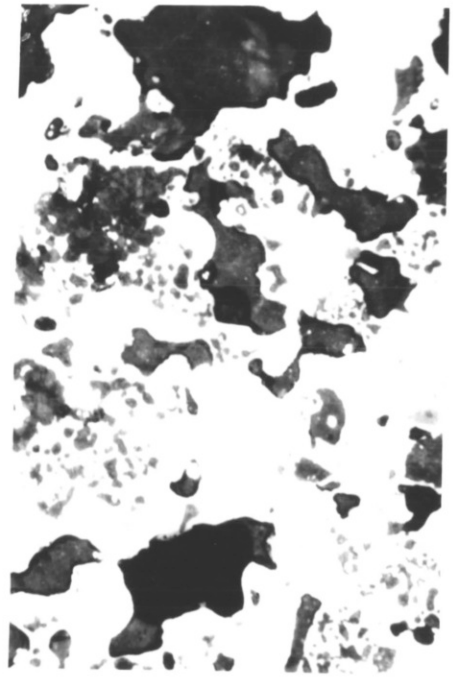
Fig (5A.20) Reduction rate during the dual treatment of CuS with lime.

PLATE 5A.6

PERIPHERY

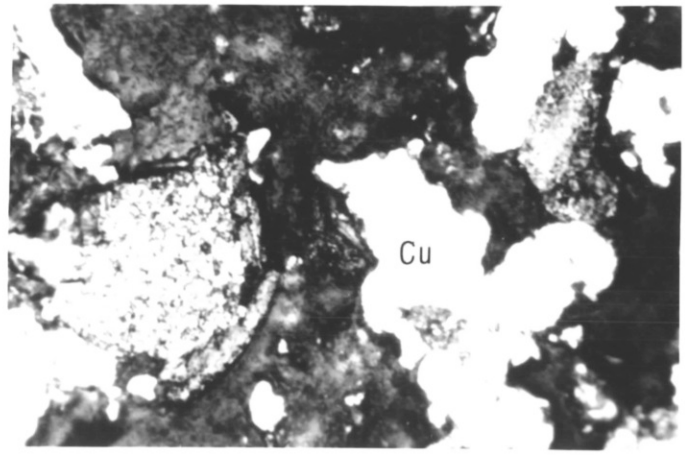


a x 300



b x 1000

CORE



c x 1000

Plate 5A.6 Heat treated CuS:CuO = 3:1 mixture mixed with lime and reduced in graphite crucible at 1000°C

(a) A large number of small Cu nuclei near the periphery
(b) The area magnified showing the evidence of eutectic liquid
(c) Grown copper from liquid matte and rejected CaS from the liquid

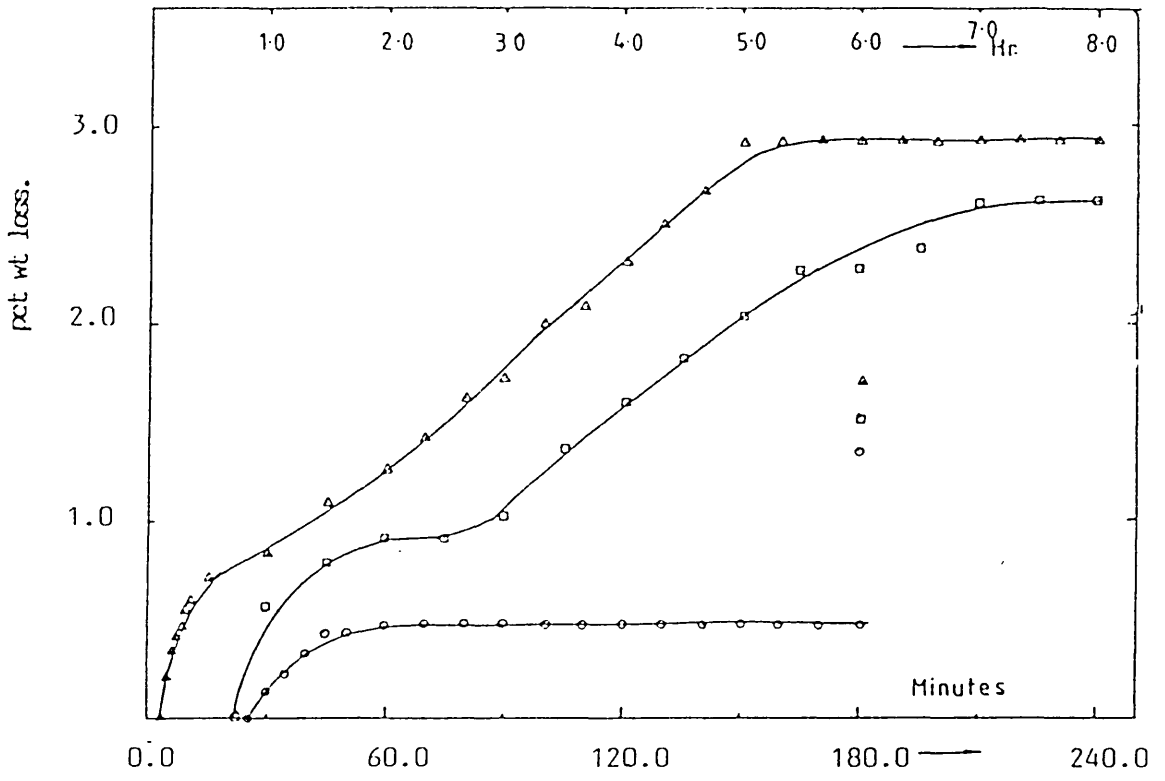


Fig (5A.21a) Rate of reduction of CuS:CuO = 3:1 preheat-treated mixture at 1000°C in argon under different conditions.

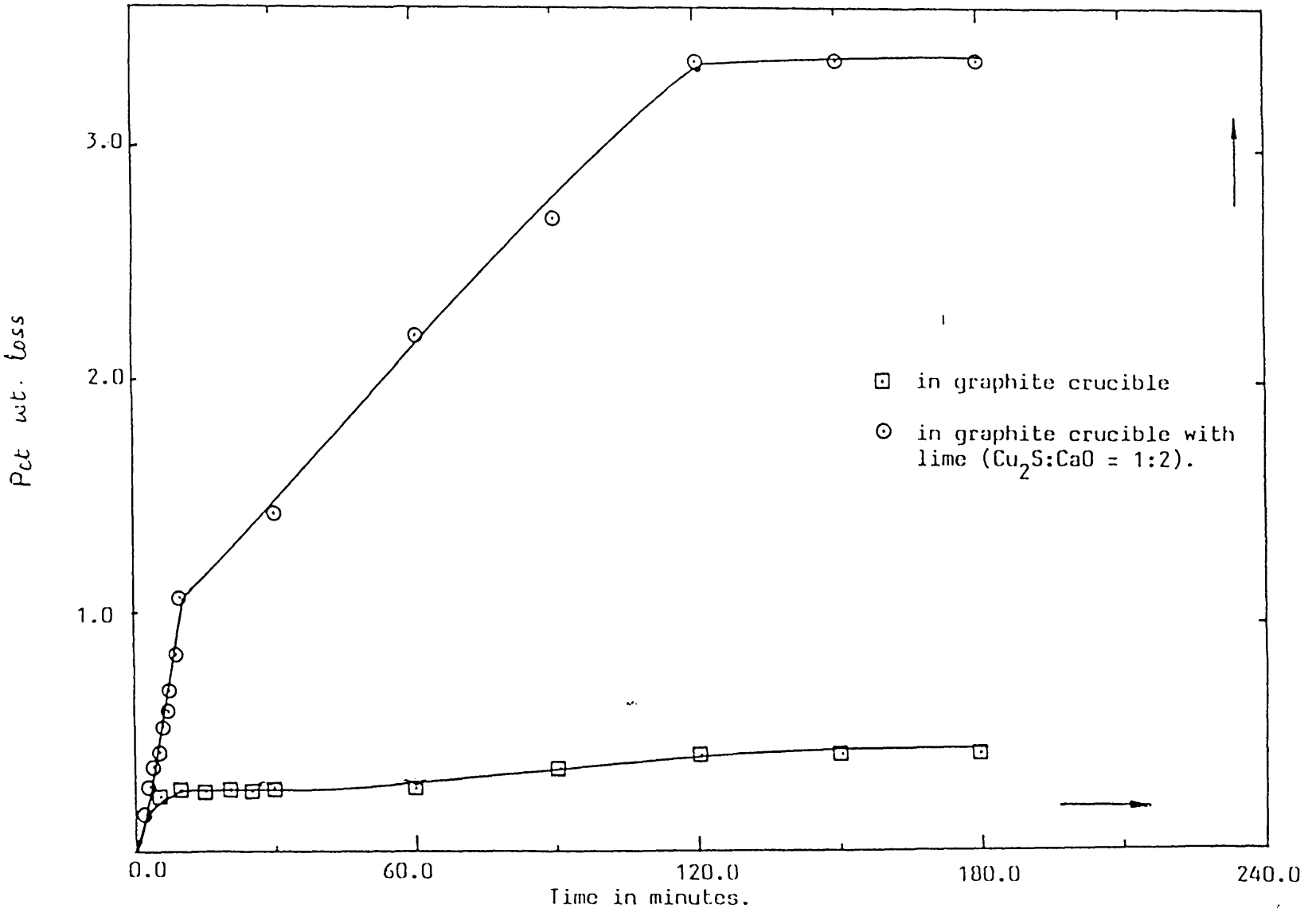


Fig (5A.21b) Rate of reduction of CuS:CuO = 2:1 preheat-treated mixture at 1000°C in argon under different conditions.

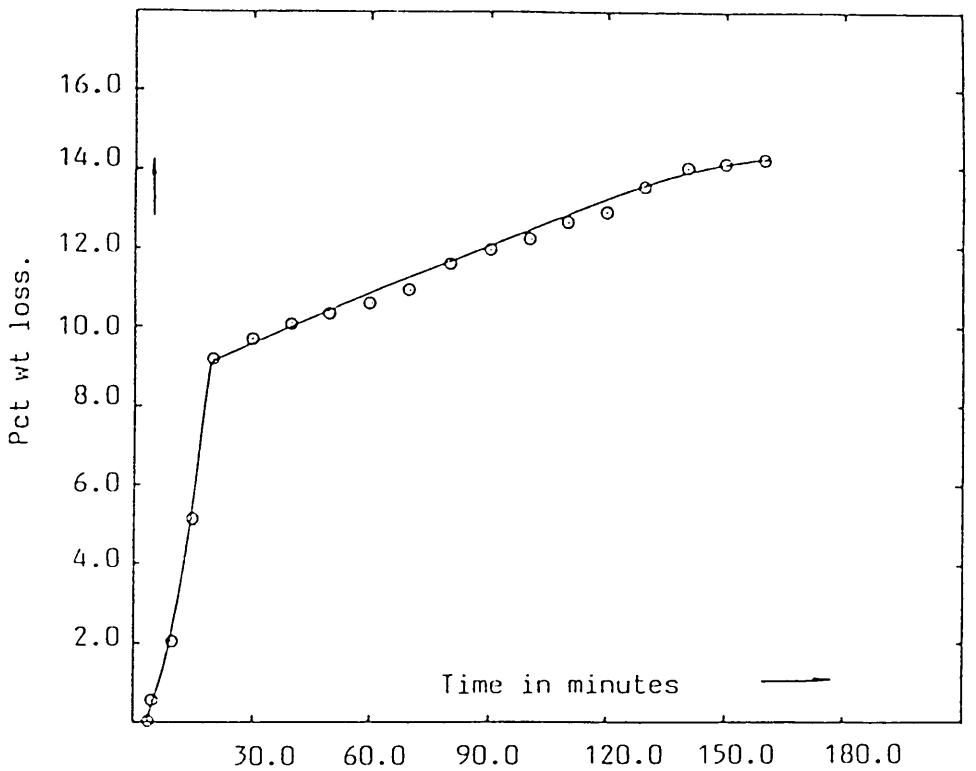


Fig (5A.21C) Rate of reduction of CuS:CuO = 1:3 preheat-treated mixture in argon at 1000°C in graphite crucible.

However, the 'O' rich mixture when reduced at 1000^{o}C in a graphite crucible proceeded remarkably well and from the rate of reduction curve it is evident that the overall rate is divided into two distinct regimes. The initial stage, see fig(5A.21)) can be ascribed to the reduction of oxide with carbon whereas the subsequent reduction was accompanied by the diffusion of O^{-2} ions, present in the liquid state, to the carbon surface. A complete agreement of the theoretical weight loss with the experiment observations shows that all the oxides are reduced. The appearance of the linear regime in this case and in the case of those mixtures with lime, indicates that the reduction of the oxysulphide liquid progresses by means of diffusion of O^{-2} ions in the liquid phase.

b. The indirect Reduction.

The indirect reduction of copper sulphides with CO in general is faster than that observed with coal or graphite. From the rate of reduction curves for CuS shown in fig (5A.9) it is obvious that there is little difference in the rates of reaction from 850^{o}C to 1000^{o}C. Whereas a remarkable difference in the reaction rate at 800^{o}C is apparent. This difference is related to the absence of oxysulphide liquid at 800^{o}C and it appears that the reduction is gas-solid in nature. It can also be concluded that the product layer of metal, if formed at the sample surface, is not dense and does not hinder the contact of the reducing gas with the oxide formed as a result of the exchange reaction becomes difficult in the later stages when the reactants are isolated by the product layer. In addition, it seems possible that a thick layer of CaS around the lime particles might have caused the cessation of the reaction at 800^{o}C.

Above 800°C, where little change in the slopes of the rate of reduction curves has been observed, a small activation energy is consistent at these temperatures. In general, the activation energy associated with chemical reactions and diffusion controlled reactions are significantly affected by change in temperature.In the present situation, it thus, appears that the rate controlling step is pore diffusion of the gaseous species for which the activation energy is of the order of 8-10Kcal per mole. At 1000°C, the rate of reduction of CuS with CO is comparable with that using coal as a reductant.

There is little similarity between the rates of reduction of CuS and Cu_2S with CO at any temperature. Comparing the rates in figs 5A.10(a) and 5A.10(b), it is evident that the rates are faster at higher temperatures but the extent of reaction is much too small in comparison to its rate. Invoking the temperature cycles used during the course of reduction of Cu_2S, it is evident that at temperatures well above the eutectic temperature in the psuedo binary section of Cu_2S- Cu_2O, the volume of oxysulphide liquid would increase with increasing temperature.A stage is reached where the liquid volume can no longer be held inside the pellet and it drains away leaving the bulk material. Under this condition the exchange reaction can no longer continue between the drained liquid and the CaO held in the bulk material. The rate curves shown in fig 5A.10(a) shows a linear regime at 950°C and 1000°C which occurs immediately after the initial reaction. The termination of the initial stage of the reaction is a function of the temperature. In the later stage, the rate follows a linear relationship with time which can be attributed to the capillary diffusion of the drained liquid to the bulk material. By the mechanism of

capillary diffusion, the drained liquid would come in contact with lime to resume the supply of oxygen and hence the subsequent reduction step would continue. Thus the extent of the reaction is purely decided by the extent to which capillary diffusion of liquid can take place. On the other hand, when no prior heat treatment was given ie the pellet was held in CO as the temperature was raised from the room temperature a higher percentage reduction was observed at 950^{o}C. Once again a sudden cessation of the reaction can be attributed to the drainage of the liquid, see fig (5A.10a).

This proposed mechanism is not necessarily valid for experiments at 900^{o}C. The pellet at this temperature was held in reducing gas from room temperature and the reduction was the slowest observed. An explanation of this reaction condition can be made in terms of the volume of the oxysulphide liquid generated. The liquid in this case, is certainly held within the pellet and does not drain away. After a fast initial stage of the reaction, a temporary cessation occurs for which an explanation has already been given. In the later stages ie beyond the plateau, the reaction rate is governed by the removal of oxygen from the encapsulated liquid. It is for this reason that the rate is extremely slow. A careful examination of the nature of the rate of reduction curve shows that the rate is parabolic in nature and decreases very slowly with time. In this situation because of the limited surface area of reaction, the reduction proceeds very slowly towards its completion.

At 850°C, which is just above the eutectic temperature the rate of reaction appears to proceed in steps ie after an initial stage the rate is totally governed by the very small volume of liquid generated. This is the reason why the reaction ceases immediately after the appearance of the first plateau. It is worth noting at this point that the stability of $CaSO_4$ increases with decreasing temperature.

The rate of reduction curve at 800°C indicates that the rate is faster than that observed at 850°C and 900°C which is related to the reduction of pure copper oxide with CO. At this temperature 800°C the reaction terminates very quickly because of the absence of the oxysulphide liquid. Thus, it can be stated briefly that for the carbon monoxide reduction of Cu_2S the presence of a volume of liquid phase at any temperature plays a dominant role.

c. The Reduction Under Reduced Pressure.

The purpose of this aspect of the present investigation is to determine the dependence of the indirect ,CO, reduction on the direct ,C, reduction. The necessary conditions were simulated using P_{CO} = 0.5 atm where, Cu_2S pellets mixed with lime and graphite (or coal) in different stoichiometric proportions were reduced at different temperatures. In general, the rate of reduction of Cu_2S was much faster than the rate of reduction of Cu_2S with graphite at the same temperature. The rates are faster than those observed in argon atmospheres because of the presence of CO gas but the appearance of the plateaux is evidently related to the retarded oxygen removal rate in the presence of graphite. Such problems can easily be overcome if coal replaces graphite and the results prove this conclusively.

There is one instance with coal where the overall reduction of sulphide proceeded beyond 100pct. This discrepancy can be explained by the formation of SO_2 see fig(5A.13). It is also worth remembering at this point that at the end of reduction there is a significant quantity of CO_2 generated in the system which has a pronounced effect on the length of the plateaux. The length of the plateaux are longer with time because of the continuously decreasing reducing condtions.

d) Relation between the length of plateau, temperature and composition

During the course of reduction of sulphide with graphite the length of plateaux was found to be dependent on the following factors:-

i. It is inversely proportional to the temperature.

ii. It is directly proportional to the initial sulphur to carbon ratio and oxygen to carbon ratio.

iii It is also dependent on the reactivity of the carbon surface.

iv. The increase in the partial pressure of CO_2 in the system increases the length of plateau.

****

5.B. Reduction of Iron Sulphide Minerals.

(i) Results

The reduction mechanism of iron sulphide ($Fe_{1-x}S$) was investigated by the determination of rate of reduction curves together with X-ray diffraction and optical microscopic analyses. The rate of reduction curves were produced using a chemical mass balance relation derived from the stoichiometry of the reaction and the amount of weight loss observed. Equation (5.2) was used to estimate the percentage reduction occuring at any time. The chemical mass balance equation governing the reduction of pyrrhotite is given below.

$$Fe_{1-x}S(s) + CaO(s) + C(s) = (1-x)Fe(s) + CaS(s) + CO(g). \qquad (5.9)$$

The reduction was carried out with various stoichiometric mixtures of lime, graphite (or coal) and pyrrhotite over a range of temperatures. The rate of reduction of pyrrhotite with graphite is shown in fig 5B(1) and from the rate curves it is evident that there exists a large temperature dependence for the reaction .For these conditions the reaction was incomplete at all temperatures. The reaction products at different temperatures were analysed using X-ray diffraction techniques. The results of X-ray diffraction analysis in terms of relative amounts of CaS, iron and graphite were consistent but the powder pattern for pyrrhotite and lime were virtually absent which was inconsistent if the reaction was incomplete. From the diffraction pattern, a large number of reflexions remained unidentified. These were discovered later to be associated with oxysulphide compounds formed during the reaction, see Table 5B.1. These oxysulphide compounds are essentially constituted from FeS and CaO. A detailed description with

possible phase combinations in this system is illustrated in Appendix 1 where an attempt to establish all possible phase relationships has been made. The appendix also covers the X-ray diffraction information of the unidentified oxysulphide compounds. From Appendix 1 it is obvious that a liquid phase exists above 835^{o}C which agrees with the work of Lapin (1.18), whereas the first liquid observed in the reciprocal system FeO-CaS appears at 880^{o}C and about 77 mole pct of FeO (2.28). The liquid formed under this condition is not the Fe-S-O liquid as observed by a few workers (2.15-2.19). If that would have been the case the liquid on cooling would have eutectically decomposed at 915^{o}C and would have formed FeO and FeS at room temperature. The formation of such a liquid at 850^{o}C is also ruled out.

The sulphide was reduced with coal over a range of temperatures and the rates of reduction of sulphides are shown in fig 5B(2). With increasing temperature, both the extent and the rate of reaction were found to increase. Contrary to reduction with graphite, at 800^{o}C significant reduction was observed with coal. Several of the reaction products were analysed using the X-ray diffraction technique and the results show that between six to seven phase combinations are possible at one temperature. In a five component system,such phase combinations are impossible according to Gibbs Phase Rule. Depending upon conditions, oxysulphides were found in the presence of lime, FeS, CaS and iron. The reduced samples were examined using the optical microscope and evidence of a liquid phase above 850^{o}C was discovered by inspecting the morphology of the product formed. The microstructure also shows, see plate 5B.1, the nucleation of iron in the matrix which was analysed using Energy Dispersive X-ray Spectral Technique and was found to be an oxysulphide compound.

Table 5B.1 Reduction of Fe-Ca-S-O

Mixture Composition	H.Tr Temp °C / Red Temp °C	Mass Balance. Pct Wt Loss	Pct Reduction	Atmos. $P_{O_2} = 10^{-30}$ atm.		X-ray Diffraction analysis. FeS	CaO	FeO	CaS	Fe	Gr	FeO.CaS	FeS:CaO	Fe,C	NO.
FeS:CaO = 1:1	950°C/800°C	0.627/2.35	-/12.09	Graphite crucible Reduction		VW	-	-	S	M	-	-	VS	-	B1
FeS:CaO = 1:1	950°C/800°C	0.627/2.10	-/12.29	Graphite in argon		VW	-	-	S	S	M	-	MS	-	B2
FeS:CaO = 1:1	950°C/800°C	0.627/6.19	-/55.66	CO atm		-	-	-	VS	S	WM	-	-	S	B3
FeS:CaO = 1:2	950°/800°C	0.538/0.208	-/1.49	Graphite crucible Reduction		-	S	-	VS	S	-	VW	M	-	B4
FeS:CaO = 1:2	950°C/800°C	0.538/2.57	-/2.57	Graphite and Argon		-	S	-	VS	MS	M	VW	VW	-	B5
FeS:CaO = 1:2	950°C/800°C	0.538/4.34	-/54.33	CO		-	S	-	S	S	WM	-	WM	S	B6
FeO:CaS = 1:1	1000°C/900°C	0.295/14.17	-/85.02	Graphite and Argon		S	-	VW	VS	VS	WM	-	-	-	B7
FeO:CaS: = 2:1	1000°C/900°C	5.11/25.97	-/111.30	Graphite and Argon		VW	WM	-	VS	VS	WM	VW	VW	-	B8
FeO:CaS = 2:5:1	1000°C/900°C	0.595/19.28	-/77.71	Graphite and Argon		VW	-	-	MS	VS	M	VW	WM	-	B9
FeO:CaS = 1:1 up to 'c' dep (5 hrs)	950°C	10.83/0.659	100	CO	Bulk	-	-	-	VS	S	-	-	-	W	B10
					Shell	W	-	-	VS	VS	-	-	-	WM	
FeS:CaO = 1:1 up to 'o' loss (3 hrs)	950°C	11.93	106.14	CO	Bulk	-	-	-	VS	S	-	-	-	-	B11
					Shell	W	-	-	VS	VS	-	-	-	-	
FeS:CaO = 1:1 up to the end of plateau 60 mins	950°C	7.66	68.15	CO	Bulk	S	-	-	VS	M	-	-	WM	-	B12
					Shell	W	W	-	VS	VS	-	-	-	-	

Table 58.1 Contd. Reduction of Fe-Ca-S-O

Mixture Composition	H.Tr Temp °C	Red Temp °C	Mass Balance. Pct Wt Loss	Pct Reduction	Atmos. $P_{O_2} = 10^{-30}$ atm.	X-ray Diffraction analysis. FeS	CaO	FeO	CaS	Fe	Gr	FeO.CaS	FeS:Ca	Fe,C	NO.
FeS:CaO = 1:1 up to the beginning of plateau 40 min	950oC		5.80	51.58	CO Bulk	VW	-	-	VS	M	-	-	M	+	B13
					Shell	VW	-	-	VS	VS	-	-	M	-	
FeS:CaO:Gr = 1:1:2	1000°C		15.80	95.80	P_{CO} = 0.5 atm	+	-	-	VS	VS	VW	-	-	VW	B14
FeS:CaO:Gr = 1:1:2	850°C		11.54	69.21	P_{CO} = 0.5 atm	VW	-	-	VS	VS	WM	-	W	-	B15
FeS:CaO:(C+Gr) = 1:1:2	1000°C		17.49	104.85	P_{CO} = 0.5 atm	-	-	-	VS	MS	-	-	W	-	B16
FeS:CaO:Gr = 1:2:2	1000°C		11.15	92.00	P_{CO} = 0.5 atm	-	S	-	VS	MS	W	-	-	-	B17
FeS:CaO:Gr+Li_2CO_3	800°C		8.09	48.49	Argon	S	VS	VW	MS	MS	WM	-	-	-	B18
FeS:CaO:Gr = 1:2:3	850°C		9.57	85.24	Argon	W	-	-	VS	VS	WM	-	M	-	B19
FeS:CaO:Gr+Coal = 1:1:2	900°C		16.51	100.99	Argon	W	VW	-	VS	VS	W	-	W	-	B20
FeS:CaO:Coal+Gr = 1:1:2	800°C		5.87	36.12	Argon	WM	WM	-	M	M	VW	M	M	-	B21
FeS:CaO:Gr = 1:2:2	1050°C		12.91	105.97	Argon	-	-	-	VS	VS	VW	-	VW	-	B22
FeS:CaO:Gr = 1:1:2	850°C		6.13	36.76	Argon	WM	-	-	MS	W	M	-	MS	-	B23
FeS:CaO:Coal = 1:1:2	850°C		10.31	62.94	Argon	W	W	-	VS	VS	W	W	M	-	
FeS:CaO:Coal (1:1:2)	900°C		16.48	100.6	Argon	W	VW	-	VS	VS	VW	VW	WM	-	B24

Table 58.1 Contd. Reduction of Fe-Ca-S-O

Mixture Composition	H.Tr Temp °C / Red Temp °C	Mass Balance. Pct Wt Loss	Pct Reduction	Atmos. $P_{O_2} = 10^{-30}$ atm.	X-ray Diffraction analysis. FeS	CaO	FeO	CaS	Fe	Gr	FeO.CaS	FeS:CaO	Fe,C	NO.
FeS:CaO:C = 1:2:2	850°C	9.96	79.57	Argon	WM	M	-	VS	M	WM	VW	M	-	B25
FeS:CaO:C = 1:2:2	900°C	13.31	106.22	Argon	-	M	-	VS	VS	WM	-	VW	-	B26
FeS:CaO:C = 1:2:2	950°C	12.62	100.11	Argon	-	M	-	VS	VS	WM	-	VW	-	B27
FeS:CaO:C = 1:2:2	1000°C	12.55	100.16	Argon	-	M	-	VS	VS	WM	-	VW	-	B28
FeS:CaO:Coal = 1:2:2	800°C	3.76	30.53	Argon	W	M	W	VS	W	VW	WM	W	-	B27
FeS:CaO:Coal = 1:2:2	850°C	7.004	56.86	Argon	VW	S	-	VS	WM	W	VW	M	-	B28
FeS:CaO:Coal = 1:2:2	950°C	12.17	98.86	Argon	W	M	-	VS	MS	VW	-	W	-	B29
FeS:CaO:Gr = 1:1:3	850°C	1.37	15.10	Argon	-	VW	-	VS	W	WM	-	VS	-	B30
FeS:CaO:Gr = 1:1:3	950°C	15.25	98.03	Argon	VW	-	-	VS	VS	WM	-	-	-	B31
FeS:CaO: = 1:2:3	950°C	11.73	98.8	Argon	VW	M	-	VS	VS	WM	-	WM	-	B32
FeS:CaO = 1:1	800°C	6.21	55.69	CO	M	WM	-	VS	VS	-	-	VW	M	B33
FeS:CaO = 1:1	850°C	7.76	69.61	CO	WM	WM	-	VS	VS	-	-	VW	WM	B34
FeS:CaO = 1:1	900°C	11.57	103.74	CO	W	-	-	VS	VS	-	-	-	VS	B35
FeS:CaO = 1:1	1000°C	13.06	117.60	CO	VW	-	-	VS	VS	-	-	VW	-	B36
FeS:CaO = 1:2	800°C	4.35	54.36	CO	-	S	-	VS	WM	-	-	WM	M	B37
FeS:CaO = 1:2	850°C	7.63	95.36	CO	-	S	-	VS	VS	-	-	M	WM	B38

Table 58.1 Contd. Reduction of Fe-Ca-S-O

Mixture Composition	H.Tr Temp °C	Red Temp °C	Mass Balance. Pct Wt Loss	Pct Reduction	Atmos. $P_{O_2} = 10^{-30}$ atm.	X-ray Diffraction analysis. FeS	CaO	FeO	CaS	Fe	Gr	FeO.CaS	FeS:C	Fe,C	NO.
FeS:CaO = 1:2	900°C		7.51	93.80	CO	-	S	-	VS	VS	-	-	WM	WM	B39
FeS:CaO = 1:2	950°C		8.05	100.58	CO	VW	S	-	VS	VS	-	-	-	W	B40
FeS:CaO = 1:2	100°C		8.87	106.71	CO	VW	S	-	VS	MS	-	VW	VW	-	B41
FeS:CaO:C = 1:1:2 with Li_2CO_3	800°C		15.59	95.39	Argon	W	W	-	VS	VS	WM	-	-	-	B42

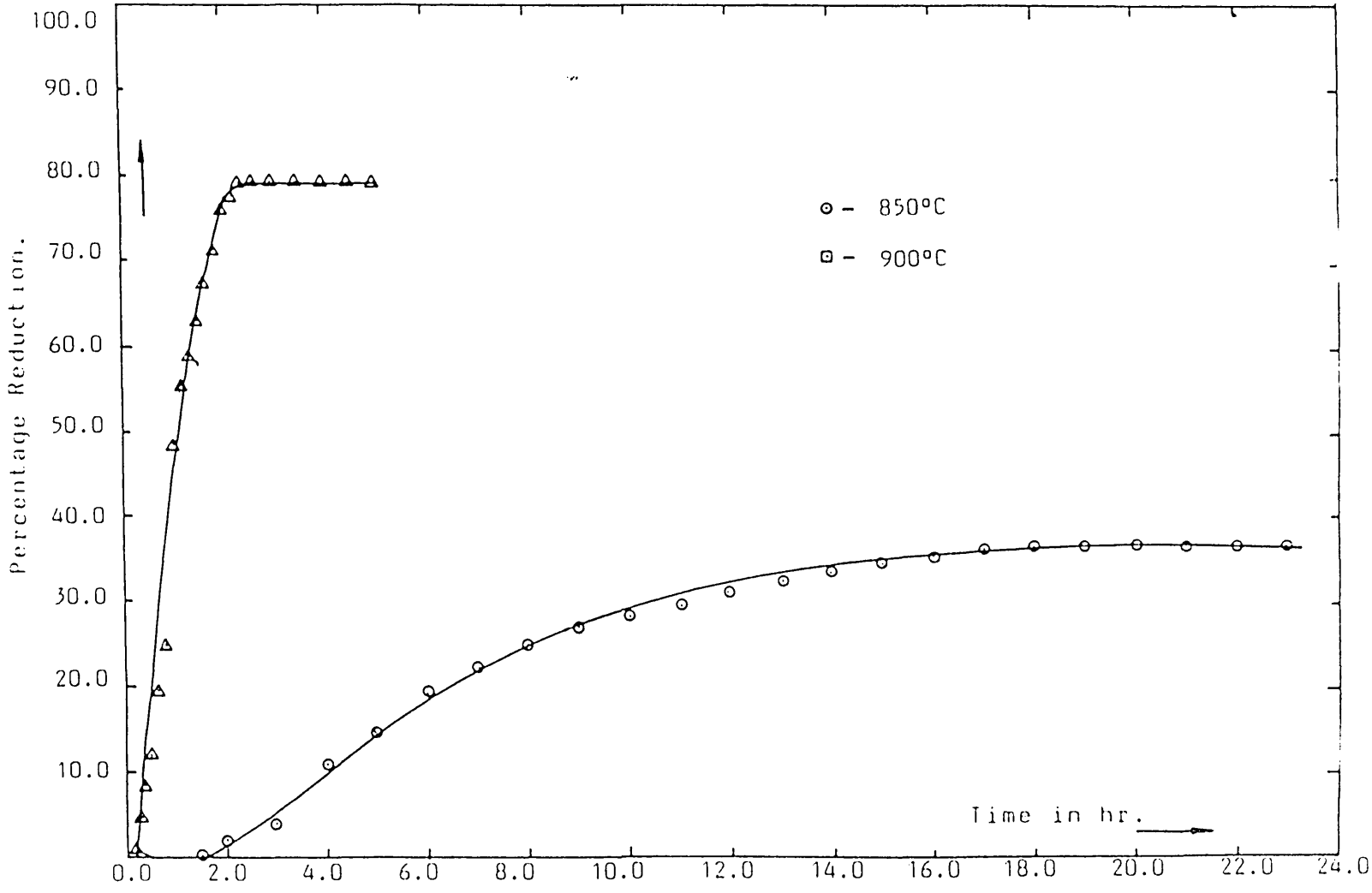
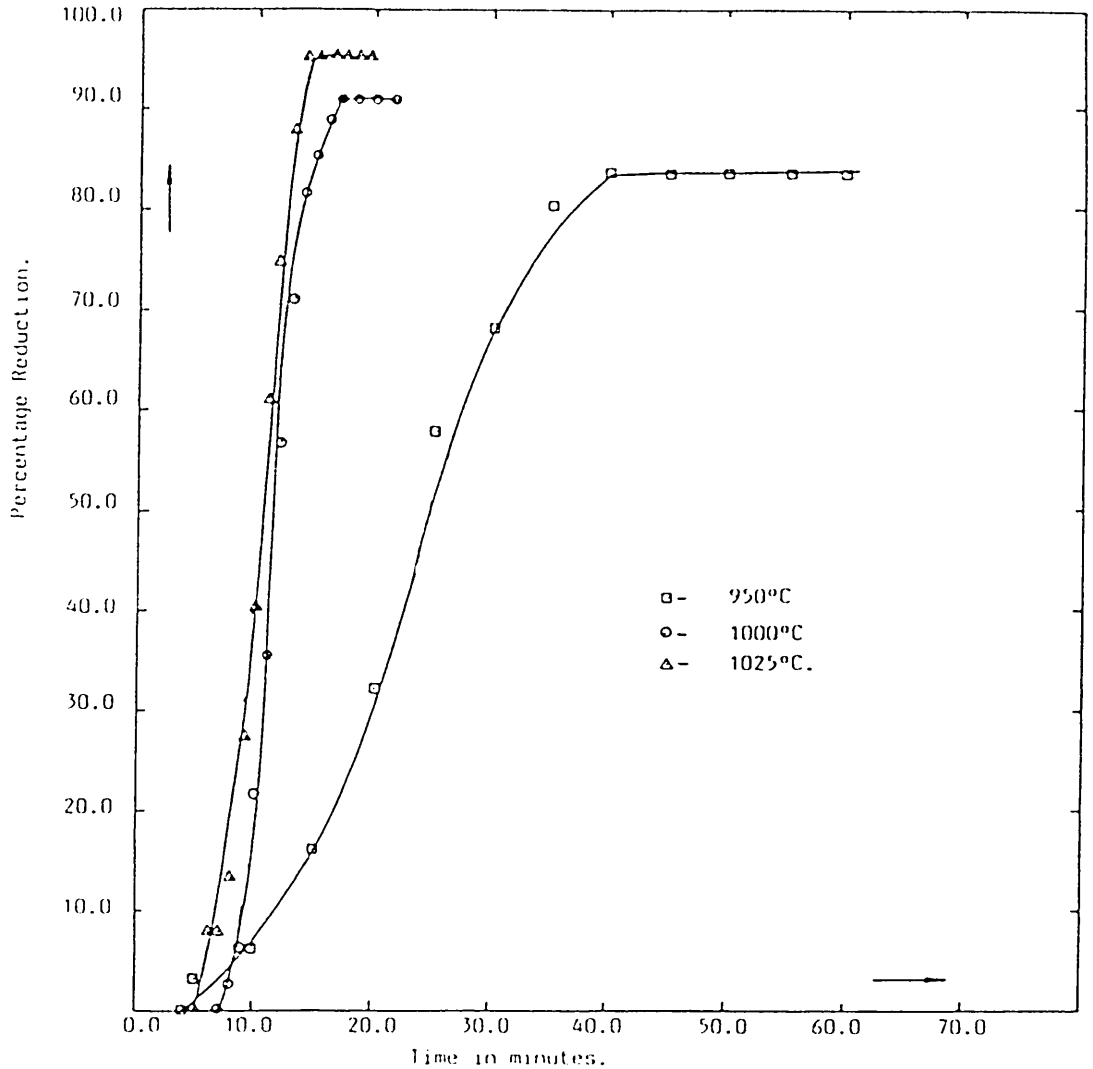


Fig. (5B.1a) Rate of reduction of iron sulphide ($Fe_{1-x}S$) in presence of lime and graphite (FeS:CaO:C = 1:1:2). Atm-Argon.



Fig(5B.1b): Rate of reduction of $Fe_{1-x}S$ with graphite in presence of CaO(S:O:C=1:1:2).

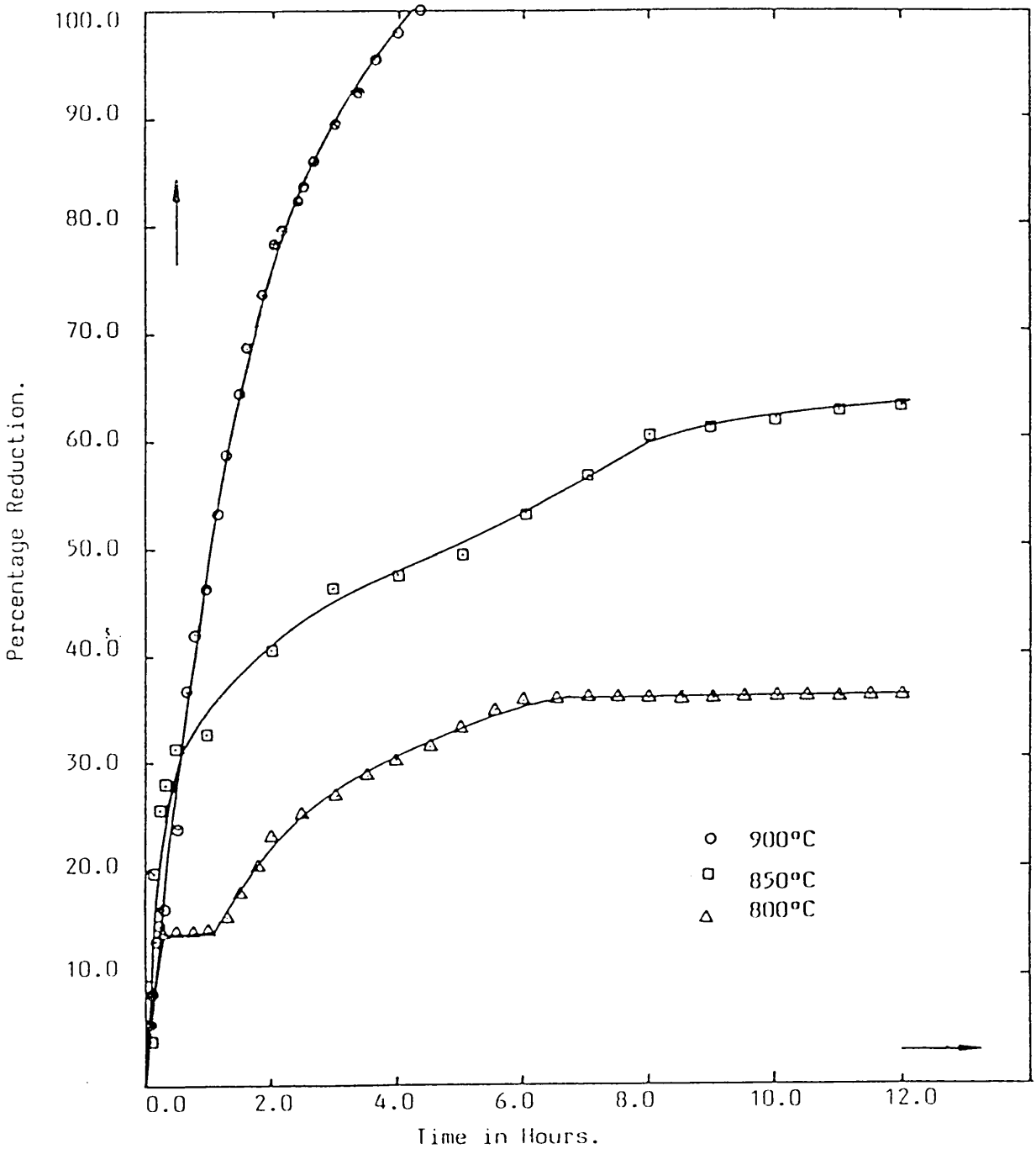


Fig (5B.2a) Rate of reduction of ($Fe_{1-x}S$) with coal in presence of lime (FeS:CaO:Coal = 1:1:2). Atm-Argon.

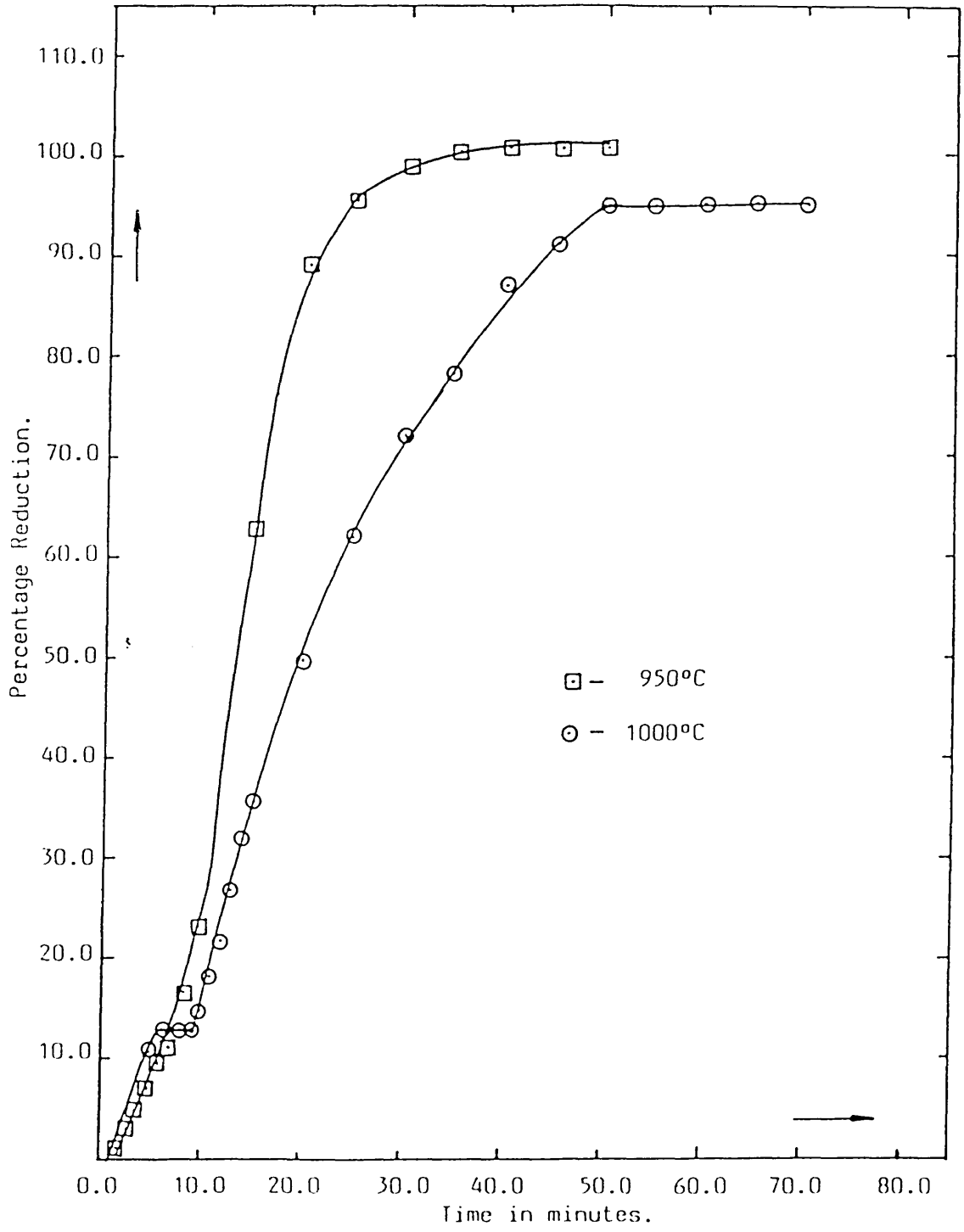
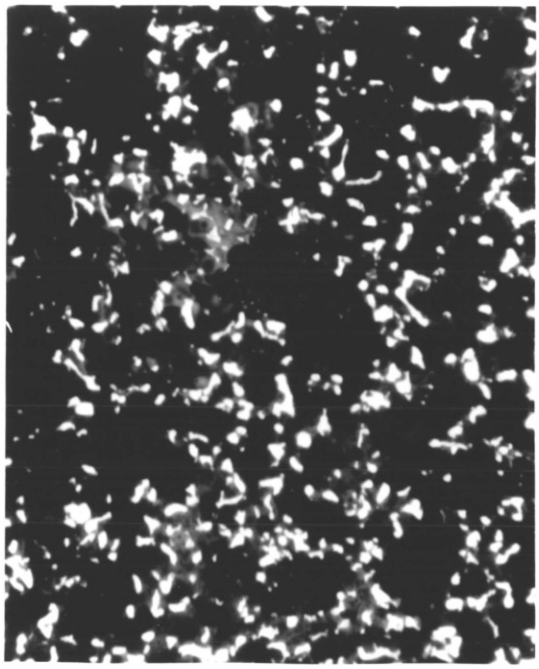
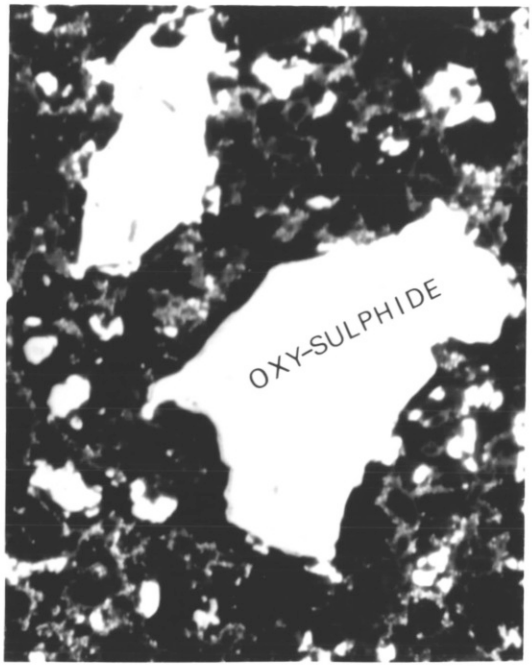


Fig (58.2b) Rate of reduction of $Fe_{1-x}S$ with coal in presence of CaO ($Fe_{1-x}S$:CaO:Coal = 1:1:2) Atm-Argon.

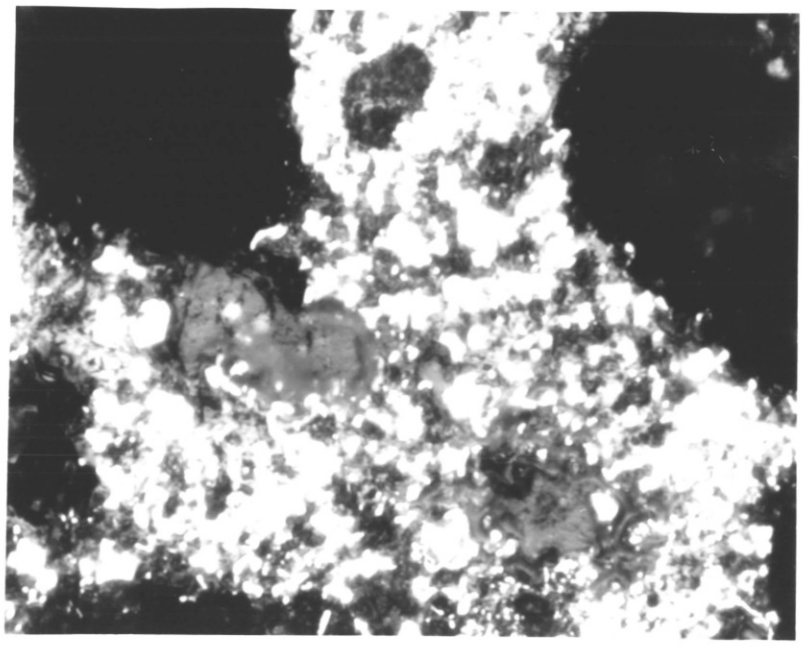
PLATE 5B.1



a x 300



b x 300



c x 300

Plate 5B.1 Reduction of iron sulphide with lime (S:O:C = 1:2:2)
(a) Small nuclei of iron growing from oxysulphide phase during the reduction at 850° with coal
(b) Formation of oxysulphide at 850°C
(c) Variation in iron nuclei size in the reduced sulphide at 900°C with coal

Temporary arrests of 5 minutes and 45 minutes were observed in the rate curves at 950^{o}C and 800^{o}C respectively. Such a feature was completely absent during the reduction of pyrrhotite with graphite.

The overall reduction reaction is governed by two steps - the exchange reaction and the reduction reaction. Since the rate of the exchange reaction can be altered by altering the quantity of lime in the pellet which governs the surface area of lime on the overall reaction, experiments were carried out with an increased lime to sulphide ratio. The effect of coal and graphite was investigated and the rates of reduction under these conditions are shown in figs 5B(3a) and 5B(3b). Although a complete reduction was observed in the case of graphite and above 900^{o}C it is evident that the reduction reaction was incomplete as confirmed by X-ray diffraction data. A higher weight loss was observed due to the presence of carbonated lime which on heating liberated CO_2. The reduction was also incomplete in the case of coal. The failure of the reaction to reach completion indicates that in the later stages problems associated with the physical separation of the reactants may be responsible for the permanent cessation. However, no microstructural evidence of the physical separation of reactants was observed. From the comparison of the rate of reduction curves, it is evident that above 900^{o}C the rates are adversely affected by the presence of the increased ratio of lime to sulphide. A possible explanation for the relative retardation of the reaction can be given by invoking the physical changes observed during the heat-treatment of FeS and CaO mixtures, illustrated in Appendix 1. Complete liquefaction

of the mixture was observed when the mixture FeS:CaO = 1:1 was heated in an argon atmosphere at 900^{o}C, whereas no such change was observed in the case of FeS-CaO = 1:2 at 900^{o}C. The mixture, after heat-treatment contained a solid phase with only about 10-15pct of liquid phase by volume. Such conditions prevail and it seems to be the relative volume of the oxysulphide melt at that temperature which determines the rate of reduction. A large volume of liquid provides a relatively large surface area for the reduction reaction.

The combined effect of enhanced proportions of lime and graphite demonstrated that at lower temperatures, lime has the significant effect on the rate of reduction of pyrrhotite, for the same carbon to sulphide ratio. Little difference in the rate of reaction was observed at higher temperatures which proves that the presence of a large volume of liquid has a dominant effect on the rate when the lime to sulphide ratio is doubled.

During the course of direct reduction of sulphide carbon monoxide gas is generated which is a potential reducing agent. This gas also participates in the reduction process and hence its effect on the rate of reduction of FeS was investigated. Stoichiometric mixtures of FeS and CaO in the form of cylindrical pellets were heated isothermally in a flowing stream of argon. Once isothermal conditions were attained, the reducing gas was introduced into the apparatus. The rates of reduction for the ratios 1:1 and 1:2 of sulphide and lime are shown in fig 5B(5a) and (5b). The rates of reduction of FeS with CO at temperatures above 950^{o}C were found to be shown than the rates observed in the case of coal and graphite. At and below 900^{o}C the rate of reduction of FeS with CO was faster than that

observed with coal and graphite. This particular variation of the rate of chemical reaction differs from the concept of its dependence on the temperature.

The Arrhenius Relationship for any chemical reaction is a universally accepted fact, so it can be conclusively said, that a change in rate controlling step occurs. Microsctuctural examination of the reduced samples was carried out and the typical results are shown in plate 5B.2 and 5B.3. The morphological difference of iron particles produced at different reducing temperatures can be seen. It is worth noticing that the nucleation of iron started around the pores at 850^{o}C and this is significantly different from observations at 950^{o}C. At 950^{o}C, the periphery of pellet appears to be richer in iron than the core, whereas at 1000^{o}C, the reduced iron resembles a eutectic cellular morphology. Above 950^{o}C in the case of FeS:CaO = 1:1 a temporary arrest in the rate of reduction curve was observed. The presence of the arrest in the rate curve indicates that gas evolution has temporarily ceased. In order to understand the mechanism of reduction along the arrest, the reaction was stopped at the beginning of the arrest, at the end of arrest, after the completion of oxygen loss and after carbon deposition has commenced. The X-ray diffraction data are summarized in Table 5B.1 and the rate of reduction curves for various stages, are shown in fig 5B(6). During the course of reduction of iron sulphide with CO, varying proportions of cementite were observed in the reduced sample. The relative amounts of cementite indicate the extent of carburization iron even when the reduction reaction was incomplete e.g at higher temperatures where cementite is less stable it formation is very difficult.

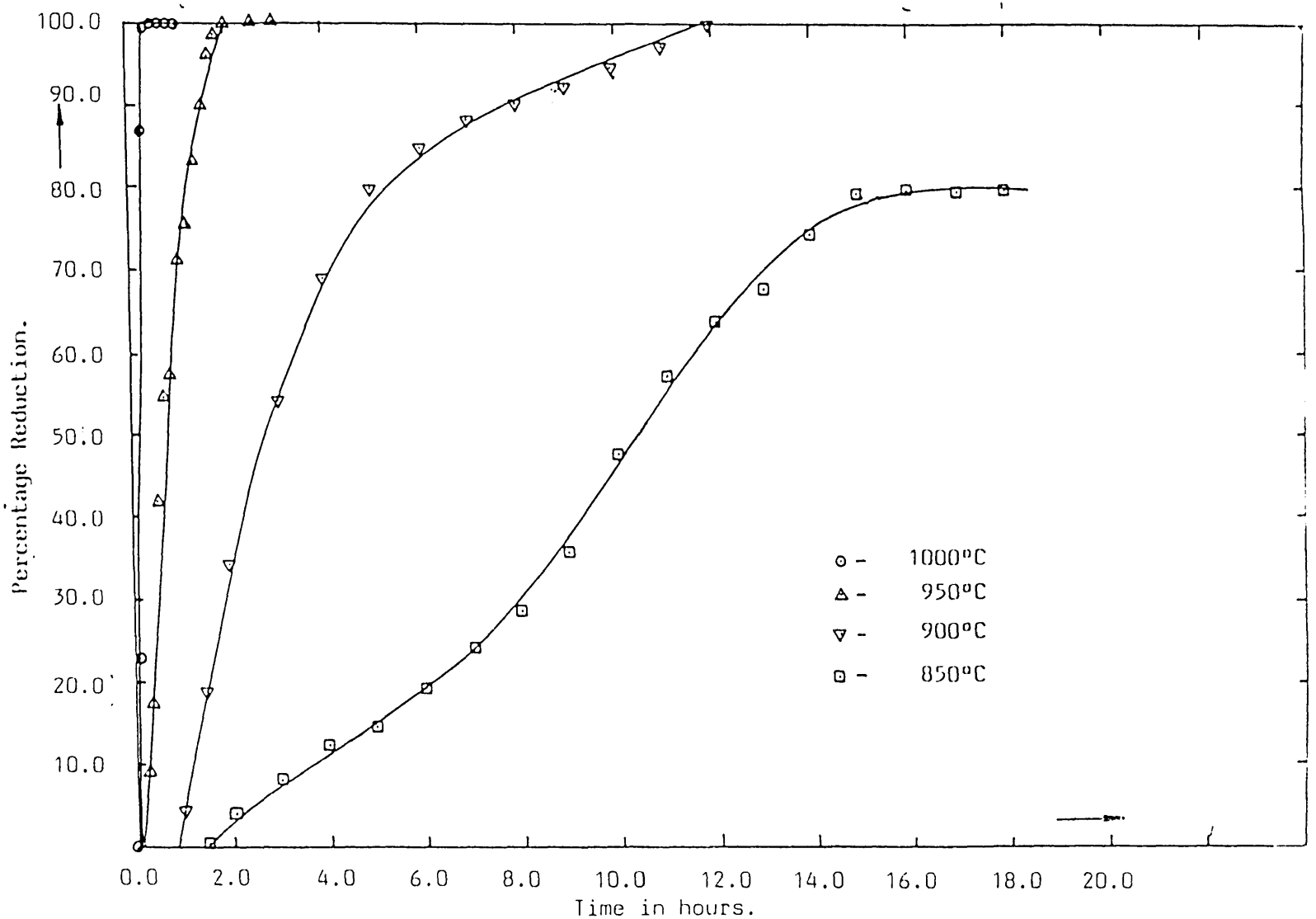


Fig (5B.3a) Rate of reduction of ($Fe_{1-x}S$) with graphite in presence of lime to sulphide ratio (FeS:CaO:C = 1:2:2).

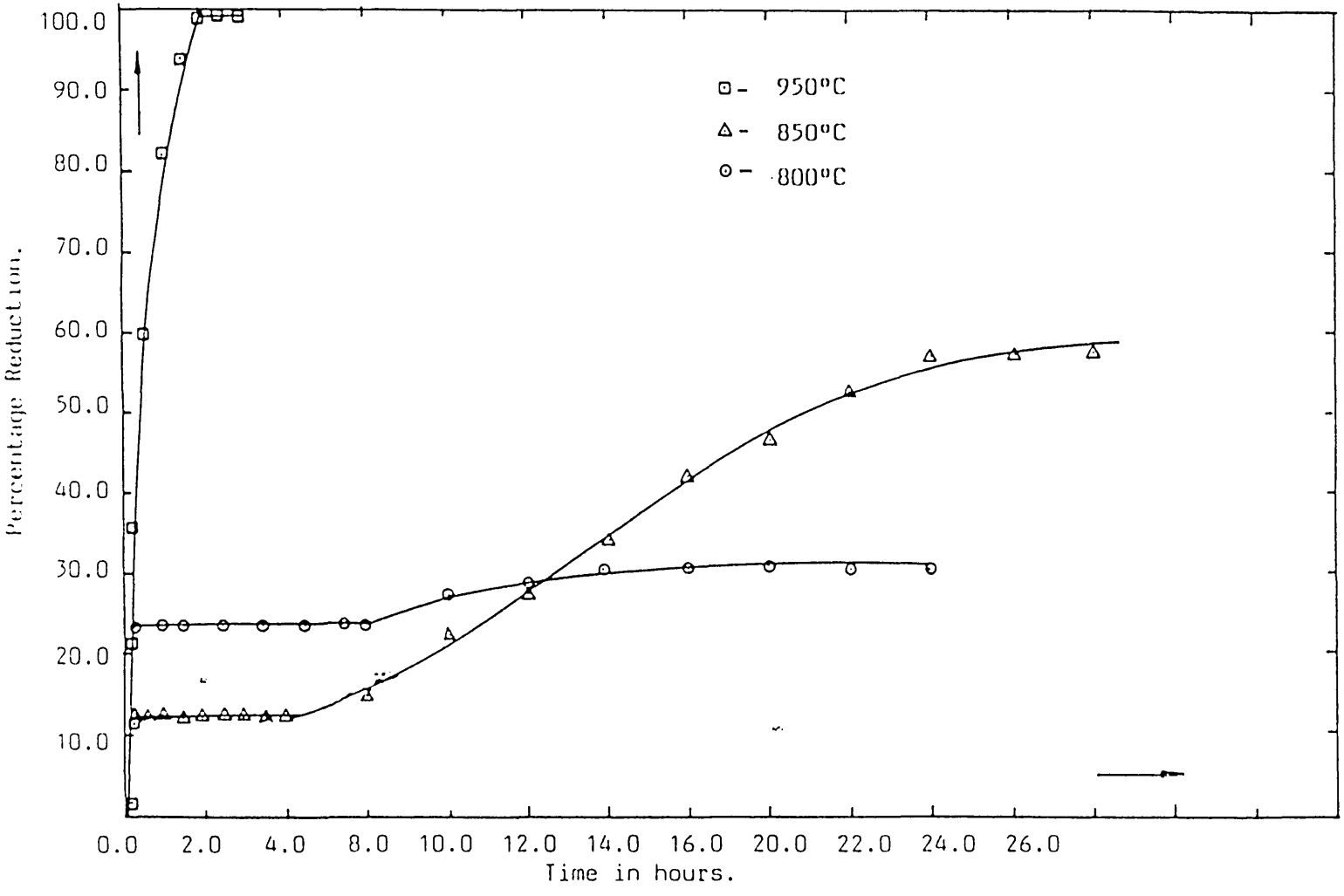


Figure (5B.3b) Rate of reduction of $Fe_{1-x}S$ with coal in presence of lime (CaO:FeS:Coal) = (2:1:2) Atm-Argon.

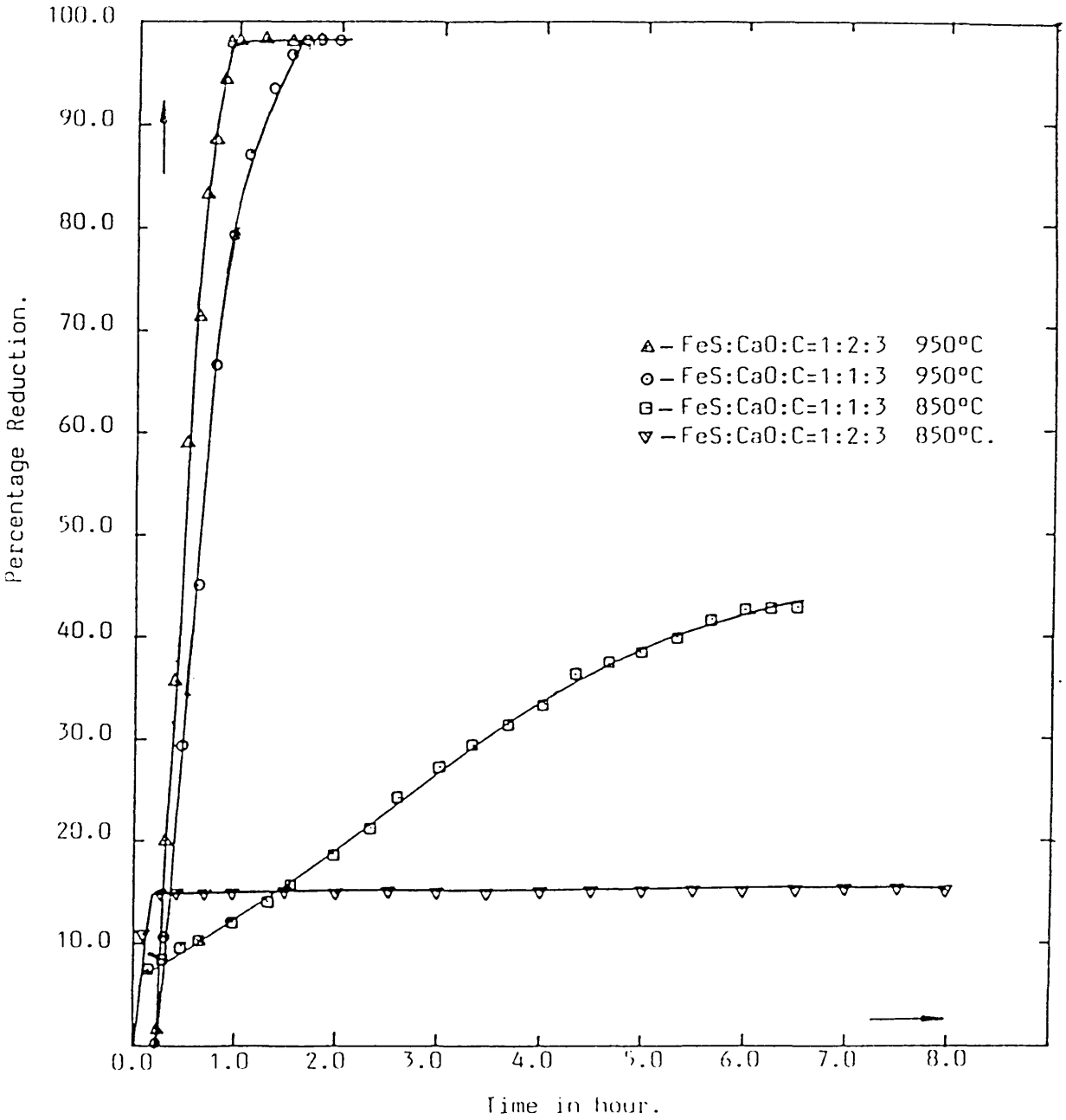


Fig (5B.4) Rate of reduction of ($Fe_{1-x}S$) with enhanced graphite to sulphide and lime to sulphide ratios.

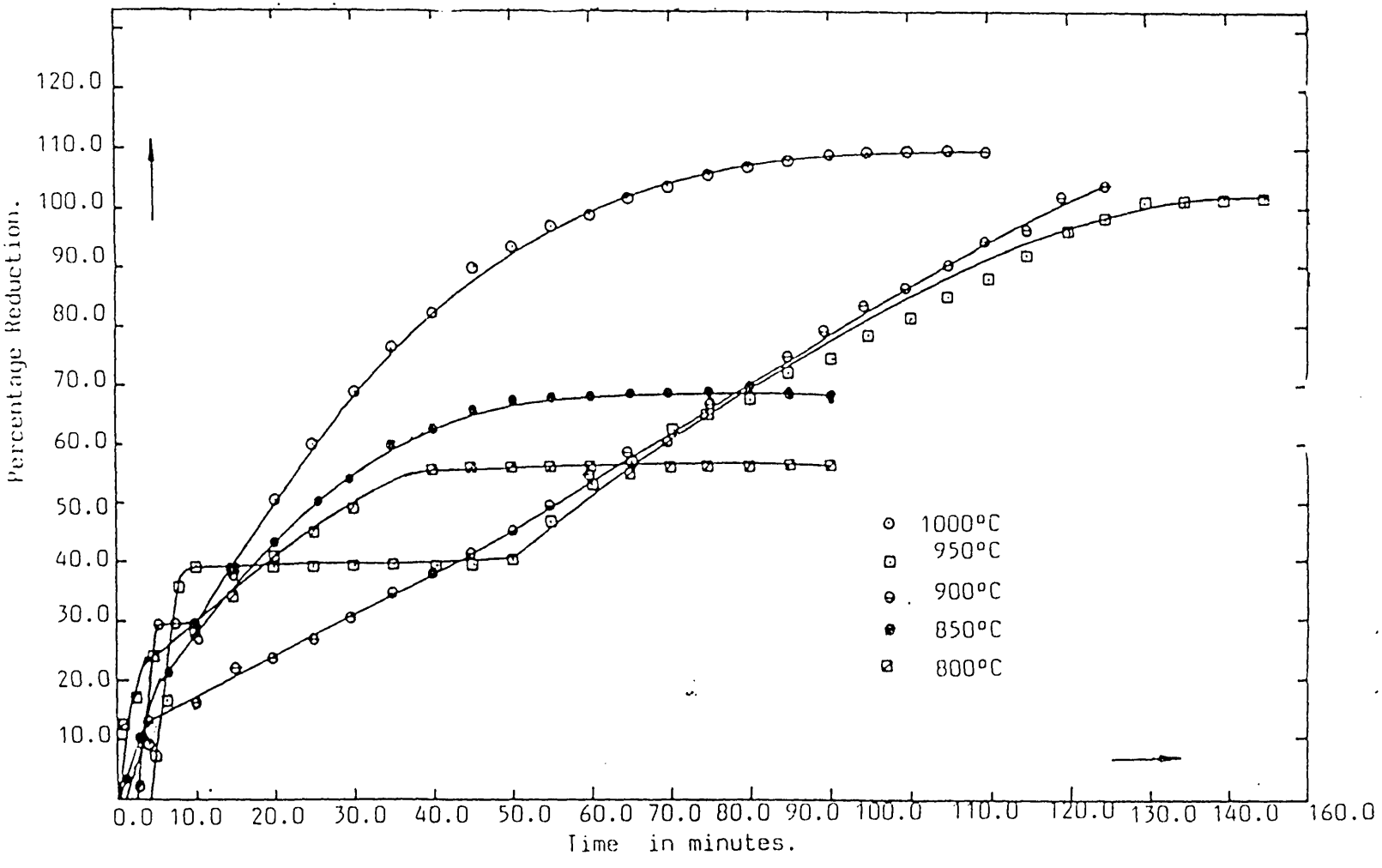


Fig (5B.5a) Rate of reduction of $Fe_{1-x}S$ with CO in presence of lime (FeS:CaO = 1:1)

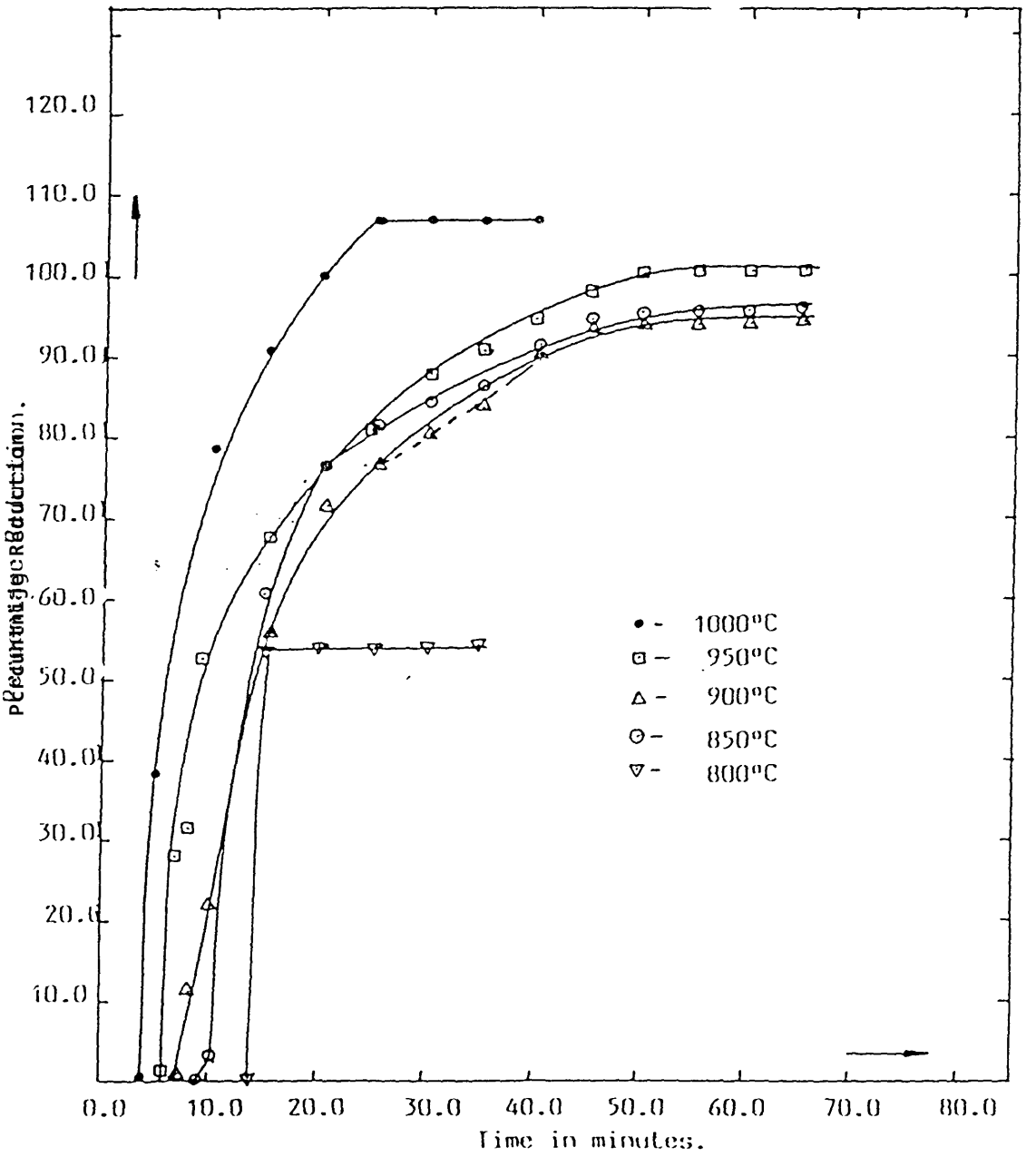


Fig (5B.5b) Rate of reduction of ($Fe_{1-x}S$) with CO in presence of excess lime (FeS:CaO = 1:2).

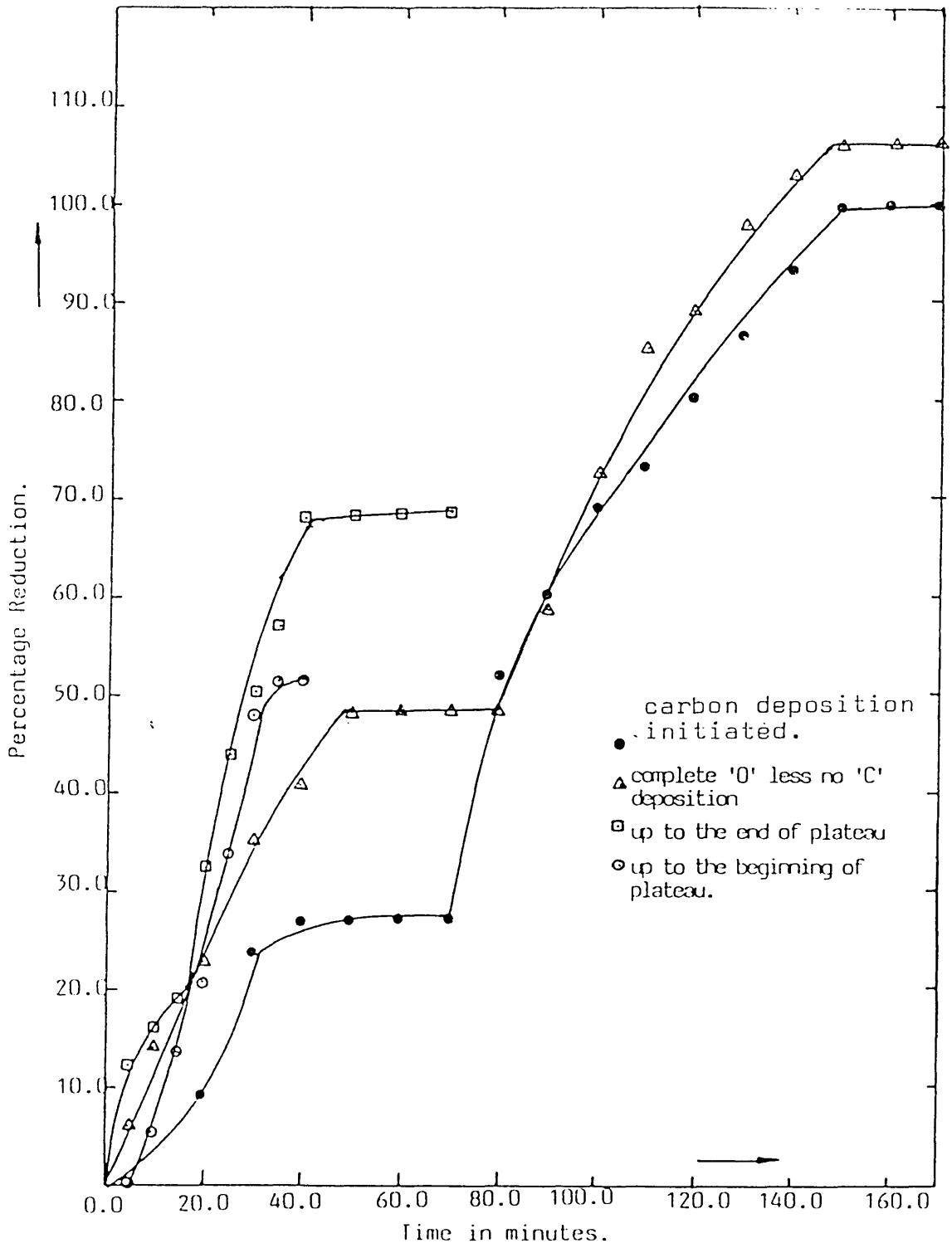
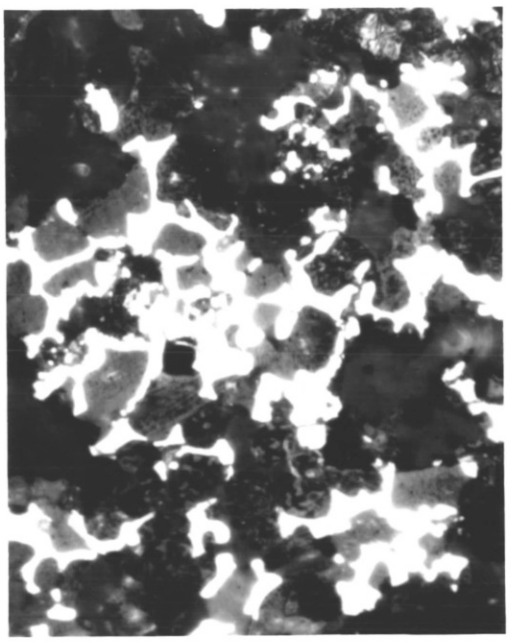
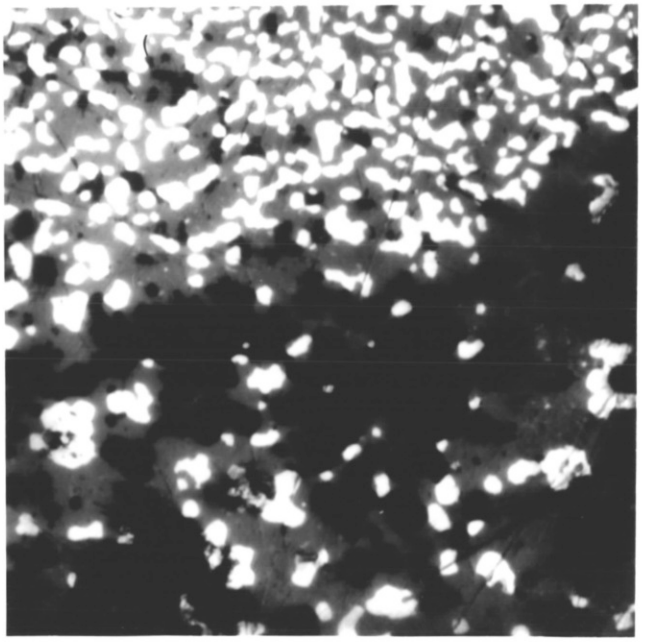


Fig (58.6) Different stages during the rate of reduction of $Fe_{1-x}S$ with CO in presence of lime at 950°C.

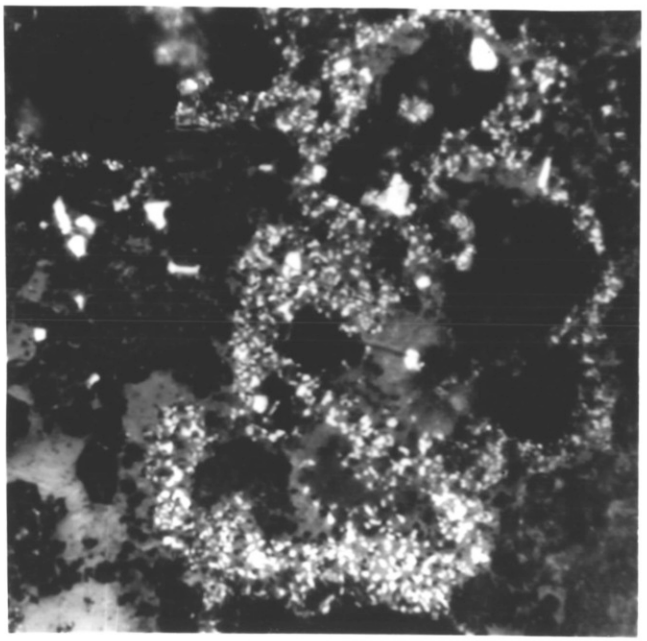
PLATE 5B.2



a x 300



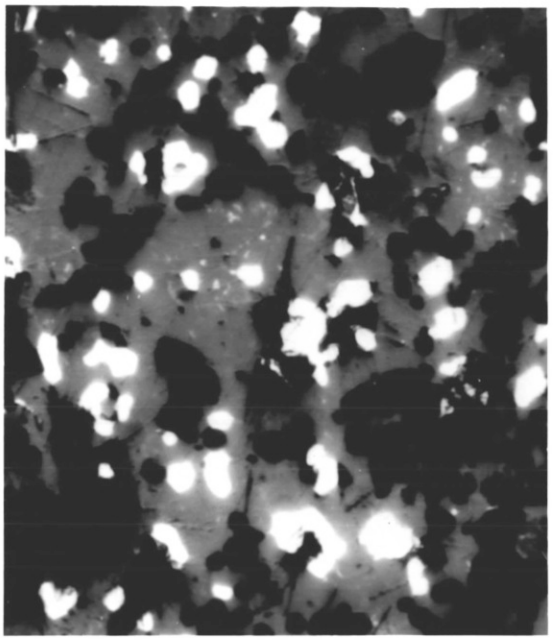
b x 300



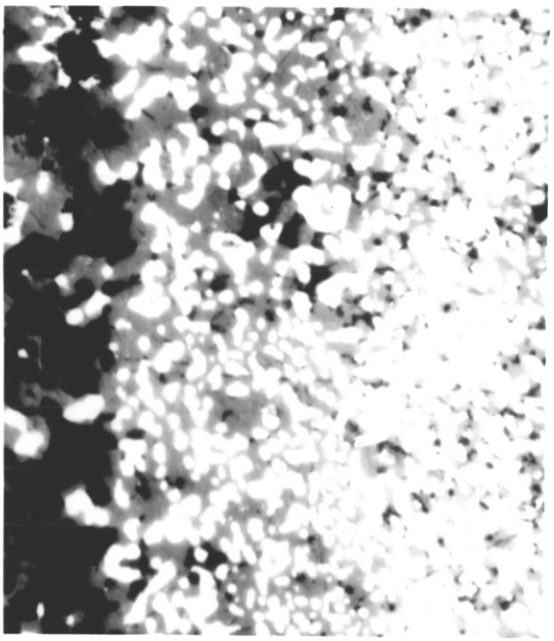
c x 500

Plate 5B.2 Reduction of iron sulphide with lime and carbon monoxide.
(a) Eutectically formed iron at 1000°C
(b) Iron rich and iron depleted regions at 950°C
(c) Very small nuclei of iron around the pores at 850°C

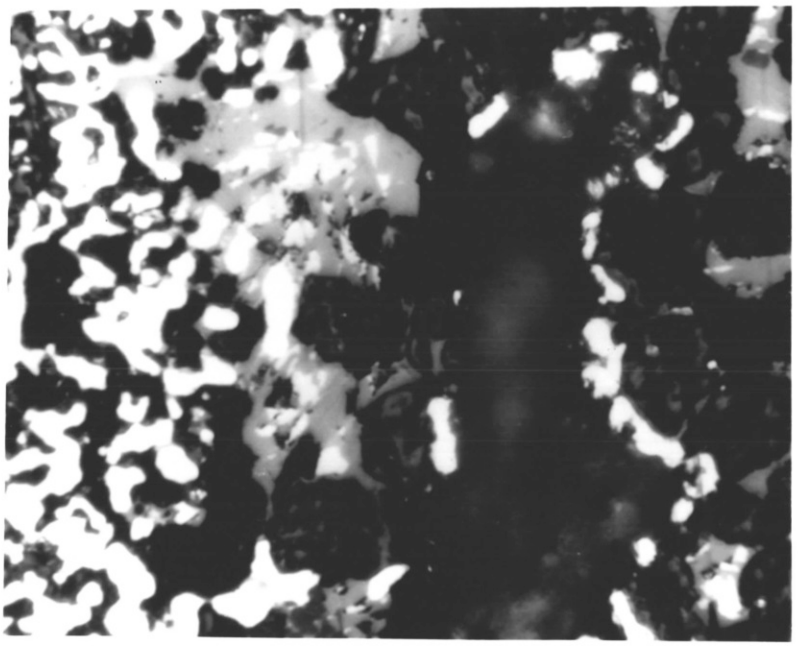
PLATE 5B.3



a x 300



b x 300



c x 800

Plate 5B.3 FeS:CaO = 1:1 at 950°C with CO.
(a) Iron from reduced oxysulphide in the core of the pellet
(b) Rim of iron formed on the periphery of pellet
(c) The boundary of dense iron rim (left) and core (right)

A very different and important physical change was observed at 1000°C. The pellet was completely deformed and its original geometry was lost. It was like a molten pool which had solidified containing many gas pores. The reduced samples at 950°C and 1000°C were examined using electron and optical microscopy. A great deal of similarity in the microstructures was observed. The scanning electron microscopic investigation shows the formation of an oxysulphide phase around the lime particles and the presence of some eutectic cellular structure at 950°C with FeS:CaO = 1:1. The cellular colonies and preferential precipitation of oxysulphide phase was also observed in the heat-treated pellets of composition FeS:CaO = 1:2 in argon at 900°C, see plates 5B.4, 5B.5 and 5B.6.

The combined effect of direct and indirect reduction was investigated by reducing FeS:CaO:Coal (or graphite) mixtures under controlled pressures of CO, showing that the rate of reduction is not affected by the relative amounts of coal, graphite and lime at 1000°C. But at 850°C, the rate of reduction is very slow and does not go to completion, see fig 5B(7). With a pellet of increased lime to sulphide ratio, several temporary arrests of short intervals were observed on the rate curve for which an explanation will be given in the next section.

None of these results provide a clear indication of the mechanism of reduction. To investigate the mechanism of reduction, mixtures of FeS and CaO in 1:1 and 1:2 ratios were heat-treated at 950°C in an argon atmosphere and these heat-treated pellets were reduced in a graphite crucible with graphite and CO respectively at 800°C. The X-ray

diffraction results with mass balance analyses are shown in Table 58.1. The rate of reduction curves are shown in figs 58(8a) from which it can be seen that the rate of reduction in the case of FeS:CaO = 1:1 with CO is almost identical with that for FeS:CaO = 1:1 at 900^{o}C with graphite. The results for the rate of reduction of this mixture in a graphite crucible and with graphite were very similar in that both exhibit a long incubation period. The rate of reaction with graphite proceeds with a temporary arrest at 800^{o}C. Comparing CO with graphite reduction and reduction in a graphite crucible the former is much faster. During the course of reduction, cementite formation and carbon deposition were observed. On the basis of mass balance analysis,the percentage weight gain curve is drawn which evidently shows two regimes one linear and one non-linear.

The effect of the catalysed carbon oxidation reaction was investigated by reducing FeS in the presence of Li_2CO_3 (refer no: B18 and B42). The extent of reaction was found to be affected by flow rate of the carrier gas. The flow rate was the only parameter which was altered during these two expeiments. In the former case where only 48pct reduction was observed a flow rate of 500ml per minute of argon was maintained where as the latter experiment was carried out at 150ml per minute. The weight loss observed in the latter case was much greater than the expected theoretical weight loss. In addition, no Li_2CO_3 or Li_2O was observed in the X-ray diffraction pattern which means that all the carbonates were evaporated during the course of reduction. No Li_2CO_3 or Li_2O was observed when the higher flow rate of argon was used. The rate of reduction curve was plotted taking into account the weight loss due to Li_2CO_3. The rate of reduction curve shows a

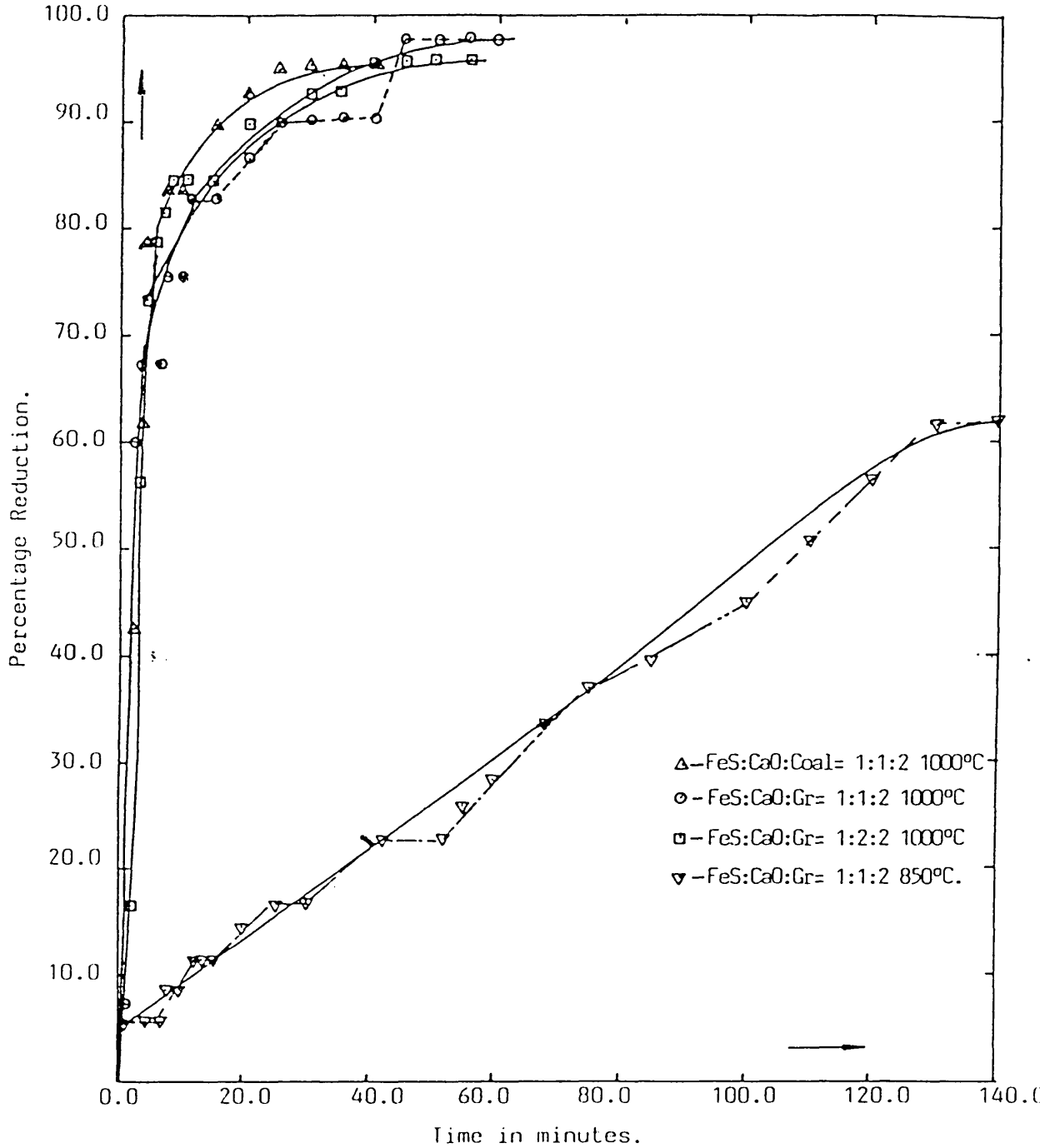
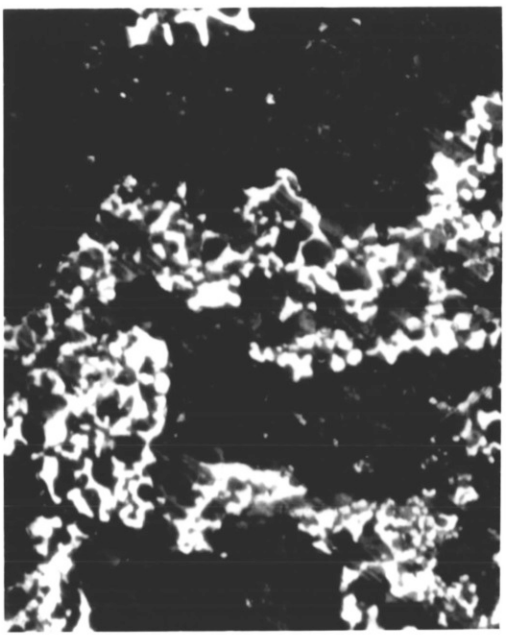
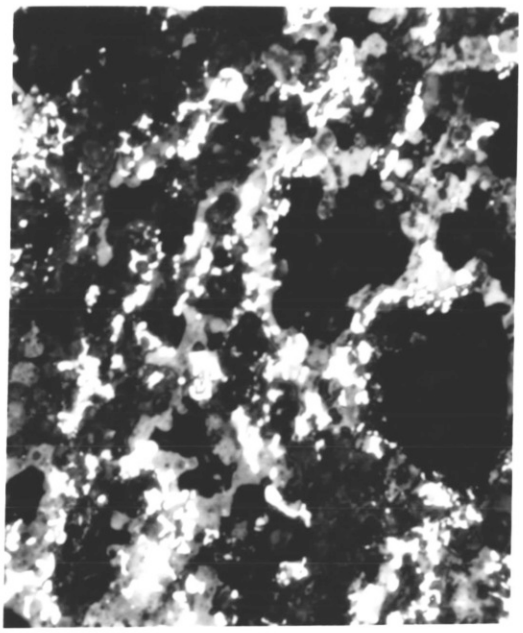


Fig 38(7) Rate of reduction of ($Fe_{1-x}S$) with graphite and coal in presence of lime under controlled atmosphere p_{CO} = 0.5 atm.

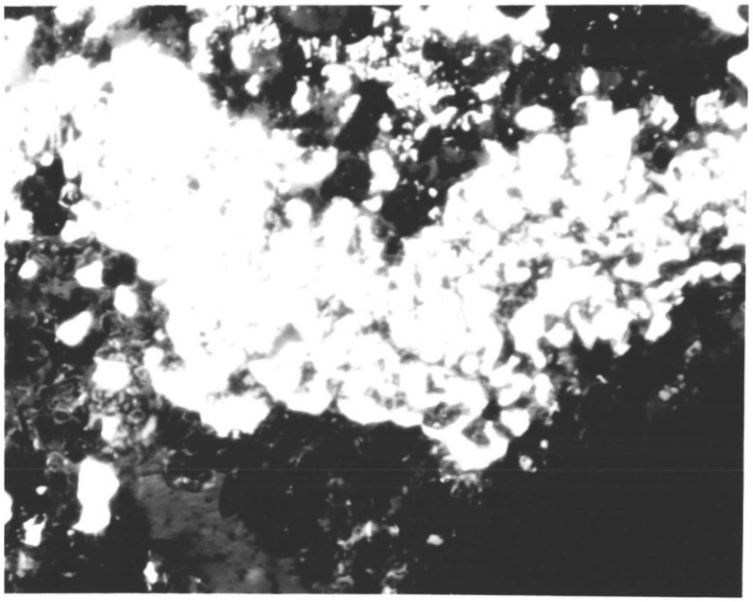
PLATE 5B.4



a x 300



b x 300

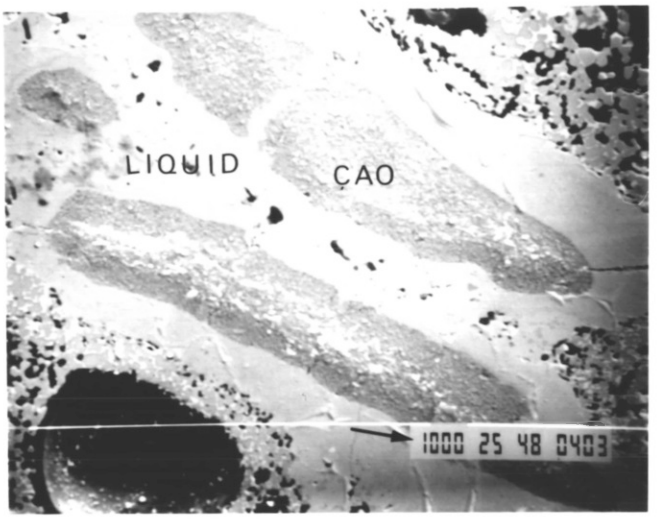


c x 300

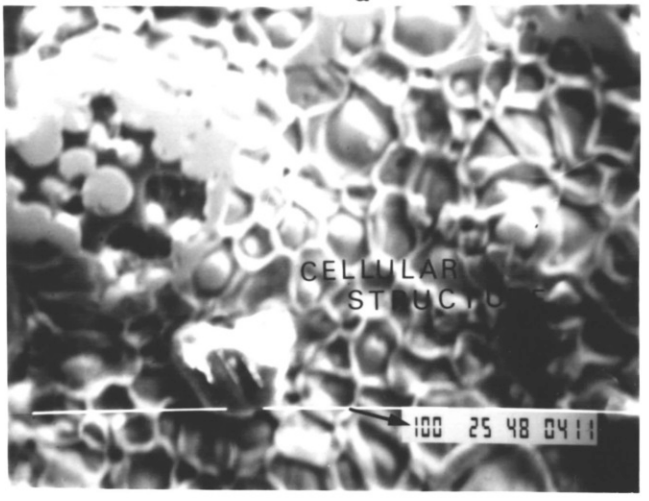
Plate 5B.4 Reduction of iron sulphide with lime.

(a) FeS:CaO = 1:2 at 900°C with CO
(b) FeS:CaO = 1:2 at 1000°C p_{CO} = 0.5 atm
(c) FeS:CaO = 1:2 at 950°C with CO

PLATE 5B.5

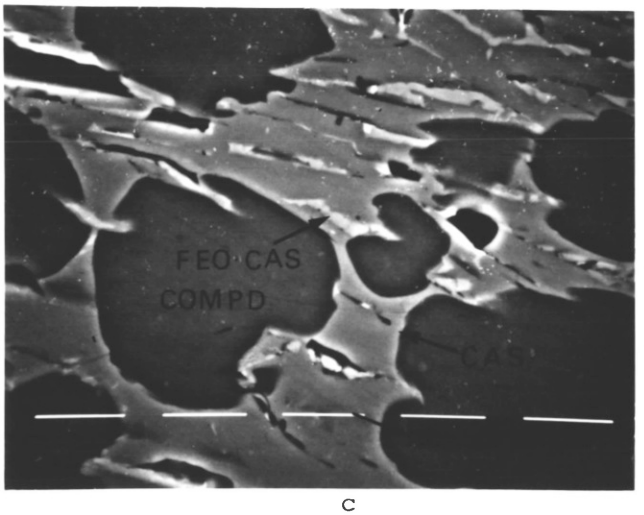


a



b

FeS:CaO



c

Plate 5B.5 Scanning electron micrograph of FeS:CaO = 1:1 pellet reduced with CO at 950°C.
(a) Oxysulphide phase around lime particles during reduction.
(b) Eutectic cellular structure grown in the pellet.
(c) Eutectic colonies formed during the heat treatment of FeS:CaO = 1:2 mixture in argon atmosphere at 900

PLATE 5B.6

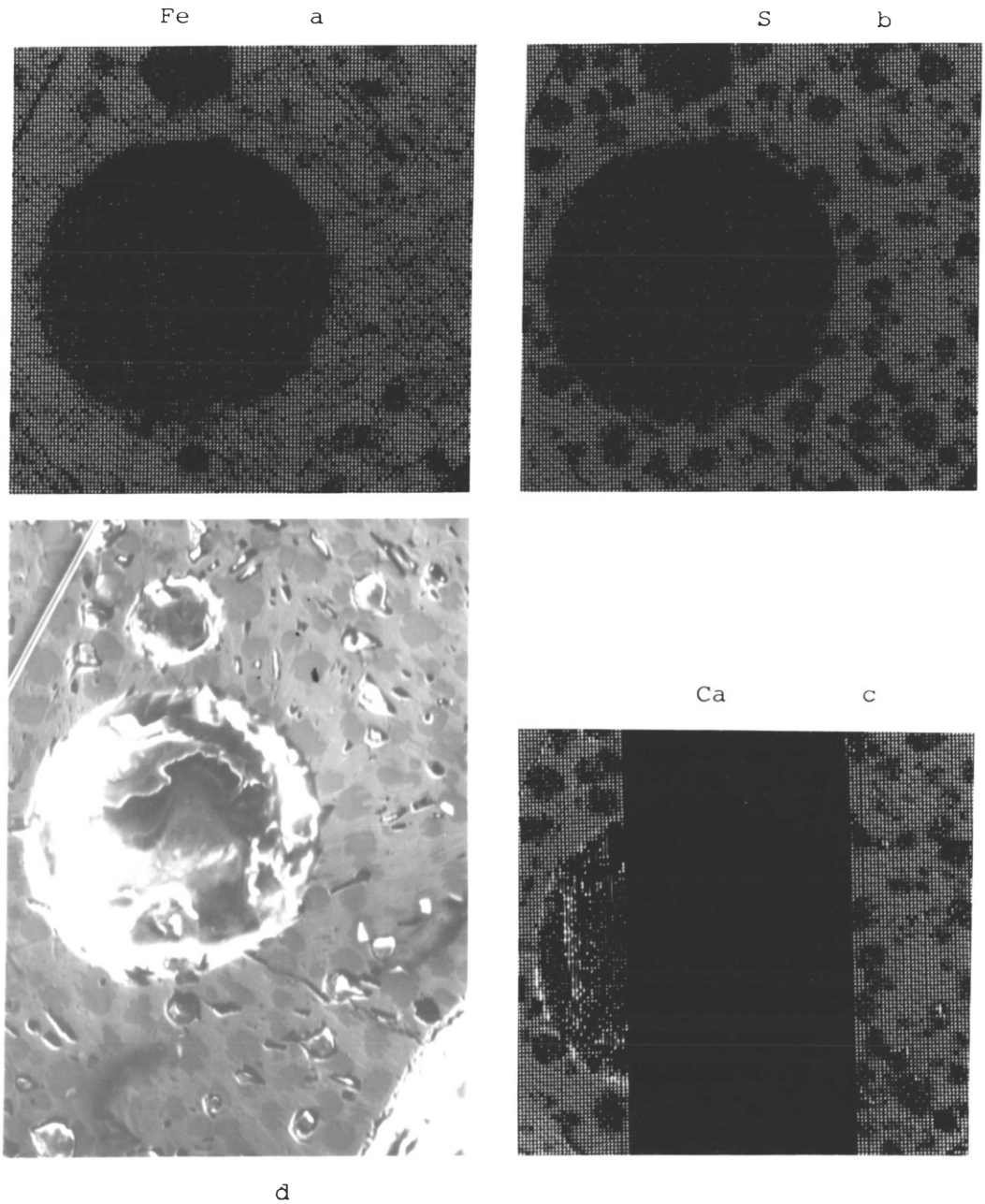


Plate 5B.6 Energy dispersive X-ray ($^{k}\alpha$) analysis of FeS:CaO = 1:2 mixture heat treated at 900°C in argon atmosphere

(a) 'Fe' Elemental distribution
(b) 'S' Elemental distribution
(c) 'Ca' Elemental distribution
(d) Sample area analysed

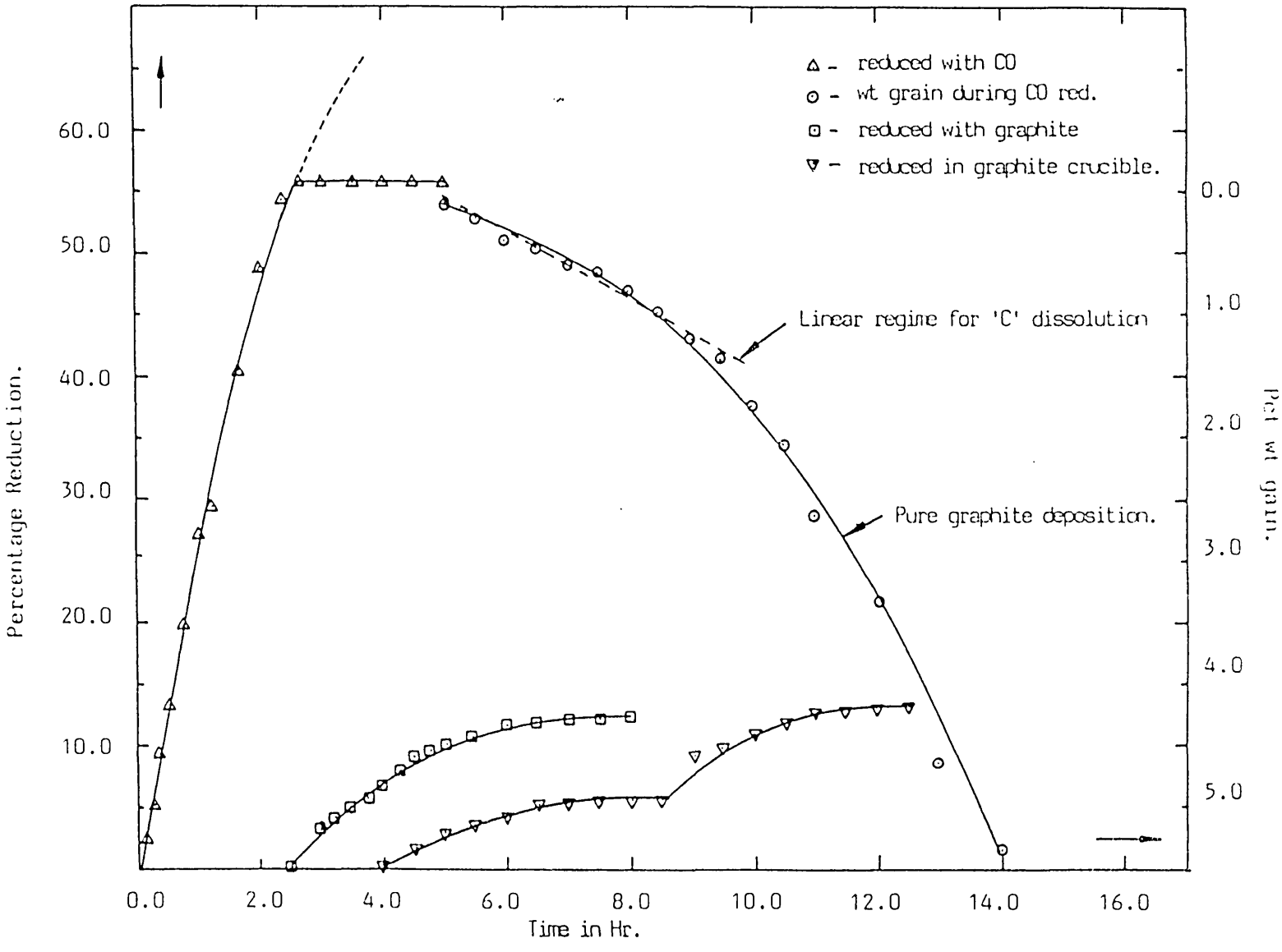


Fig 5B (8a) Rate of reduction of preheat-treated (FeS:CaO = 1:1) mixture at 800°C under different conditons. Preheat-treatment temperature - 950°C.

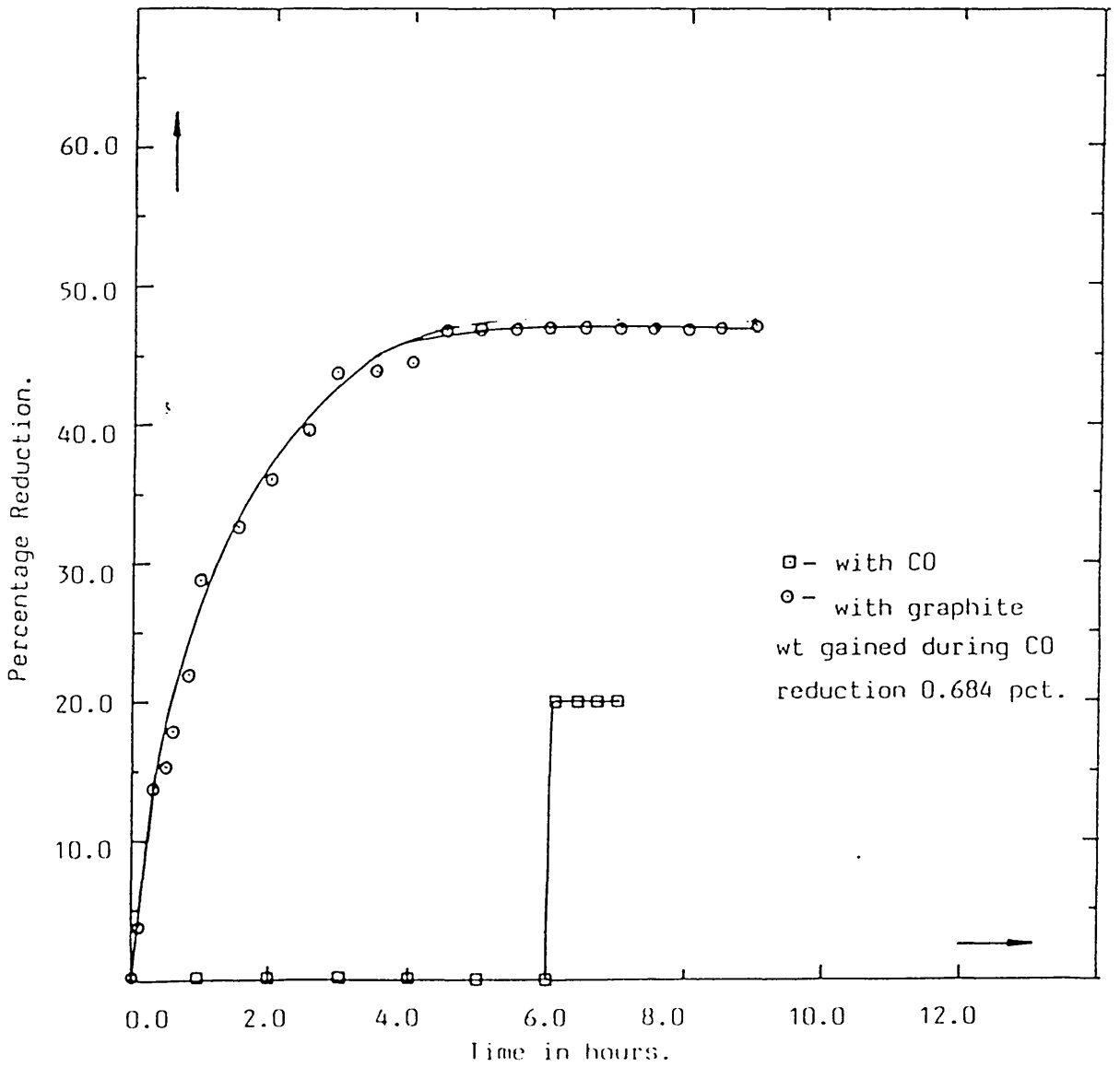


Fig (5B.8b) Rate of reduction of preheat-treated FeS:CaO = 1:2 mixture at 800°C under different conditons. Preheat-treatment temp 950°C.

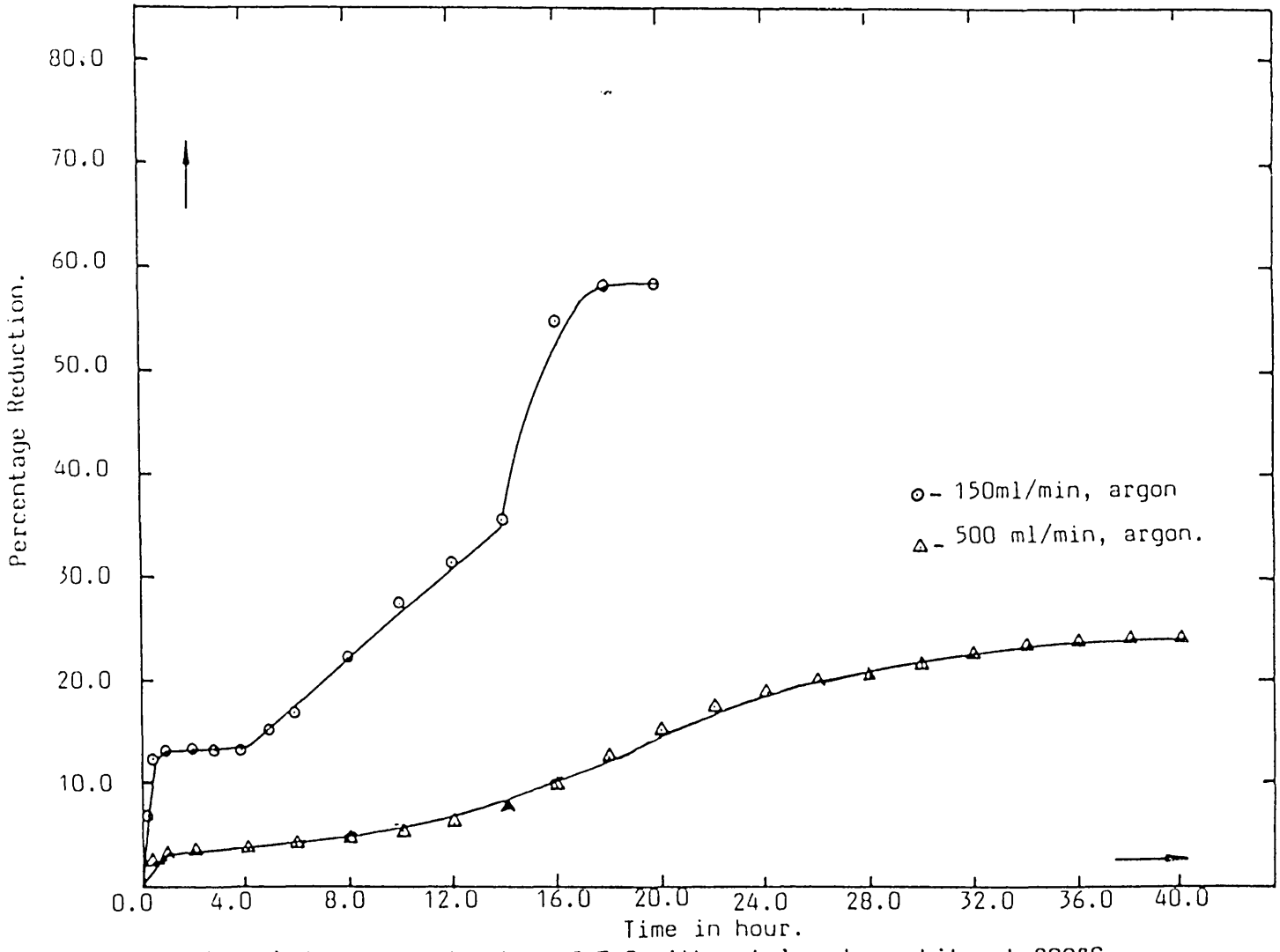


Fig (5B.9) Rate of reduction of FeS with catalysed graphite at 800°C (FeS:CaO:C = 1:1:2) with 4 pct Li_2CO_3.

plateau after an initial stage of reduction, see fig 5B(9). At a low flow rate of argon, the reaction proceeds at a linear rate which abruptly changes at 14hrs and the remainder of the reaction occurs within 4 hrs. At a higher flow rate, the rate progresses very steadily up to 25pct. in 40 hours after which it does not proceed any further. From the X-ray diffraction analysis (no:B18 and B42) it can be seen that there is no oxysulphide compound at 800°C in the presence of Li_2CO_3 but a small quantity of FeO was confirmed. A trace of lime and FeS was observed at the end of reaction with the lower flow rate of argon, which indicates that the reaction has proceeded near to completion.

(ii) Discussion of the Results of Iron Sulphide Reduction

a) Phase Relationships and Mechanism of Reaction:-

The phase relations of the reduced product show that during the course of the reduction either the quaternary oxysulphide liquid or the compound C_{II} is the dominant phase. The compound C_{II} lies in the FeS-CaO pseudo binary section (reference appendix 1). The possibility of the formation of iron as a result of the reaction between FeO and FeS is ruled out because of a large positive free energy for the reaction

$$FeS(s) + 2FeO(s) = 3Fe(s) + SO_2(g) \qquad (5.10)$$

$$\Delta G^o_T = 76390 - 28.02T$$

The equilibrium partial pressure of SO_2 is of the order of 10^{-7} atm at 1000°C. Considering the exchange reaction between FeS and CaO which shows that FeO and CaS are the equilibrium phases.

$$FeS(s) + CaO(s) = FeO(s) + CaS(s) \qquad (5.11)$$

$$\Delta G^{o}_{T} = -5470 + 2.18T$$

According to equation (5.11) the reaction is thermodynamically less feasible at higher temperatures. Using the data of Turkdogan (6.9) the standard free energy equation shows a negative enthalpy change and a positive entropy change ie $\Delta G^{o}_{T} = -4505 - 0.35T$. Evidently, the reaction is thermodynamically possible at any temperature. From the heat-treatment experiments of sulphide and oxide it is seen that FeO and CaS are not the equilibrium phases but a compound is formed which is in equilibrium with CaS. By forming the compound C_{II}, the activity of FeO is much less than unity. Therefore, the reduction proceeds at a much lower driving force. From the available literature (5.1) there is a kinetic barrier for the reduction of solid FeO with carbon at these temperatures, yet in the present investigation the reaction was found to proceed at a significant rate. Although in the present situation the driving force for the reduction of the compound C_{II} is smaller than pure FeO, the reason the reaction proceeds is thus obviously kinetic in nature. The presence of a liquid phase enhances the surface area of reaction many fold. The kinetic barrier to the progress of the reduction reaction can be appreciated from the results where no liquid was present during reduction. A quantitative estimate of driving force for the reduction of iron sulphide via compound C_{II} is not possible because of the non-availability of data on the free-energy of formation of the compound C_{II}. However, this particular observation indicates that the reaction proceeds despite the fact that it is thermodynamically less feasible than with the pure oxide.

The phase relationships in the reciprocal binary systems FeO-CaS and FeS-CaO are dealt with in Appendix 1 where this work is compared with Tromel (2.28) and Lapin's (1.18) work. Phase combinations observed during the heat-treatment of reciprocal mixtures and the reduction of iron sulphide can be explained using Tromel's phase diagram. To explain the reduction mechanism of iron sulphide it is essential to consider a suitable ternary section eg mixture FeS:CaO = 1:1 after the heat-treatment lies in the C_I-CaS-C_{II} ternary area shown in fig 58(10a) where this composition represents an equilibrium between CaS and compounds C_I and C_{II}. When oxygen is removed from this mixture by reduction, the change in composition is represented by an appropriate tie line, which is shown in fig 58(10a). The composition in this ternary phase field has been estimated on the basis of the X-ray diffraction results which show that after heat-treatment neither FeS nor CaO is present. The tie line through composition (1) is drawn such that it is parallel to the CaO-CaS and FeO-FeS edges which means that during the course of reduction the composition moves away from the oxygen rich corners of the quaternary . Such a tie line intersects the C_{II}- CaS phase region at 1 where it is in equilibrium with CaS and C_{II}. Explaining the mechanism in terms of a chemical equation then

$$\underset{C_I}{3(CaS\text{-}FeO)} + C = \underset{C_{II}}{2(CaO\text{-}FeS)} + CaS + Fe + CO \qquad (5.12)$$

Such a reaction sequence is consistent with quaternary section presented by Tromel (2.28). The liquid phase field diminishes with decreasing temperature until the compounds C_I and C_{II} appear. The above phase relationships show that compound C_I is relatively unstable in the

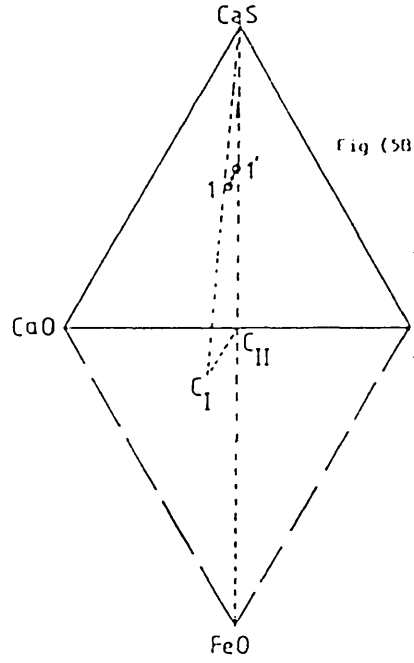


Fig (58.10a) Reduction path of iron sulphide in reciprocal system.

1 - FeS:CaO = 1:1 after heat-treatment.

1 - During reduction. Arrow head shows the path followed during the course of reduction.

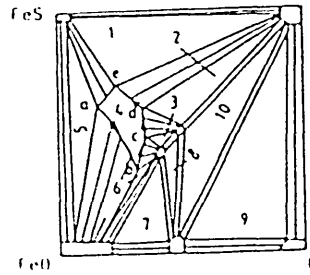


Fig (58.10b) FeO-FeS-CaO-CaS Section at 900°C as shown by Trömel et al.

1. FeS + L + CaS
2. L + CaS + II
3. L + I + II
4. L
5. FC + I + FeS
6. FC + L + I
7. FC + I + C_2F
8. C_2F + I + II
9. CaS + C_2F + Cf
10. C_2F + II + CaS

I - FeO:CaS compd
II - FeS.CaO compd
C_2F - Dicalcium ferrite
Cf - CaO-FeO SS
FC - FeO-CaO SS

presence of a reducing atmosphere. This is the reason why the quantity of C_I diminishes as the mixture is reduced and explains why the quantity of C_I reduces in the presence of Fe during the heat-treatment. All these factors can be understood in terms of the higher activity of FeO in compound C_I compared to C_{II}. It seems that the presence of iron and carbon controls the oxygen partial pressure in the system which leads to the stabilization of the phase C_{II}. The above invariant phase relations represented by equation (5.12) show that under reducing conditions the ternary peritectoid decomposition of compound C_I takes place. The recombination process is purely controlled by kinetics and the appearance of compound C_I at room temperature is expected.

From the above phase relations and the experimental evidence, compound C_{II} reduces to iron and CaS

$$(CaO\text{-}FeS)_{C_{II}} + C(gr) = Fe + CaS + CO(g) \qquad (5.13)$$

The above phase considerations represent the course of reduction which operates as long as solid compounds are present and the path of the reduction will be decided according to the above mechanism. The reduction sequence of preheatreated FeS-CaO mixtures at 800°C provides support of this mechanism. Under conditions, when a liquid phase exists with compounds C_I and C_{II}, the reduction mechanism is different. Once again C_I would reduce to C_{II} according to the previously presented mechanism but at the same time liquid also reduces. Later in the course of reduction only C_{II} and the liquid phase are present. The liquid phase first forms at 835°C and N_{FeS} = 0.65 so that, with increasing temperature, the liquid phase field predominance area in any isothermal section increases. It is worth

noting that the liquid phase contains less CaO than the compounds see fig 58(10b). This means that the liquid phase is continuously supplied with CaO by the compound C_{II} under reducing conditions and hence the reduction process is sustained. This means when the reduction of FeS commences in presence of lime, the liquid which forms first has composition on the ab surface which moves along this boundary until it establishes equilibrium with C_I. From this point onwards the path of reduction follows the curve bc along which C_I reduces to C_{II} followed by cd along which C_{II} reduces. If this liquid cools down the precipitation of these three phases takes place under conditions where this liquid loses contact with the compound C_{II} the supply of oxygen ceases such that in the limiting case when the activities of CaS and FeS approach unity, the precipitation of FeS and CaS occur. Proof of this mechanism can be appreciated from the indirect reduction of iron sulphide with CO. Since the compound C_I melts congruently it decomposes into a liquid and a solid phase C_{II} which is typical in the case of a peritectic transformation. Since most of the reduction was carried out in the composition range close to S:O = 1:1, peritectic transformation plays a very significant role during the reduction. A situation can occur where the liquid is isolated with a layer of C_{II} growing on C_I at any temperature between 1100°C and 880°C.

(b) The Kinetics of the Direct Reduction of Iron Sulphides.

Under any conditions, the rate of reaction is directly related to the temperature according to the Arrhenius Relationship. The significant difference in the slopes of various rate curves can be attributed to the relative volume

of quaternary oxysulphide liquid which determines the surface area of reaction. The sudden cessation of the reaction particularly at lower temperatures and with graphite is related to the continuous decrease in the volume of liquid and hence the isolation of liquid from the reducing agent at that temperature. This effect is very dominant at 900°C when the reaction enters a linear regime. The linear regime (in no B26 and B24) shows a steady state of diffusion condition has been established across which the concentration gradient is linear. In particular this happens at 900°C, as a result of the balanced volume of liquid which is neither too high nor too low. The weight loss analysis shows more than 100pct reduction has been observed under this conditon which can be accounted for due to drainage of the liquid. If the drained liquid maintains a pore diffusion mechanism to feed the material on the reducing surface, a linear regime is observed in the rate curve, otherwise it remains isolated from the bulk. Conversely,this liquid might drain completely from the pellet during the reaction giving a higher weight loss even with incomplete reduction. The weight loss due to drainage of the liquid can be supressed by using an active reducing agent ie if the rate of reduction is extremely fast, the liquid is reduced to metallic iron before it can drain.

The X-ray diffraction results of the reduced sulphide show that the existence of the compounds C_I and C_{II} is also dependent upon the rate of the reduction reaction. If an active reducing agent is used the decomposition of compound C_I controls the subsequent reduction of compound C_{II} at all temperatures. Two possible reasons for the coexistence of compounds C_I and C_{II} during reduction can be given :

i) If the compound C_I decomposes to C_{II} and liquid and this is encapsulated by the compound C_{II}, it would not be reduced directly by the reducing gas or the solid reducing agent. The supply of oxygen in this situation is maintained from the compound C_I through C_{II} to the C_{II}- liquid interface. This, the decomposition of C_I would be governed by a pure diffusion mechanism which is expected to be a slow step.

ii) In the absence of liquid phase, C_{II} can shield C_I from the reducing atmosphere and hence its existence is expected.

Both these conditions for the coexistence of C_I and C_{II} are governed by a single factor ie the concentration gradients of O^{-2} and S^{-2} ions across the product and the reactant layers. Under the conditions of the combined effects of direct and indirect reduction which prevails during the reduction of FeS-CaO-Gr (or coal) pellets under a controlled atmosphere of CO ie p_{CO} = 0.5 atm, the reaction rates are exceedingly high at 1000^{o}C because of the increased volume of liquid present and the rate of reaction is also very fast because of the presence of both CO and the solid reducing agent.

The catalysed reaction with Li_2CO_3 has been greatly affected by variation in the flow rate of argon. Since most of the lithium compounds which catalyse carbon gasification reaction according to an oxidation mechanism volatilize at low temperatures. A high flow rate of argon enhances the volatilization of Li_2CO_3 which cannot

participate in the carbon gasification reaction. From the results, it appears that gasification was initiated very slowly and has a pronounced effect on the rate of reduction of the sulphide. A fast gasification reaction precedes a fast reduction reaction and hence a sudden increase in the rate of reaction has been observed. In the situation where the reaction is incomplete in the presence of Li_2CO_3 at 800°C, FeO was observed in the partially reduced pellet. During the course of reaction compound C_I must have formed and been reduced by CO. The reason why FeO remains stable in the presence of carbon and catalysed gasification reaction is related to the mechanism of the overall reaction. Since the reduction reaction always follows the exchange reaction as a result of which compounds C_I, C_{II}, FeO and CaS form. Therefore, it seems possible that during the course of reduction FeO might have been isolated from the reducing gas and remained unreduced.

(c) The Kinetics of Indirect Reduction of Iron Sulphide

The indirect reduction of iron sulphide has been investigated in order to determine its contribution during the course of direct reduction. The rate of indirect reduction and its extent were found to be dependent on two parameters - temperature and the lime to sulphide ratio. In general, the rates were found to be faster with increased lime to sulphide ratio and the possible explanation for this is the relatively higher oxygen potential at which compound C_I exists. If a composition is produced which is in equilibrium with FeO and C_I, the rate of reduction is expected to be faster than when the equilibrium is determined by C_{II}. In the case of FeS:CaO = 1:1 the rate of reaction has been affected by three factors:-

i) If the rate of reduction is slow the liquid reduces slowly and it is possible under these circumstances that the liquid drains from the pellet. Subsequent reduction of this liquid is only possible when the liquid is fed back to the pellet by a pore diffusion mechanism where it re-establishes the exchange reaction. This step is particularly effective in the temperature range of 850°C - 900°C.

ii) In the case of intermediate reaction rates, the liquid formed is encapsulated by the product iron layer e.g. reduction at 950°C and hence drainage is prevented. In this situation, the rate is governed by pore diffusion of product gas through the metallic iron shell where O^{-2} ions are reduced by CO to generate two electrons which are discharged in the bulk to form metallic iron.

iii) At and above 988°C the material becomes completely liquid and in this liquid the precipitation of iron takes place. The reaction is extremely fast and once it commences, the risk of loss of liquid from the crucible is minimised.

The indirect reduction of iron sulphide above 850°C, is consistent with the fact that during the course of reduction the liquid composition moves along the different surfaces as indicated in the previous section, see fig 5B(10b). In the limiting case when oxygen supply to this liquid ceases, the liquid composition moves to the corner 'e'. During the cooling of this liquid precipitation of FeS and CaS is expected. This is the reason why FeS was observed in conjunction with CaS in the rim of iron at 950°C. The surface of the pellet reduces first and then

the reaction progresses slowly inwards. The X-ray data for the reduction at 950°C indicates that the transfer of oxygen from the bulk of material takes place towards the shell and in the limiting condition of oxygen solubility in the liquid, during cooling CaO precipitates instead of forming compound C_{II}. The reason why CaO precipitates is evident from the relative stability of CaO and compound C_{II}.

The rejected material from the liquid inside the cellular structure of iron at 1000°C is pure CaS, which can only happen when iron sulphide is completely reduced ie the liquidus surface has merged with CaS corner. Thus from the above phase relationships and the existence of the liquid phase, the whole reduction mechanism can be explained.

d) Cementite Formation During Iron Sulphide Reduction.

During the reduction process, cementite formation was observed and it seems that the mechanism of cementite formation is not grossly affected by the sulphurous atmosphere. Fruehan (5.2) has shown the effect of H_2S on the carburization of iron at 1000°C. The carburization rate was found to be reduced by a factor of 10 at this temperature with 0.2 pct H_2S. Calculating the partial pressure of sulphur in the equilibrium gas mixture which would change if sulphur starts occupying favourable sites on the iron surface.

$$H_2(g) + \tfrac{1}{2} S_2(g) = H_2S$$

$$\Delta G^{o}_{T} = -21580 + 11.58T$$

$$K_{1273} = \frac{P_{H_2S}}{P_{H_2}} \cdot (P_{S_2})^{\frac{1}{2}} = 14.93$$

From Fruehan's work at T = 1000°C

$$P_{H_2S}/P_{H_2} = \left(\frac{0.2}{50}\right), \quad P_{S_2} = 7.17 \times 10^{-8} \text{ atm.}$$

$$P_{H_2S}/P_{H_2} = \left(\frac{0.005}{50}\right), \quad P_{S_2} = 4.486 \times 10^{-11} \text{atm.}$$

This indicates a very small partial pressure of sulphur is necessary to alter the course of carburization. In the present system the partial pressure of sulphur is in equilibrium with CaS. C_I and C_{II} where P_{S_2} is much lower than the values shown above which indicates a very low coverage of sulphur at the preferred sites on the iron surface and thus CO is allowed to commence the carburization step. Cementite formation can take place at temperatures up to the eutectic in the iron-carbon diagram. The tendency of cementite formation is higher at lower temperatures because of its relative stability and it is expected to cease once the diffusion of carbon becomes increasingly difficult to sustain the reaction. This effect can be seen fig 5B(8a) where carbon deposition has commenced immediately after the linear regime of cementite formation.

****

5(c) Reduction of Complex Iron- Copper Sulphide Minerals:-

(i) Results.

The reduction mechanism of complex copper iron sulphide minerals has been investigated using a basis the results of copper sulphide and iron sulphide reduction. To investigate the reduction mechanism of complex sulphides, chalcopyrite and bornite minerals were chosen. The investigation was initiated with a heat-treatment of chalcopyrite mineral at 800^{o}C in an argon atmosphere. The chalcopyrite decomposed extremely slowly and at the end of 18 hours of heat-treatment when the sample was quenched and analysed using X-ray diffraction technique to identify the phases, high-temperature forms of chalcopyrite and bornite solid solutions were present in conjunction with FeS. According to several workers (3.1,3.6) as discussed in chapter 3, the decomposition of chalcopyrite results in the formation of two stable condensed phases, bornite (Cu_5FeS_4) and pyrrhotite (FeS_x). But according to the Cu_2S-FeS phase diagram (chapter 2, fig (2.5)) a wide range of solid solubility is expected of bornite with iron sulphide and chalcopyrite with iron sulphide. In the terminal range, where FeS saturation is attained, FeS would exist as a pure phase and depending upon the quenching rate, the solute will be held in solution because of the depression of the solvus. Therefore, under these conditions the bornite solid solution is the phase expected from the phase diagram, see table 5C.1. To identify these phases, the heat-treated pellet was examined by optical microscopy after etching the sample with luke warm acidified potassium dichromate. Two complex

sulphide phases were found, see plate 5C.3.

The carbothermic reduction of sulphides, proceeds in two steps which are complementary to each other ie the exchange reaction and the reduction reaction. In order to identify any changes occuring during the exchange reaction, heat-treated chalcopyrite, bornite mineral and chalcopyrite minerals were mixed with lime in stoichiometric proportions and then heat-treated over a range of temperatures. Depending upon the heat-treatment temperature and the type of mixture, different types and quantities of products were observed and they are shown in Table 5C.1. It is evident from the crystallographic data that metallic copper is present and its quantity varies with temperature and the type of the mixture.From the phase combinations, it is evident the metallic iron is not present in all cases except where heat-treated chalcopyrite was treated with lime. The compound C_{II} (FeS - CaO type) was in general absent and the stable compound from the Fe-Ca-S-O quaternary was C_I. On one occasion, Fe_3O_4 was found in conjunction with Fe after heat-treatment. A quinary compound possibly (FeS-CaO - Cu_5FeS_4) type was found in conjunction with the (FeO-CaS) compound. The presence of magnetite with iron together with C_I appears consistent with the phase relationships illustrated in Appendix 1. Thus, the heat-treatment experiments indicate that the metallization of copper is possible even in the absence of carbon and most of the iron in the system remains present in the form of complex compounds. The formation of copper cannot be justified without any evolution of SO_2 from the system, which results in a weight loss.

The mechanism of carbothermic reduction was investigated by adding graphite to the above lime-sulphide mixtures. The reduction was carried out in argon atmospheres. The amount of carbon added to the mixtures was decided by their initial stoichiometry. The weight loss observed during reduction was correlated with the following stoichiometric relations for chalcopyrite and bornite minerals.

$$CuFeS_2(s) + 2CaO(s) + 3C(s) = Cu(s) + Fe(s) + 2CaS(s) + 3CO(g) \qquad (5.15)$$

$$Cu_5FeS_4(s) + 4CaO(s) + 4C(gr) = 5Cu(s) + Fe(s) + 4CaS(s) + 4CO(g) \qquad (5.16)$$

An excess of carbon was used in order to ensure the total weight loss is only due to carbon monoxide and the contribution of carbon dioxide is insignificant. On the basis of the observed weight loss compared with the stoichiometric weight loss, at any time a percentage reduction was determined. The rate of reduction curve was constructed by plotting percentage reduction against time, and for the reduction of heat-treated lime-chalcopyrite and lime-bornite mixtures, these curves are shown in fig 5C(1). The lime-bornite mixture was initially reduced at 900^{o}C but after some initial reduction, the reaction ceased. At the end of 100 minutes the temperature was raised to 950^{o}C, when the reduction reaction resumed. A significant progress in the reaction was observed which finally ceased at about 28pct. From the phase analysis of the product, it is evident that both iron and copper have formed during the course of reduction but there is no evidence of the presence of lime, quinary compound or quaternary compound, which were observed during the heat-treatment step with lime. This indicates that most of these compounds were reduced and any unreacted sulphide is present in the

form of a high temperature bornite solid solution phase. Crystallographic data indicate that the reduction is incomplete. The incompleteness of the reduction process was also confirmed from mass balance analysis. Contrary to the reduction of bornite lime mixtures, chalcopyrite-lime mixture reduction was much faster at 900°C. It also continued uninterrupted at 900°C but was deliberatly stopped in order to identify the intermediate phases during reaction. From the crystallographic data it is evident that there was no iron present in the partially reduced pellet where as most of the C_I compound had converted to C_{II}. This conversion was already observed in the case of iron sulphide reduction, which supports the present evidence. The quinary compound was also found coexisting with C_{II}. This indicates that during the course of reduction of the chalcopyrite mineral, most of the iron is distributed between C_{II} and the quinary compounds and it is from these two compounds, finally iron is obtained. This is the reason why no iron was observed in the partially reduced pellets. The reduction mechanism of bornite mineral was investigated, because bornite is the stablest complex sulphide at higher temperatures in the Fe-Cu-S system as the other sulphides decompose.

In view of the above investigation, the reduction of synthetic chalcopyrite was carried out by mixing it with lime and graphite (or coal) in stoichiometric proportions. The rate of reduction curve with graphite is shown in fig 5C(2). The rate was found to increase with increasing temperature and it was delineated into different regimes, an initial non-linear regime and an intermediate linear regime which contributes significantly to the overall reduction process. The analysis of these two regimes will be dealt with in the next section where a discussion on

the mechanism of reduction will be presented. The X-ray diffraction results show that the quinary compound is present at the end of the reduction and it is from this phase, both iron and copper metals are generated. The absence of C_{II} and C_I shows that the primary steps in the reduction process have ceased.

The reduction with coal using the same lime to sulphide ratio is much faster and proceeds to a higher extent. The reaction under this conditon appears to proceed in stages. With graphite, no temporary arrests were observed on the rate curve whereas with coal at 900^{o} and 850^{o}C arrests appeared consistently. Good agreement in the length of the plateaux was observed during the reduction of chalcopyrite in the presence of lime with coal, figs 5C(1) & 5C(3) . Evidently the plateaux are an indication of a physical barrier associated with chemical reaction which needs further investigation. The microstructure of partially reduced chalcopyrite with graphite is shown in plate (5C.4), where the areas rich in copper and iron can be appreciated. From the micrograph, it appears that copper has grown from a liquid matte phase leaving an iron rich matte yet to be reduced. Observing such noticeable changes in the microstructure, selected areas were analysed using Energy Dispersive X-ray Analysis. From this analysis the elemental distribution maps were produced and are shown in plates 5C.1 and 5C.2 and these elemental maps confirm the optical microscopic observations. On a fewer areas of the reduced pellet EPMA was carried out to determine the quantities of individual components. These values are summarized in Table 5C.2.

Table 5C.1 Heat-Treatment of Chalcopyrite and Bornite Minerals.

Mixture Composition	Temp °C	Pct Wt loss	Pct Reduction	Atmosphere $P_{O_2} = 10^{-30}$ atm	$CuFeS_2$ High form (ss)	High form Bornite (ss)	$FeS/FeS.CaO$	$FeO/FeO.CaS$	CaS	CaO	Cu	Fe	Gr	Fe_3O_4	Ternary compound.
$CuFeS_2$	800	6.54	-	Argon	VS	M	M	-	-	—	-	-	-	-	-
Heat-treated $CuFeS_2$ at 800°C + CaO = 1:0.45	900	2.51	-	Argon	-	-		VS	VS	-	WM	VW	-	VW	S
Cu_5FeS_4:CaO = 1:4	900	1.017	-	Argon	-	-	-		VS	WM	M	-	-	-	MS
Cu_2S:FeS = 2:1	900	1.47	-	Argon	$Cu_{196}S$ -S Cu -w	VS	-	-	-	-	M	-	-	-	-
Cu6:FeS = 2:1															
Heat-treated at 900°C and then heated in lime surrounding	900	0.898	-	Argon	-	-	VS	VW	S	MS	S	-	-	-	MS
$CuFeS_2$:CaO = 1:2	1000	4.83	-	Argon	Cu_2FeS_6	W	-	-	M	VS		WM	-	-	-	S
$CuFeS_2$:CaO = 1:2	900	0.787	-	Argon	Cu_5FeS_6 -WM	-	-		WM	VS	-	WM	-	-	-	Med
CuFeS:CaO = 1:2	800	0.719	-	Argon	Cu_5FeS_6 -WM	-	-		WM	VS	WM	-	-	-	-	-

Table 5C.1 Heat-Treatment of Chalcopyrite and Bornite Minerals. Contd..

Mixture Composition	Temp °C	Pct Wt loss	Pct Reduction	Atmosphere $P_{O_2} = 10^{-30}$ atm	$CuFeS_2$ High form (ss)	High form Bornite (ss)	FeS/FeS.CaO	FeO/FeO.CaS	CaS	CaO	Cu	Fe	Cr	Fe_3O_4	Quinary compound.
$CuFeS_2$:CaO = 1:2 with total 'o' loss	850°C	9.45	8.722	CO	-	-	-	-	VS	W	S	S	-	-	W
$CuFeS_2$:CaO = 1:2 with 'c' deposition	850°C	10.64	100.76	CO	-	Fe_3C -WM	-	W	VS	VW	S	WM	-	-	W
$CuFeS_2$:CaO = 1:2	900°C	12.11	114.68	CO	-	Fe_3C -W	WM	-	VS	VW	S	WM	-	-	W
$CuFeS_2$:CaO = 1:2	950°C	11.30	107.58	CO	-	Fe_3C -WM	WM	-	VS	-	W	VS	VW	-	M
$CuFeS_2$:CaO = 1:2	1000°C	10.07	95.45	CO	-	-	M	M	VS	VW	M	S	-	-	W
$CuFeS_2$:CaO:C = 1:2:3	First 950°C then 1125°C	18.67	110.05	Argon	-	-	-	-	VS	-	M	M	VW	-	-

Table 5C.1 Heat-Treatment of Chalcopyrite and Bornite Minerals. Contd.

Mixture Composition	Temp °C	Pct Wt loss	Pct Reduction	Atmosphere $P_{O_2} = 10^{-30}$ atm	$CuFeS_2$ High form (ss)	High form Bornite (ss)	$FeS/FeS.CaO$	$FeO/FeO.CaS$	CaS	CaO	Cu	Fe	Gr	Fe_3O_4	Quinary compound.
$CuFeS_2CaO$ = 1:2:3	First 850°C for 4-5hr then 925°C	11.74	69.74	Argon	-	-	-	-	VS	S	S	MS	W	-	VW
$CuFeS_2$:CaO:C = 1:2:3	1000°C	14.45	85.50	Argon	-	-	-	-	VS	WM	S	S	WM	-	VW
$CuFeS_2$:CaO:C = 1:2:2.75	950°C	15.53	84.16	Argon	-	-	-	-	VS	VW	S	MS	W	-	VW
$CuFeS_2$:CaO:C = 1:2:2.75	900°C	13.90	75.38	Argon	-	-	-	-	VS	WM	VS	MS	W	-	VW
$CuFeS_2$:CaO (Coal + Gr) = 1:2:3.31	800°C	14.27	84.27	Argon	-	-	MS	VW	VS	-	WM	-	VW	-	M
$CuFeS_2$:CaO (coal + Gr) 1:2:3.31	900°C	17.77	105.13	Argon	-	-	-	-	VS	VVW	M	S	VW	-	W
$CuFeS_2$:CaO (coal + Gr) 1:2:3.31	950°C	15.90	94.43	Argon	-	-	-	-	VS	VW	S	S	VW	-	W
$CuFeS_2$:CaO: (coal + Gr) 1:2:3.31	1000°C	18.45	107.52	Argon	-	-	-	-	VS	VW	S	S	VW	-	VVW

Table 5C.1 Heat-Treatment of Chalcopyrite and Bornite Minerals. Contd..

Mixture composition	Temp °C	Pct Wt loss	Pct Reduction	Atmosphere $P_{O_2} = 10^{-30}$ atm	$CuFeS_2$ High form (ss)	High form Bornite (ss)	FeS/FeS.CaO	FeO/FeO.CaS	CaS	CaO	Cu	Fe	Gr	Fe_3	Other compounds
Cu_5FeS_4:CaO = 1:4 Heat-treated at 900°C and reduced with Gr.	900°C	4.17	28.79	Argon	-	M	-	-	VS	-	VS	WM	W	-	-
$CuFeS_2$:CaO = 1:2 at 900°C then reduced with 'Gr'	900°C	5.16	30.53	Argon	-	-	VS	-	MS	-	S	-	WM	-	M
$CuFeS_2$CaO = 1:2 at 800°C Heat-treated and then reduced with 'Gr'	900°C	7.13	42.17	Argon	-	-	VS	-	MS	-	MS	-	WM	-	S

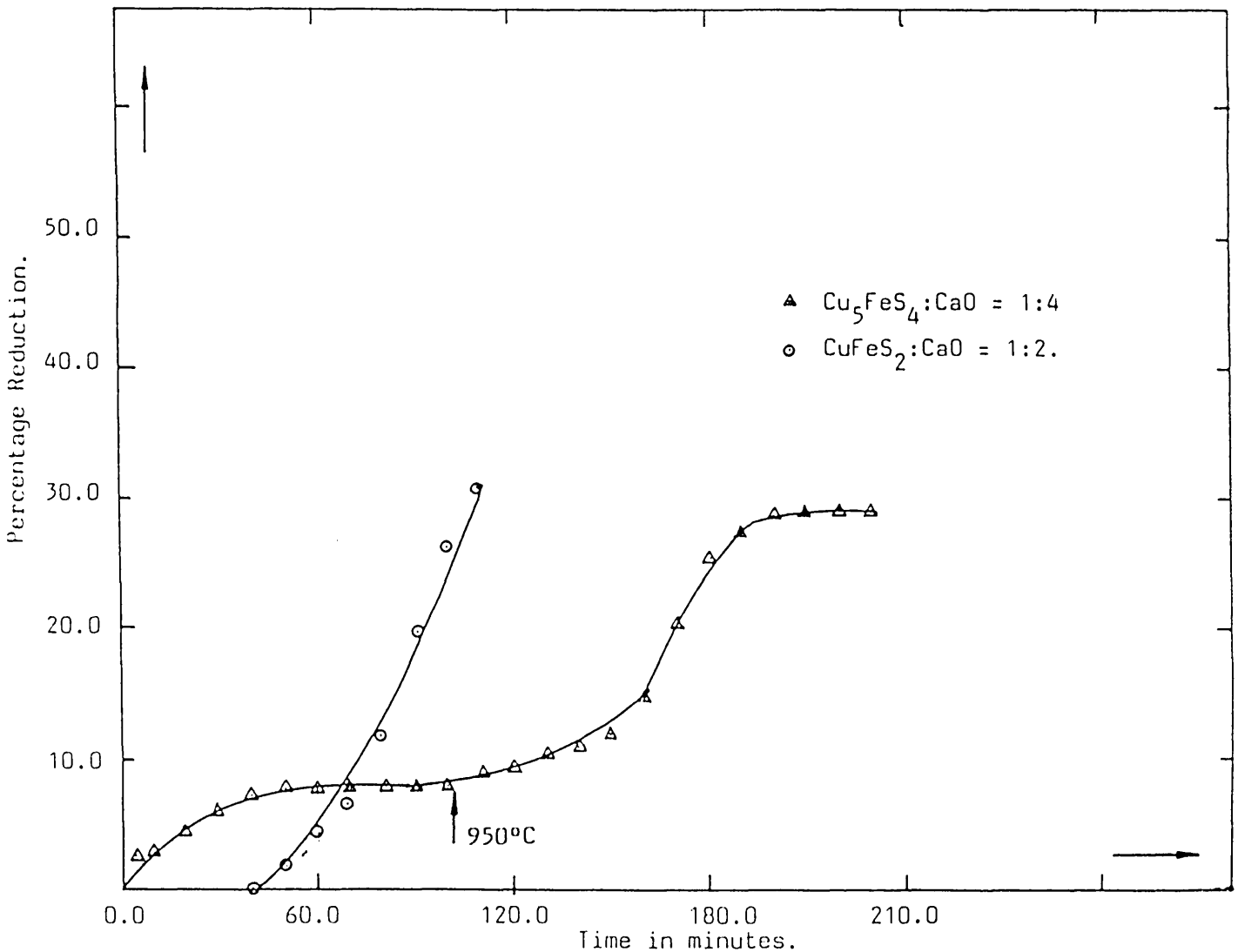


Fig (5C.1) Rate of reduction of preheat-treated complex sulphides and lime mixture with graphite. Atm-Argon. Reduction and heat-treatment temperature 900°C.

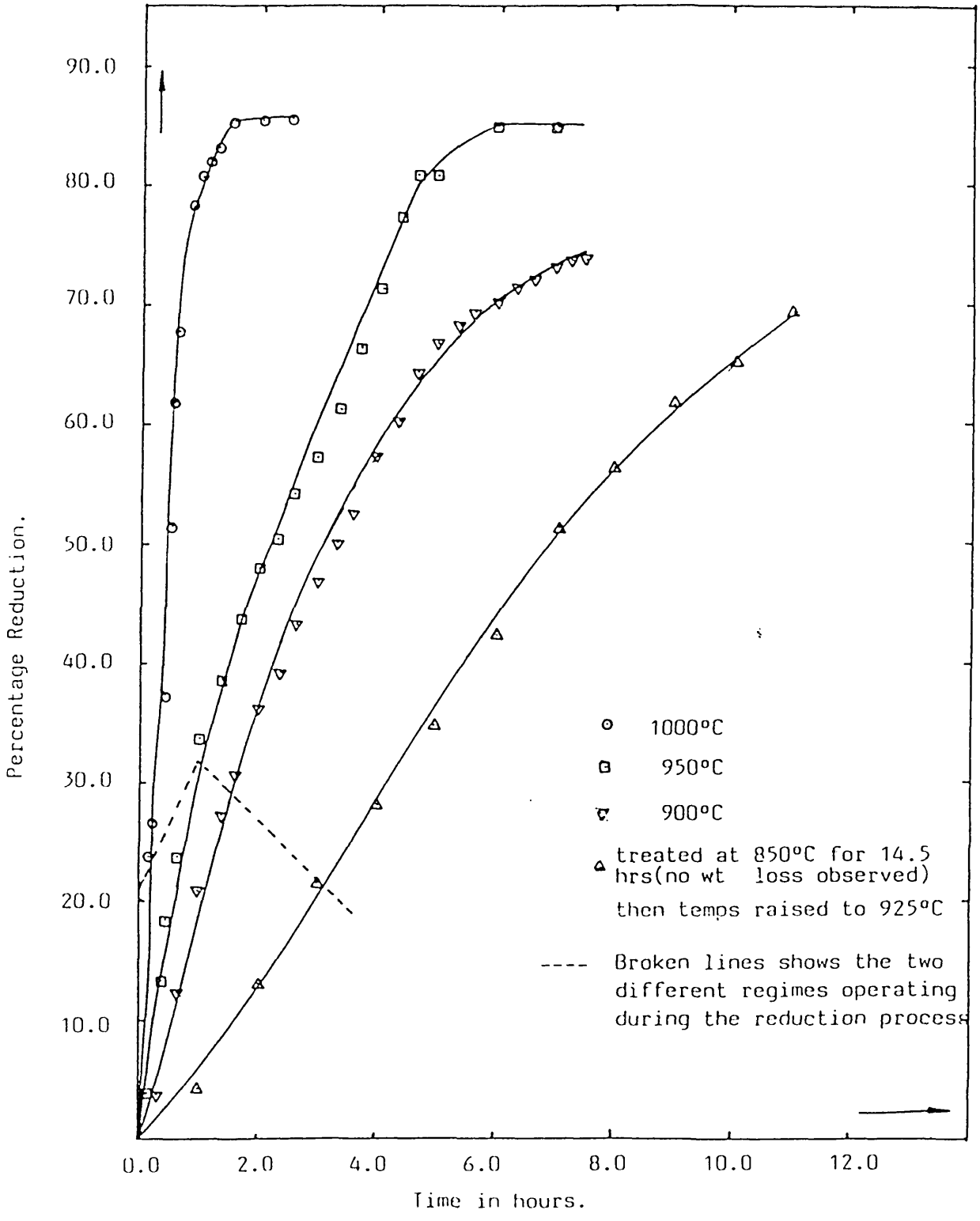


Fig (5C.2) Rate of reduction of chalcopyrite ($CuFeS_2$:CaO:C = 1:2:3) with graphite in presence of lime.

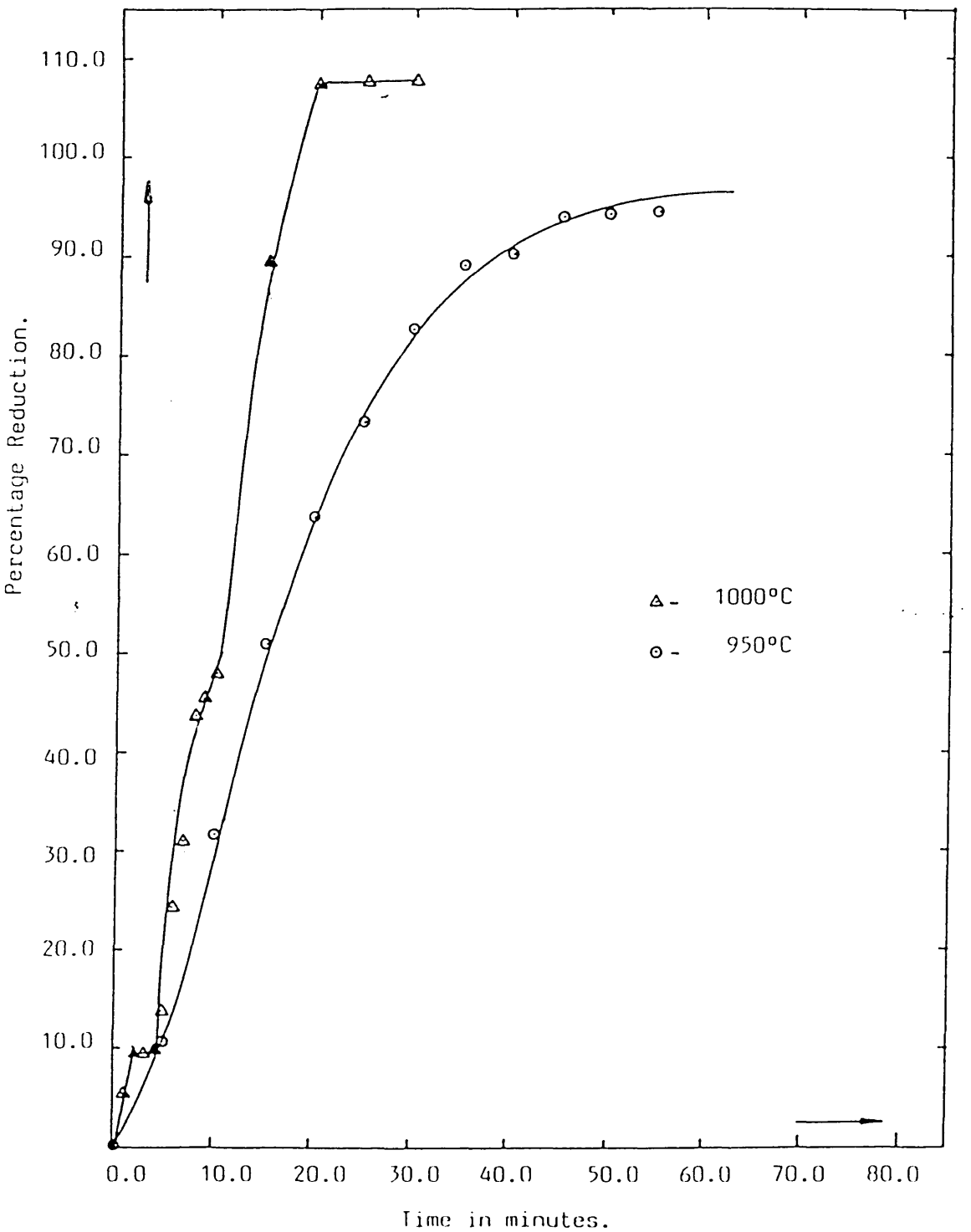


Fig (5C.3a) Rate of reduction of chalcopyrite with coal in presence of lime ($CuFeS_2$:CaO:C = 1:2:3).

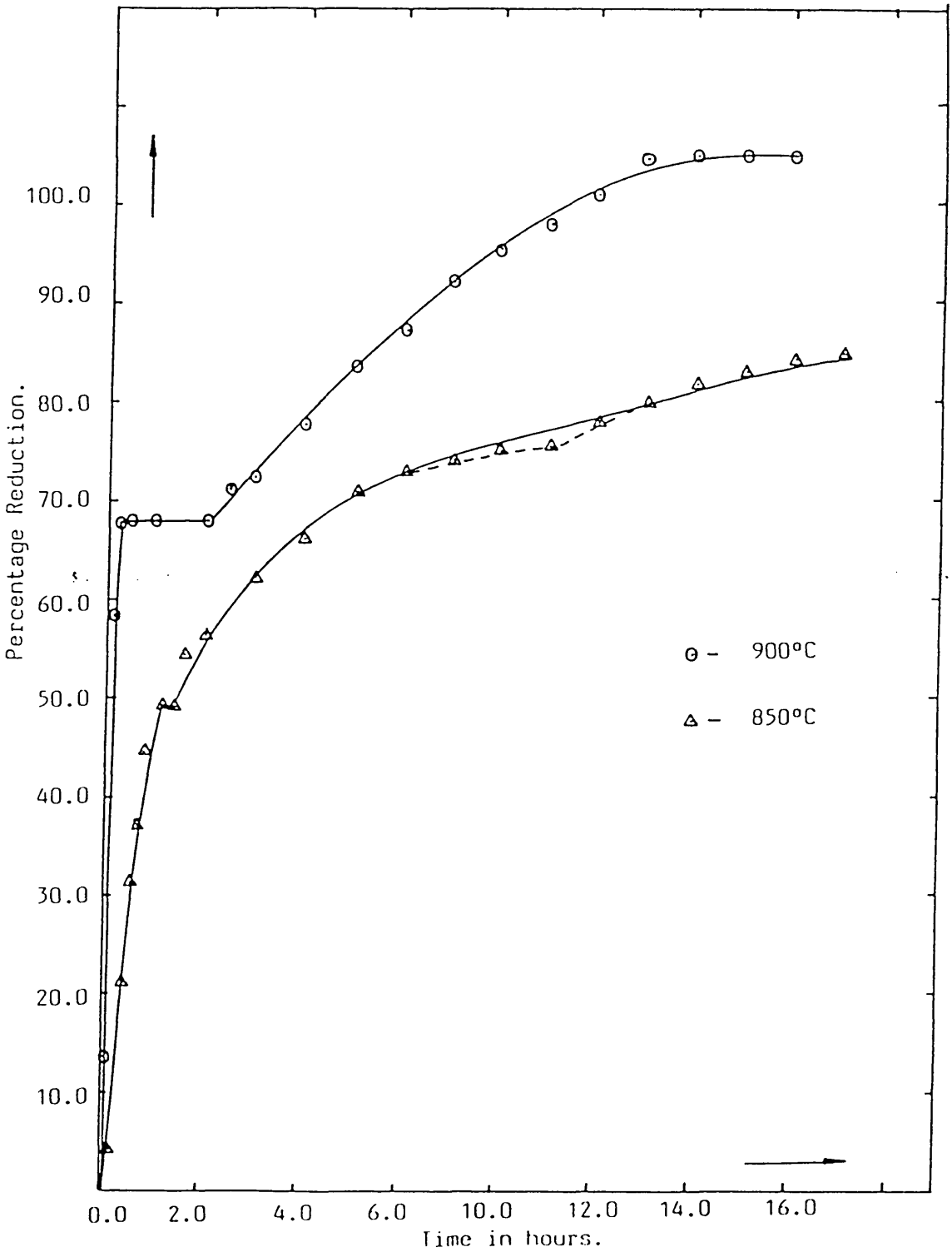


Fig (5C.3b) Rate of reduction of $CuFeS_2$ with coal in presence of lime ($CuFeS_2$:CaO:Coal + Gr = 1:2:3).

PLATE 5C.1

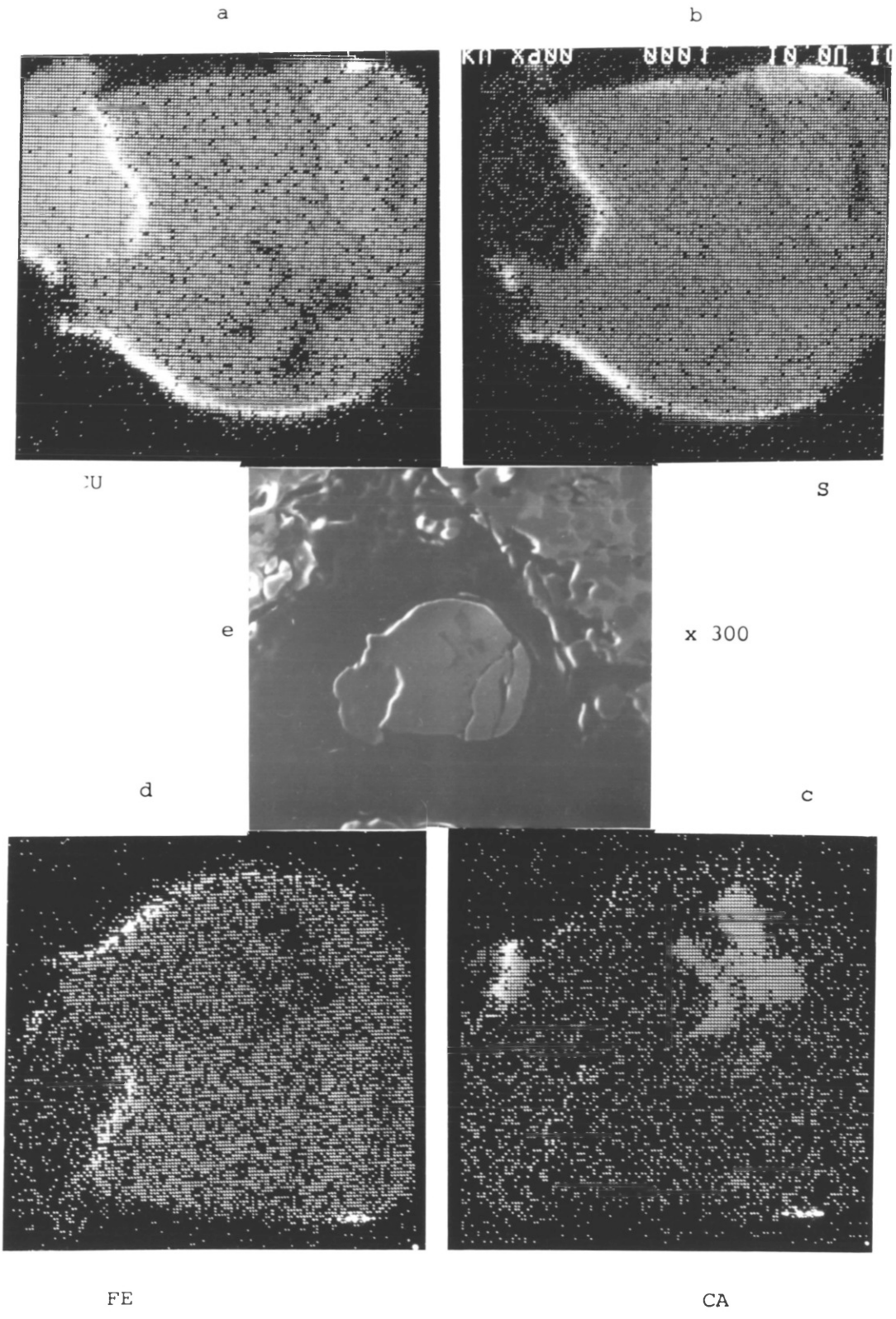


Plate 5C.1 Energy dispersive X-ray ($^{k}\alpha$) analysis of $CuFeS_2$:CaO:C = 1:2:2 reduced at 1000°C in argon atmosphere

(a) 'Cu' Elemental distribution
(b) 'S' Elemental distribution
(c) 'Ca' Elemental distribution
(d) 'Fe' Elemental distribution
(e) Sample area analysed

PLATE 5C.1

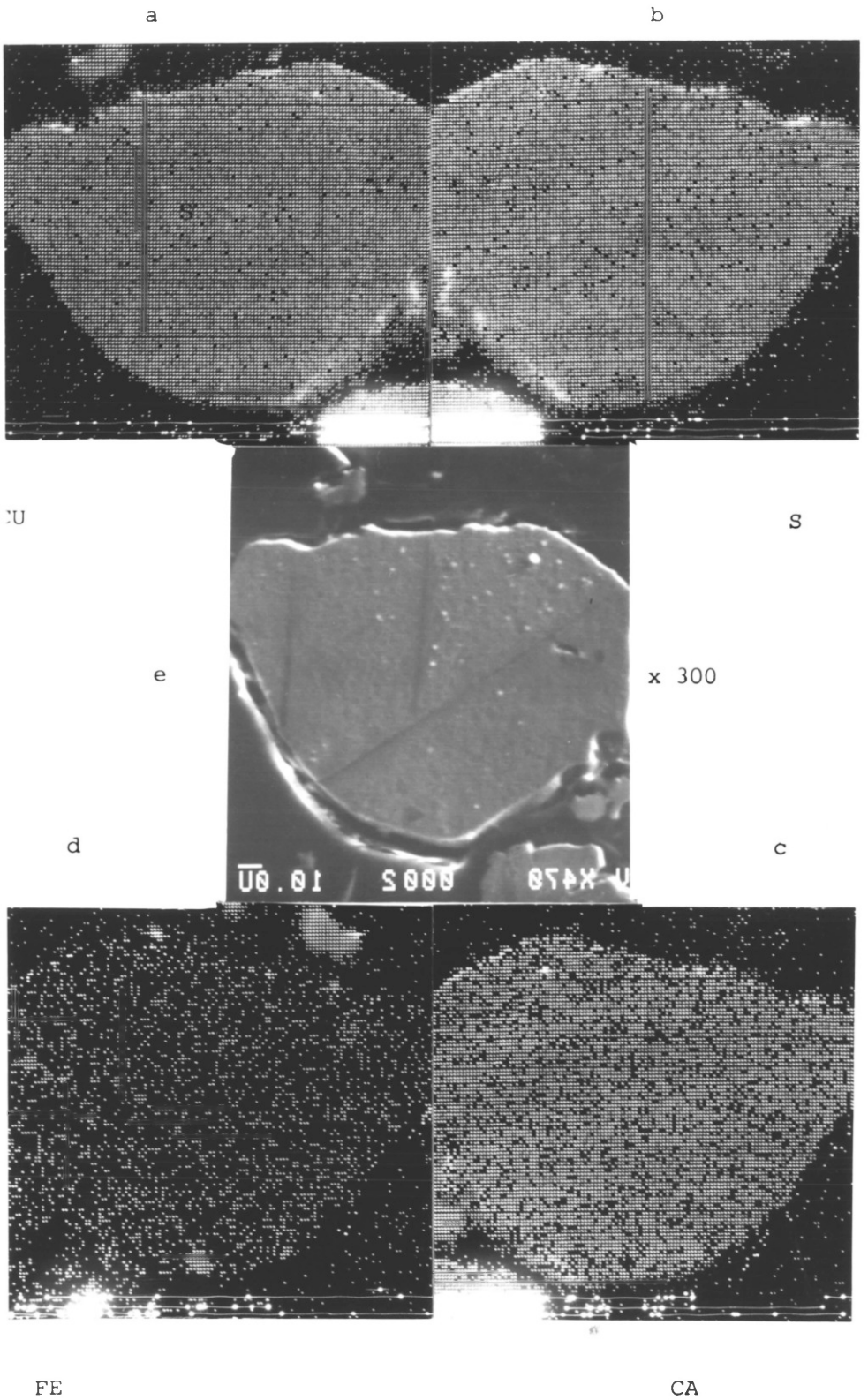
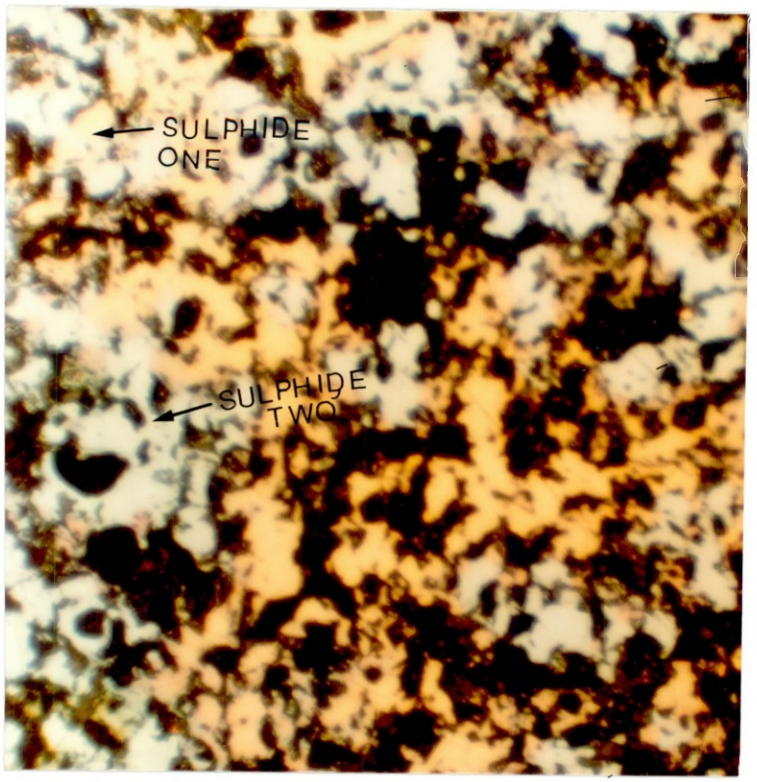


Plate 5C.1 Energy dispersive X-ray ($^{k}\alpha$) analysis of $CuFeS_2$:CaO:C = 1:2:2 reduced at 1000°C in argon atmosphere

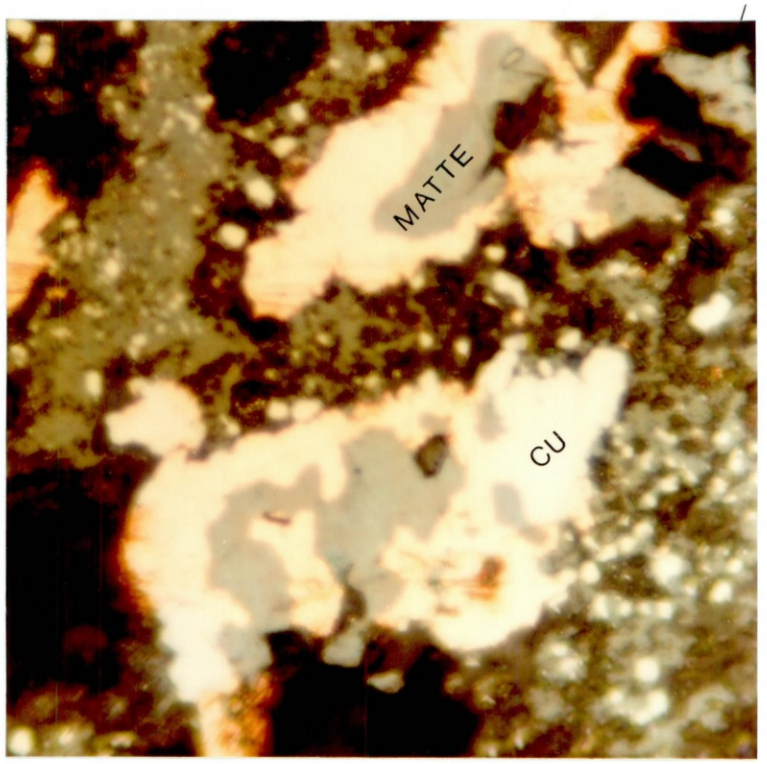
(a) 'Cu' Elemental distribution
(b) 'S' Elemental distribution
(c) 'Ca' Elemental distribution
(d) 'Fe' Elemental distribution
(e) Sample area analysed

PLATE 5C3



A

x260



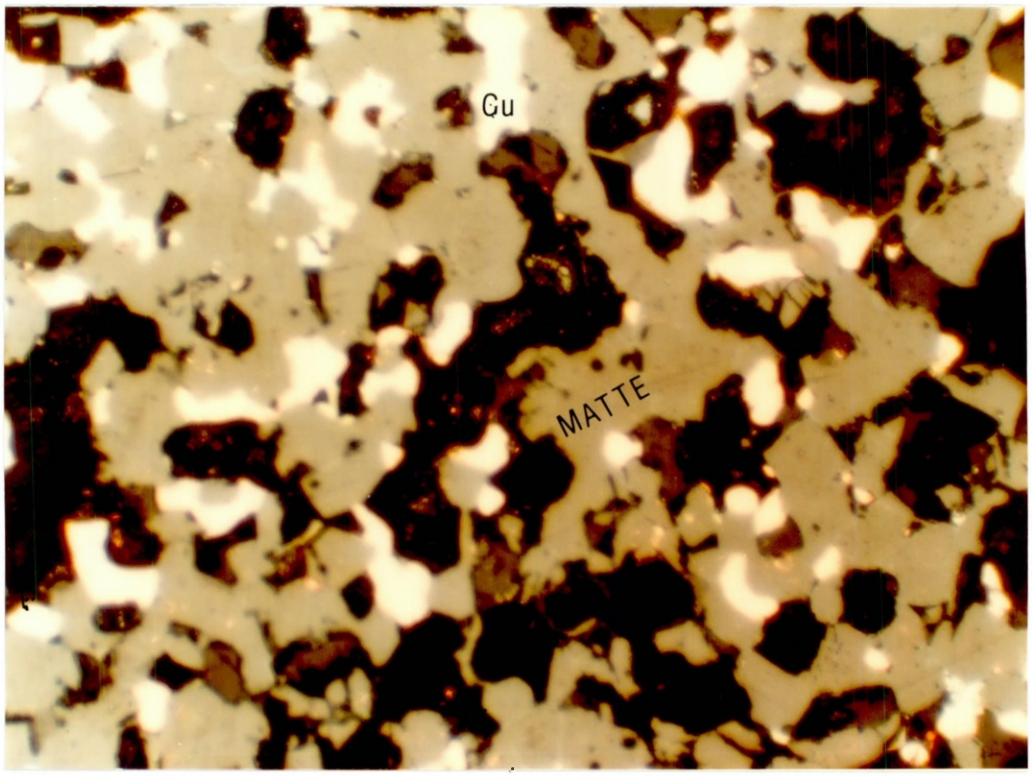
B

x260

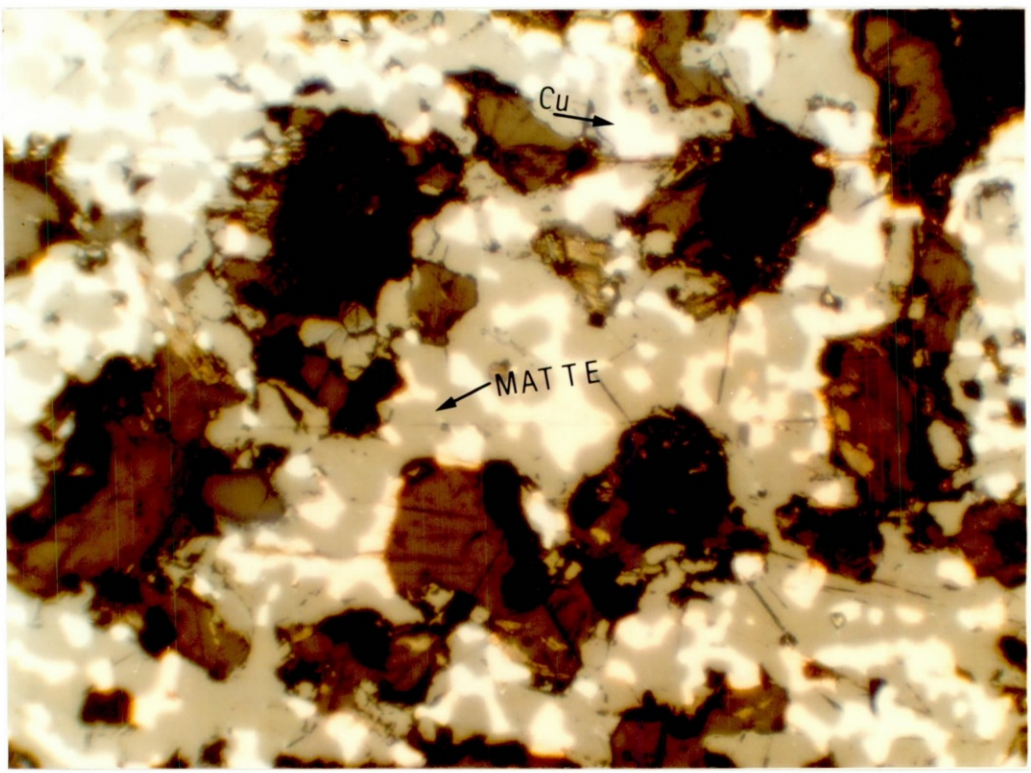
Plate 5C.3: a) Decomposition of Chalcopyrite into two sulphides at 800°C in argon. Sample etched with acidified $K_2Cr_2O_7$.

b) Formation of copper during the heat eratment of $CuFeS_2$ with lime. T=900°C. Atmosphere- Argon.

PLATE 5C·4



A X 260



B X 260

Plate 5C.4; Reduction of chalcopyrite with lime and graphite(2S:O:C=1:2:2).

a)950^{o}C iron rich matte with copper.

b)1000^{o}C iron rich matte with copper.

Table 5C.2: Electron Probe Micro - Analysis of Chalcopyrite reduced with graphite at 1000°C. $CuFeS_2$:CaO:Gr = 1:2:3 Atmosphere Argon.

Selected Area	Normalized Results, pct.				
	S	Ca	Fe	Cu	O
Area 1	21.45	0.281	12.22	53 33	12.72
Area 2	21.75	0.111	11.78	58.04	8.31
Area 3	21.59	0.01	11.38	57.18	9.87

These results are normalized in order to determine pct 'O' by difference in the selected areas. This has been determined by deducting other elements quantities from 100 pct. Using the normalized results, hence the percentage of Cu_2O, Cu_2S, FeS, FeO, CaO and CaS can be determined. Since these areas were essentially those from where copper had grown from the matte phase, the EPMA results also prove that the matte is richer in iron and metallic copper formed is in equilibrium with this matte under the prevailing conditions. A great deal of similarity was observed in the two mattes produced under different conditions - a) the matte produced during the heat treatment of chalcopyrite with lime, b) the matte produced during the reduction of chalcopyrite which indicates similar reaction sequences might be occuring in the two situations.

The effect of indirect reduction on the rates of direct reduction of sulphide was investigated by reducing chalcopyrite pellets in a carbon monoxide atmosphere. From the rate of reduction curves shown in fig 5C(4), it is evident that the reduction of chalcopyrite at temperatures 850°C, 900°C and 1000°C proceeds at a similar rate but the reduction

kinetics at 950°C are much slower than the above. It also proceeds producing several plateaux on its way to completion. Optical microscopic investigation was carried out on this pellet and it showed two well defined regions, - a region rich in iron on the periphery and a region which was depleted in iron with a few scattered copper nuclei, see plate 5C(5). The iron rim resembled very closely to those observed during the reduction of iron sulphide with CO, see plate 5B(3). A rim of this kind was observed at 1000°C also but it was located in a very small section of the periphery. Geometrically, the pellet after reduction at 1000°C was slightly deformed indicating the presence of liquid. No such evidence was observed at 850°C or 900°C. From the X-ray diffraction results, a variable amount of C_I and C_{II} compounds in conjunction with quinary compound was found which can be correlated with the extent of reduction taking place at any temperature. The crystallographic data does not agree with the mass balance and the reasons why a higher proportion of Cu is formed in preference to iron, can be explained in terms of SO_2 evolution which accounts for the higher weight loss. The presence of oxysulphide compounds were observed in conjunction with metallic copper during the heat-treatment of chalcopyrite and bronite in presence of lime in argon atmosphere. Also no drainage of liquid was observed during this heat-treatment which could possibly account for a higher weight loss. If this would have occured the relative amounts of copper and iron in the remainder of the sample would have proportionately decreased. Therefore, during the reduction of chalcopyrite and bornite with CO it is the weight loss due to SO_2 which gives a value of weight loss higher than the expected stoichiometric value.

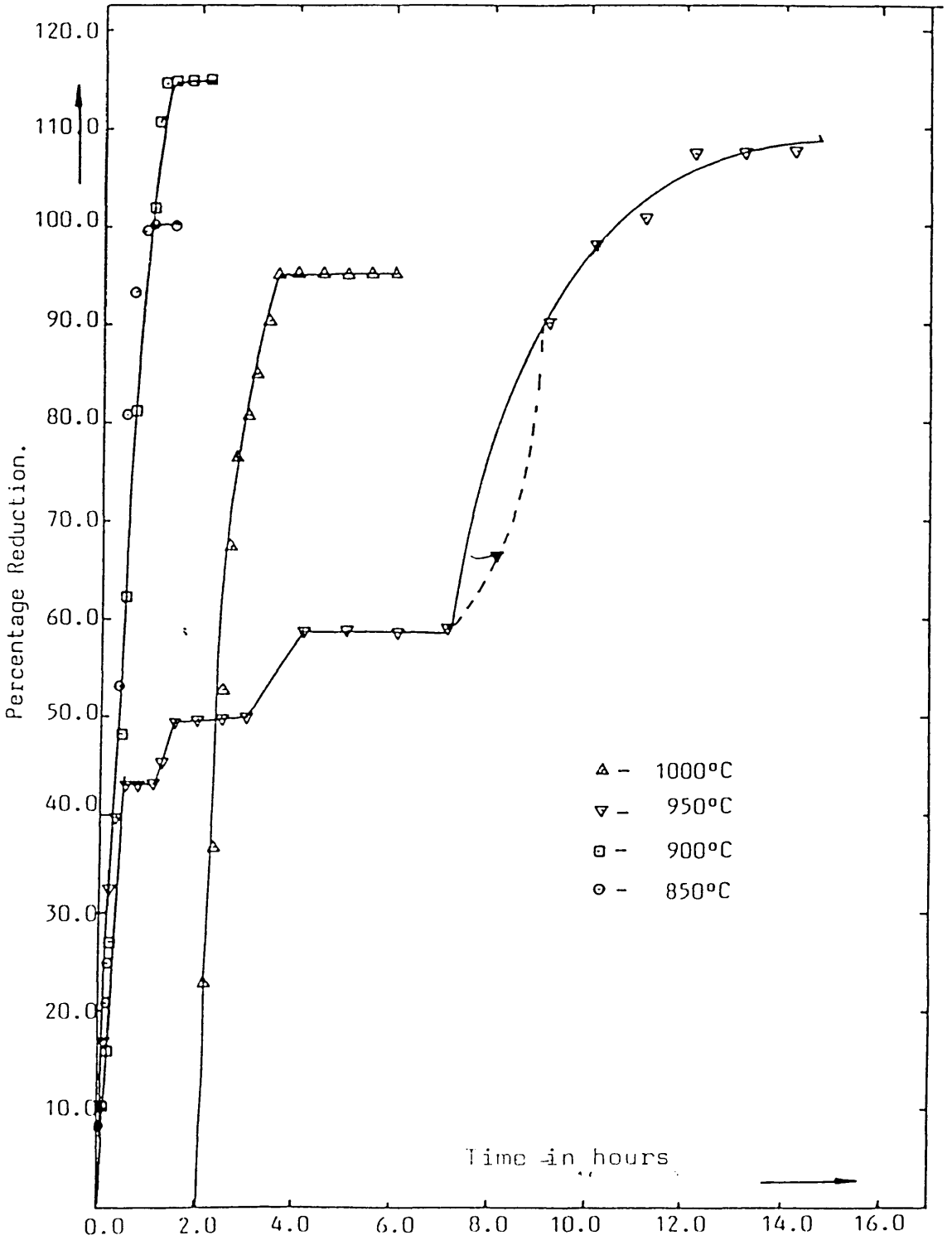
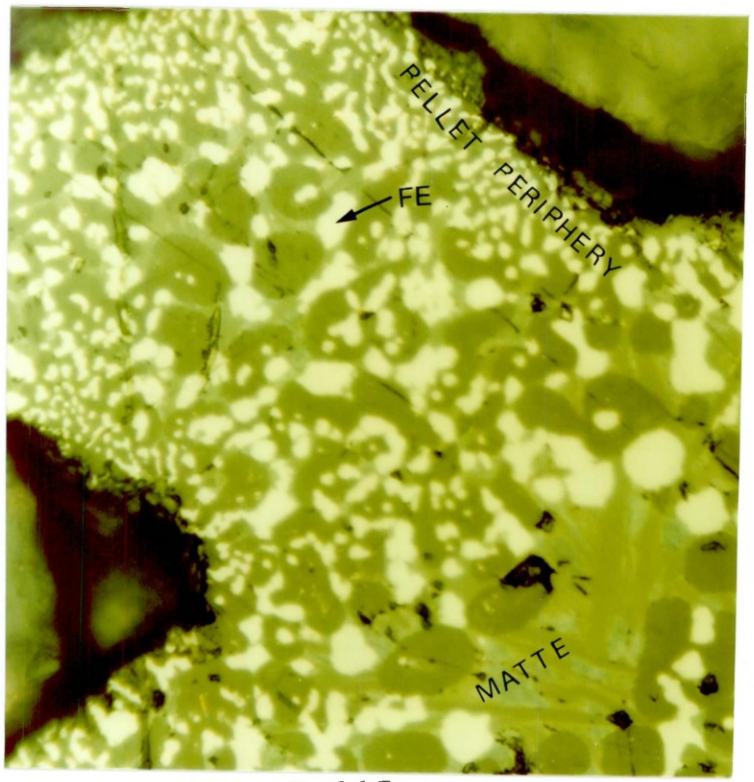


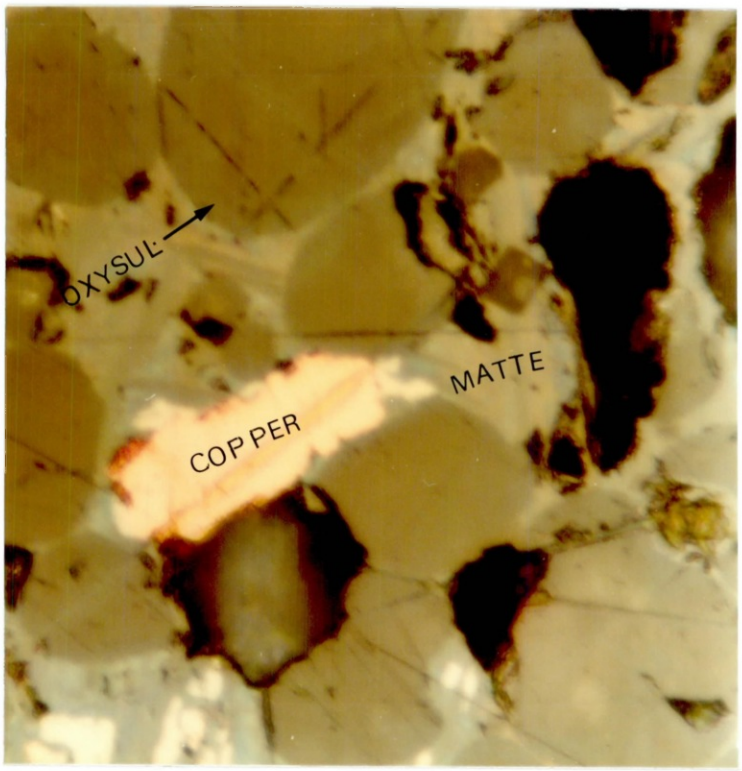
Fig (5C.4) Rate of reduction of chalcopyrite with CO in presence of lime ($CuFeS_2$:CaO = 1:2).

PLATE 5C.5



a

X 1265



b

X 1265

Plate 5C.5: Reduction of $CuFeS_2$:CaO=1:2 at 1000°C with CO.

a) Formation of iron rich rim and eutectic colonies.

b) Core slightly richer in metallic copper.

(ii) Discussions:-

(a) Thermodynamics of the Reduction Mechanism.

The reduction of chalcopyrite mineral proceeds in the presence of lime as an exchange medium. During the course of reaction copper metal is produced by the exchange reaction. Considering bornite is the stablest mineral at the operating temperature, it can be written:-

$$Cu_5Fe\ S_4(s) + 6Cu_2O(s) = 17Cu(s) + FeS(s) + 3SO_2(g) \qquad (5.17).$$

In the above equation, the standard state of copper oxide has been considered as pure solid. The standard free energy change for bornite ($Cu_5Fe\ S_4$), has been calculated from INCRA reports and by drawing the best line whose equation is $\Delta G^o_T = 45839 - 84.48T$. The Standard Gibb's Free Energy change for equation (5.17) is $\Delta G^o_{17} = -9011 - 120.96T$ cals which gives the value of the equilibrium constant as 5.74×10^{24} at 900°C for which the activity of Cu_2O at unit activity of FeS and at a $^pSO_2 = 1.0$ atm is $^aCu_2O = 7.47 \times 10^{-5}$, under this condition, a unit activity of FeS cannot be expected because of the existence of a liquid phase which has been observed during the experiment. Thus, under the conditions of one atmosphere of SO_2 a more appropriate relationship can be derived on the basis of above equilibrium i.e.:-

$$6 \log a_{Cu_2O} - \log a_{FeS} = -\log K \qquad (5.18)$$

At any temperature, if a_{FeS} decreases, the value of $^{a}Cu_2O$ would also simultaneously decrease. In the present situation, the activity of FeS is lowered in the presence of lime to form compounds C_I and C_{II} or a liquid. Qualitatively, it can be said, at the temperature where the quinary compound or quinary liquid exists, a decrease in the activity of Cu_2O is expected. In the presence of carbon as a reducing atmosphere, the value of $^{a}Cu_2O$ would decrease further to form copper and carbon monoxide or carbon dioxide gas. This equilibrium has already been discussed earlier in this chapter.

(b) Related Phase Fields and the Path of Reduction.

From the observations made on the reduction of bornite and chalcopyrite minerals it can be appreciated that the compounds C_I, C_{II} and the quinary compound exist under different sets of conditions. In order to illustrate their presence it is essential to construct a relevant phase diagram. A correlation between the phases is drawn in Fig 5C(5). From the X-ray diffraction results, it is evident that compounds C_I and the quinary co-exist only in the absence of any reducing agent. From the results of iron sulphide and from Appendix 1, we know that the existence of C_I is possible in an oxidizing condition. It is for this reason C_I, the quinary and CaS co-exist together during the heat-treatment when no reducing agent was present. This also justifies the presence of magnetite and iron during the heat-treatment of preheat-treated chalcopyrite with lime at 900°C. In this case, C_I and the quinary are present and are in equilibrium with CaS. The existence of CaS in relatively high oxidizing conditions can be interrogated but the reason why CaS is not oxidized to $CaSO_4$ is because of the presence of Fe which controls the oxygen potential in the system. In the previous section it has already been shown that compound C_I is unstable under

Fig (5C.5a)

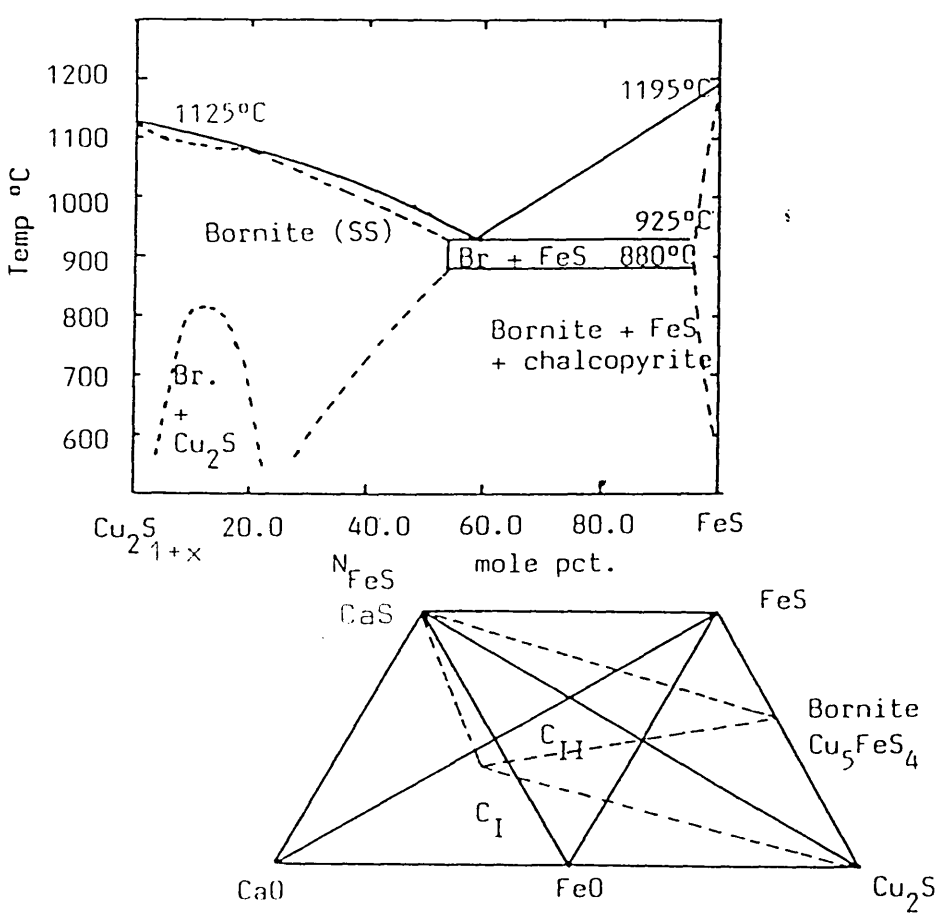


Fig (5C.5b)

Fig (5C.5) a - Cu_2S-FeS psuedo binary section

b - CaO-FeS-CaS-FeO-Cu_2S section.

reducing conditions, hence C_I decomposes to C_{II} and CaS. From then onwards, the reduction of C_{II} proceeds to give iron and CaS as discussed earlier. From the crystallographic data summarized in Appendix 1, the presence of the compound C_{II} appears to produce conditions which stabilize the quinary compound. The phase stabilization may be related also to the similarity of the crystal structures of C_{II}, bornite and the quinary compound. They all exhibit unit cells which are basically tetragonal. By comparing the 'd' spacings of C_{II}, the quinary, and bornite, many similarities are observed. Once the quinary and C_{II} are the only phases present the two composition co-ordinates move concurrently towards the CaS corner to give Fe, Cu and CO gas. Thus, it can be summarized that in the initial stages copper is formed as a result of the exchange reaction and during this process FeO-CaS forms because of the higher oxygen potential prevailing in the system. In the early intermediate stage C_I reduces to C_{II} and finally C_{II} and quinary compound reduces together to give metals.

(c) The Rate Governing Steps.

The rate of reduction curves, shown in figs 5C(1) to 5C(3) indicates clearly that different routes have been taken during the course of reduction of the sulphides. If all the rate curves for the direct reduction of sulphides are considered the effect of the reactivity of the carbon seems to be significant. The rate of reduction curves for graphite can be divided into two regions the initial non-linear region during which copper is generated purely as a result of the exchange reaction. Also, in the initial stage, the activity of Cu_2O appears to be higher and is reduced by generating SO_2. The linear intermediate stage represents the reduction of the compounds or the relevant liquid - the first to reduce is C_I to C_{II} (or liquid) and then the reduction of C_{II} (or liquid) commences simultaneously with that of the quinary compound. From X-ray diffraction data it is evident that the reduction of the quinary compound or liquid continues until the reaction

is complete, hence it is the reduction of the quinary compound or liquid by carbon which governs the overall rate of reduction. It is believed that the quinary compound probably melts between 900-950^{o}C and its existence at room temperature is caused by its formation during cooling. The rate of reduction curve with coal can only be compared in terms of relative rates of reduction. Above 950^{o}C, the rate of reduction of chalcopyrite with coal is much faster than graphite but the overall reduction is much slower with coal below 900^{o}C. The reaction at 850^{o}C and 900^{o}C proceeds by forming a plateau. The initial rates of reduction above 900^{o}C are comparable which indicates the mechanism of reduction above 900^{o}C in the case of coal and graphite, is identical. This is also evident from the comparison of slopes of these rate curves that the reasons for the appearance of plateaux could be the following:

a) If the relative rates of reduction of compounds are significantly different, in that situation, it may be possible that C_I and C_{II} are easily reduced by carbon, the quinary would not be produced hence the reaction would temporarily cease.

b) If a layer of calcium sulphide has formed around CaO, the reaction might temporarily stop.

c) If the volume of liquid at a particular temperature is relatively small in comparison to solid, the reduction reaction would proceed relatively slowly and a situation may arise during which the oxygen transport mechanism is affected by the separation of the liquid and the reducing solid surface.

Amongst the above reasons, the last appears more reasonable because if the other two had been dominating the reaction, they should definitely have been effective in the case of reduction with graphite. The chances of existence of a sulphide layer around lime particles is remote as both the ternary Cu-S-O and quaternary Fe-Ca-S-O liquid exist above 840^{o}C. It is also evident from the comparison of the slopes of rate curves with graphite at 950^{o}C and 900^{o}C, which appear to be parallel indicating that the mechanism of reaction is similar. Since the rate of reduction with graphite is much slower than with coal the reduction reaction would be sustained all the time without the formation of the plateau as at any instant of time, a significant volume of liquid will be present to maintain the transport of oxygen to the carbon surface. Oxygen transport is impossible if the reduction is fast enough to consume all the liquid. The mechanism of reduction is slightly different at 1000^{o}C where a eutectic between iron and iron sulphide exists. This might be the reason why the reaction is extremely fast at 1000^{o}C and is only altered by the relative reactivity of the carbon particles.

From the rate curves obtained for the reduction of preheat-treated lime-chalcopyrite and lime-bornite mixtures, the reaction proceeds in the former case whereas in the latter, it stops and recommencement was only possible at higher temperatures. From the X-ray data no iron was generated in the former case but all C_I has converted into C_{II}. So the partial reduction curve shows the primary step involved in the production of iron. The cessation observed in the latter case throws some light on the fact that the quinary compound probably melts at 950^{o}C and from then onwards the reduction mechanism is altered.

In the case of indirect reduction of chalcopyrite, it is evident that the rate is independent of temperature except at 950°C. The rate curves are parallel showing the mechanism of reduction is identical. A similar observation was made during the reduction of a cupric sulphide with lime. The reaction appears to be controlled by a pore diffusion mechanism and hence the rates are insignificantly affected by the temperature. On the other hand, the rate is drastically affected and is much slower at 950°C. It proceeds by forming several plateaux. As discussed earlier a solid layer of iron has formed around the periphery indicating that the rate of removal of oxygen associated with iron has a major affect on the overall reaction. The plateaux in this situation indicates a sufficient time is required to maintain a transport of O^{-2} ion at the gas-solid interface from the bulk. This aspect needs further investigation as far as preferential deposition of iron on the peripheral surface is concerned. From the reduction curve it appears that cementite formation is prevalent at all temperatures except 1000°C. With increasing temperature cementite formation becomes more difficult and in the present situation it is not affected by the partial pressure of sulphur in the system. At 1000°C, no cementite was observed because of the higher activity of Cu_2O in the system which offers a higher pressure of CO within the system. At other temperatures where relatively large amounts of copper are produced, such a condition does not prevail and cementite formation commence. At 950°C, most of the cementite formation has taken place around the peripheral iron.

NOTE:- The presence of quinary and quaternary compounds at 800^{o}C shows that both iron and copper are tied up in the form of compounds not as a pure sulphide phase. Habashi and Dugdale (1.20) observed a decrease in iron removal beyond 0.2gm of CaO per gram of bornite. From the quaternary phase diagram on Fe-Ca-S-O system it is evident that the two compounds are possible and can occur with the quinary. The amount of lime used for bornite reduction at which 100 pct iron removal was expected must be a critical value beyond which the compound formation tendency commences. Hydrogen reduction of such compounds is expected to be very difficult in the solid state where product morphology might be the most important factor to govern the rate of removal of iron. These worker's results appear to be very anamolous because in the same system where lime beyond 0.2gm/gm of bornite appears to adversely affect the removal of iron from the bornite at 800^{o}C, it helps the removal of iron in the case of chalcopyrite, see fig (1.5) and (1.6). These results are not substantiated by the results of the investigations carried out by above workers using hydrogen as a reducing agent.

Chapter 5.

5.1 P.C. Hayes Internal Report. Univ. of Strathclyde 1977

5.2 R.J. Frueham Met. Trans vol. 4 1973 pp 2123 - 2132

Chapter 6.

Calcination of Calcium Sulphate.

6.A. INTRODUCTION.

This chapter has been devoted to the investigation on the mechanism of calcination of calcium sulphate in both reducing and inert atmospheres. In addition to being important with respect to the major subject of study in this investigation, this subject has drawn attention in the past pertaining to the desulphurization of limestone (6.1,6.2). Pyrites is invariably associated with natural lime stone, and during its calcination process, it decomposes to pyrrhotite resulting in CaS, SO_2 and CO formation according to the following chemical equlibrium:-

$$3FeS(s) + 3CaCO_3(s) = Fe_3O_4(s) + 3CaS(s) + CO(g) + 2CO_2(g) \qquad (6.1).$$

At the reaction front because of the generation of S_2 vapour a gaseous reaction with S_2 and CO_2 may possibly give rise to CO and SO_2. SO_2 generated in this way reacts with CaO to form $CaSO_4$. It is likely that the decomposition of pyrite to pyrrohtite may result in the conversion of $CaCO_3$ to CaS according to equation (6.1). Also depending upon the temperature, it is possible that FeS may form an oxysulphide matte as a result of S^{-2} ion exchange with lime. Little is known about the existence of the oxysulphide phase (1.18,2.12,2.26,2.28), in which CaS could dissolve. Consideration of results in a recent publication of Turkdogan and Martonik (6.3) clearly indicate that this liquid has a significant solubility of CaS and on cooling it gives FeO, CaS & FeS.

This aspect has been discussed at greater length in Chapter 5 where the investigation of the reduction mechanism of iron sulphide was considered. The thermodynamics of calcination have been studied by Darken and Wriedt (6.4). A detailed thermodynamic investigation related to the phase diagram and the possible univariants and invariants has been carried out by several workers (6.5,6.6,6.7,6.8) at different temperatures. From these thermodynamic investigations, two probable mechanism for the calcination of $CaSO_4$ anhydrite suggested as below:-

$$CaSO_4(s) + CO(g) = CaO(s) + SO_2(g) + CO_2(g) \qquad (6.2)$$

$$CaS(s) + 3CO_2(g) = CaO(s) + SO_2(g) + 3CO(g) \qquad (6.3)$$

and the related equlibrium constants are:-

$$\log K_1 = \log ({}^{P}CO_2/{}^{P}CO),\ {}^{P}SO_2 = \frac{20325.3}{T} - 9.481 \qquad (6.4)$$

$$\log K_2 = \log ({}^{P}CO/{}^{P}CO_2),\ {}^{P}SO_2 = -\frac{20,000}{T} + 9.27 \qquad (6.5)$$

The calcination of sulphate has been investigated in order to relate this reaction mechanism which occurs during the carbothermic reduction of copper sulphide. During the reduction calcination of $CaSO_4$ the equilibria are represented by the following chemical equations (6.9):

$$CaSO_4(s) + 2C(s) = CaS(s) + 2CO_2(g) \qquad (6.6)$$

$$\Delta G^{o}_{6.6} = 30230 - 75.06T$$

$$CaSO_4(s) + 4CO(s) = CaS(s) + 4CO_2(g) \qquad (6.7)$$

$$\Delta G^{o}_{6.7} = -49740 + 7.2T$$

Once the sulphide is formed the calcination may proceed according to the following reactions:

$$3CaSO_4(s) + CaS(s) = 4CaO(s) + 4SO_2(g) \qquad (6.8)$$

$$\Delta G^{o}_{6.8} = 222670 - 151.96T$$

For the conversion of sulphate to lime in a reducing atmosphere the governing chemical equilibria are:

$$CaSO_4(s) + C(s) = CaO(s) + SO_2(g) + CO(g) \qquad (6.9)$$

$$\Delta G^{o}_{6.9} = 83030 - 77.32T$$

$$CaSO_4(s) + CO(g) = CaO + SO_2 + CO_2 \qquad (6.10)$$

$$\Delta G^{o}_{6.10} = 43220 - 36.19T$$

In the investigation carried out by Turkdogan and Vinters, on the reduction calcination of calcium sulphate, it has been shown that the rate of reduction varies with the reactivity of the carbon and hence reaction (6.8) suffers accordingly limiting the rate of sulphur elimination if the rate of oxygen removal from the system is rapid. The calcination of the sulphate in the presence of calcium sulphide appears to be gas diffusion controlled ie when the reaction is carried out with a light inert gas the desulphurization rate of the sulphate and sulphide is enhanced. A relationship between temperature and the rate of reaction has been shown that the theoretical reaction rate and the observed rate vary by an order of magnitude. The reason for this discrepancy lies in the equilibrium value of the partial pressure of sulphur dioxide calculated from the standard Gibbs Free Energy change for the reaction (6.8). The entropy change in the free energy data appears to be very high and has been confirmed by data from two sources (6.10,6.9). The variation

of the rate of reaction with temperature, when calculated using the following rate equation (6.11) was found to be in good agreement with that observed by Turkdogan and Vinters.

$$n_{SO_2} = \frac{Z}{RT} (p^e_{SO_2} - p^b_{SO_2}) \qquad (6.11)$$

n_{SO_2} = rate of SO_2 evolution

Z = proportionality constant

R = gas constant

T = temperature in degree Kelvin

$p^e_{SO_2}$ = pressure of SO_2 at the reaction front = equilibrium pressure.

$p^b_{SO_2}$ - bulk gas SO_2 partial pressure = 0

The rates calculated by Turkdogan and Vinters and those calculated according to equation (6.11) are shown in fig (6.1). Glasson and O'Neil (2.25) have reviewed the mechanism of reaction (6.8) and have studied the stability of various phases. Considering the route of reaction via an intermediate phase $CaSO_3$ the modified equation can be represented in the following form:-

$$3CaSO_4 + CaS = 4CaSO_3 = 4CaO + 4SO_2 \qquad (6.12)$$

The predominance area of $CaSO_3$ and the equilibrium constant for the decomposition of sulphite to oxide and SO_2, and its disportionation to sulphate and sulphide are shown in fig (6.2). It is evident that the sulphite is unstable above 705^oC and the predominance area contracts with increasing temperature. On the other hand, from fig (2.11)[2.12] it is evident that the sulphate and sulphide can only

coexist together only up to 700°C in agreement with Glasson and O'Neils calculation.

During the calcination of $CaSO_4$ either in the presence of carbon or with CaS in inert atmosphere , the conversion of sulphate to lime takes place presumably via a gaseous species SO_3 in agreement with the predominance area diagram shown in fig (6.2) ie increasing SO_2 pressure decreases the predominance area of CaO. Thus according to Glasson and O'Neil:-

$$3CaSO_4 = 3CaO + 3SO_3 \qquad (6.12)$$

$$CaS + 3SO_3 = CaO + 4SO_2 \qquad (6.13)$$

The rates of these reactions are apparently fast and according to Turkdogan and Vinters (6.1) the activation energy of the reaction is identical to the enthalpy change involved in this reaction ie ΔH^o = 55.9 Kcal/mole of SO_2. The activation energy of such magnitude indicates that the rate is not governed by pore diffusion of SO_2 into the bulk gas phase. Such a activation energy falls in the range of 5-10 Kcals. This shows the anomaly of the rate controlling step. From the value of activation energy observed by Turkdogan and Vinters, it seems that heat transfer from the surface to the reaction interface plays a significant role and could give rise to a high activation energy.

During the calcination of $CaSO_4$ in the presence of carbon, it may be possible that CaS is oxidized directly by CO_2 according to reaction (6.3) which only happens if sufficient CO_2 is generated within the system ie parallel progress of reactions (6.2), (6.6), (6.7) and (6.10) is necessary.

Thus it follows that under the condition of high pCO_2/p_{CO}, the sulphate-oxide univariant would be prevalent which agrees with the univariant relationship shown in fig (6.3)[6.9] . Attempts have been made to elucidate the mechanism of calcination (2.25) in terms of crystal structure and bonding. The reaction (6.8) with $CaSO_3$ intermediary is identical with the dissociation reaction and involves the breaking of S-O bonds to release a SO_2 molecule. The stability diagram shown in fig (6.2) justifies the decomposition thermodynamics and the remaining oxygen is co-ordinated with the metal ion. The channel within the structure are bounded by six Ca^{+2} ions each connected to sulphite groups via oxygen. Arrangements of groups around the channel is such that the pyramidal SO_3^{-2} species have their apical sulphur directed towards the centre of the channel, thus oxygen can be bonded to this sulphur to form tetrahedral SO_4^{-2} group, the oxygen is donated by SO_2 molecule see fig (6.4). The resulting SO could react with SO_3^{-2} to give sulphur. Both SO_2 and SO have been found to be present in the effluent gas. Thus the sulphur can:

a) associate with another sulphur atom to form a diatomic molecule which could escape from the structure.

b) exchange with an oxygen attached to Ca^{+2} to form CaS

The complete mechanism suggested by Glasson and O'Neil is depicted in the form of a schematic diagram shown in fig (6.4).

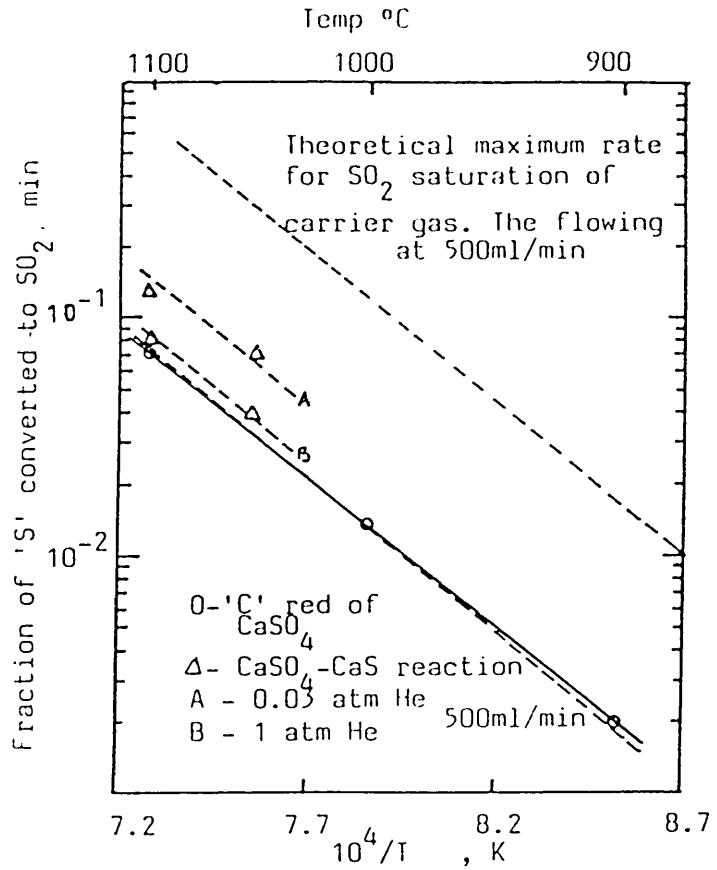


Fig (6.1) Temperature dependence of rate of $CaSO_4$-CaS reaction

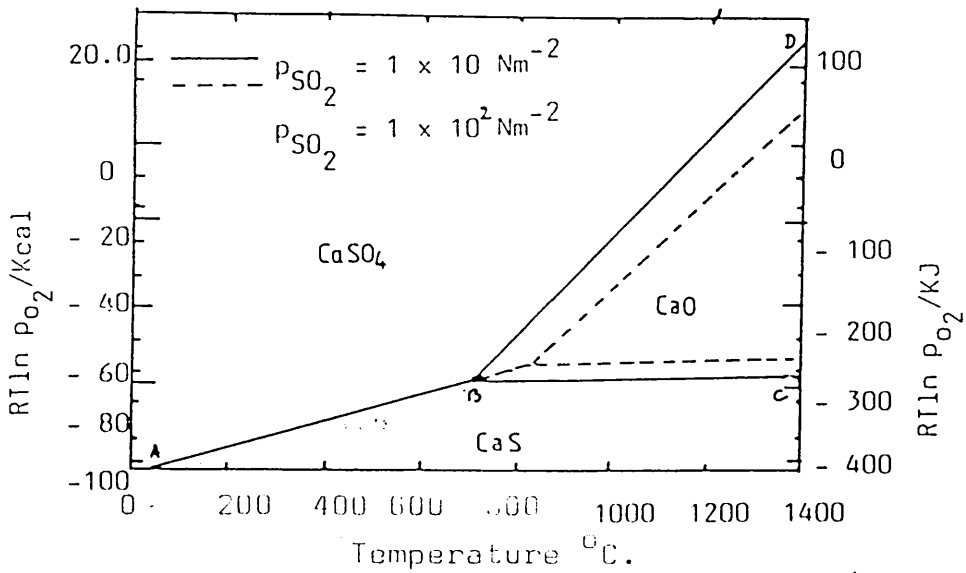


Fig (6.2) Predominance diagram for CaO, CaS, $CaSO_4$ and 'O' gas

AB - 0.5 CaS + O_2 = 0.5 CaSO4

BC - CaS + O_2 = CaO + SO

BD - 2CaO + SO_2 + O_2 = $2CaSO_4$

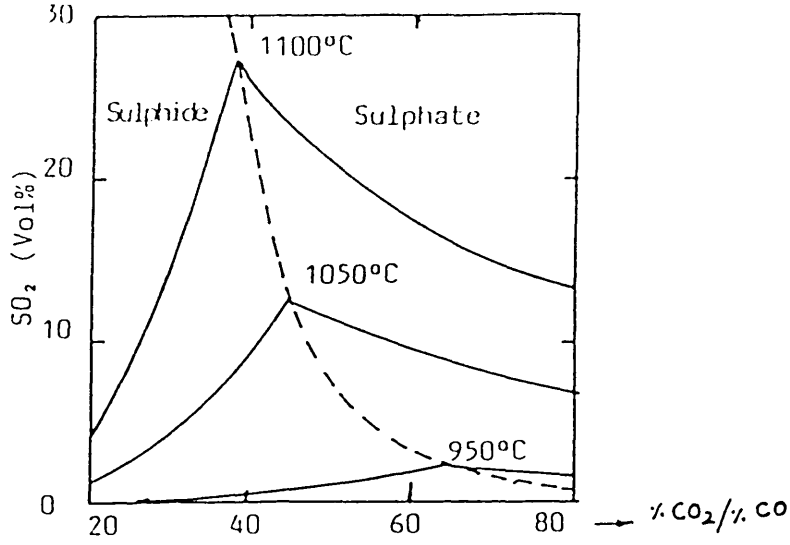


Fig 6.3 SO_2 content and (CO_2/CO) ratio of gas in equ. with CaO-CaS and CaO-$CaSO_4$ at indicated temperatures and total presure of 1 atm.

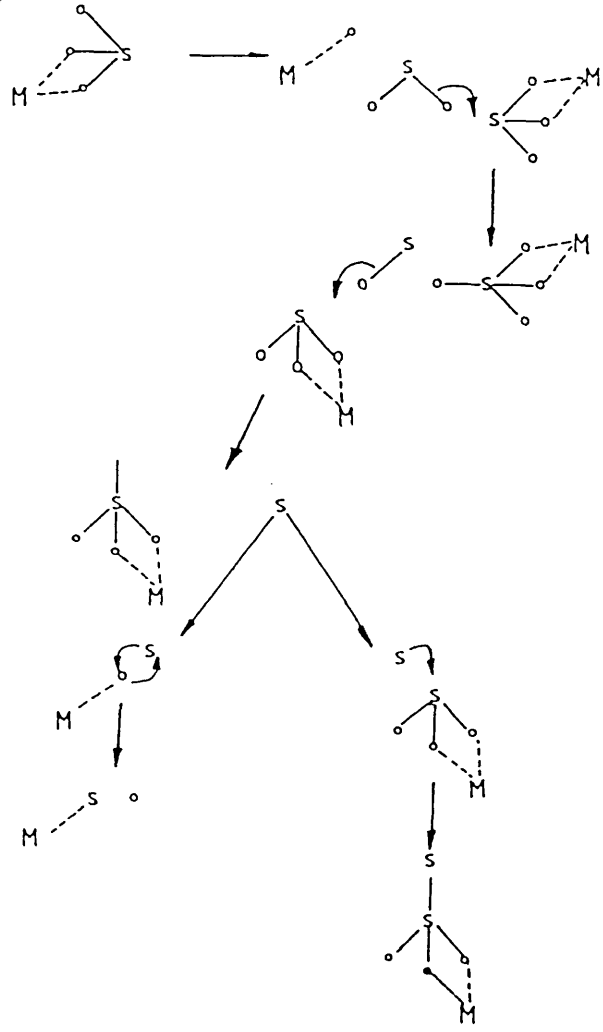


Fig 6.4. Possible reaction steps involved in the thermal decomposition of alkaline earth metal sulphites.

6.B. EXPERIMENTAL TECHNIQUE.

The experiments to investigate the kinetics of calcination were carried out in a similar manner to the carbothermic reduction experiments discussed in Chapter 4. The investigation was carried out with A.R. Grade $CaSO_4$ granules which were preheated in air at 1000^oC to liberate any water of crystallization present. The calcined $CaSO_4$ was then crushed and mixed with A.R. Grade calcium sulphide (CaS) also dehydrated and calcined in a dry intert atmosphere. To understand the kinetics of calcination of $CaSO_4$ in the presence of CaS, two types of experiments were carried out:

a) with stoichiometric mixtures of $CaSO_4$ and CaS according to equation (6.8) in an inert atmosphere

b) with $CaSO_4$ - CaS composite pellets in their respective stoichiometric proportions in an inert atmosphere.

For reduction calcination of sulphate, the powder was mixed with spec pure graphite. In addition, reduction with CO was also carried out with $CaSO_4$ pellets. For reduction of $CaSO_4$ pellets with CO a gas flow rate of 500 ml per minute was maintained through the double wall silica tube.

6.C. RESULTS

i. The Reduction of Calcination of Calcium Sulphate

The investigation on the rate of reduction of calcium sulphate in the presence of carbon was carried out using mass balance analysis according to the following equilibrium:

$$CaSO_4(s) + 4C(Gr) = CaS(s) + 4CO(g) \qquad (6.14)$$

and plotting the weight loss observed at a particular instant of time. From the construction of rate curves and from the X-ray diffraction analyses, a complete analysis was carried out. The results of the mass balance analysis and the X-ray diffraction analysis are arranged in the Table 6.1.

Table 6.1: Observations on the Reduction Calcination of Calcium Sulphate.

				Mass balance analysis		X-ray diffraction analysis.					
	Mixture Composition	Temp °C	Atmos. $P_{O_2} \cdot 10^{30}$ At.	Pct wt loss	Pct red.	CaS	Ca(OH)$_2$	CaO	$CaSO_4$	$CaCO_3$	Gr.
6.1	$CaSO_4$:C • 1:4	1000°C	Ar	46.74	77.04	VS	M				
6.2	$CaSO_4$:C • 1:4 with Cu	1000°C	Ar	46.25	75.97	VS	M	WM	Cu-WM	WF	M
6.3	$CaSO_4$:C • 1:4	950°C	Ar	45.62	74.96	VS	WM	-	-	-	M
6.4	$CaSO_4$:C • 1:4 with Cu	950°C	Ar	41.51	68.55	VS	WM	-	- Cu-W	W	M
6.5	$CaSO_4$	950°C	CO	47.05	99.94	VS	-	-	VVW	-	-

The phase combinations shown in Table (6.1) are given in terms of their relative intensities on the diffraction pattern. Although the above mixtures were stoichiometrically adjusted for the aformentioned chemical equation, in the X-ray diffraction pattern calcium oxide and calcium hydroxide($Ca(OH)_2$) were observed which could only occur if the desulphurization of sulphate commenced simultaneously according to equation (6.8). Turkdogan and Vinters (6.1) in their investigations had observed the desulphurisation of sulphate with stoichiometrically inadequate amounts of carbon, ie $CaSO_4$:C = 1:2. The rates of reduction of $CaSO_4$ at different temperatures are shown in fig (6.5). From Turkdogan's work, it is evident that the amount of sulphur converted to SO_2 is relatively high with inactive carbon and the reaction is essentially governed by the reactivity of the carbon surface. The presence of catalysed carbon reduces the amount of SO_2 evolution from the mixture. A comparison of sulphur converted as SO_2 and as CaS is shown in fig (6.6) [6.1].

From the rate curve shown in fig (6.5), it is evident that there is no effect on the rate of reaction at 1000°C with copper additions whereas at 950°C the rate of reduction has been significantly affected by the presence of copper. Calcium carbonate was observed after reaction in the case of direct reduction of sulphate. Although calcium carbonate is unstable above 900°C in the present situation possible reasons for its existence will be discussed later in the text. Furthermore, the reduction of sulphate with carbon monoxide was found to be much faster than with graphite. It proves that the faster removal of oxygen from the sulphate does not allow the reaction (6.8) to proceed thus no lime nor SO_2 is generated as a result of reduction.

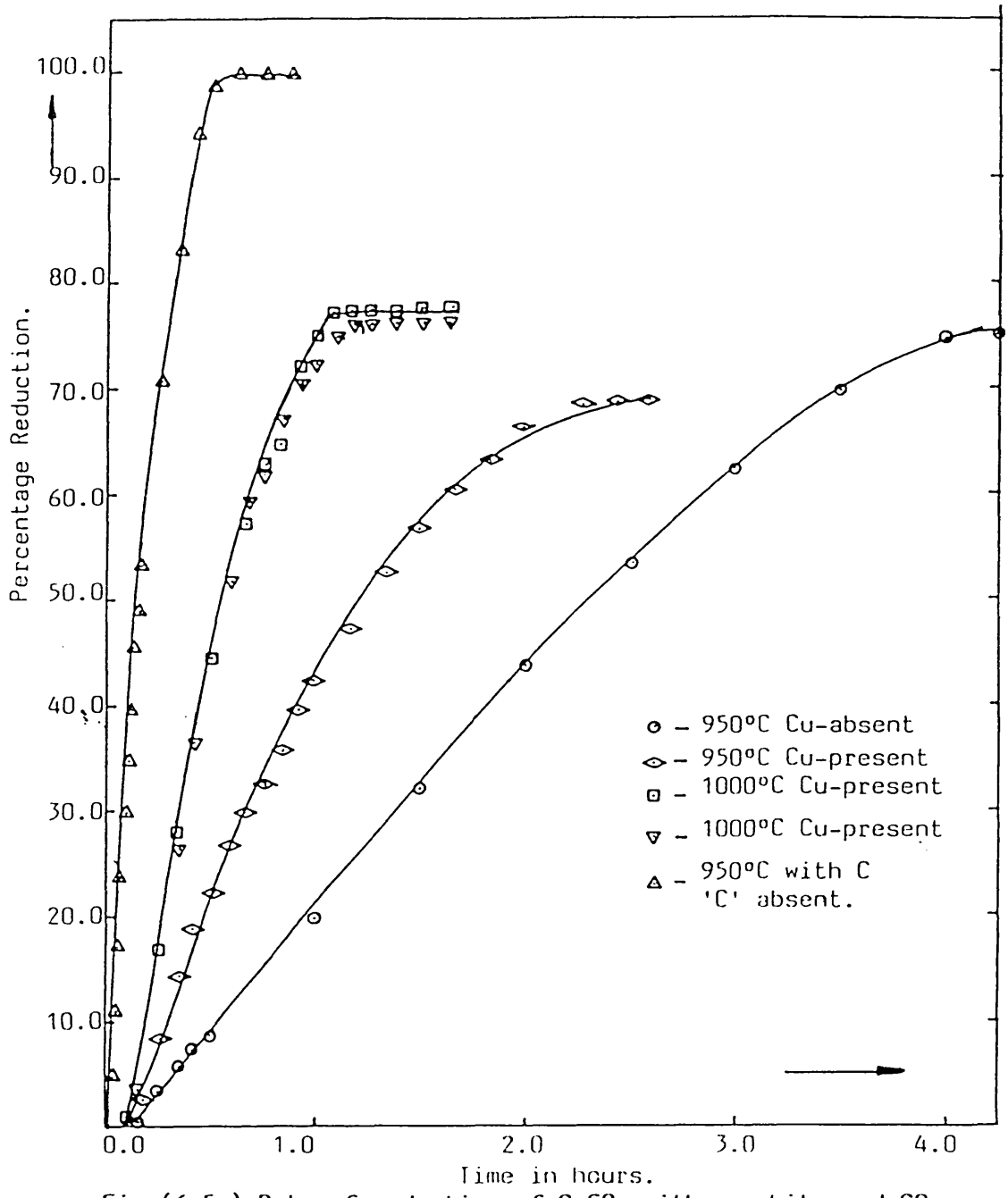


Fig (6.5a) Rate of reduction of $CaSO_4$ with graphite and CO. Argon atmosphere maintained during the reduction with graphite (Argon-200ml/min).

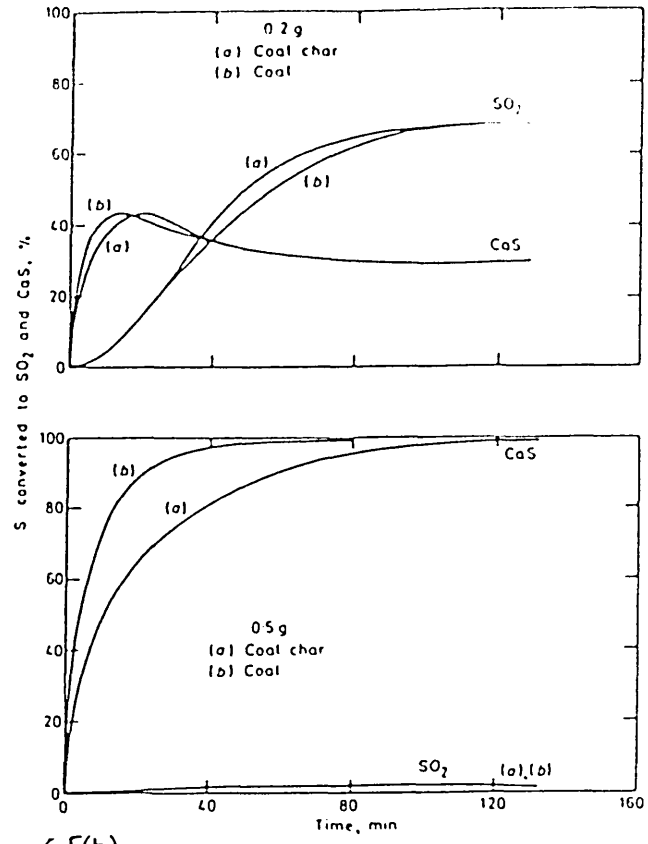


Fig. 6.5(b) Extent of conversion of $CaSO_4$ to CaS accompanied by evolution of SO_2 as affected by the amount of coal or coal char mixed with 1.6 g of $CaSO_4$ and treated at 1000°C

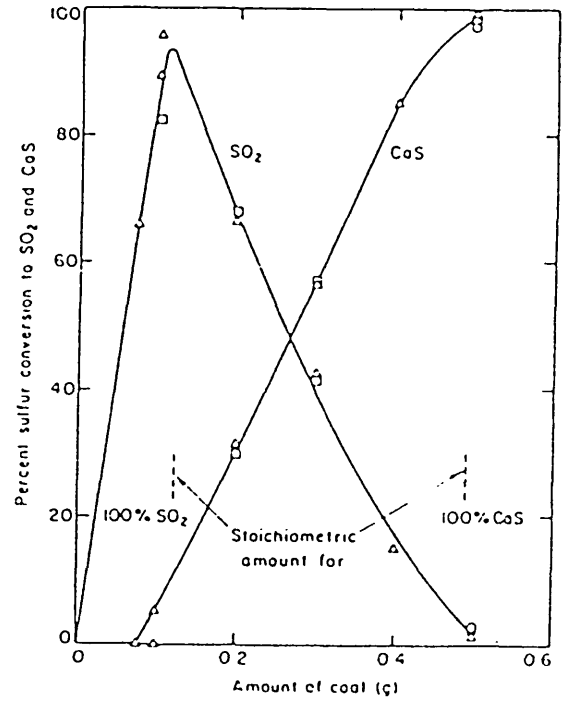


FIG. 6.6 Conversion of sulfur in calcium sulfate (1.65 g) to SO_2 and CaS at temperatures of (○) 1900, (△) 1000, and (□) 1100°C as a function of amount of coal in the mixture.

ii Inert Atmosphere Calcination of Calcium Sulphate.

During the reduction calcination of sulphate, the presence of lime showed that part of the desulphurization of the mixture proceeds according to equation (6.8). This aspect was separately analysed to understand the combined mechanism of calcination. Following the equilibrium represented by equation (6.8), the rate of calcination curves were drawn on the basis of the stoichiometry of the chemical reaction. The mass balance analyses together with X-ray diffraction data on the stoichiometric mixtures of sulphate and sulphide are arranged in Table 6.2 for the different temperatures:

Table 6.2: Observations on the Inert Atmosphere Calcination of Calcium Sulphate.

				Mass balance analysis		X-ray diffraction analysis.			
	Mixture Composition	Temp °C	Atmos $P_{O_2} \cdot 10^{-30}$	Pct wt loss	Pct Red.	CaO	CaS	$CaSO_4$	$Ca(OH)_2$
6.6	$CaSO_4$:CaS • 3:1	900°C	Argon	41.83	78.44	M	WM	M	M
6.7	$CaSO_4$:CaS • 3:1	950°C	Argon	51.33	96.24	W	W	VW	VS
6.8	$CaSO_4$:CaS • 3:1	1000°C	Argon	38.41	72.02	-	M	S	S
6.9	$CaSO_4$:CaS • 3:1	1000°C	Argon	38.93	73.01	-	-	-	-
6.10	$CaSO_4$:CaS • 3:1	1000°C	Argon	37.33	70.00	-	-	-	-
	Temperature raised to	1050°C	Argon	11.20	21.00	-	-	-	-
6.11	$CaSO_4$CaS • 3:1	1050°C	Argon	51.09	95.80	-	W	WM	VS
6.12	$CaSO_4$CaS • 3:1	1000°C	Argon	49.75	93.29	-	-	-	-
	Coarse particle of $CaSO_4$ - 153μ • 104μ								

The rate curves drawn on the basis of equation (6.8) shows that over a range of temperature 900°C to 1050°C the operative mechanism of overall reaction varies with temperature see figs (6.7) and (6.8). One mechanism appears at 1000°C and 1050°C and the difference in the slope of the rate of calcination curves is related to the apparent activation energy of the reaction in this temperature range. The other noticeable fact from the rate curves, at these temperatures, is the extent to which the reaction proceeds. At 1000°C, it is evident that the reaction has suddenly stopped. The sudden cessation of the reaction at 1000°C will be discussed later in the text. On the other hand, when a dual temperature treatment was given to the mixture, the reaction at 1050°C proceeded at much slower rates than expected from the results of the 1050°C single treatment. From the observations made in this temperature range, a significant difference in the rate was observed with coarser particles of $CaSO_4$ (-153μ + 104μ). This, once again proves that some parameter is influencing the overall rate to a large extent and is very sensitive to temperature and particle size.

A large difference in the slope of the rate of reactions at 950°C and 1000°C was observed although, the initial rates up to about 5% reduction, at these two temperatures were reasonably similar. An approximate comparison of the slopes at different temperatures is shown in fig (6.7). It is also evident from the comparison of rates at 900°C and 950°C, after the initial reaction that the reaction seems to follow a similar mechanism (a linear portion of these two curves) followed by a short parabolic regime. From then onwards at 900°C, the reaction proceeds at a linear rate. The quantitative mass balance is carried out in the

discussion section of this chapter where the significance of different reaction regimes will be considered.

The influence of particle size, the sudden cessation of reaction and its further progress at a slower rate at $1000^{o}C$ suggests that the progress of chemical reaction is probably inhibited in some ways which seems to be related to sintering.

Microscopic analyses were carried out on the calcined samples and the indications are the product layer grows from the outside of the pellet to inside. Energy Dispersive X-ray (EDX) analysis was carried out across the interface of the product and the reactant. On the basis of EDX analysis elemental distribution maps were produced. The schematic diagram for the growth of product layer is shown in fig (6.9). The morphological information obtained from the Scanning Electron Microscopy and from the elemental mapping of the calcined pellets show that the product layer is very dense with very few pores, see plate (6.1a). The microscopic analysis shows that a considerable amount of densification of the product layer has taken place during the course of calcination. In view of these observations, a correlation involving the thickness of the product layer, its densification characteristics, the rate of calcination and the equilibrium partial pressure of SO_2 will be discussed in the next section of this chapter.

Concerning the mechanism of the reaction at any temperature, the reaction between calcium sulphide particle should stop after some initial chemical reaction ie when a product lime layer is formed at the $CaSO_4$-CaS interface, but contrary to this, the reaction proceeds at the same rate at higher temperatures.

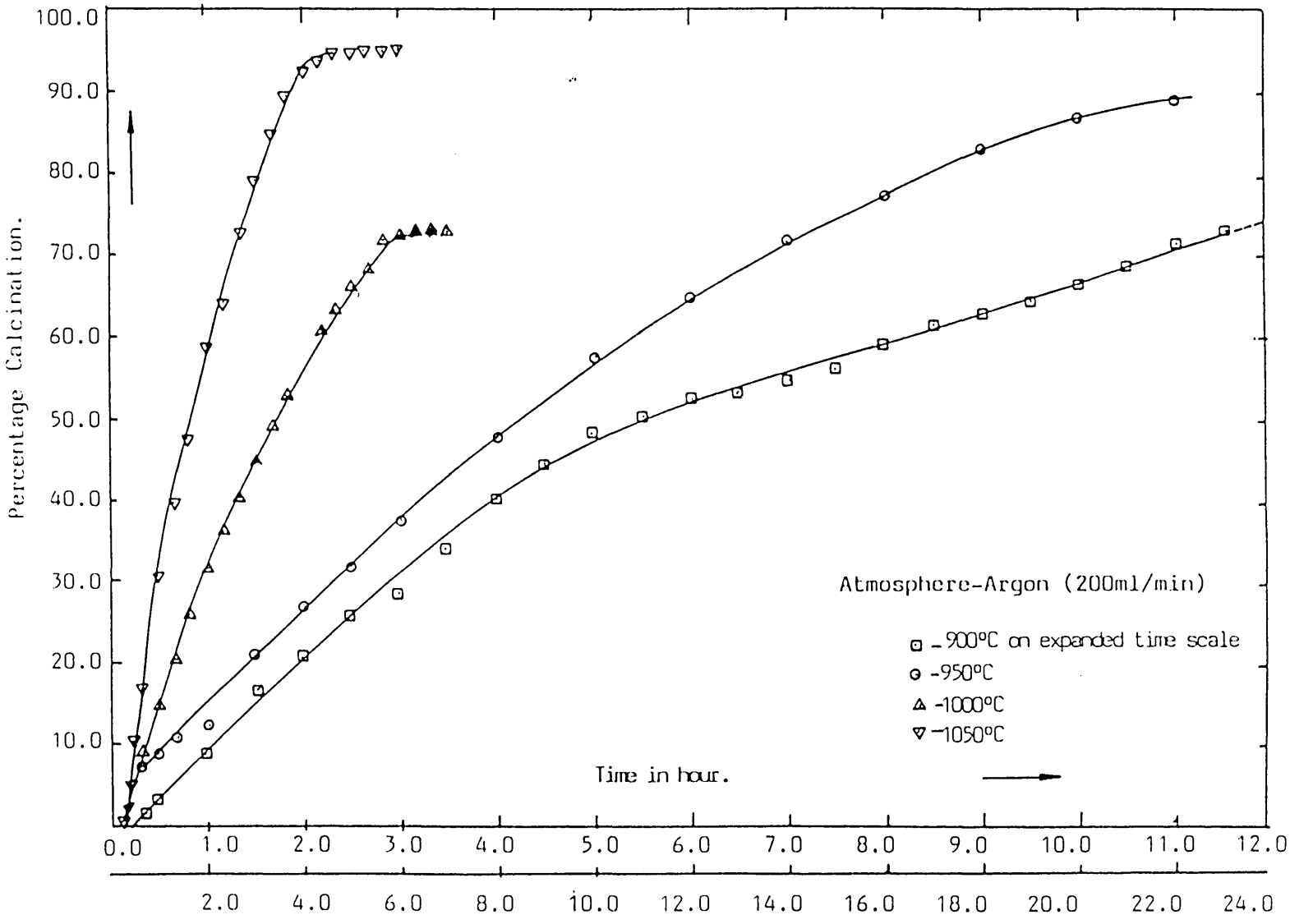


Fig (6.7) Rate of calcination of $CaSO_4$ in presence of CaS ($CaSO_4$:CaS = 3:1).

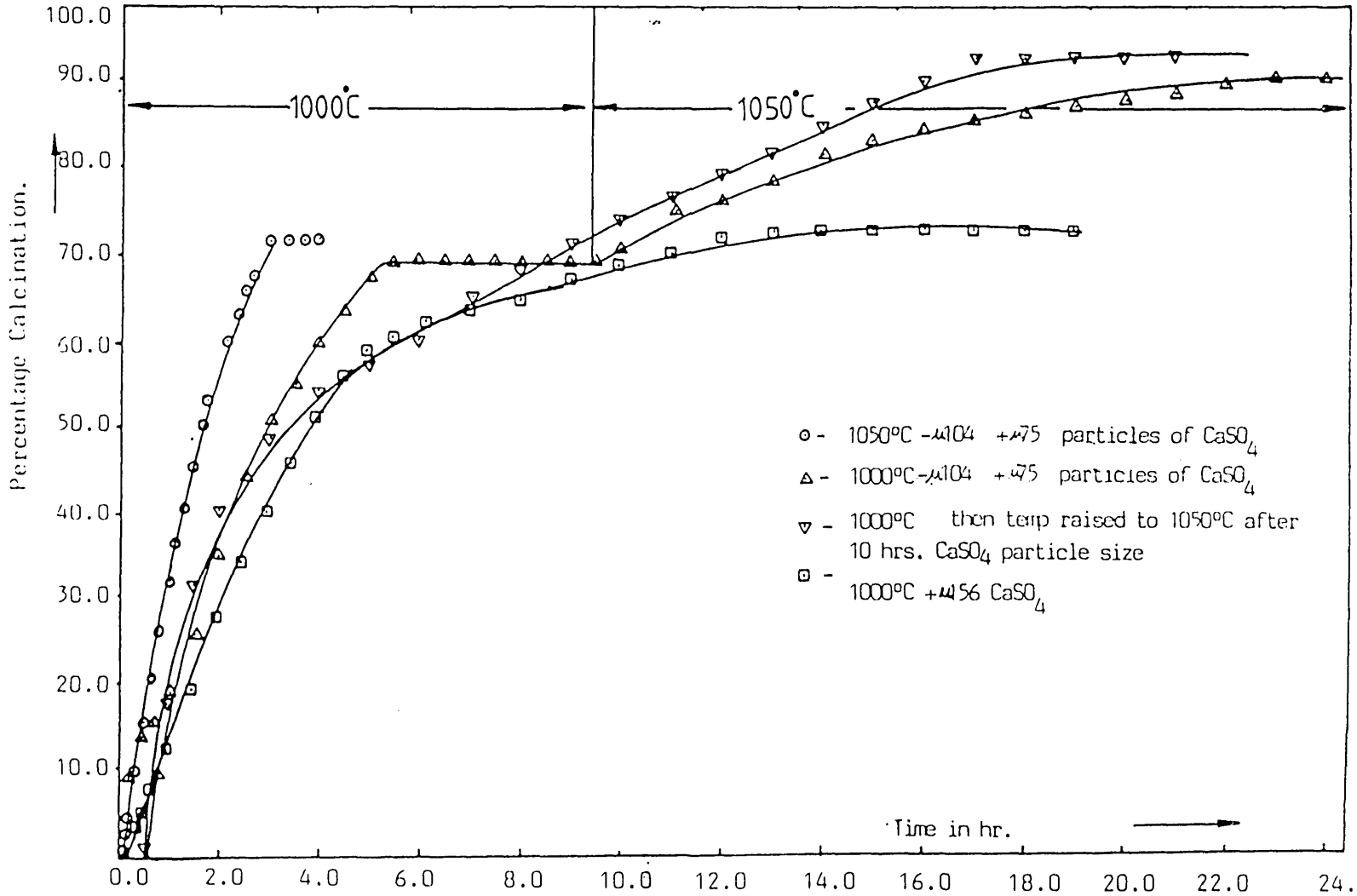


Fig (6.8) Rate of calcination $CaSO_4$ in presence of CaS in argon atmosphere ($CaSO_4$:CaS = 3:1).

At lower temperatures it undergoes completion with a change in reaction regime. This results in a large difference in the temperature coefficients of reaction, as evident from the slopes, indicating that the various mechanisms are extremely sensitive to temperature changes. Assuming that the nature of the chemical reaction changes after an initial stage and the subsequent reaction proceeds with the decomposition of calcium sulphate with a product gas intermediary ie:

$$CaSO_4(s) = CaO(s) + SO_2(g) + \tfrac{1}{2}\ O_2(g). \qquad (6.15)$$

$$\Delta G^{o}_{T} = 110370 - 56.82T$$

For which the equilibrium constant for the unit activities of lime and sulphate at T = 1273^{o}K is:-

$$K_{(6.15)} = 2.95 \times 10^{-7} = p_{SO_2}\ p^{\frac{1}{2}}_{O_2} = 2\ (p_{O_2})^{3/2}$$

ie $p_{O_2} = 2.78 \times 10^{-5}$atm.

For the equilibrium

$$CaS(s) + \frac{3}{2}\ O_2(g) = CaO(s) + SO_2(g) \qquad (6.16)$$

For which the equilibrium partial pressure of oxygen at T = 1275^{o}K is $p_{O_2} = 2.83 \times 10^{-29}$atm. The equilibrium partial pressures of oxygen for these two reactions (6.15) and (6.16) show that the decomposition of $CaSO_4$, under a stream of purified argon ($p_{O_2} = 10^{-30}$atm), would create conditions for the oxidation of the sulphide to lime and as a result desulphurisation could take place from the mixture. The partial pressure of oxygen in the flowing stream of argon makes conditions suitable for the decomposition of $CaSO_4$ to SO_2 and O_2.

In line with these assumptions experiments were designed to understand the possible operating mechanisms of calcination. These experiments were carried out with $CaSO_4$-CaS composite pellets of various sizes under identical conditions. The data obtained from these experiments are summarized in Table 6.3. The following are the most important features of the rate of calcination $CaSO_4$-CaS composite pellets:

i) The length of the incubation period for the calcination is directly proportional to the amount of $CaSO_4$ present in the composite ie the height of $CaSO_4$ portion of the composite pellet.

ii) It is inversely proportional to the temperature

iii) The rate of the overall reaction is inversely proportional to the height of the $CaSO_4$ portion of the pellet at any temperature.

iv) The extent to which the calcination takes place is inversely proportional to the height of $CaSO_4$ pellet in the composite

v) Deposition of lime was observed only around the periphery of $CaSO_4$ pellet and not around the CaS pellet.

vi) Once the product had formed at the CaS-$CaSO_4$ interface a loss of CaS was observed with increasing time.

Table 6.3: Results of Composite Pellet Experiments Argon Atm. ($p_{O_2} = 10^{-30}$ atm).

	Experimental Pellet Comp.	$\frac{CaSO_4}{CaS}$ wt ratio	Temp deg C	A	B	C	D	% wt loss	% red.	Incubation period in Min	Calculated wt. of lime from volume from volume (grams).
1	$CaSO_4$-CaS	6.66	950°C	0.31	0.275	0.22	-	7.38	13.84	480.0	0.0549
2	$CaSO_4$-CaO-CaS	6.66	950°C	0.1075	0.0704	0.085	0.009	1.68	3.15	60.0	0.0125
3	$CaSO_4$-CaS	3.032	1000°C	0.58	0.29	0.37	0.156	31.60	59.60	80.0	0.01296
4	$CaSO_4$-CaS	3.955	1000°C	0.56	0.59	0.39	0.185	19.93	37.37	140.0	0.1030
5	$CaSO_4$-CaS	2.815	1000°C	0.46	0.29	0.435	0.047	20.11	37.67	65.0	0.0776
6	($CaSO_4$-CaO)mix CaS	1.345	1000°C	-	-	-	-	$\frac{7.76}{9.97}$ +	$\frac{14.56}{18.68}$+	30.0	0.0197
7	$CaSO_4$-CaS	1.649	1000°C	0.37	0.85	0.80	0.62	28.33	53.12	5.0	0.076
8	($CaSO_4$-CaO)mix CaS	1.499	1000°C	-	-	-	-	$\frac{22.27}{33.8}$+	$\frac{41.74}{63.24}$+	60.0	0.0652
9	CaS-$CaSO_4$	6.55	1100°C	1.23	0.25	0.415	0.06	14.32	26.66	120.0	0.1033
10	CaS-$CaSO_4$	3.321	1100°C	0.844	0.5	0.5	0.40	17.19	32.23	65.0	0.0666
11	CaS-$CaSO_4$	1.683	1100°C	Undefined			layers	35.02	65.66	5.0	0.0903
12	CaS-CaO-$CaSO_4$	6.65	1100°C	0.638	-	-	-	8.64	16.18	-	-
13	($CaSO_4$-CaO)mix CaS	1.35	1000°C	0.6	0.625	0.625	0.55	9.97	18.68	20min	-

* Calculated from the stoichiometric relation given by (6.8) equation

\+ Pct wt. loss and pct. reduction calculated excluding the weight of lime.

All dimensions in mm.

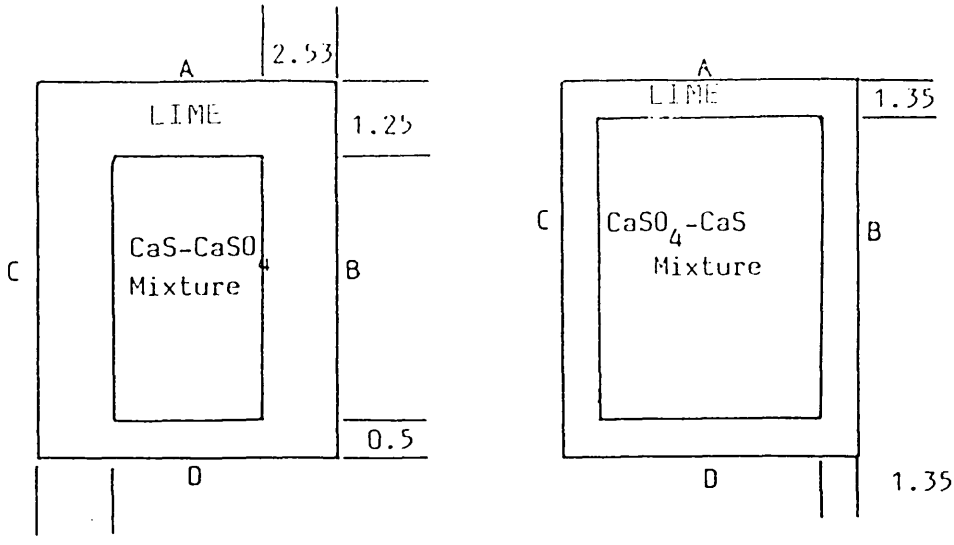


Fig (6.9) Schematic diagram of the product morphology after the calcination of $CaS-CaSO_4$ mixtures.

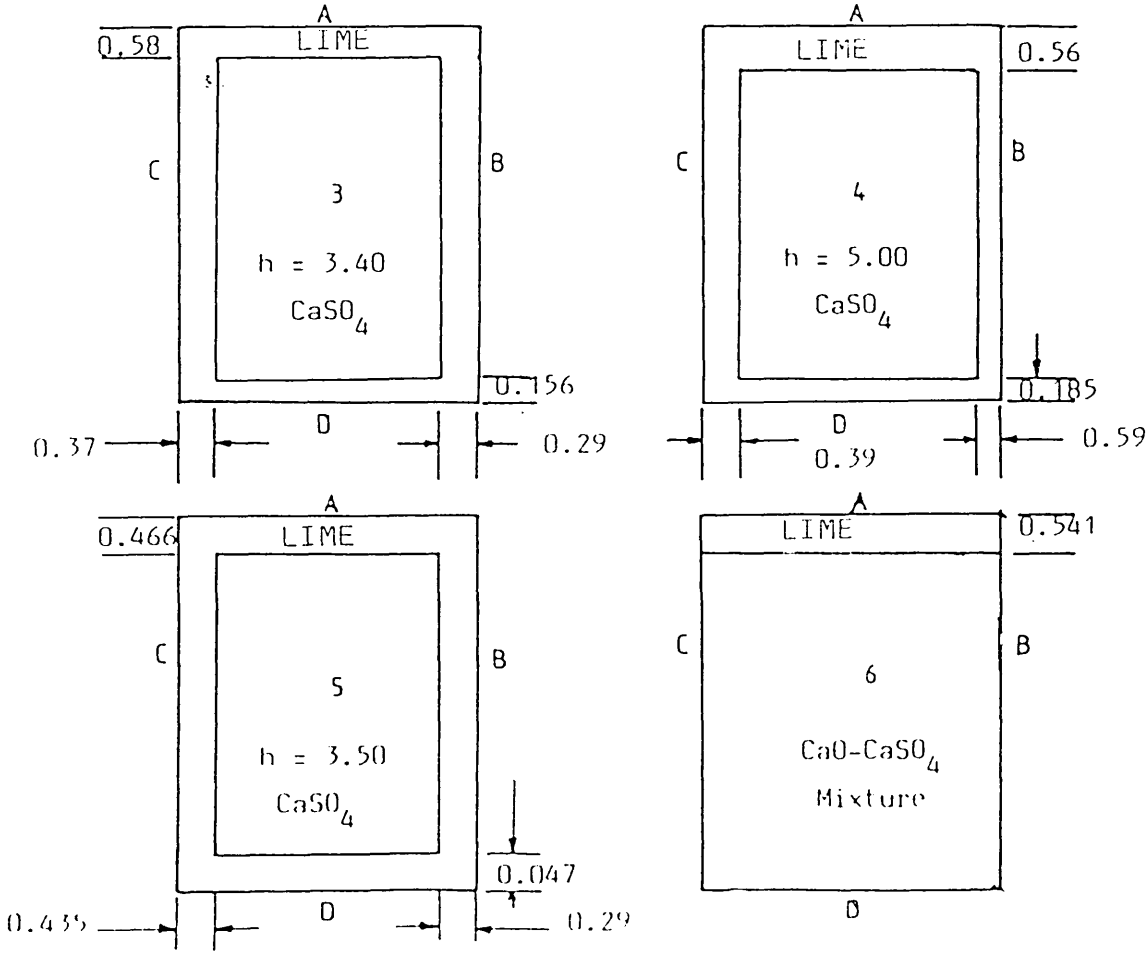


Fig (6.10) Schematic diagram of product morphology after the calcination of $CaS-CaSO_4$ composite pellets (contd).

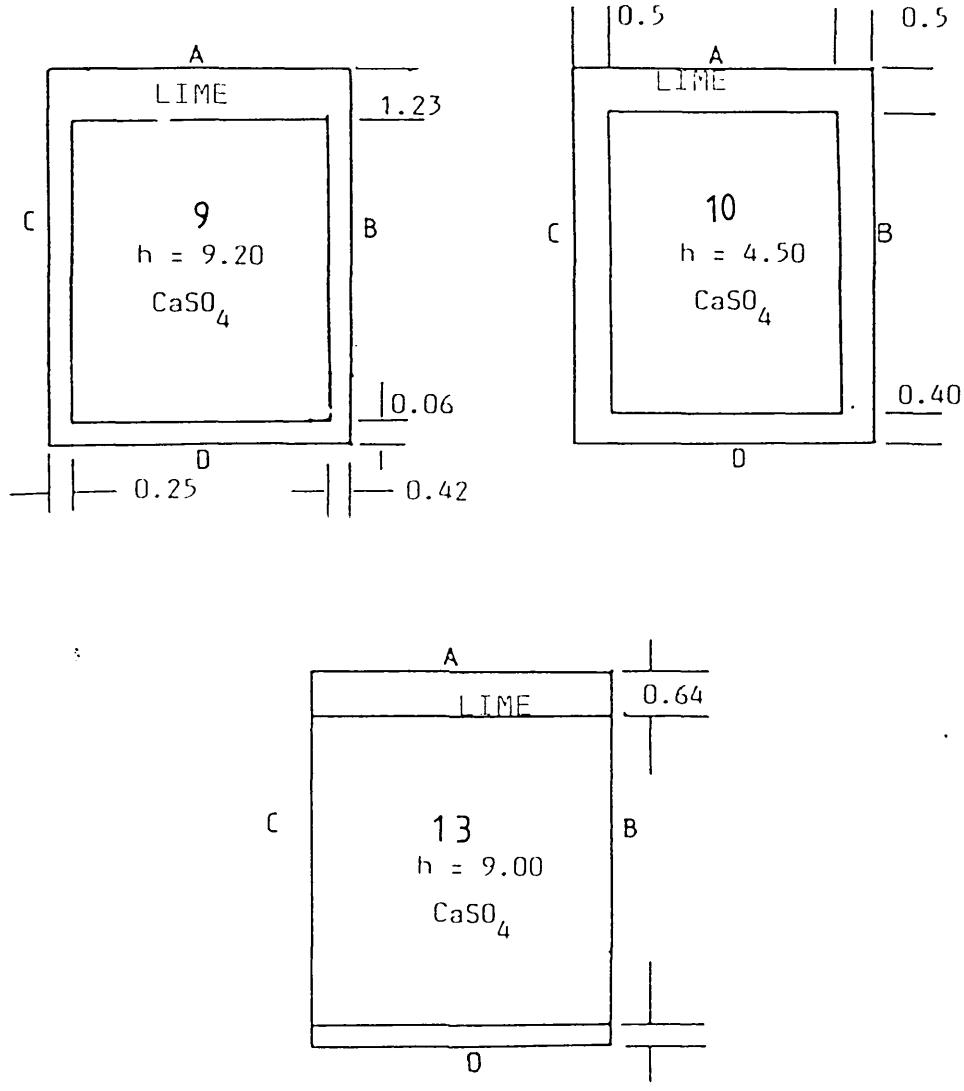
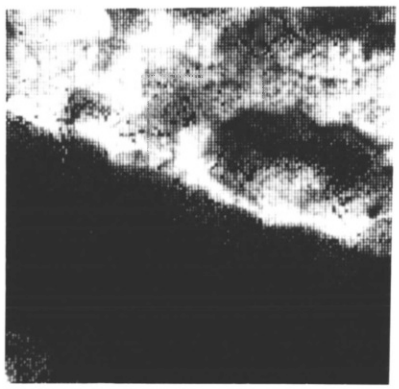


Fig (6.10) contd:- Schematic diagrams of product morphology after calcination of CaS-$CaSO_4$ composite pellets.

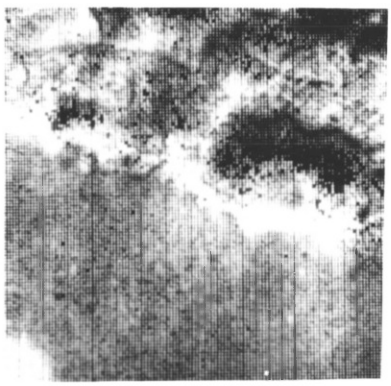
PLATE 6.1



x 650

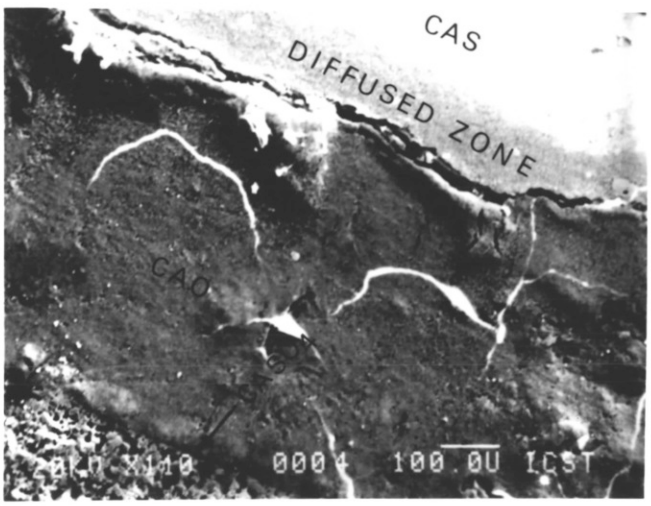


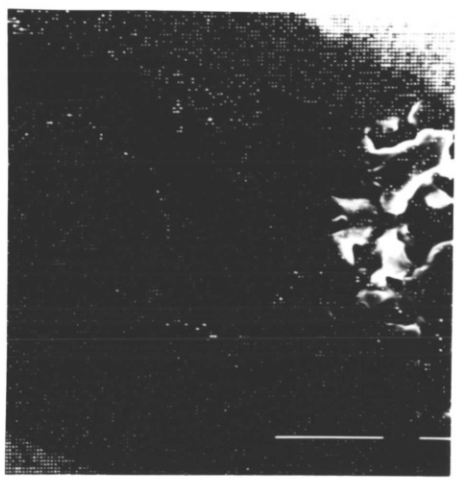
SULPHUR



CALCIUM

(A)





x 110

(B)

Plate 6.1 Calcination of calcium sulphate

(a) $CaSO_4$:CaS = 3:1 mixture at 900°C in argon sulphur and calcium distribution shown

(b) $CaSO_4$ - CaS composite pellet at 1100°C in argon sulphur distribution shown

The data for the extent of reaction, the amount of $CaSO_4$ in the composite and the amount of lime deposited around the peripheral regions and at the original CaS - $CaSO_4$ interface are summarized in Table 6.3. The areas of lime deposition on the periphery of the $CaSO_4$ pellet have been defined and shown in the form of a schematic diagrams in fig (6.10). Typical rate of calcination curves for different temperatures and with different proportions of sulphate are shown in figs (6.11a) and (6.11b). In one experiment a composite pellet in which the CaS - $CaSO_4$ interface was isolated with a lime layer was prepared and the calcination was carried out at 950^oC. It was found that the length of the incubation period for calcination had decreased considerably for the same geometry of $CaSO_4$ pellet in the composite. A sharp decrease in the incubation period for the reaction was subsequently confirmed using a ($CaSO_4$ - CaO mixture) - CaS composite pellet. For calcincation of these pellets, the length of the incubation period was inversely related to the height of $CaSO_4$ pellet and the temperature see fig (6.11c). It also appears although during the course of reaction there is a presence of lime which otherwise would have delayed the commencement of the reaction but still in those situations the geometry of $CaSO_4$ pellet with lime in the mixture has an overwhelming effect in determining the speed of reaction. The presence of lime eliminates the barrier for nucleation. Another very important feature of these rate of calcination curves, see fig (6.11c), is the decrease in rate of reduction with increase in the height of $CaSO_4$ pellets. The preferential peripheral and interfacial deposition of lime was once again observed in all experiments carried out in the presence of lime. This is an indication

that lime deposition at the periphery is unaffected by its presence as an external nucleating agent. Furthermore non-uniform peripheral deposition of lime was observed with the tallest $CaSO_4$ pellet at 1100^oC ie a comparitively thick layer of lime near to the original $CaSO_4$-CaS interface. To justify this evidence a composite and a mixture pellet of lime and $CaSO_4$ were made without CaS and heat-treated at 1000^oC. Microscopic observations indicate that the peripheral deposition of lime has taken place around the $CaSO_4$ pellet whereas hetrogeneous pockets of lime were observed in the case of the mixture see table (6.3). Although these two experiments were similar,a considerable difference in the incubation period was observed see fig (6.11d). The difference in the incubation period is probably due to the area effect of the particle to particle contact affecting the commencement of reaction. It is also well known (6.5) that $CaSO_4$ has a limited solubility in CaO above 900^oC so the necessary time to establish this equilibrium of CaO with $CaSO_4$ will also affect the incubation period for calcination reaction.

In this investigation, the calcination of $CaSO_4$ was carried out in pure and in impure argon atmospheres and a massive weight loss was observed during the calcination of sulphate in pure argon ($^Po_2 = 10^{-30}$atm). The X-ray diffraction analysis showed the relative amounts of lime and $CaSO_4$ present in the pellet. Whereas an insignificantly small weight loss was observed when impure argon was used ($^Po_2 = 10^{-6}$atm). The following observations were made:

i) The decomposition of $CaSO_4$ takes place in an argon atmosphere according to equation (6.15).

ii) The extent and the rate of decomposition of $CaSO_4$ is inversely proportional to $^Po_2$ in the gas phase.

iii) The rate of decomposition of $CaSO_4$ in the case of a

mixture with CaO and with a CaO composite is identical

iv) The incubation period in these two expeiments with CaO and in the case of decomposition of $CaSO_4$ is related to the equilibration of lime with $CaSO_4$. The incubation period for the decomposition of sulphate was smallest when no lime was used.

The lime formed during the reaction or the lime used in the pellet as an external nucleating agent tends to slow down the overall calcination because of the limited solubility of $CaSO_4$ in CaO. On the basis of these observations, it can be conclusively be said that the calcination of sulphate and sulphide composites in a pure stream of argon proceeds simultaneously in two ways:

a) The calcination of $CaSO_4$ in the presence of CaS according to equation (6.8)

b) The thermal decomposition of sulphate in pure argon according to equation (6.15).

The deposition of lime at the CaS-$CaSO_4$ interface is confirmed by EDX Scan analysis and the sulphur element mapping is shown in plate (6.1b).

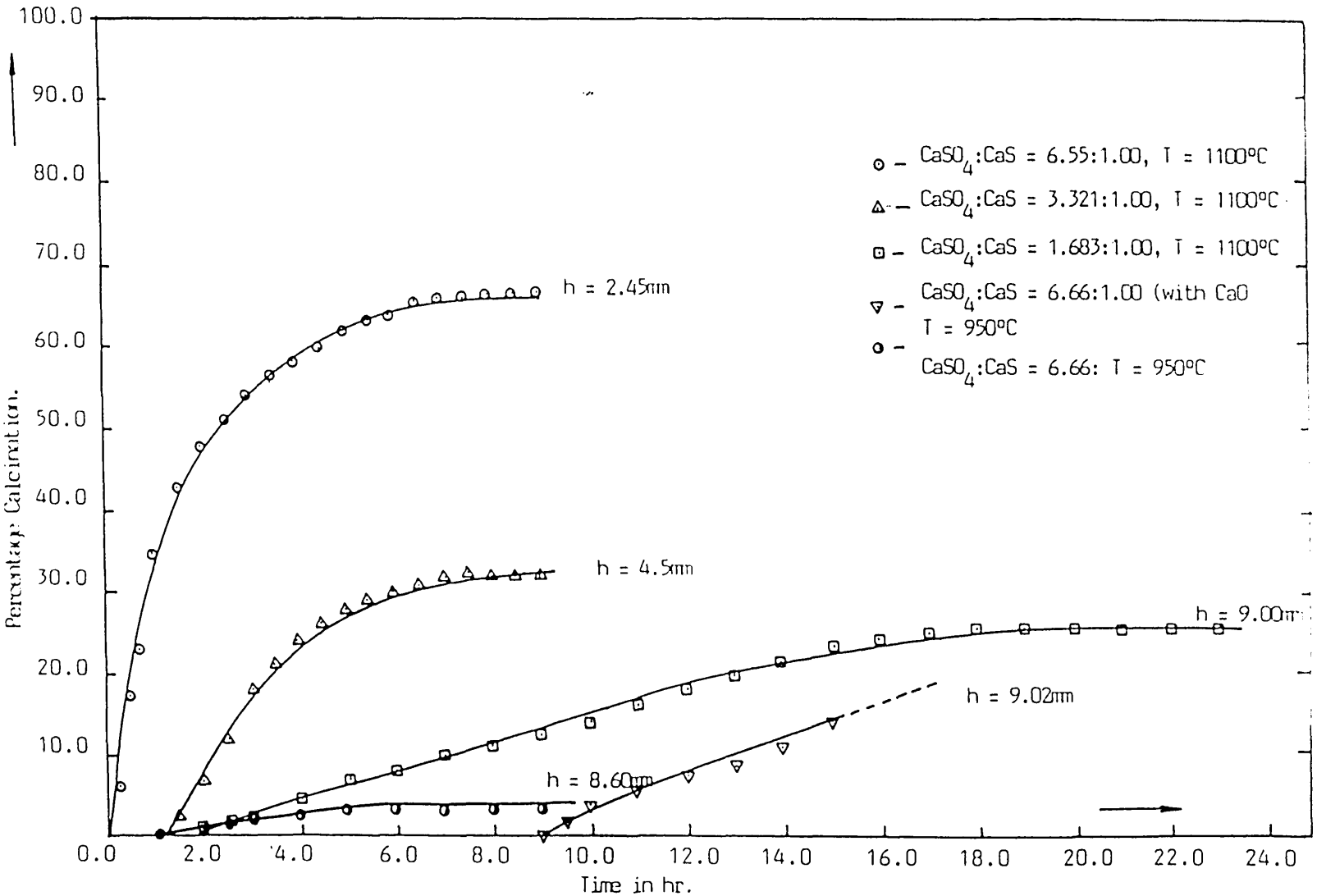


Fig (6.11a) Effect of temperature and height of $CaSO_4$ pelle on the calcination of $CaSO_4$ - CaS composite.

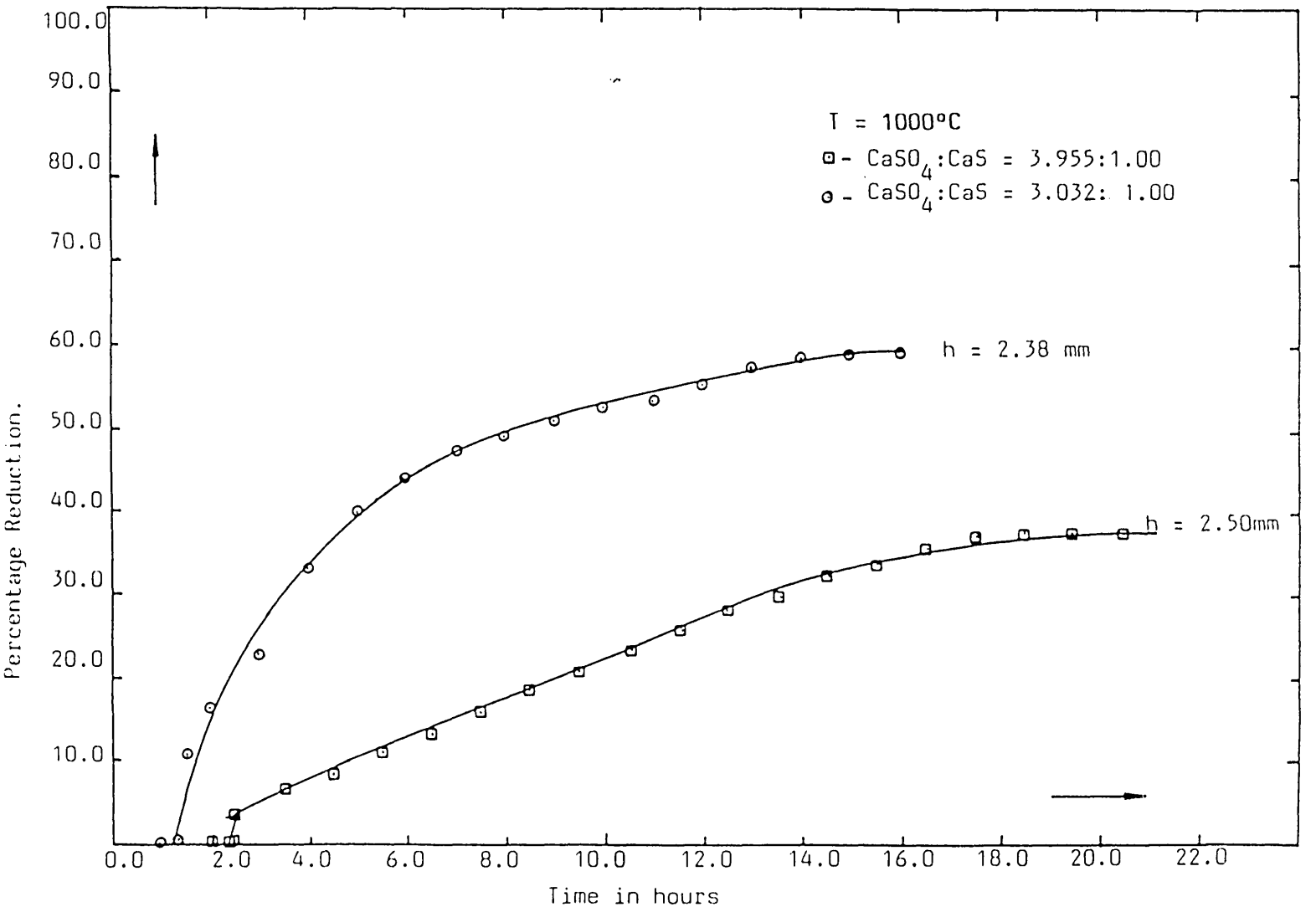


Fig (6.11b) Rate of calcination of $CaSO_4$-CaS composites in argon atmosphere.

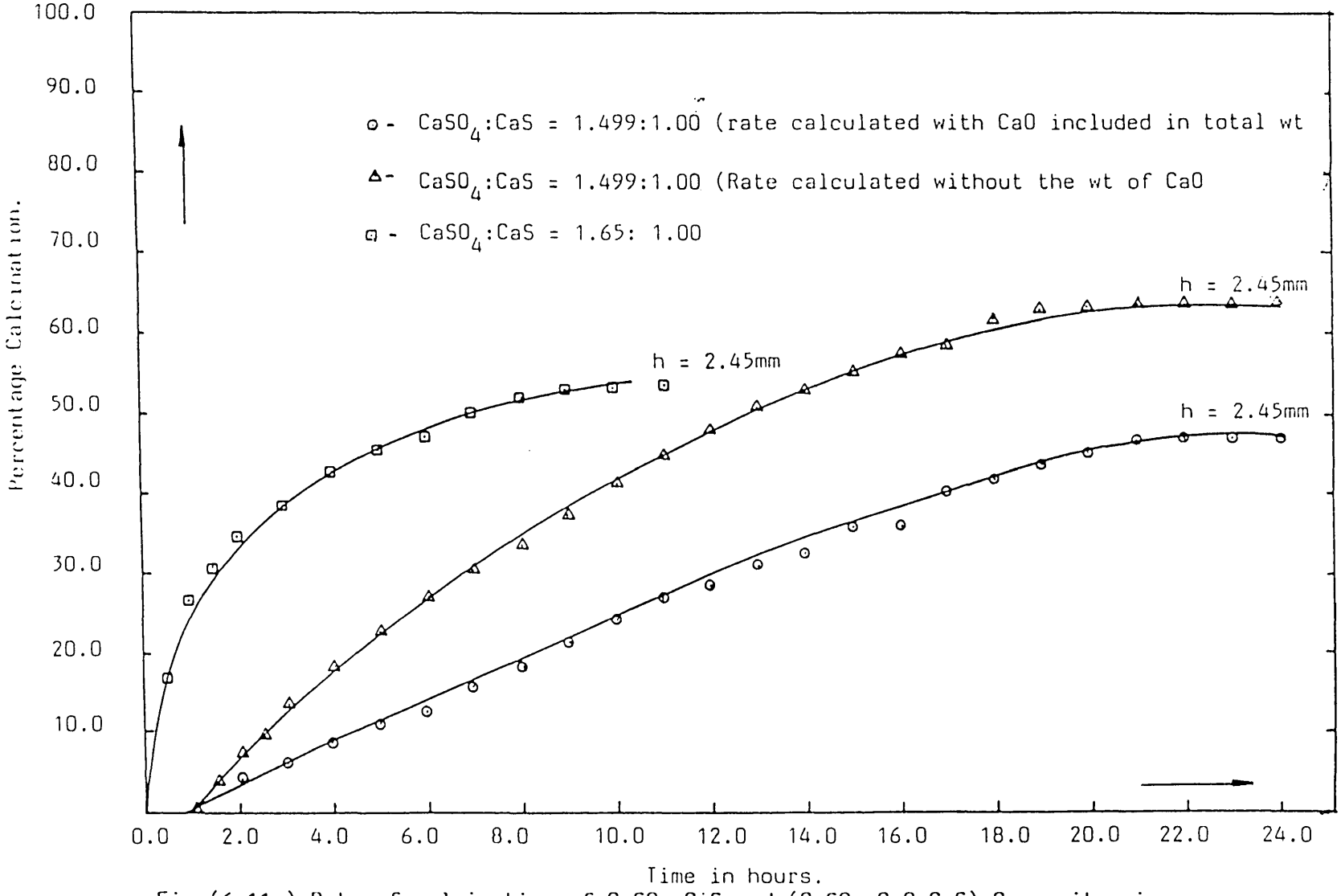


Fig (6.11c) Rate of calcination of $CaSO_4$-CaS and ($CaSO_4$:CaO-CaS) Composites in argon atmosphere (200ml/min) at 1000°C.

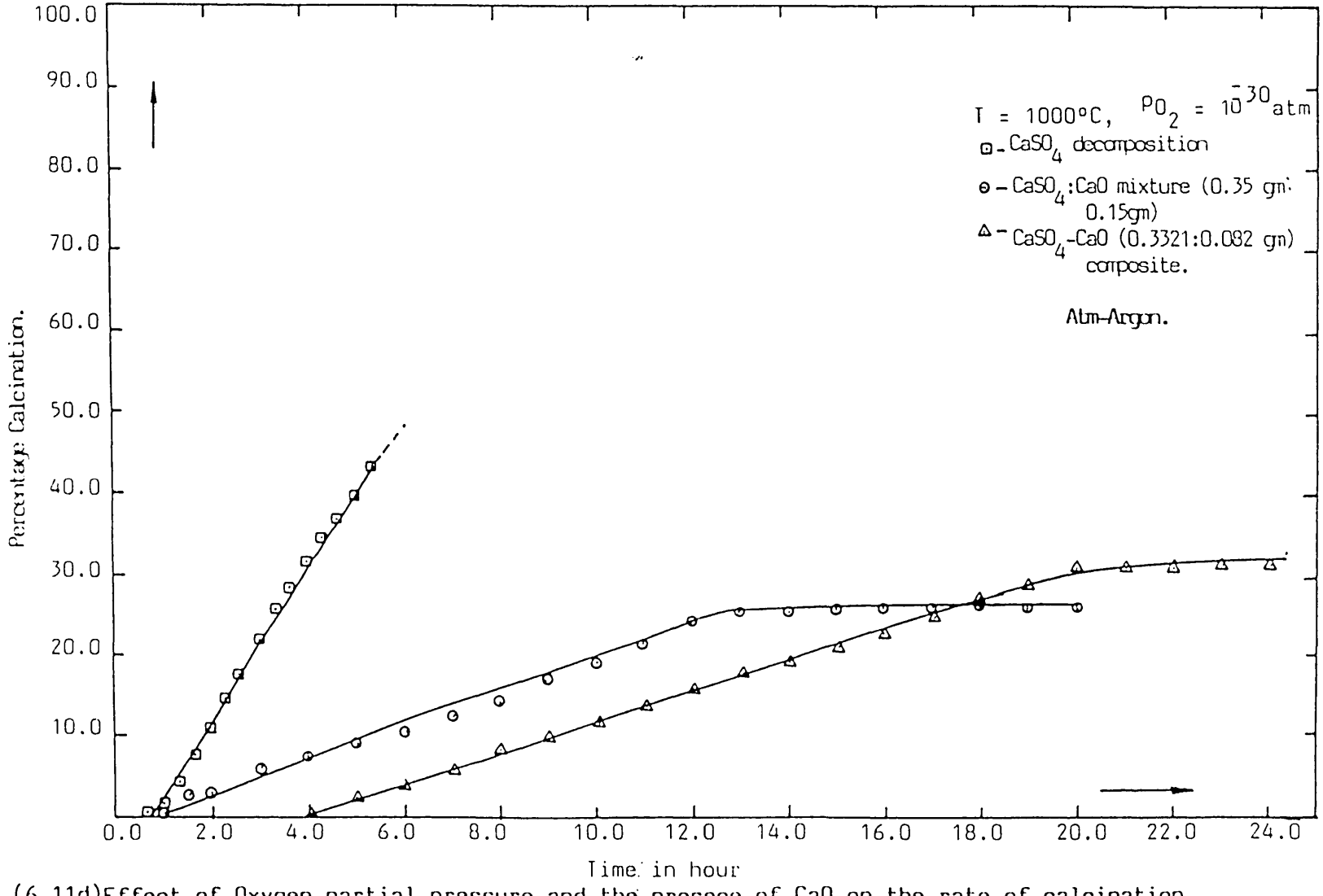


Fig (6.11d)Effect of Oxygen partial pressure and the presece of CaO on the rate of calcination of calcium sulphate.

Table 6.4: Thickness of Lime on the CaS Pellet Measured from Original Interface.

Experimental Pellet Comp	$\frac{CaSO_4}{CaS}$ wt ratio	Temperature	Thickness in mm	Remarks
$CaS-CaSO_4$	6.55	1100°C	99μ = 0.099	
$CaS-CaSO_4$	3.321	1100°C	16.87μ = 0.167	about 50-30μ thick diffused layer.
$CaS-CaSO_4$	3.032	1000°C	145.00μ = 0.145	at the interface, lime-CaS was very diffused.
$CaS-CaSO_4$	2.815	1000°C	125.5 μ = 0.127	105μ-165μ diffused layer
$CaS-CaSO_4$	3.955	1000°C	157.5 μ = 0.157	150μ-165μ diffused layer
$CaS-CaSO_4$	1.649	1000°C	112.5 μ = 0.1120	75μ-105μ diffused layer.

Table 6.5: Thickness of Product Layer During Calcination of $CaSO_4$ with Lime in Oxygen Free Argon (10^{-30}) and Impure Argon (10^{-15})

Experimental Pellet Comp.	$\frac{CaSO_4}{CaS}$ wt ratio	Argon Atom	Temp	Thickness of Lime Layer in mm				% wt loss	% red.	Incubation period in mm.
				A	B	C	D			
$CaSO_4$-CaO mixt	-	$P_{O_2} = 10^{30}$	1000°C	-	-	-		17.64	29.28	60.
$CaSO_4$-CaO	-	$P_{O_2} = 10^{-30}$	1000°C	0.075	0.0437	0.37	0.325	37.42	64.46	240
$CaSO_4$	-	$P_{O_2} = 10^{-30}$	1000°C	Non Uniform Layer				30.74	51.68	40
$CaSO_4$	-	$P_{O_2} = 10^{-15}$	1000°C	Non Uniform Layer				2.012	3.42	-
$CaSO_4$-CaS	3.317	$P_{O_2} = 10^{-15}$	1000°C	0.375	0.10	0.20	0.025	13.98	26.19	15 minutes.

6.0. DISCUSSIONS

i) The Mechanism of the Calcination of Calcium Sulphate in the inert atmosphere:-

The chemical equilibrium for the calcination of sulphate represented by equation (6.8) shows that the reaction has a large endothermic heat and a large entropy change associated with it. Under the condition of unit activity of all the condensed phases the equilibrium temperature at which P_{SO_2} = 1.0atm, ie ΔG^o = 0 is T equilibrium = 1190^{o}C. The system reaches equilibrium at 1456^{o}K. From our observations, it is evident that the reaction commences at 900^{o}C. Using the equilibrium data at any temperature, the equilibrium pressure of SO_2 can be calculated from the following relationships considering unit activity of all the condensed phases.

$$(P_{SO_2})_T^{\text{equilibrium}} = \exp\left(-\Delta G^o/RT\right)^{0.25} \qquad (6.17)$$

where ΔG^o = 222670 - 151.96.T

The reason for the commencement of the reaction at a temperature much below the equilibrium temperature can be explained on the basis of Le Chatelire's Principle. The calcination has been carried out in a flowing stream of argon where $P_{O_2} = 10^{-30}$atm, and this partial pressure of oxygen is much lower than the equilibrium partial paressure of oxygen in the system $P_{O_2} = 10^{-15}$at 900^{o}C. This difference of 15 orders of magnitude in the partial pressure of oxygen established a large chemical potential gradient for the reaction to commence. The experimental system never allows the product gas to accumulate and influence the back reaction. This also explains the decomposition of calcium sulphate in a stream of pure argon.

At this point, it is worth noting that the equilibrium represented by equation (6.16) does not prevail as the flowing stream of argon does not allow oxygen to have a sufficient residence time to react with CaS to form CaO and sulphur dioxide in the case of composite pellets. However, these thermodynamic calculations do not substantiate the mechanism of calcination.

From our results it is evident that the presence of lime is essential and the nucleation of lime is a barrier for the commencement of the calcination reaction from the rate data, it is evident that the incubation period is a function of size and geometry of $CaSO_4$ pellet in the composite and is dependent on the temperature; which means that the important factor is influenced by these two parameters. From the data summarized in Table 6.4, it is evident that as the reaction progresses the height of the CaS pellet in the composite diminishes. The $CaSO_4$ - CaO interface is mobile whereas CaO-CaS interface is stationary with the thickness of CaS layer in diminishing with time. This evidence together with the parabolic nature of the rate curves justifies hypothesis of diffusion of one of the reacting species being influenced by these parameters.As mentioned earlier,the calcination proceeds in two ways ie a chemical reaction between CaS and $CaSO_4$ and the pure decomposition of sulphate to lime and SO_2, it is evident from our observations that the first mode of calcination is governed by the diffusion of these participating ionic species.

Considering the data from the deposition of lime at the periphery and at the interface and correlating the observed weight loss with the thickness of product layer it can be inferred that the ratio between the peripheral or interfacial, lime to the total weight of lime generated is slightly greater than 1:2. This means an equal proportion

of lime generated at $CaSO_4$/CaS and the $CaSO_4$/gas interface and the consistency suggests that they ought to be connected in some stoichimetric manner which will establish the mechanism. The possible mechanisms related to the observed stoichiometry are shown below:

At the interface

$$2CaSO_4(s) + CaS(s) = 2CaO(s) + SO_2(g) + Ca^{+2} + 2e \quad (6.18)$$

At the periphery

$$Ca^{+2} + 2e + CaSO_4(s) = 2CaO(s) + SO_2(g) \quad (6.19)$$

Adding these two equations would give equation (6.8).

The equilibrium represented by equation (6.18) shows that calcium ions and SO_2 are generated at the interface. This mechanism is supported by the experimental observations eg the nucleation of lime presents a barrier and the height of the $CaSO_4$ pellet is an important factor in governing the rate of reaction. For the continuation of the interfacial reaction, it is necessary that the product is removed from the interface. The gaseous product is liberated by pore diffusion and is swept away by the inert gas, whereas Ca^{+2} ions and electrons create a chemical potential gradient for transport. Such a transport mechanism of those species is essentially Chemical Diffusion and is much faster than self-diffusion. This concept explains why the rate of calcination is affected by the geometry of $CaSO_4$ as the diffusion distance governs the reaction rate. The electrons can diffuse easily and their diffusion is not expected to be the rate controlling step. Diffusion of Ca^{+2} ions through the $CaSO_4$ lattice is a much slower process while

S^{+6} ion diffusion is fast because of its small ionic radius. In contrast, O^{-2} ions are large in comparison to Ca^{+2} ions, so that O^{-2} ion transport would reduce calcination reaction to a very slow process. Considering the crystal structure of $CaSO_4$, it is evident that O^{-2} ions are essentially distributed in a closed packed arrangements with Ca^{+2} and S^{+6} ions occupying interstitial sites, resulting in the easier movement for the latter ions. Since during the transport process S^{+6} ion movement does not occur, it is the diffusion of Ca^{+2} ions which govern the rate of reaction. Therefore, once the conditions for peripheral reaction are satisfied by the establishment of the transport of ions, CaO generation and SO_2 evolution take place according to equation (6.19). This mechanism explains every possible variation in the reaction rate discussed. In order to prove the validity of this mechanism experiments were carried out in impure argon and the weight losses and the thickness of the product lime layers were correlated. These data were in agreement within the experimental error mainly due to the formation of porous lime. These experimental results are arranged in Table 6.5. The rate curves are shown in fig (6.13a) and fig (6.13b).

Once the lime layer develops at the interface, the mechanism of reaction alters. The growth of lime at the interface separates the $CaSO_4$ and CaS and the further reaction only proceeds via diffusion of the sulphate and sulphide ions through calcium oxide. Turkdogan et al (6.5) have investigated the solubility of sulphate and sulphide in lime and solubility data is shown in fig (6.12). The partial solubility of SO_4^{-2} of S^{-2} ions in lime have been verified by EDX analysis, see plate (6.1b) where the

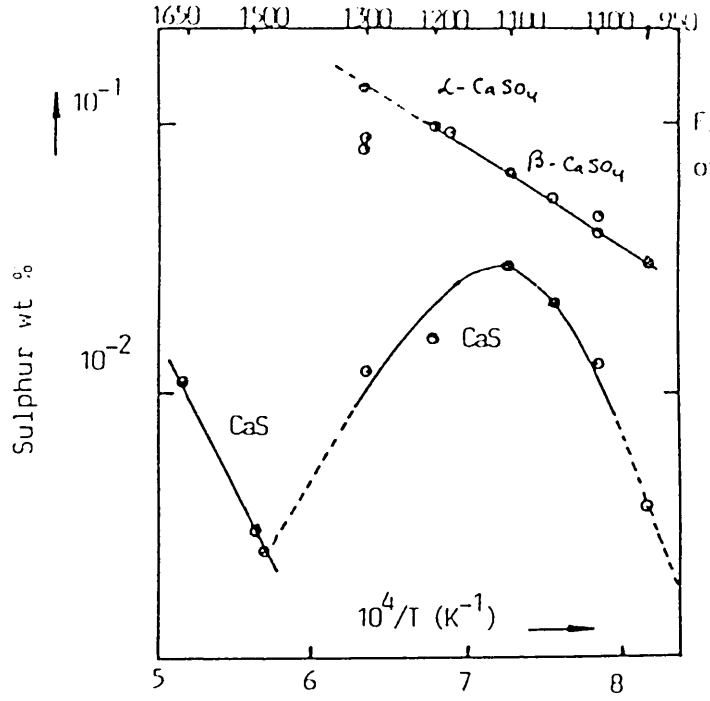


Fig (6.12) Variation of solubility of CaS and $CaSO_4$ in CaO with temp.

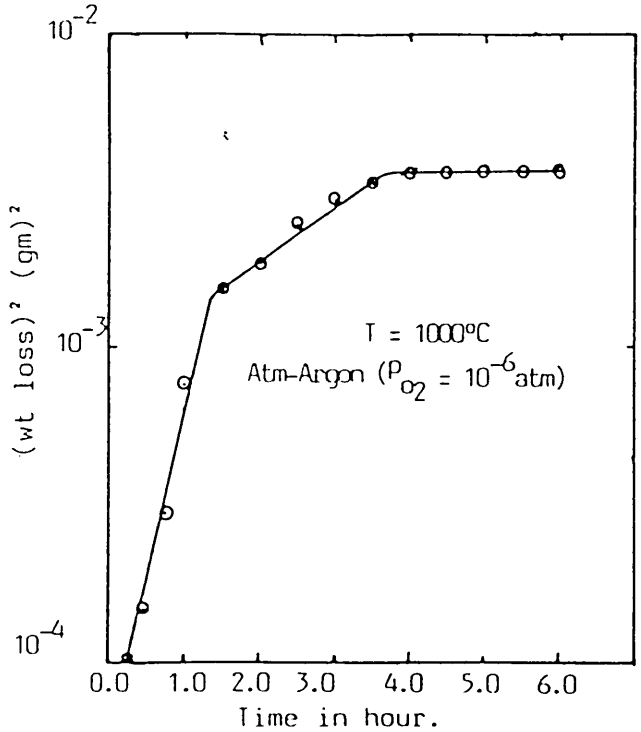


Fig (6.13a) (wt.loss)² vs time relationship for the calcination of CaS-$CaSO_4$ composite in impure argon at 1000°C.

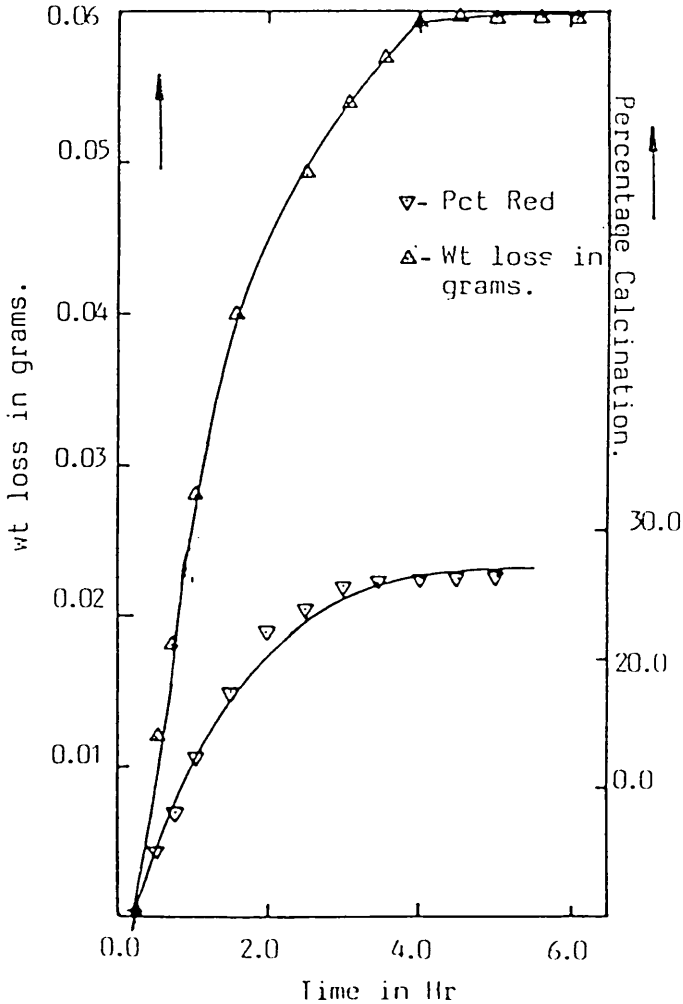


Fig (6.13b) Rate of calcination of $CaSO_4$-CaS composite in impure argon.

presence of sulphur diffused into CaO can be seen. This plate shows the penetration depth of S^{-2} ion in CaO during the course of reaction. The mechanism of calcination of composite pellets indicates that the presence of lime has a pronounced effect on the rate of calcination. The rate of calcination of calcium sulphate is remarkably affected by the way lime is made available inside the pellet as an external nucleating agent. If lime-$CaSO_4$ composite is made, the incubation period is much longer than the case where lime is mixed with $CaSO_4$ particles, see fig (6.11c) and fig (6.11d). In presence of lime, it is the total surface area of contact between $CaSO_4$ and CaO which governs the initiation of the reaction as the surface area determines the area over which the equilibrium between lime and $CaSO_4$ is taking. This equilibrium is essentially due to the solubility of SO_4^{-2} ions in CaO at that temperature. Thus in case of composites where the diffusion distance is relative larger the equilibration time is also longer before the calcination reaction commences. An approximate calculation has been carried out to determine the diffusivity of S^{+6} ion for the given geometry of pellet.

For L = 1.1mm, t = 3hrs = 3 x 3600 secs, and for an unidirectional flux of S^{+6} ion towards the CaO pellet, the value of fraction saturation F = 3.00

$$\frac{Dt}{L^2} = F \quad \text{ie} \quad D = 2.77 \times 10^{-6} \text{ cm}^2/\text{sec}$$

which means the diffusion of S^{+6} ion is extremely fast and hence the saturation can be attained very quickly. A third factor in addition to the diffusion of ionic species and their solubilities in CaO, appears to influence the reaction. ie the densification of the lime layer. This factor seems to

have affected the overall reaction by bringing it to a permanent halt. Sintering of the lime layer presents an impervious layer through which SO_2 diffusion is retarded in the later stage. This effect can be seen in fig (6.13) where the reaction has suddenly stopped. From the rate data at different temperature and sintering characteristics of the lime layer it is apparent that the densification is maximum at $1000^{o}C$.

From our experimental results it is evident that calcination is faster with small heights of $CaSO_4$, and a correlation between temperature and rate has been established. Thus, a geometric factor (g) has been considered and is defined as the area to volume ratio of $CaSO_4$ pellet (in mm^{-1}) and attempts have been made to correlate it with the initial slope of the calcination reaction. The data are arranged in the Table (6.6) and the correlation is shown in fig (6.14). Plotting (-) log $\frac{dR}{dt}$ vs g (mm^{-1}) a relationship was established for two temperatures. From this graph, it is apparent that the mechanism is identical at higher value of 'g' where a different mechanism is operative. Had there been no change in the mechanism, the curves would have been parallel. Since the diffusion distance plays a very important role in the reaction, the increase in the volume to area ratio (1/g) causes the rate to decrease.

Considerations of the dependence of rate with the geometric factor shows that both the diffusion process and the partial pressure of SO_2 is exponentially related with the temperature. The difference in the activation energy of the diffusion process is related to the parallel portion of the curve but an alteration of the mechanism can be seen at lower temperatures with lower 'g'. If the diffusion distance and the equilibrium partial pressure of SO_2 are affected

Table 6.6: Relation of Geometric Factor (g) With Temperature.

Pellet Comp	Temp ^{o}C	Interface 'A' in mm	Vol of Int. A $(mm)^3$	Int. 'A' Mass in Grams	Calculated wt of lime at int. 'A' from wt. loss.	p_{O_2} in atm.
$CaSO_4$ - CaS	950°C	0.31	9.82	0.032	0.0241	10^{-30}
$CaSO_4$ - CaS	1000°C	0.58	18.37	0.061	0.0567	10^{-30}
$CaSO_4$ - CaS	1000°C	0.56	17.73	0.0586	0.0451	10^{-30}
$CaSO_4$ - CaS	1000°C	0.466	14.76	0.0487	0.0340	10^{-30}
$CaSO_4$ - CaS	1000°C	0.37	11.71	0.0387	0.0333	10^{-30}
$CaSO_4$ - CaS	1100°C	1.23	38.95	0.1285	0.0452	10^{-3}
$CaSO_4$ - CaS	1100°C	0.844	26.73	0.088	0.0300	10^{-3}
$CaSO_4$ - CaS	1000°C	0.375	11.86	0.039	0.0261	10^{-15}

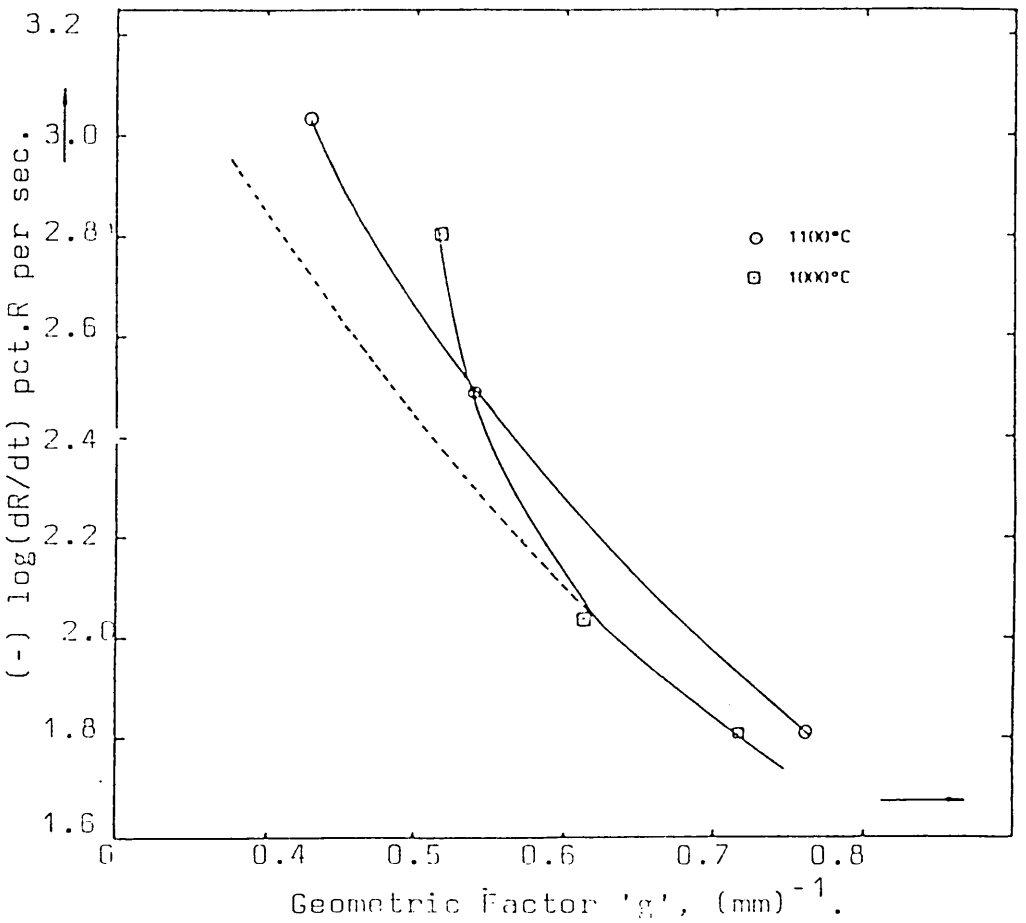


Fig (6.14) Relationship between rate of calcination of $CaSO_4$ and CaS, and the geometry of the pellet at different temperature.

by sintering a change in the mechanism may be expected. Thus, a steeper slope at lower 'g' is observed at 1000^{0}C and is related to the sintering of lime. Also, the more product produced around the periphery the greater is the sintering tendency because it produces a lower number of pores in a large volume by reducing the surface energy of the particles in the bulk. The sintering of lime layer thus alters the mechanism much more dramatically than any other parameter. This results in virtual sealing of all pores creating a greater and greater barrier for the pore diffusion of SO_2.

(ii) The Mechanism of Calcination of $CaSO_4$ and CaS Mixtures.

On the basis of the results and discussions on composite pellets reaction, the mechanism of calcination of $CaSO_4$ in the case of mixtures can be explained. The basic mechanism of calcination remains the same except, all the individual particles of $CaSO_4$ and CaS represent a composite pellet ie particle-to-particle contact. In a flowing stream of argon having $P_{O_2} = 10^{-30}$atm the calcination proceeds according to equation (6.18) by generating Ca^{+2} ions and electrons followed by their migration so that reaction (6.19) can proceed producing time and SO_2. Both steps commence simultaneously at the solid-gas interface which is tentamount to saying that the reaction front moves from the outside inwards. As the reaction commences, SO_2 is swept away from the reaction front to maintain reaction in the forward direction. Thus over a certain duration of time one expects product interfacial movement.

The comparison of the incubation period and the rate of calcination of sulphate in mixtures and composites are remarkably different. The incubation period in the mixture

is very small compared to the composites. The rate, on average is 3-4 times faster than that for composites. One peculiar feature of the reaction in the mixture is that it enters different regimes. Comparing the rate of reaction in the mixtures at different temperature, it is evident that the rate follows the Arrhenius Relationship. But the extent of reaction at 1000^{o}C is smaller than that at other temperatures. Dual temperature treatment of a mixture pellet was carried out at 1000^{o}C when 70 pct calcination was observed at which point the temperature was raised to 1050^{o}C and the rate of calcination was smaller. The reaction proceeded at a very slow rate. Microscopic examination revealed CaO, which was very dense in nature, around the periphery of pellet and sealed off the pores eliminating gas diffusion. The cessation of SO_2 removal became the critical factor which brought the reaction to a halt. It is also apparent from our investigation that sintering is an extremely rapid process at 1000^{o}C and it overtakes the chemical reaction in the later stages. An increase in temperature to 1050^{o}C in the case of dual temperature treatment, leads to an increase in pressure of SO_2 via the pore diffusion mechanism.

At every temperature, there is a fast initial step which prevails for a few minutes and is followed by a distinct linear region at 950^{o}C and 900^{o}C see fig (6.7). The linear stage terminates at 41 pct calcination and a parabolic regime commences at these two temperatures but is absent at 1000^{o}C and 1050^{o}C. There the rate curve is similar to an 'S' curve broken into different regimes. The parabolic regime is essentially related to the growth of the lime front from the outside reducing the rate with time. In this case a perfect balance of rate of sintering, the rate of chemical diffusion and the equilibrium partial pressure of SO_2 is established allowing the reaction to proceed to completion.

The rate of reaction proceeds in a slightly different manner at 900°C. In the later stages of reaction when the parabolic regime terminates, the reaction again enters a linear regime where the pore diffusion mechanism was established for SO_2 removal and governed the overall rate. The rate of sintering at this temperature was not significant enough to provide a barrier to the reaction. In this regime, the rate of reaction proceeds linearly and calculating the flux of gas through the pores has been estimated.

The linear rate equation for the flux of SO_2 across the product layer can be represented in the following form with a simplified picture of the reaction front. In reality, the reaction front moves with time and such a flux equation would be valid if an assumption of a stationary interface is made for a certain duration of time ie a quasi steady state condition.

$$J_{SO_2} = \frac{De_{Ar\text{-}SO_2}}{\delta . RT} \left(p^{i}_{SO_2} - p^{b}_{SO_2}\right) \qquad (6.20)$$

where J_{SO_2} = Flux of SO_2 (mole sec^{-1})

$De_{Ar\text{-}SO_2}$ = Effective diffusivity of SO_2 into the carrier gas argon

δ = Thickness of the product layer (cm)

R = Gas Constant (litre-atm (g $mole^{-1}$) $(K)^{-1}$)
= 82.05 cm^3atm (g mole)$^{-1}$ $(^oK)^{-1}$

T = Temperature (^oK)

To calculate the flux of SO_2 the effective diffusivity has been calculated on the basis of Binary Diffusion of SO_2 in Argon ie $D_{Ar\text{-}SO_2}$ where

$$D_{Ar\text{-}SO_2} = \frac{0.0018583 \left[T^3 \left(\frac{1}{M_{Ar}} + \frac{1}{M_{SO_2}} \right) \right]^{0.5}}{p \cdot \sigma^2_{Ar\text{-}SO_2} \cdot \Omega_{Ar\text{-}SO_2}} \qquad (6.21)$$

M_{Ar}, M_{SO_2} - Molecular Weight

p - Total pressure (atm)

$\sigma_{Ar\text{-}SO_2}$ - Collision Diameter (Angstrom)

Ω - Dimensionless function of temperature

Using data (6.11), (6.9), the value of binary diffusion was calculated at T = 1173°K. $D_{Ar\text{-}SO_2}$ = 1.144 $cm^2\ sec^{-1}$. From Turkdogan (6.12) et al data on the calcination of limestone, $De_{Ar\text{-}O_2}$ at 835°C = 0.30 $cm^2\ sec^{-1}$. To determine $De_{Ar\text{-}SO_2}$ an approximation has been made, the ratio of binary diffusion of O_2 and SO_2 in argon was used and it was assumed that the ratio is fixed for the effective diffusivity. the same geometry of pores and their distribution. With this approximation and the temperature correction $De_{Ar\text{-}SO_2}$ has been calculated to be 0.147 $cm^2\ sec^{-1}$. Substituting this value into equation (6.20), we have J_{SO_2} = 0.02 gm $(hr)^{-1}$.

$$\text{and } J_{eff,\ SO_2} = J_{SO_2} \times \frac{De}{D_{Ar\text{-}SO_2}} \qquad (6.22).$$

for which $J_{eff.\ SO_2}$ = 2.568 x 10^{-3} gm per hour. From fig (6.7) taking the average of the weight loss per hour from 13 hours onwards, $\frac{\Delta W}{\Delta t}$ = weight change per hour = 7.783 x 10^{-3} gm per hour.

The observed and the estimated values differ by a factor of 3 which seems reasonable in the light of the assumptions made and the experimental error. The relation given in equation (6.20) shows the linear dependence of the pressure on flux of SO_2 and the pressure in the equation has been assumed to be the equilibrium partial pressure given by equation (6.17). If a quantitative estimate on the rate of sintering with the particle size and the temperature is made the overall rate equation for calcination can be formulized with all factors taken into consideration.

A more rigorous analysis on the flux of SO_2 across the product layer can be carried out using a cylindrical flux equation with moving interface boundary conditions. This aspect of mathematical analysis of the present problem has been left over because such an analysis is very laborious.

(iii) Mechanism of Calcination of Sulphate in Reducing Atmosphere

Although investigation of the reduction of calcium sulphate with different types of carbon has been carried out by Turkdogan and Vinters (6.1) and according to these workers the presence of lime during the course of reduction depends solely upon the temperature and the amount of carbon present in the mixture. The desulphurization of sulphate takes place under conditions such that the rate of oxygen removal is relatively slow so any CaS formed can react with the remainder of the $CaSO_4$ to give lime and SO_2. It is evident from Turkdogan and Vinters (6.1) results that under certain conditions the desulphurisation and deoxidation reactions are competitive and this has been confirmed in the present work. The lime formed during the course of reaction was partially converted into calcium hydroxide and calcium carbonate because of prolonged exposure in the atmosphere, subsequently verified by X-ray diffraction results.

From the rates of calcination shown in fig (6.5a) it is apparent that carbon monoxide reduction of $CaSO_4$ is very fast. The equilibrium represented by equation (6.7) has been attained during reduction and the rate controlling step is the effective diffusivity of the product gas CO_2 ie De_{CO_2} through the product layer. The back reaction is never involved because the product gas established an unsteady state flux which is intrinsically governed by the binary diffusion of the two gaseous species. An equilibrium P_{CO_2} = 69.27 atm is achieved at P_{CO} = 1.0 atm. Since it is an equimolar counter diffusion situation the bulk velocity of the reducing gas CO would not alter such a rate.

The direct reduction of $CaSO_4$ with graphite is very different from indirect reduction. The overall reaction can be considered as two equilibria ie:

$$CaSO_4 + 4CO = CaS + 4CO_2$$

$$4CO_2 + 4C = 8\ CO \qquad (6.23)$$

At the start it is the direct reduction of $CaSO_4$ which prevails and it is feasible that both CO and CO_2 form as a result of direct reduction but mechanistically direct reduction cannot be sustained after contact between graphite and sulphate particles is lost. Subsequent reduction can only progress when CO generation occurs according to the solution loss or Boudouard Chemical Reaction(6.23).It is at this stage when an active carbon surface can play a significant role in promoting the reaction. Graphite being very inactive takes a relatively long time to initiate the oxidation of carbon as can be seen from the rate of calcination curves. At 950^{o}C the rate of calcination in the absence of copper is much slower than the copper catalysed Boudouard Reaction. It is also noteworthy that the effect of catalyst is effective. According to the Electron Theory of catalysts, metals accept electrons from the graphite surface destabilizing the carbon-carbon bonds and stabilizing the carbon-oxygen

bond. The oxygen occupies favourable sites to initiate oxidation. The mechanism $(CO_2) + C \longrightarrow [CO]^+ + C\,[O]^-$ represents the formation of a (C-O) bond and brackets represent a strongly chemisorbed oxygen, and the parentheses a weakly chemisorbed CO molecule. The formation of a strongly chemisorbed negatively charged oxygen is accompanied by the formation of a positively charged chemisorbed CO molecule. Thus, Cu metal accepts electrons to initiate oxidation of graphite and is very sensitive to temperature.

The rate curves for the direct reduction of sulphate indicates that the reduction is incomplete but there is virtually no $CaSO_4$ left. This is because of the simultaneous desulphurization of $CaSO_4$ to form lime which sinters very rapidly in this temperature range. The rapidity of CaO sintering influences the reaction and forces to cease due to lack of passage of gas through the sintered layer. Thus, once again sintering of lime affects the reduction process.

****

Chapter 6.

6.1 E.T. Turkdogan and J.V. Vinters IMM Trans C. 1976 pp 117

6.2 E.T. Turkdogan and B.B. Rice. SME AIME Trans vol 254 1973 pp 28.

6.3 E.T. Turkdogan and L.J. Martonic J.I. Iron and Steel of Japan Vol 83 pp 83.

6.4 L.S. Darken and H.A. Wriedt. SME AIME Trans vol 254 1973 pp 254.

6.5 E.T. Turkdogan et al Met Trans. vol 5 July 1974 pp 1527

6.6 F.D.Richardson and E.W. Dewing Trans Faraday Soc. 1959. vol 55 pp 611.

6.7 F.D. Richardson and C.J.B. Fincham Proc. Roy. Soc. 1954 vol. A223 pp 40-62.

6.8 T. Rosenqvist Trans AIME Vol. 191 1951 pp 534-40

6.9 E.T. Turkdogan The Physical Chemistry of High Temp Tech. Academic Press, 1980.

6.10 O. Kubacheswki and C.B. Alcock - Metallurgical Thermochemistry. Pergamon Press 1967

6.11 R.B. Bird, W.E. Steward and E.N. Lightfoot Transport Phenomena Wiley Int. Edition 1960.

6.12 E.T. Turkdogan et al SME Trans Vol 254 1973 pp 9.

Chapter 7

Mechanism of Growth of Bi-Partite Whiskers.

7.1 Introduction.

The mechanism of whisker growth remains a fascinating area to explore and in the past several theories have been propounded to explain nucleation and growth mechanisms. Broadly, these theories can be classified into two major catagories:-

a) the mechanism of whisker growth during the vaporization of metallic compounds, which involves the solid and vapour phases.

b) whisker growth of products following chemical reaction especially metals during the reduction of their oxides and sulphides.

Whisker growth from the vapour phase has been thoroughly investigated on the basis of rigorous theoretical model and sound experimental proof.

Many discrepancies still exist in the explanation of whisker growth during the reduction of oxides and sulphides of metals. However there exists some similarities between the two methods of whisker formation. G.W. Sears (7.1) suggested that whisker growth commences under conditions of supersaturation of the growing species insufficient for two dimensional nucleation. He also proposed that whiskers are perfect except that they contain a single axial screw dislocation. Whisker growth assisted by a single screw dislocation is thoroughly understood and has been observed on many occasions. J.W. Cahn (7.2) has mathematically analysed this situation and proved that energetically second phase growth of this type occurs on a screw or edge dislocation. An alternative mechanism of whisker growth

is based on growth around impurity particles, where a single screw dislocation is generated. This mechanism seems to operate in the case of growth of potassium halide (7.3) rods produced from aqueous solutions. Such crystals circumventing a single screw dislocation grows at constant radius to form a rod. The production of crystal of fixed radius, in such situations, is determined by the constant quantity of volume free energy dissipated to create a new surface. Brenner and Sears (7.4) suggested that there must be an initial critical supersaturation necessary to produce a whisker from a screw dislocation,which has a critical seperation distance from a neighbouring dislocation. When screw dislocations are more closely spaced the supersaturation necessary for growth increases. In other words, higher supersaturations are expected to yield more closely spaced whiskers. This theory establishes an upper limit for the supersaturation essential for a whisker growth. A system of very closely spaced screw dislocations allows planar growth with respect to surface rather than a grwoth in perpendicular direction.

Brenner (7.5) also investigated whisker growth by reduction of metal salts. In this case, the growth takes place from the tip and there seems little doubt that growth occurs by condensation of freshly formed metal from the vapour. Whisker grwoth with a wide variety of shapes and degrees of perfection takes place under these conditions. Near perfect whiskers which exhibit high strength are bounded by smooth surfaces. Brenner claims that whiskers bigger than 8μm are rarely perfect. Coleman and Sears (7.6) observed the growth of zinc whiskers by vapour deposition of the pure phase in the presence of an inert gas. Whiskers of much greater length were obtained in the presence of a gas atmosphere than by vacuum deposition. The diameters of the whiskers were found to diminish with increasing inert gas

pressure. The only reason for the diminition in the diameter of whiskers in the presence of increasing pressure of inert gas could be the mutual collisions between metal gas vapour and the inert gas molecules. It seems reasonable that this would reduce the probability of condensation of the metal vapour on the metal surface. This is logical because at higher pressures of inert gas more molecules will be present reducing the mean free path of the metal vapour in the system.

7.2 Existing Models on the Nucleation and Growth of Whiskers during the Reduction of Metal Sulphides and Metal Oxides.

The models and principles developed for whisker growth from the vapour phase can be applied to whisker growth during the reduction of metal oxides and metal sulphides. Brenner's observation on the need for low supersaturation conditions during whisker growth was also observed by Carl Wagner (7.7). Wagner's mechanism is based on his investigation on the reduction of transition metal oxides and sulphides. A large number of these oxides and sulphides are non-stoichiometric and with excess anions. During the course of reduction, the activity of metal ions increases as excess anions are removed from the compound lattice. Once conditions of low supersaturation are attained, whiskers nucleate around an active surface e.g. dislocations.
A very important question arises at this junction concerning the views of various authors. Why is there a need for low supersaturation conditions? Although this view was first propounded by Brenner and Sears (7.4) it needs further explanation. It is our view that the necessity for low supersaturation is based on the classical theory

of nucleation, Cahn's (7.2) theory on the growth of second phases on dislocations and the Brenner-Sears's view. The degree of supersaturation in the system determines the equivalent amount of volume free energy which can be invested in creating new surface. The larger the volume free energy the larger will be surface created to accomodate the loss of this energy. A large surface energy, which is equivalent to large volume free energy, would give rise to large surface in forms of defects which would not happen if the whole process commences with small volume free energy. The other very important factor during the second phase nucleation is its wetting on the substrate which, in case of two condensed phases (solid) is the matching planes of the product and the substrate. The extent of matching between these two planes of the substrate and the product can be determined by the initial supersaturation and the surface morphology of the substrate. Since perfect matching of planes is never achieved, this means, a slight mismatch would create dislocations, which later in the process play a very significant role during the growth mechanism. This is the reason why whiskers have very few defects whereas the epitaxy which grows in a planar direction leaves a lot of defects.

Wagner (7.7) determined the degree of supersaturation required during the reduction of metal sulphides and oxides and it is related with the chemical potential of anionic species in the crystalline phase and the related gas molecule in the gas phase.

The concept that screw dislocations intersecting a surface are responsible for the growth of crystals from the vapour phase at very low supersaturation was made by Frank (7.8), Burton and Cabrera (7.9) in 1949. The theory based on the movement of a monomatomic ledge was propounded by these authors (7.10, 7.11), who confirmed this hypothesis during the growth process (7.12,7.13,7.14). During the process of whisker growth angular bends and twists have been observed (7.15,7.16,7.17) and several reasons have been suggested for these morphological charactristics of a growing whisker. On the basis of the work carried out, no significant conclusions can be drawn about the prevalent mechanism. Wagners mechanism is the first relating to whisker growth during the reduction of metal sulphides and oxides. During the reduction of iron oxides, iron whiskers have been observed by several workers and different explanations have been presented. Wenzel (7.18) suggested that iron whisker growth occured by the decomposition of a sub-oxide to iron and oxygen. However, this theory was discarded because no suboxides were found to exist in the vapour phase.Finnstrom (7.19,7.20) suggested that metallic whiskers can grow from the tip on the basis of Gibbs-Thompson effect (7.21) which suggests that a curved surface has higher energy than a flat surface. In the case of whisker growth, a convex tip has a high surface energy due to curvature and because of the presence of screw dislocations, which makes the surface energetically unstable. Thus, if the diffusing species can be carried to the tip growth occurs from this point preferentially. Finnistrom suggested that absorbed metal ions exist during the course of metal oxide reduction and the favourable sites for such adsorption is the surface of the oxide or the side of the whisker. Between the two sites for metal ion adsorption, the

former appears to be very reasonable whereas, the latter is less convincing as the most favourable site on a whisker is the tip which is energetically unstable.

Observations made by Lu (7.22) on iron whisker growth mentioned the formation of 'Young' and 'Mature' whiskers. 'Young' whiskers are thin and short and become thicker and longer with increasing time. His observations on 'Mature' whiskers gave no indication that the tops of these whiskers were always thinner than the base. Lu also reported that the starting size of a nucleus of metallic iron should be in the order of tens or hundreds of angstroms. It is reasonable to expect that these nuclei would grow laterally rather than upwards to become extremely thin whiskers. The preference for lateral growth rather than longitudinal growth is acceptable in relation to the large initial surface area where several screw dislocations exist. The main objection to Lu's work is that no reason is given for the lack of lateral growth when whisker growth is initiated. He concluded that growth may result from the clustering of rejected impurities which originated in the oxide phase. Considering the repetative nucleation of whiskers on the substrate, such clustering of impurities and hence the provision of heterogenous sites for nucleation seems reasonable and is in accordance with his observation. However, it gives rise to a serious objection that if impurities all invariably present during whisker growth processes what reason exists for whiskers grown by vaporization of halides exhibiting a different morphology. An explanation for the stubby growth of whiskers will be given later.

The growth of metal fibres (7.23,7.24,7.25,7.26) was observed during hydrogen reduction of non-ferrous metal sulphides in the presence of lime. In case of nickel sulphide (7.23) growth was suggested to proceed because of the presence of a liquid Ni_3S_2 and Ni mixture and in all other cases Wagner's mechanism seems to be responsible. Similar explanations were given by several workers.Wagner's mechanism vividly explains the nucleation mechanism of whiskers on the energetically favourable sites but it does not explain the mechanism of growth nor can an explanation be offered for the morphology of whiskers. The energetics of growth and the related morphology has been discussed earlier, and explains how the volume free energy is expended to give whisker growth of defined morphology.

In general,the favourable conditions for whisker growth can be stated as follows (7.27):

a) structural anisotropy in the crystal lattice
b) additive-induced growth due to the presence of impurities
c) active sites for nucleation (catalytic interfaces of screw dislocations).

Whiskers started to grow in a number of distinct stages:-

a) an induction period resulting in nucleation
b) a primary growth stage known as leader growth, sometimes followed by step (c) or directly by step (d)
c) a secondary thickening or over growth
d) slowing down or cessation of growth

These steps represented schematically in fig (7.1) have been observed by Finnstrom (7.19) from direct observation during reduction of wustite with CO/N_2 = 40:60 mixture.

7.3 Conditions for Whisker Growth

In this section growth mechanisms influenced by various factors are presented briefly to justify the conditions for their growth as stated in the previous section.

a) Structural Anistropy:

The majority of crystals have anistropic structures to a varying degree so that the external crystal faces have differing surface energies depending on the type of atomic bonding and the extent of atomic packing.

b) Additive or Poison Induced Growth:

In this case, whisker growth results from impurities. Two possible mechanisms have been suggested on the basis of the surface of a crystal which could have either surface vacancies or surface adatoms.

i) In case of a surface adatom, the presence of impurities enhances the value of the surface diffusion coefficient by providing a preferential site on a specific crystal faces. Hence, it influences the development of other planes by harnessing the existing anistropy of the crystal besides creating additional anistropy. Mathematically if D_S is represented by an equation of the type:

$$D_S = \left(\frac{ni}{No}\right) \cdot f_1 \left(\frac{na}{No}\right) \cdot f_2 \left[\exp\left(\frac{-\Delta Ha^{o}}{RT}\right)\right] \qquad (7.1).$$

where

D_S = is surface diffusion coefficient

na = no. of adatom on a particular crystallographic plane

No = no. of favourable sites where adatoms can move in the absence of impurities

ΔH_a^o = enthalpy of formation of an adatom

T = temperature

R = gas constant

ni = no of impurity atoms on the surface.

Thus, by providing impurities on the surface, the enthalpy of adatom formation is reduced enhancing the value of D_S ie adatoms associate preferably with impurities to those favourable sites on the crystallographic plane.

ii) In the case of surface vacancies, the movement of a vacancy is enhanced because of the presence of certain impurities which are smaller in size than the substrate atoms. The vacant site on any crystallographic plane will move faster in the presence of such an impurity as the impurity atoms would always have a tendency to associate with atoms on that plane. If 'β' is the binding energy of the impurity atoms then the impurity vacancy complex ($^nVI/N_o$) is related to the concentration of free vacancy (nv/N_o) and impurity concentration (n_I/N_o) by

$$\left(^nVI/N_o\right) = \frac{(n_I)}{No} \quad \exp\left\{\frac{\beta}{RT} \cdot \frac{n_I}{N_o}\right\} \qquad (7.2)$$

hence an increase in D_S will result. This is essentially true when there is a negative heat for absorption and the impurity size is smaller than the substrate atom.
On the other hand, if the jump frequency of the vacancy or adatoms are sufficiently reduced because of the slow movement of the impurity atoms (when the size of the impurity atoms is bigger) then D_S would significantly decrease. Collins & Shewmon (7.28) and Gjostein (7.29) have given the experimental proofs and theoretical model for this aspect of surface diffusion.

c. Whisker Nucleation:

In whisker nucleation and in some mechanism of their growth it is usually necessary to postulate an active sites on the substrate, such as an existing screw dislocation or the presence of impurities. Generally, the mechanism of nucleation is governed by Wagner's theory.

7.4. The Anistropy of Surface Free Energy - The Shape and Faceting of Surfaces.

The surface of a crystalline solid is structurally imperfect because of the existence of number of 'broken bonds' and the surface energy of each crystalline surface plane is related to the number of broken bonds present on each plane. It is for this reason that the surface energy of each plane varies leading to anistropic values. By way of explanation, a two dimensional crystal with chemical bonds associated with nearest neighbour atoms has been considered and a rigorous analysis was presented by Mullins.

A crystal surface substending an angle θ to the crystal plane (001) is made of a series of terraces and steps with a minimum number of broken bonds. The surface has been created from a region of a perfect crystal separation from its intersecting surface for which the energy needed is U_b times the number of broken bonds f(θ) where f(θ) is the number of broken bonds on each surface corresponding to a unit distance along the (001) base, see fig (7.2).

$$f(\theta) = \frac{1}{a} + \tan\theta/a \qquad (7.3)$$

where 'a' is the interatomic distance and the first term in equation (7.3) represents the number of broken bonds in an (001) plane. Whereas, the second term for the vertical broken bonds is related to:-

$$\sigma_\theta = \text{the surface free energy} = \frac{U_b\, f(\theta)}{2/\cos\theta} \qquad (7.4)$$

where $2/\cos\theta$ is the total surface created in unit volume. Substituting (7.3) in equation (7.4)

$$\sigma_\theta = \frac{U_b}{2}\left[\frac{1}{a} + \frac{\tan\theta}{a}\right]\cos\theta$$

$$= \frac{Uh}{2a}(\cos\theta + \sin\theta) \qquad (7.5)$$

ie $$\sigma_\theta = \frac{U_b}{a(2)^{\frac{1}{2}}}(\cos(\theta - \pi/4) \qquad (7.6)$$

which is the equation for a circle in polar co-ordinates having diameter $\frac{U_o}{a\sqrt{2}}$ subtending an angle $\Pi/4$ to the positive axis and passing through an origin 'O'. Calculations have been carried out for three dimensional crystals where different bond energies are considered for both the first and second nearest neighbours. Such calculations provide a value of surface energy as a function of orientation for different values of bond energy ratio ρ where a graph of surface energy in these terms is called a σ - plot. The polar σ - plot allows a clear demonstration of the Gibbs-Wulff theorem ie for any total surface free energy represented by an area integral of the function $\sigma\, dA$, the solution of the theorem predicts an equilibrium shape.

Investigations on the anistropy of surface free energy of bcc and fcc metals were carried out by Sundquist (7.31). As expected the faceting of planes (100) and (111) is seen with fcc metal crystals (1μm) and (110) and (100) facets with bcc metals. Some of these equilibrium shapes are shown in fig (7.3) and fig (7.4). Comparing Sundquist's observed equilibrium shapes and theoretically predicted shapes for fcc metal it can be concluded that the observed and predicted shapes are in excellent agreement.

According to Gibbs, the adsoption of impurities can reduce the surface energy, σ, and the change in surface energy associated with an impurity is given by:-

$$d\sigma = -\Gamma_2\, d \ln a_2 \qquad (7.7)$$

where Γ_2 is the surface excess of impurity component and a_2 is the activity of the impurity in the gas phase. In the case of oxygen, as a gaseous impurity the activity is related to the square root of partial pressure of the gas reaches a maximum when a monoatomic layer is formed with adsorption. This for $a_2 = RT \ln p_2^{\frac{1}{2}}$

$$d\sigma = \frac{\Gamma_2}{2} RT \; d \ln p_2 \qquad (7.8)$$

$$\text{ie} \qquad \Gamma_2 = -\frac{2}{RT} \left[\frac{d\sigma}{d \ln p_2} \right]_{T, p_2} \qquad (7.9)$$

This equation gives a value of the reduction in surface energy due to a impurity adsorption and can be experimentally determined if the observations on the variation of the surface energy with partial pressure of oxygen are made. On this basis, it has been found that the lowest energy plane for copper is {110} contrary to the observations of Sundquist who showed that the lowest energy planes in fcc metals are {111} and {100}.

Indeed, the faceting of a surface is the same problem as that associated with the development of an equilibrium shape. In general, faceting occurs with the production of crystallographic planes close in orientation to low-energy planes, such as {111} plane in silver.

In the present work, various aspects of structural changes are covered where both surface energy and anisotropy of surface energy appear to play a significant role.

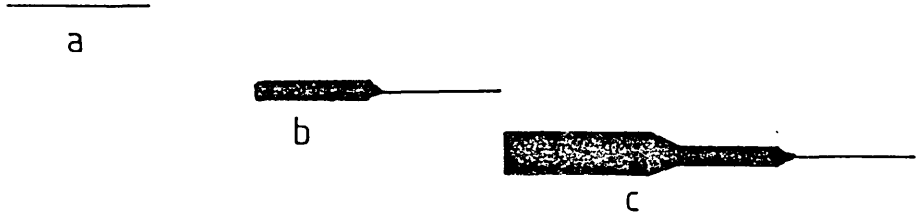


Fig (7.1) Schematic representation of whisker growth process.
a - Leader growth b - Secondary growth
c - Cessation of growth.

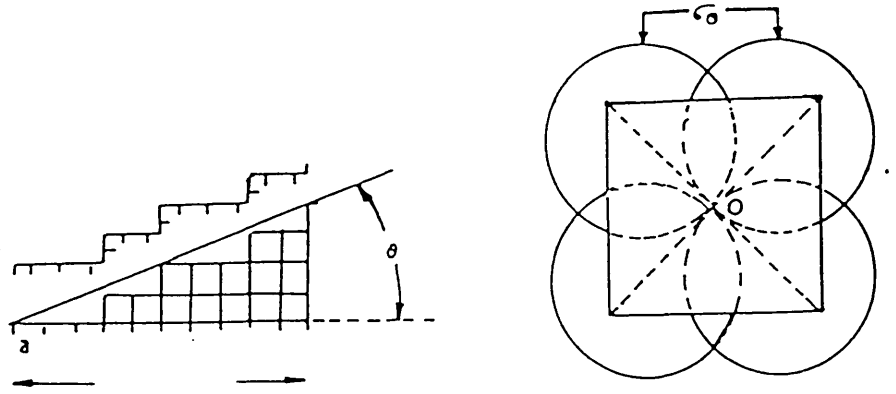


Fig (7.2) (a) showing a surface plane at an overall angel θ to a close packed plane (001) in a simple two dimensional cubic crystal together with the 'matching' surface. (b) The expected variation of surface energy as a function of θ bonds formed to nearest neighbours only.

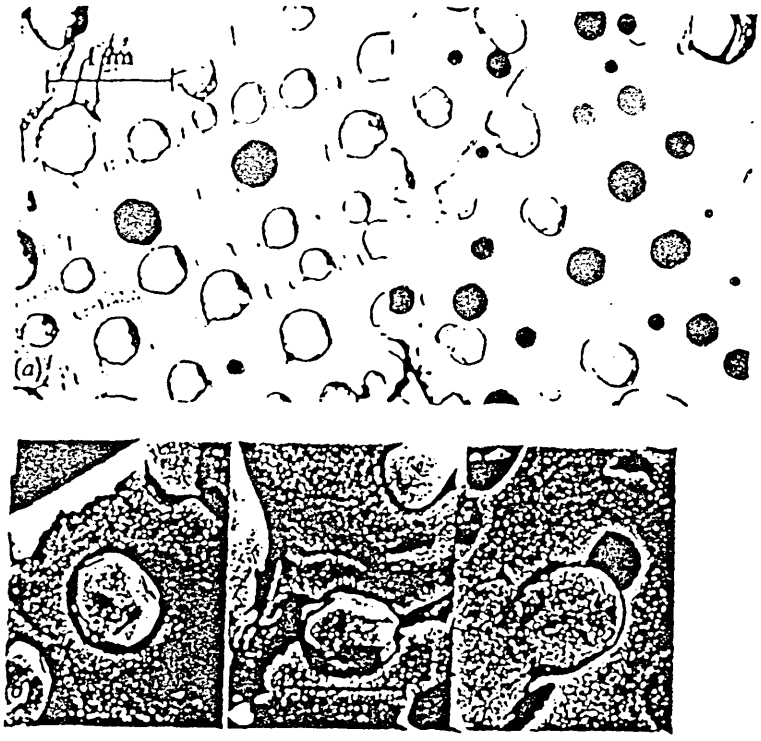


Fig. 7-3 Examples of (*a*) profiles and (*b*) typical replicas of small f.c.c. nickel particles annealed in dry hydrogen at 1273 K for 100 hours. The equilibrium shape is faceted, but with rounded corners and edges. (After Sundquist 1964, courtesy of *Acta Met.*)

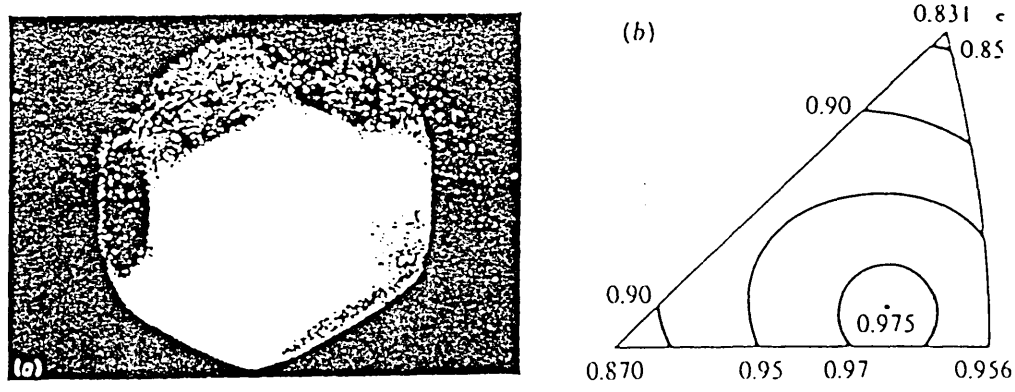


Fig. 7-4 (*a*) Model of the experimentally determined typical equilibrium shape of f.c.c. crystals. (*b*) The σ-plot that would give rise to this experimentally determined shape, scaled for comparison with Sundquist's calculated model illustrated in fig. 4.8(*d*). The hexagonal faces in (*a*) are the {111} planes and square faces {100}. (After Sundquist 1964, courtesy of *Acta Met.*)

7.5 Experimental Procedure.

The experimental apparatus used has already been described in Chapter 4. The experiments were broadly divided into two categories - the mixtures and the composites. Stoichiometric mixtures of copper sulphides and copper oxides were prepared and heat-treated in an argon atmosphere. These mixtures were subsequently reduced at 1000^{o}C in argon atmospheres in a graphite crucible packed with graphite as shown in fig (7.5). Any weight change which occured during the reduction was recorded on the chart recorder and the overall weight change using an analytical balance. Composite pellets of cuprous oxide and cuprous sulphides were prepared and heat-treated in argon atmospheres at 1000^{o}C for different lengths of time. The weight changes which occured were recorded in a similar manner. The heat-treated oxysulphide mixtures, ie the reduced pellets and the heat-treated composites, were examined using optical and electron microscopy to determine morphological changes which occured during the course of reaction. The heat-treated oxysulphide mixtures were also analysed using an X-ray diffraction technqiue to identify the phases present.

On the JEOL Scanning Electron Microscope, semi-quantitative analyses of the desired areas were carried out by considering the relative intensities of the Energy Dispersive X-ray spectra. A few experiments with sulphide and lime mixtures in their stoichiometric ratios were carried out at 1000^{o}C with graphite and in CO atmospheres.

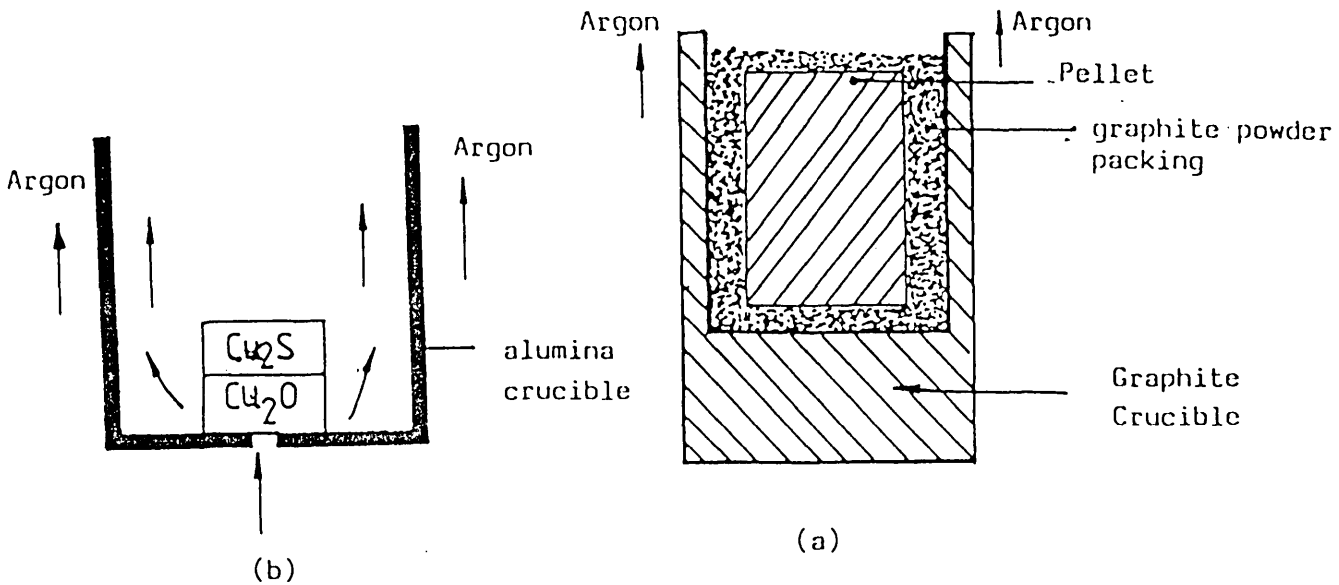


Fig (7.5) a) Arrangement of composite pellet inside alumina crucible
b) Arrangement of pellet in graphite crucible.

7.6 Results.

a) Whisker Growth in the Case of Oxysulphide Mixtures.

Oxysulphide mixtures heat-treated in argon atmosphere were reduced in graphite crucibles at 1000°C. Prior to reduction, the related phase relationships for different compositions are shown in fig (5.5) in Chapter 5.
The mass balance analyses and X-ray diffraction results are summarized in Table 7.1. Thermodynamic calculations carried concerning equilibria which exist in ternary section have been discussed in length in Chapter 5. During the course of reduction of the mixtures presented in Table 7.1, morphological changes were observed and these changes together with weight losses are summarized in table 7.2. From Tables 7.1 and 7.2 it is seen that the compositions of oxysulphide mixtures lying in the (L + Cu Cu_2S) phase field have undergone immense morphological changes. The reduced pellet showed many thin, long fibres produced at the gas-solid surface. The Scanning Electron Microscopic results shown in plate 7.1 show that the extent to which these fibres or whiskers grow is phenomenal in such a small time. The length of these 'thin' whiskers was measured to be greater than 5000μ in length. The tips of the whiskers were examined using Scanning Electron Microscopy and are illustrated in plate 7.2. It is obvious from the Scanning Electron Micrographs that the tips consist of a liquid phase. The presence of a crystal, a frozen drop and platelets at the tip of these whiskers supports the view that more than one phase exists. The various structures present at the tip have been analysed using the EDX technique and the results are shown in Table 7.5. The variations in Cu/S ratio for these tips substantiates the compositional variations of the material deposited.

Table 7.1 Heat-Treatment of Copper Oxide - Copper Sulphide Mixtures at 1000°C in Argon Atmosphere.

Mixture Composition	Temp. °C.	Mass balance		Atmos. $p_{O_2} = 10^{-30}$ atm.	Cu_2S	$Cu_{1.96}S$	$Cu_{1.93}S$	Cu_2O	CuO	Cu	CuS.
		Pct. wt loss	Time in hr.								
1 CuS:CuO = 3:1	1000°C	15.21	3.00	Ar	VS	VS	VS	WM	W	-	-
2 CuS:CuO = 2:1	1000°C	14.72	3.00	Ar	VS	VS	VS	WM	W	VW	-
3 CuS:CuO = 1:1	1000°C	18.10	3.00	Ar	S	S	S	S	M	S	-
4 CuS:CuO = 1:3	1000°C	19.33	3.00	Ar	-	-	-	VS	-	MS	-
5 Cu_2S:CuO = 1:1	1000°C	14.35	3.00	Ar	M	M	M	S	WM	VS	-
6 Cu_2S:CuO = 4:1	1000°C	4.30	3.00	Ar	VS	VS	VS	WM	WM	M	-

Table 7.2 Reduction of Preheat-treated Oxide Sulphide Mixture of 1000°C in Graphite crucible in a flowing stream of Argon.

Initial Comp of mixture	Temp °C	Pct wt.loss during red	Atmos. $p_{O_2} = 10^{-30}$	Time in hr.	Comp. in Cu-S-O ternary prior to reduction	Structural Changes				
						Thin Whiskers	Thick Whiskers	Faceted Shapes	Liq. phase	Precipi tates.
1R CuS:CuO = 3:1	1000°C	0.113	Ar	3.00	L + Cu_2S	-	-	-	-	-
2R CuS:CuO = 2:1	1000°C	0.791	Ar	3.0	L + Cu + Cu_2S	Yes	Yes	Yes	Yes	Yes
3R CuS:CuO = 1:1	1000°C	3.74	Ar	3.0	L + Cu	-	Yes	-	Yes	-
4R CuS:CuO = 1:3	1000°C	14.2	Ar	3.0	Cu+ Cu_2O	-	-	-	-	-
5R Cu_2S:CuO = 1:1	1000°C	0.236	Ar	3.0	L + Cu	-	Yes	-	Yes	-
6R Cu_2S:CuO = 4:1	1000°C	0.295	Ar	3.0	L + Cu + Cu_2S	Yes	Yes	-	Yes	Yes.

Table 7.3 Reduction of Sulphides with CO and Graphite in presence of lime at 1000°C.

Mixture Comp.	Temp°C	Total pct wt loss	pct 'O' lost	Time	REMARKS.
Cu_2S:CaO = 1:1	1000°C	5.40	72.56	2 hrs.	Formation of liquid phase during the reduction.
x CuS:CaO = 1:1	+1000°C 800°C	13.75	32.51*	4 hrs.	Evolution of SO_2 and S_2 during the experiment. Crystals of Cu_2S grew from the top of the pellet.
x CuS:CaO:C = 1:1:2	850°C	4.68	32.21	8 hrs.	$CaSO_4$ was found during the course of partial reduction of sulphide.

* Pct reduction calculated from the weight loss occured during CO redution.

\+ The mixture first heat-treated in argon at 1000°C and reduced with CO at 800°C

x Pct weight loss includes sulphur weight loss ie total weight loss.

Table 7.4 Heat-Treatment of Copper Oxide and Copper Sulphide composite.

	Composite Specification	Diam. of Composite in cm	Temp. ^{o}C	Atmos.	Time in hrs.	Mole pct of SO_2 lost.	Structural Changes				
							Thin Whiskers	Thick Whiskers	Faceted Shape	Liquid Phase	precip-itates
10	Cu_2S-Cu_2O	0.635	1000	Argon	20.0	0.0195	-	Yes	Yes	Yes	Yes
11	Cu_2S-Cu_2O	1.27	1000	Argon	0.75	-	-	Yes	-	Yes	-
12	Cu_2S-Cu_2O	0.635	1000	Argon	7.25	0.022	-	Yes	-	Yes	Yes
13	Cu_2O-Cu_2S *	0.635	1000	Argon	7.25	0.018	-	-	-	Yes	-
14	Cu_2S-Cu_2O	1.27	1000	Argon	24.00	0.2706	-	Yes	-	Yes	-
15	Cu_2S-Cu_2O	0.635	1000	Argon	8.00	0.0934	-	Yes	Yes	Yes	Yes
16	Cu_2S-Cu_2O +	0.635	1000	CO_2	24.00	0.0778	-	Yes	Yes	Yes	-
17	Cu_2S- Cu_2O	0.635	1000	Argon	24.00	0.0583	-	Yes	-	Yes	-
18	Cu_2S-Cu_2O	0.635	750	CO_2	15.00	0.0231	-	-	Yes	-	-
19	CuS-CuO *	0.635	1000	Argon	16.00	0.505	-	Yes	-	Yes	-
20	Cu_2S-Cu_2O	0.635	1000	Argon	15.00	-	-	Yes	Yes	Yes	-

* Cu_2O positioned in upward position and Cu_2S down.

\+ Cu_2O and Cu_2S surface seperated by slitted pt-foil.

*Mole pct of S_2 lost in no 19 0.1389

Table 7.5 Energy Dispersive X-ray analyses of the various morphologies developed during the treatment of the various pellets. The analyses is semi-quantitative in nature because of the intensity peaks obtained on the spectrum are calibrating against pure copper $Cu_{2-x}S$, $Cu_{2-x}O$, CuO and CuS.

Intensity Ratios:- Cu_2S, Cu/ S = 1.66. CuS: Cu/S = 0.735, Cu, Cu peak height = 99.0
Cu_2O, Cu Peak Height = 70.0, CuO, Cu Peak Height = 45.
EDX Analysis carried out in terms of Cu/s Ratio

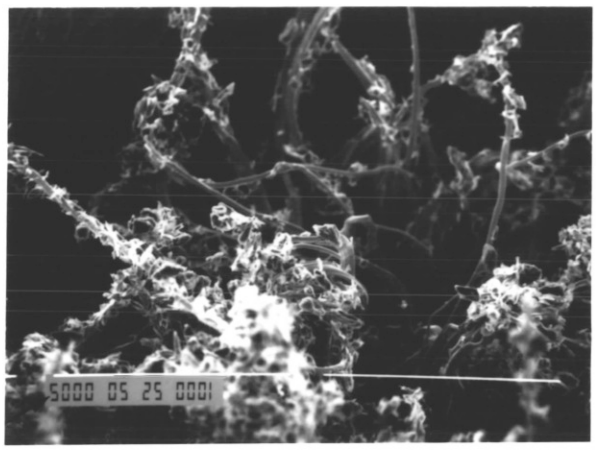
Expt No.	Temp °C	Atmos.	Tip of Thin Whisker	Stem of Thin Whisker	Tip of Thick Whisker	Stem of Thick Whisker	Precipitate on Whisker	Faceted Surface. 1	2	3	4	5	6	7
2R	1000	Argon	2.20 2.66 2.72 4.6 5.51 -	- - - 3.05 - -	73.0 14.93	77.0 25.0	12.8	1.635	-	-	-	-	-	-
3R	1000	Argon	-	-	81.0 -	81.0 -	-	-	-	-	-	-	-	-
5R	1000	Argon	2.5 -	4.4 -	- -	- -	-	-	-	-	-	-	-	-
6R	1000	Argon	1.38 2.09 2.5 2.74 3.97 5.97	- 6.27 - - 1.33 -	25.0 35.0	25.0 35.0	3.60	-	-	-	-	-	-	-
7	1000	CO	- -	-	55.0 -	55.0 -	3.30	-	-	-	-	-	-	-

Symbols Used: 1. Regular Hexagon 2. Irregular Hexagon
3. Square 4. Rectangle 5. Irregular Shape
6. Circular Shape 7. Others. * Bi-crystals see plate (7.6(D)
8*. The pellet first heated at 1000°C in argon atmosphere and the pellet was reduced with CO.

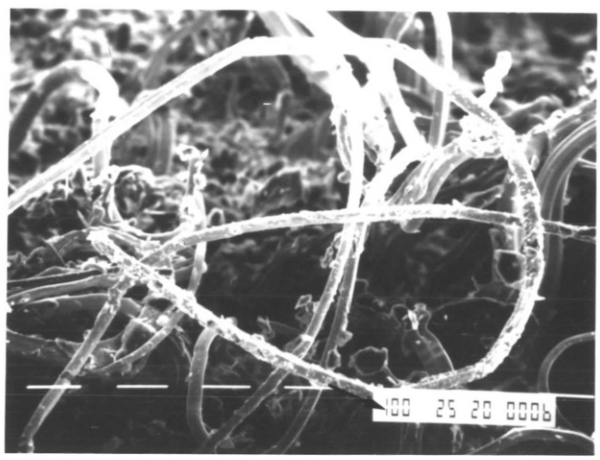
Table 7.5 Contd...

Expt No.	Temp °C	Atmos.	Tip of Thin Whisker	Stem of Tin Whisker	Tip of Thick Whisker	Stem of Thick Whisker	Precipitate on Whisker	Facted Surface						
								1	2	3	4	5	6	7
8⊙	1000	CO	1.65 1.68 1.75 -	1.65 1.68 1.75 -	-	-	-	-	-	-	-	-	-	-
9	850	Argon	-	-	55.0 50.0	55.0 50.0	-	-	-	-	-	-	-	-
10	1000	Argon	3.12 3.31 4.68 -	3.12 5.7 - -	- -	- -	7.14	1.68 1.77	-	56.8	50.0	-	-	Qua 8.4
12	1000	Argon	-	-	37.0 - - 45.0	38.0 - - -	2.40	-	-	-	-	-	-	-
14	1000	Argon	-	-	56.0 - - 45.0	56.0 - - 45.0	-	-	-	-	-	-	-	-
15	1000	Argon	-	-	45.0 - - 51.0	45.0 - - 51.0	Eutectic 2.02	10.19 36.8	2.98 2.89	7.9	-	3.78	7.11	Ri 5.
16	1000	CO_2	-	-	75.0	75.0	-	-	3.13*	-	-	-	-	Spi 75.
17	1000	Argon	-	-	74.0	74.0	2.31 1.22	-	-	-	-	-	-	
18	750	CO_2	-	-	-	-	-	4.20		-	-	-	-	Spi
19	1000	Argon	9.8	9.8	67.0 - - 65.0	67.0 - - 65.0	- -	-	-	-	-	-	-	
20	1000	Argon	4.5 3.5 2.5 -	3.5 3.3 - -	-	- -	- -	1.635	2.9	3.0	8.1	-	3.52	8.3

PLATE 7.1



A



B

Plate 7.1 Growth of bi-partite whiskers during the reduction of copper oxide - copper sulphide pellet preheat-treated in argon at 1000°C.

(A) CuS:CuO = 2:1 pellet reduced in graphite crucible for 3 hours

(B) Cu_2S:CuO = 4:1 pellet reduced in graphite crucible for 3 hours

PLATE 7.2

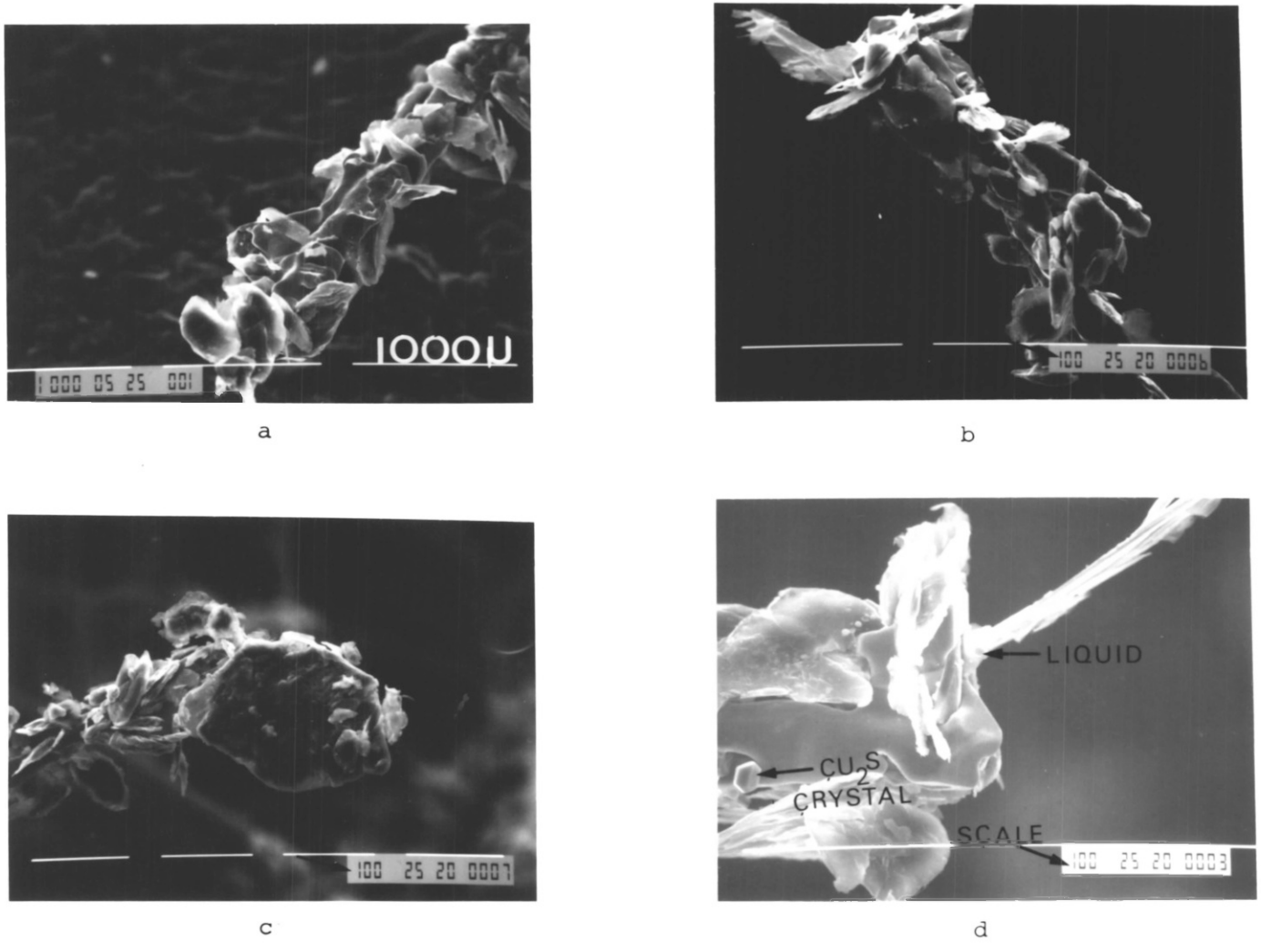
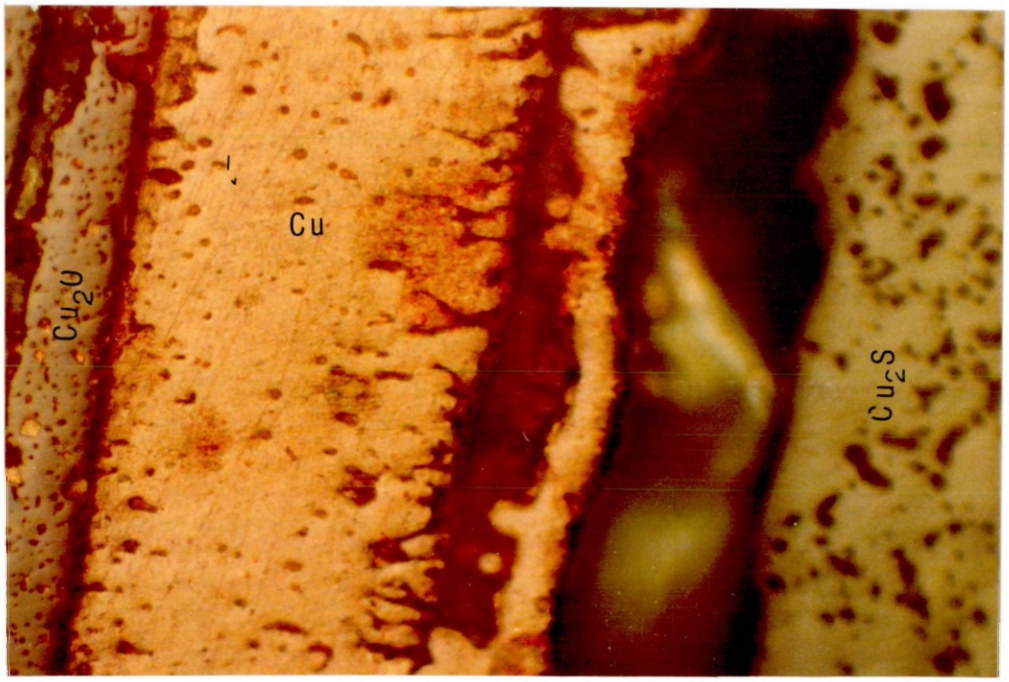


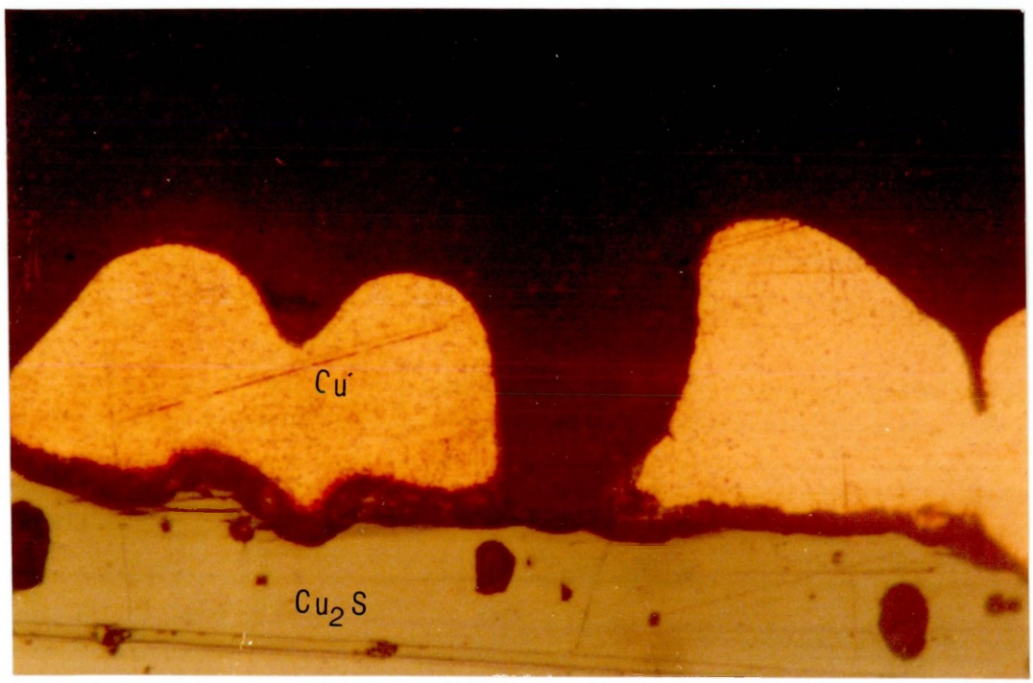
Plate 7.2 Scanning electron photo micrograph of the tip of bi-partite whiskers.

(a) & (b) CuS:CuO = 2:1
(c) & (d) Cu_2S:CuO = 4:1

PLATE 7.3



A X 44

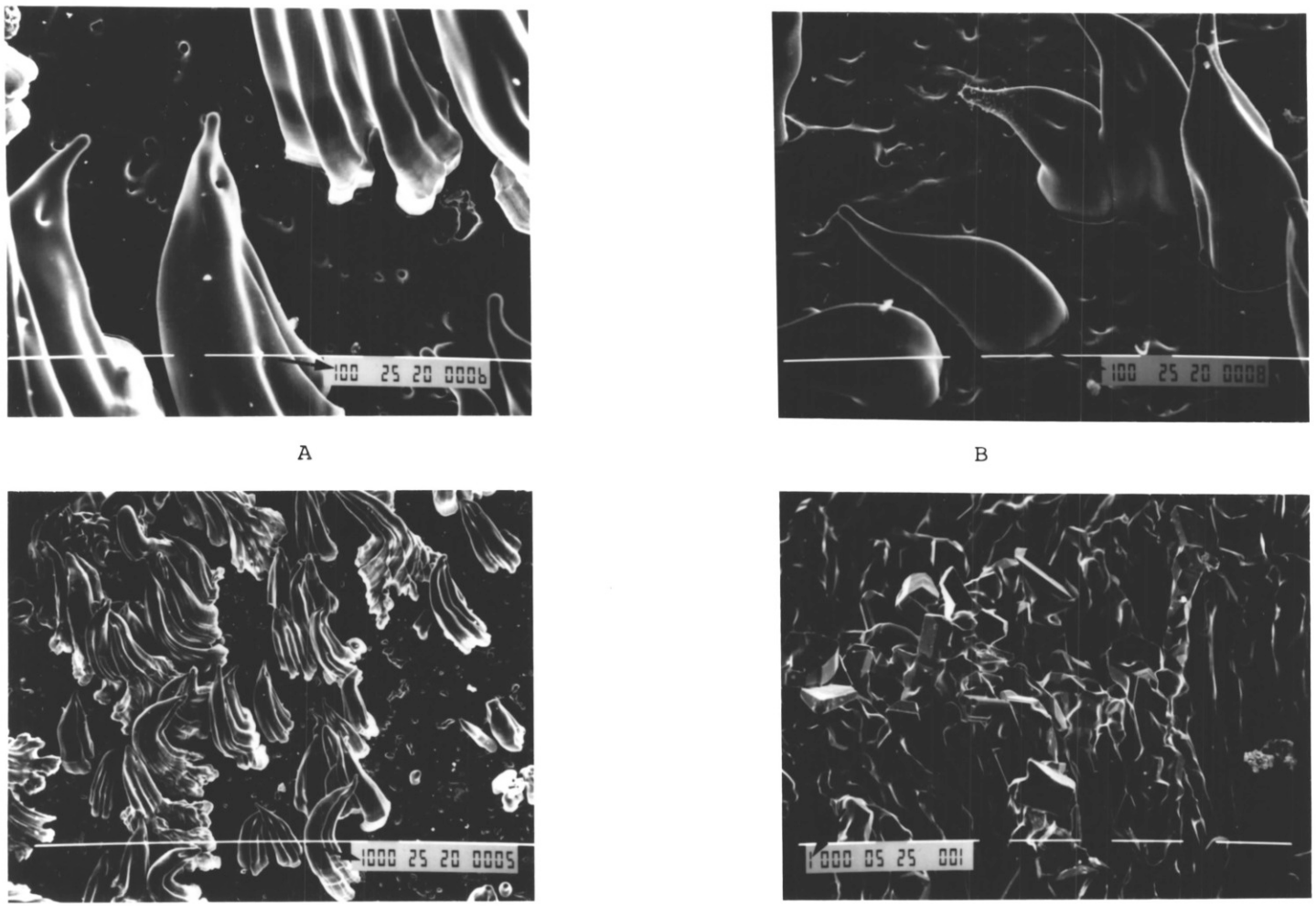


B X 180

Plate 7.3: Heat treatment of Cu_2S-Cu_2O composite in argon atmosphere at 1000 °C.

A) At Cu_2S-Cu_2O interface deposition of copper.

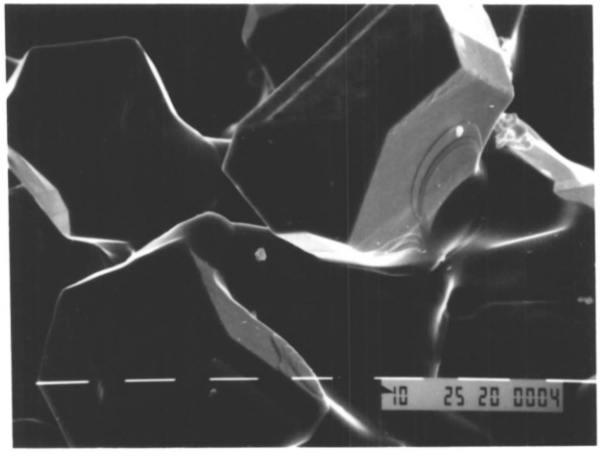
B) Growth of copper from the top surface of Cu_2S.



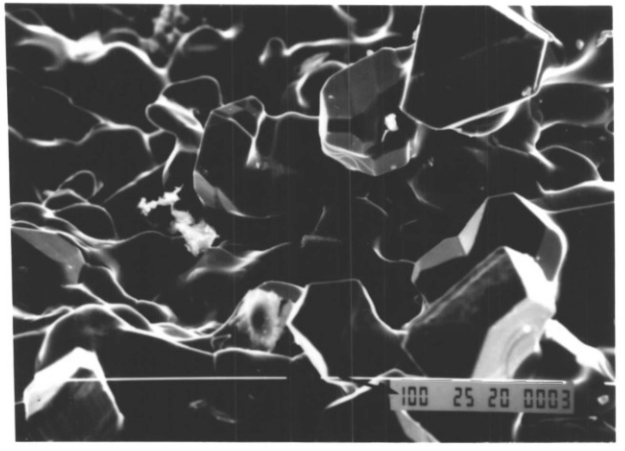
A B C D

Plate 7.4 Growth of copper whiskers from the surface of Cu_2S during the heat treatment of Cu_2S - Cu_2O at 1000°C. (Argon)

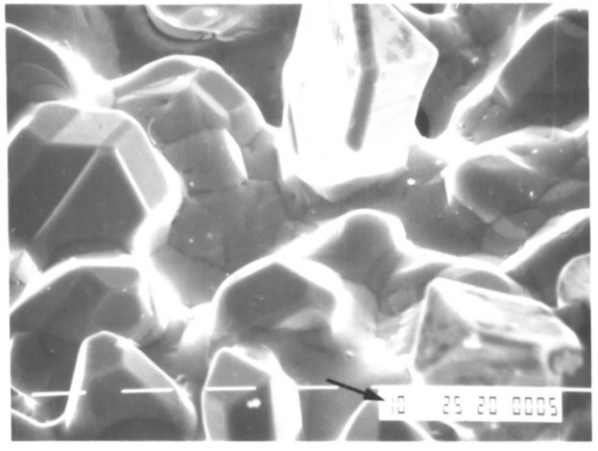
(A) and (C) 8 hrs (B) 4 hrs (D) 20 hrs



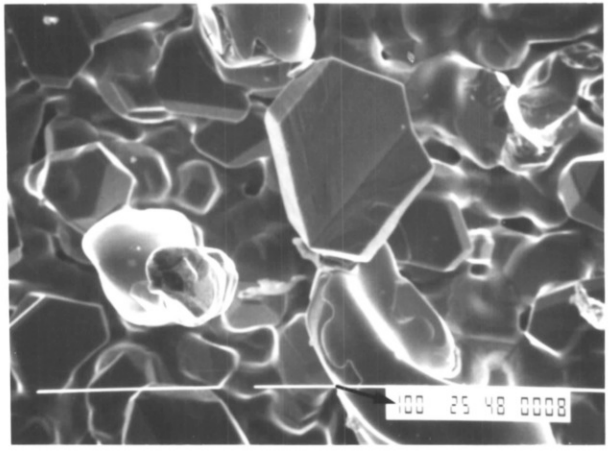
A



B

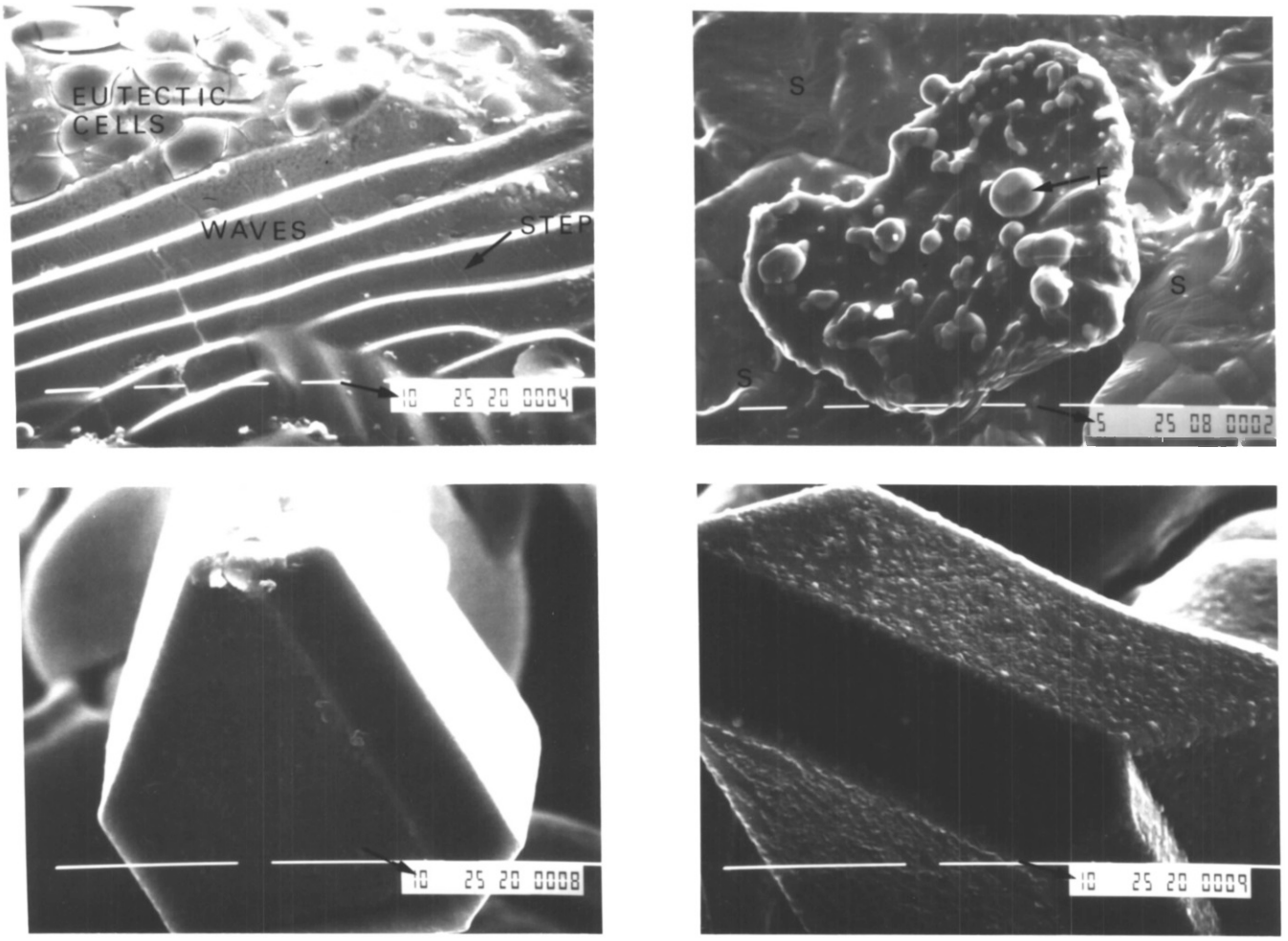


C



D

Plate 7.5 Faceting of on the surface of Cu_2S during the heat treatment of Cu_2S - Cu_2O composite at 1000°C in argon

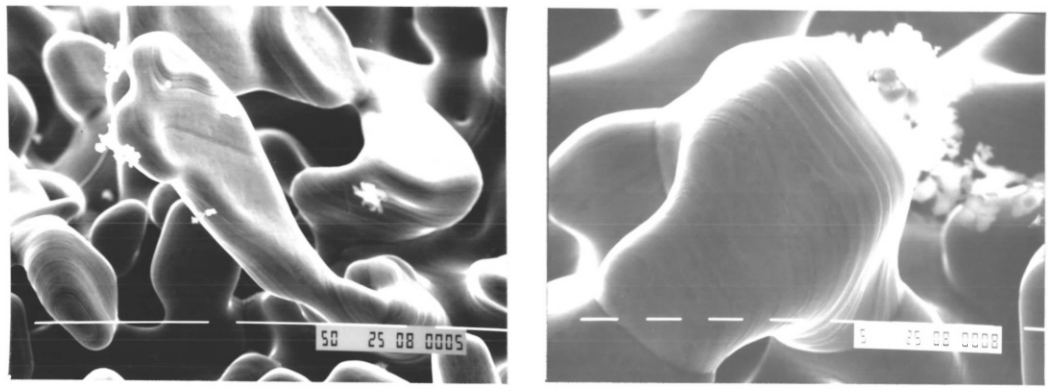


C D

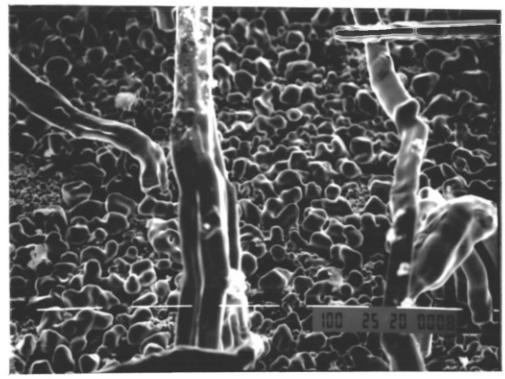
F - facet S - striations

Plate 7.6 Morphological changes occurred on the surface of Cu_2S during the heat treatment of Cu_2S - Cu_2O composite at 1000°C in argon

PLATE 7·7



A B



C

Plate 7.7: Growth of Cu_2S crystals during the dual treatment of CuS:CaO mixture in CO and growth of pure Cu whiskers in case of CuS-CaO reduction with carbon.

PLATE 7·8

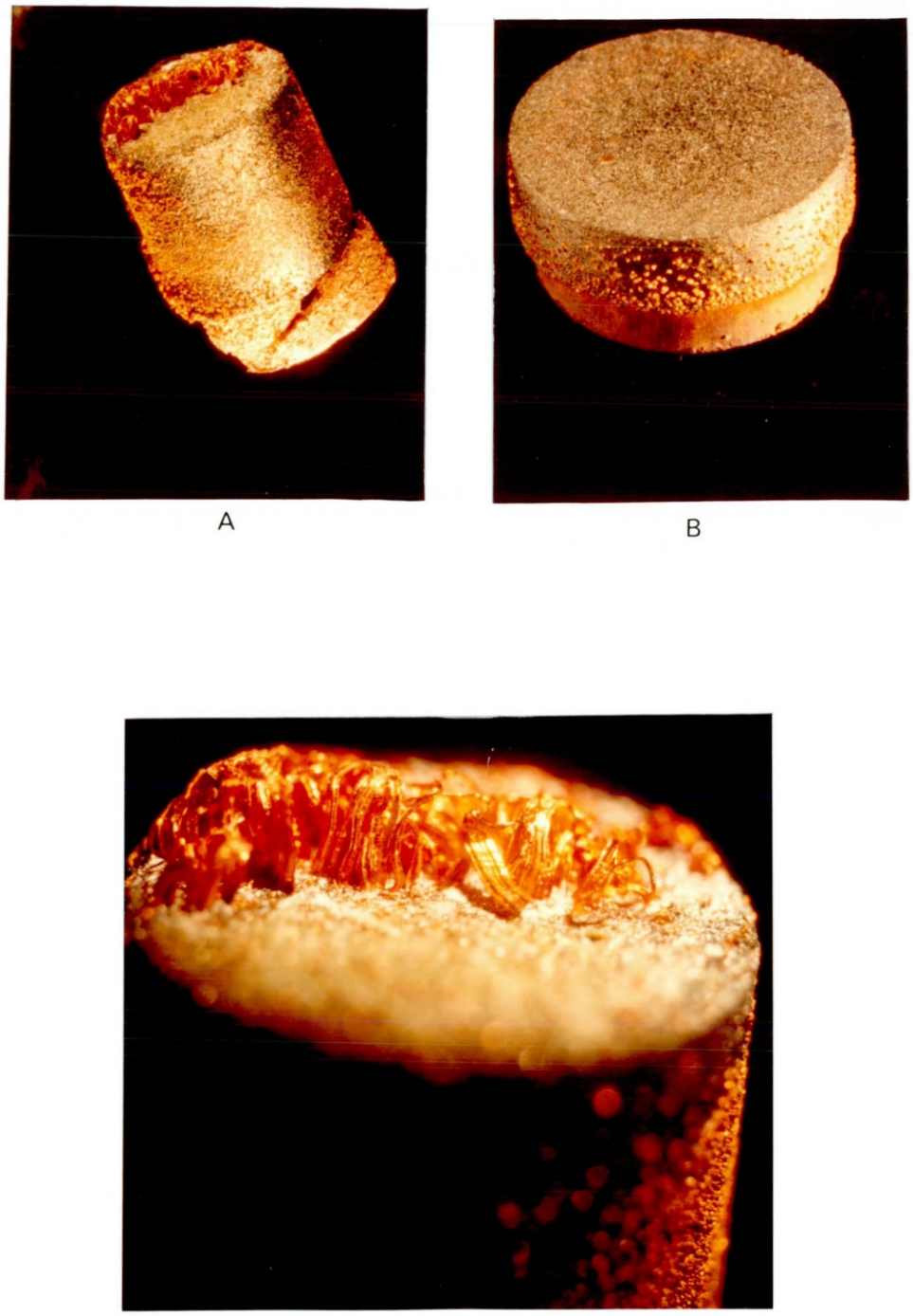
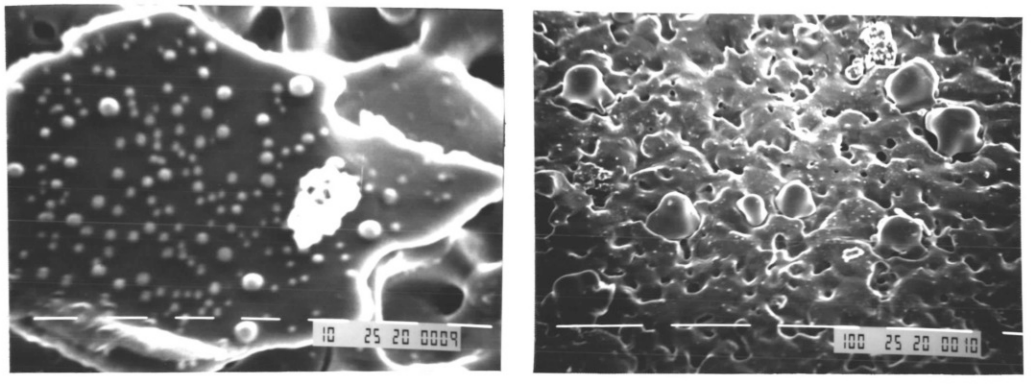


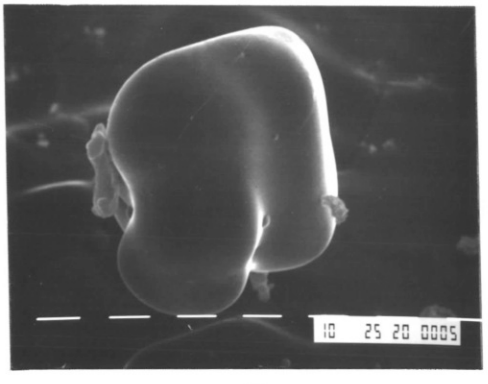
Plate 7.8: Photographs of Cu_2S-Cu_2O composite pellets with Cu whiskers.

a) 20hrs b) 45 minutes c) 20hrs.

PLATE 7·9



A B



C

Plate 7.9: Whisker growth during the heat treatment of Cu_2S- Cu_2O composite at 750^{o}C in CO_2.

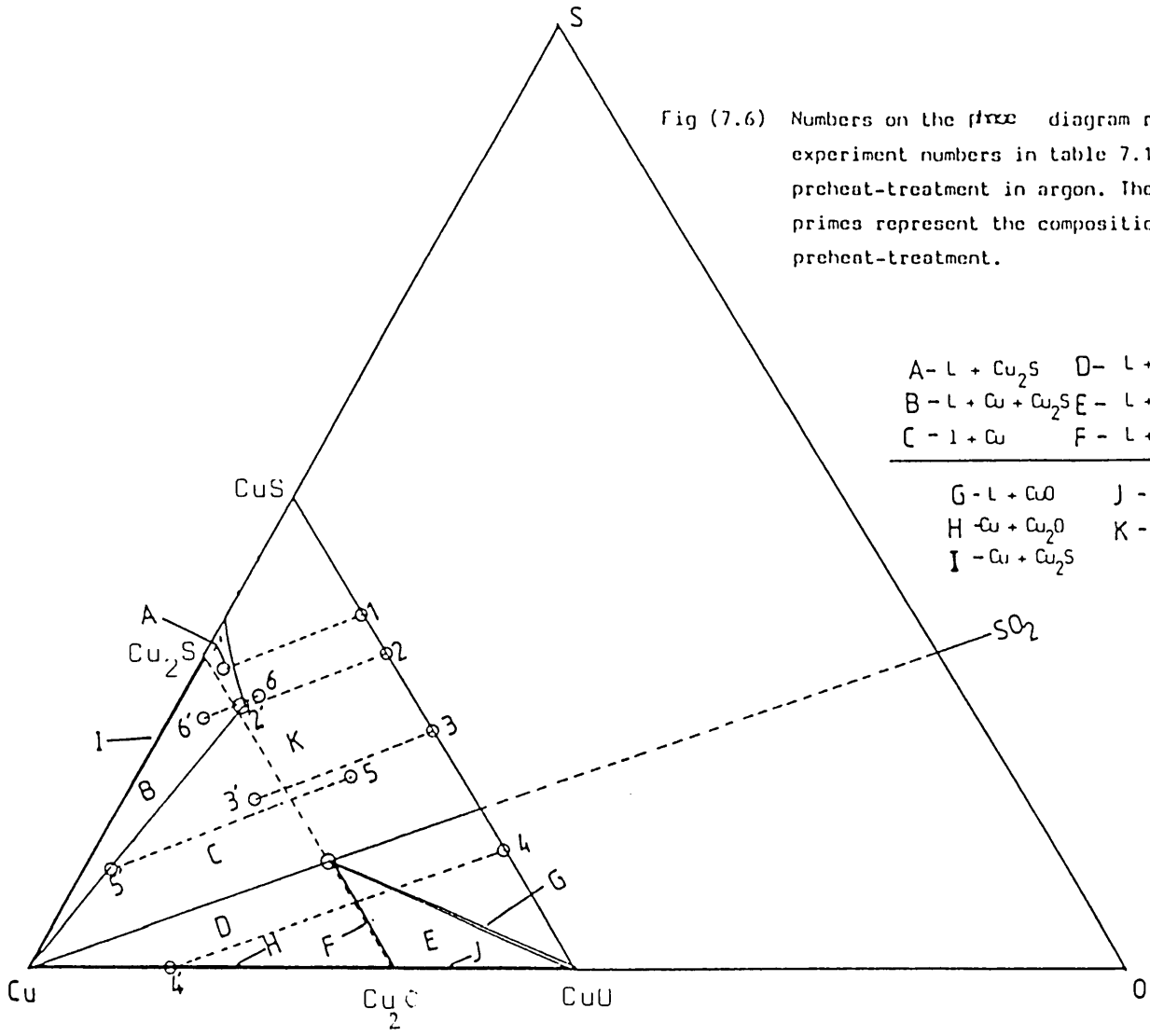


Fig (7.6) Numbers on the three diagram refer to the experiment numbers in table 7.1 prior to preheat-treatment in argon. The numbers with primes represent the compositions after preheat-treatment.

A- L + Cu_2S D- L + Cu + Cu_2O
B - L + Cu + Cu_2S E - L + CuO + Cu_2O
C - L + Cu F - L + Cu_2O

G - L + CuO J - CuO + Cu_2O
H - Cu + Cu_2O K - Liquid.
I - Cu + Cu_2S

Similar variations were observed on the stem of the whiskers.

In addition to these 'thin', 'long' bi-partite whiskers a few whiskers of different morphology were also observed on the exposed surface of the pellets. These whiskers were 'short' and 'thick'. The morphologies of these short whiskers is shown in plate 7.1(8) as indicated by an arrow head. The EDX spectral analysis of these whiskers which are in a minority shows that their composition are very close to the composition of pure copper. From the weight loss results observed during the course of reduction it can be concluded that the oxides present in the mixture after the heat-treatment must be partly reduced and as a result of this copper has nucleated. From the relative positions of the two mixtures (no:2 and no:6) within the Cu-S-O ternary, it is evident that a slightly higher weight loss would be expected in case of no:2 which is reduced in graphite crucible.

The oxysulphide mixtures represented by no:3 and no:5 whose compositions fall in the univariant (L + Cu) phase field developed one type of whisker after reduction in graphite crucible at 1000^{o}C. The whisker grown under this condition was of latter morphology ie 'short', 'thick' whiskers. The compositions for these mixtures after heat-treatment are shown in the Cu-S-O ternary diagram see fig (7.6) and from the compositions the relative amount of oxides can be estimated which accounts for the weight loss. The similarity of the composition of these whiskers are confirmed by the EDX analysis shown in Table 7.5. No whiskers were observed during the reduction of composition 1 whereas a large quantity of copper was observed on the surface of the pellet when mixture 3 was reduced. This mixture contained

a large quantity of oxide and hence the greatest weight loss was observed. No fibrous growth was observed in either case and the reasons for these structural changes will be discussed later in this section.

b) Whisker Growth During the Reduction of Sulphides in Presence of Lime with CO and Graphite.

Mixtures no: 7 and no: 8 were reduced with CO for different lengths of time and during the course of reduction the morphological changes observed in these pellets were significantly different although the atmospheric conditions were identical. Pure copper whiskers were observed in the former case whereas in the latter pure Cu_2S crystals grew, see plate (7.7), as confirmed by EDX analysis. The presence of pure copper whiskers was also observed when CuS and CaO mixtures were reduced with graphite at $850^{o}C$ see Tables (7.3) and (7.5). There was a striking similarity in the morphology of the copper whiskers which grew in different conditions and similar observations were made, in the case of the reduction of an oxysulphide mixture in a graphite crucible. Under all conditions where only pure copper whiskers grew the density of whiskers on the surface of the pellet was small. Both bi-partite whiskers and pure copper whiskers always grew at the solid or liquid gas interface which means that the gas phase plays a very significant role during the growth of these whiskers.

c) Growth of Whiskers during the heat-treatment of Oxide-Sulphide composites.

Composites of Cu_2S - Cu_2O when heat-treated in a flowing stream of argon at $1000^{o}C$ produced significant macrostructural changes. These macrostructural changes were largely related to the presence of a liquid phase in the Cu_2S - Cu_2O

pseudo binary section at 840°C as discussed in the Chapter 5. The macrostructural changes are discussed below in all those situations except experiment nos: 13,16 and 18, see Table (7.4) and (7.5).

i) Whiskers of copper were observed on top of the Cu_2S pellet.

ii) Many nuclei of copper in the form of protruded surface entities appeared on the peripheral surface see plate 7.8.

iii) Voids were observed at Cu_2S-Cu_2O interface.

iv) The peripheral surface of the Cu_2O portion of the pellet was coated with copper.

v) A substantial amount of shrinkage was observed in the Cu_2O pattern of the pellet.

The pellets after heat-treatment and scanning electron microscope analysis were prepared for optical microscopic examination. The following are the inferences drawn on the basis of optical microscopic examination:-

i) Morphologically both the whiskers and tiny nuclei of copper were very dense ie no porosity was observed although SO_2 was evolved ie neither macropores nor micropores were observed.

ii) The coating of copper on the peripheral surface of Cu_2O was found to be porous in nature, indicating some gases were evolved during the formation of copper which did not happen when whiskers were observed, see plate 7.3.

iii) Cracks, which were uniquely seen in Cu_2O composites at the interfaces, were observed and they were almost parallel to the interfacial plane.

iv) No copper layer was observed at the Cu_2S surface.

v) Diffusion of copper in the Cu_2O pellet is manifested in the microstructure in the form of small particles well distributed in this matrix, see plate 7.3.

vl) Few copper particles were observed in the matrix of Cu_2S.

vii) Copper growth was also observed on the periphery of Cu_2S, see plate 7.3.

On the basis of the scanning electron microscopic analyses, the variation in length of the copper whiskers with time has been shown in Table 7.6.

Table 7.6: Variation of the length of copper whiskers with time.

Experiment no.	Time in hr.	Length in Microns	Atmos.	Temp^{o}C
no 10	20.0	3000 - 3200	Argon	1000^{o}C
no 12	7.25	600 - 700μ	Argon	1000^{o}C
no 14	24.00	> 3500μ	Argon	1000^{o}C
no 15	8.00	850 - 1000μ	Argon	1000^{o}C
no 20	15.00	2000 - 2500μ	Argon	1000^{o}C
no 19	16.00	700 - 1000μ	Argon	1000^{o}C
no 17	24.00	50 - 60μ	Argon	1000^{o}C
no 16	24.00	very undefined	CO_2	1000^{o}C
no 18	15.00	5μ - 10μ	CO_2	750^{o}C

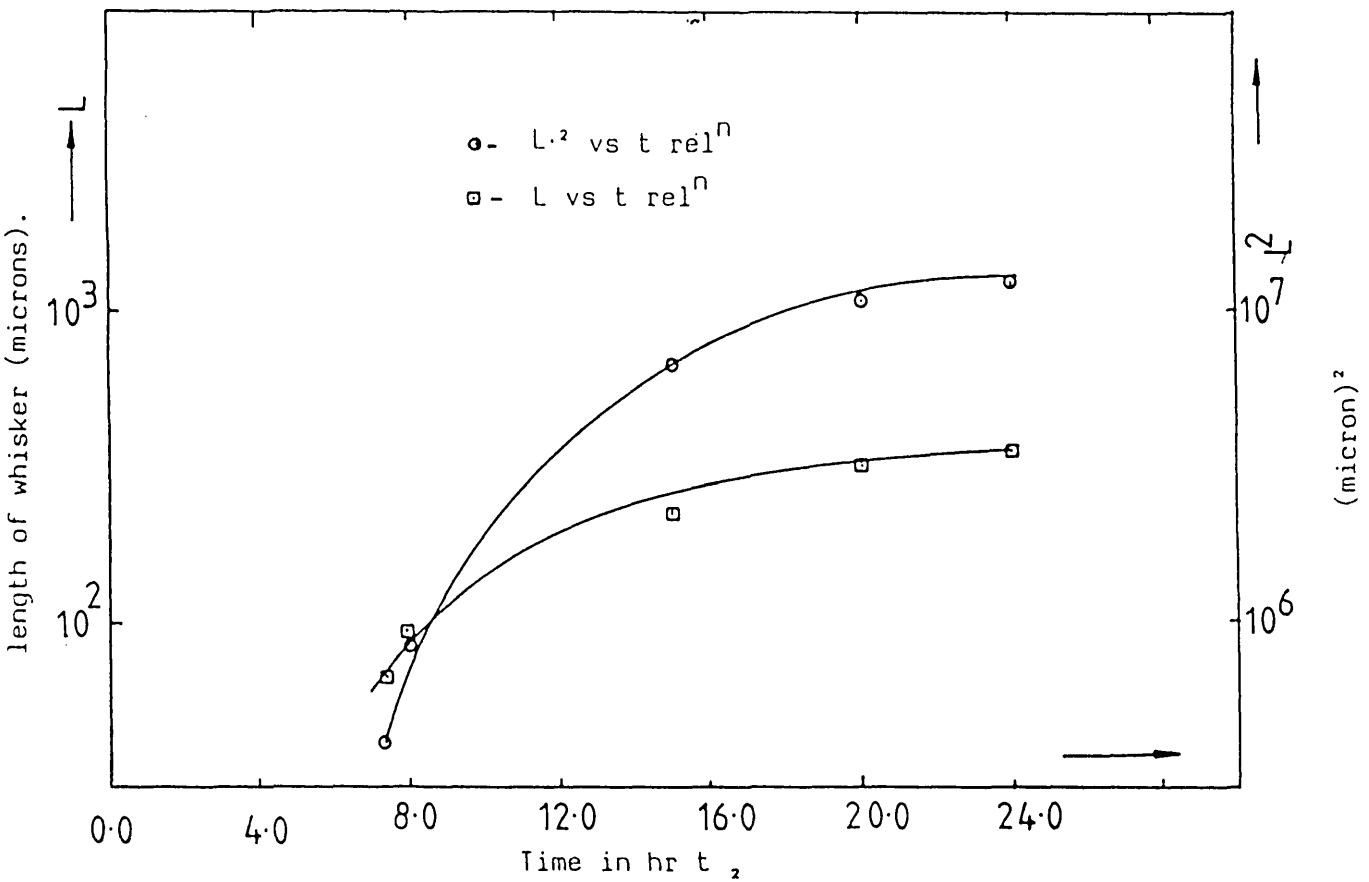


Fig (7.7a) Length vs time and (length)^2 vs time relationship during the whisker growth in case of Cu_2S-Cu_2O composite pellet. Temp^r 1000°C Atm-Argon.

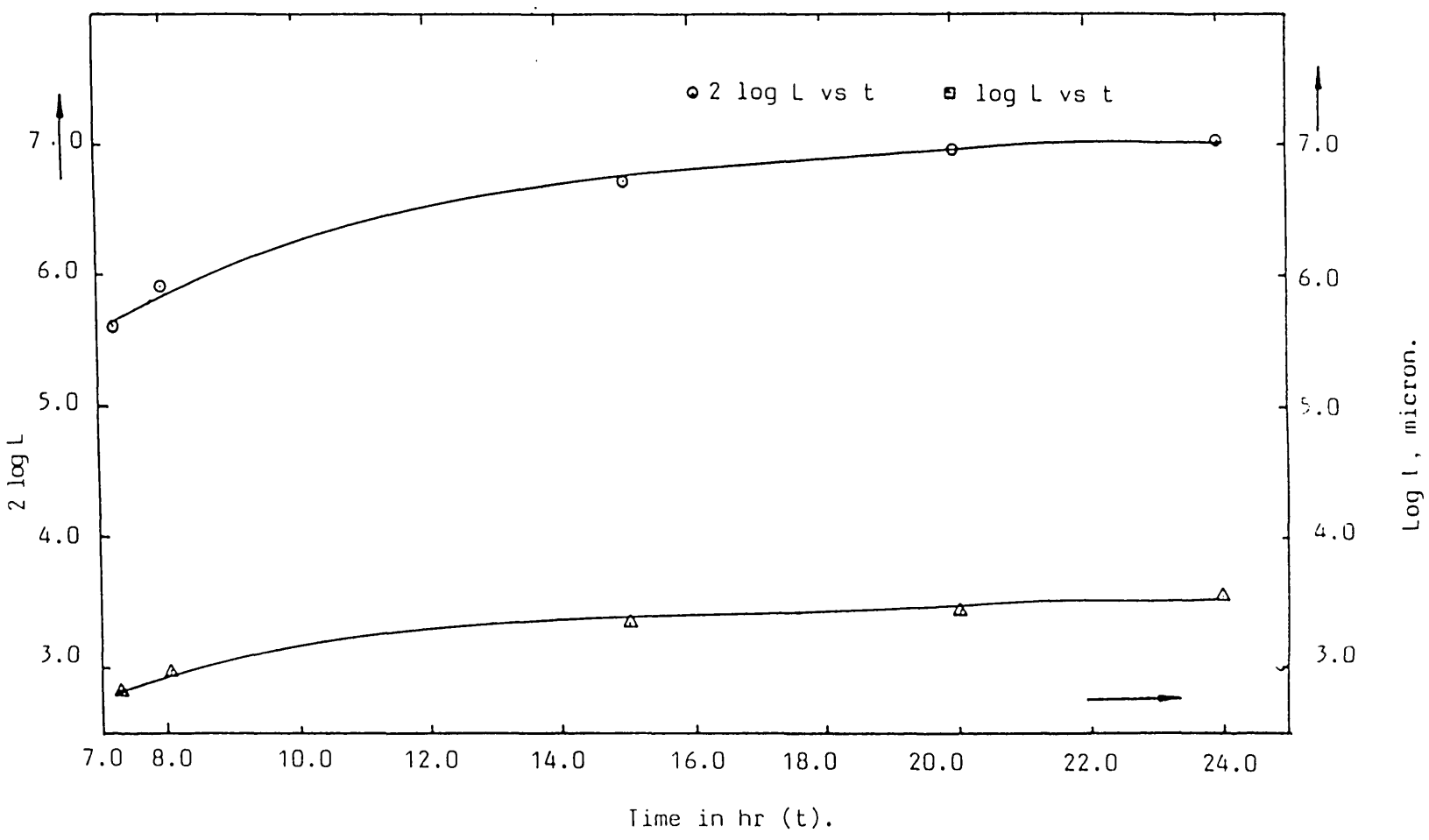


Fig (7.7b) Logarithmic relationship of length of whiskers with time in case of Cu_2O - Cu_2S composite heat-treatment at 1000°C in argon atmosphere

The tabulated values on the length of whiskers indicate that length increases with time and a correlation between the length of the whiskers and time is shown in fig (7.7) The relationship is a typical 'S' type curve. From the tabulated data, it is also obvious that the growth of whiskers is directly related to the structure of the Pt-foil (expt no:17) whereas in CO_2 atmospheres massive oxidations of Cu_2S has resulted in the formation of copper. A very unusual feature of the deposited copper at 1000^oC and on unaltered Cu_2S at 750^oC was observed to be a typical spiral growth, which was very similar in structure to striations shown in plate 7.6(B). From plate 7.8 it is seen that whisker growth is also affected by the contact surface area at the Cu_2S - Cu_2O interface. It can be seen in this photograph that the whiskers are only grown on selective areas at the top of Cu_2S pellet. This selective area is continually fed by a supply of copper from the Cu_2S - Cu_2O interface. The areas with no whiskers had undergone remarkable morphological changes. A few of them are shown in plates 7.5 and 7.6. E.D.X. Scan analysis of these areas were carried out to quantify the compositions and a wide variation in the compositions were observed as summarized in Table 7.5. A complete section has been devoted to explain the development of such morphological changes.

7.7 Discussion.

a (i) Discussion of Results of Reduction of Oxysulphide Mixtures in Graphite Crucibles.

The reduction mechanism and the morphological changes associated with it is related to the composition of the oxysulphide mixtures after heat-treatment, see fig (7.6)

The compositions indicate the relative amounts of material present in the Cu_2S - Cu-CuO ternary system. Evidently, the presence of a liquid phase in this ternary phase field is only possible at $^{p}SO_2$ = 1.0 atm as all these mixtures were heat-treated and subsequently reduced in a graphite crucible with p_{Total} = 1.0 atm. Therefore, depending upon the composition the mechanism of the reduction will be decided by the:

a) gas-liquid reduction mechanism
b) solid-liquid reduction mechanism
c) solid-solid reduction mechanism

The first mechanism is expected to contribute little because of the continuous flow of argon gas. Any carbon monoxide generated will be continuously swept away from the system. For this reason, the kinetics of reaction are slow with a very small extent of the total oxygen removed. Thus, in this process, oxygen is removed from the oxysulphides mainly by solid-solid reduction mechanism. The removal of oxygen from any composition can be represented by drawing a tie line from the oxygen corner of the ternary phase diagram through the composition co-ordinate which would eventually intersect the Cu-Cu_2S edge.

ii) Growth Mechanism of Bi-partite Whiskers

It is quite clear from the ternary phase diagram that the thermodynamic properties are invariant in the (L + Cu + Cu_2S) phase field which means the compositions and activities are constant at a particular temperature and pressure. Since the liquid is in equilibrium with pure copper metal and pure Cu_2S solid therefore, the liquid must reject Cu and Cu_2S to keep its activity constant as oxygen is removed. Thus, the

concomitant deposition of two materials on the removal of oxygen is consistent with the thermodynamics of the system. On the basis of the Lever Rule, variations in composition along the length of a whisker can be explained, if copper whiskers are growing near bi-partite whiskers, in that situation Cu_2S and Cu will be precipitated at the expense of each atom of oxygen is removed. The relative proportion at each stage remains the same but the material is distributed between copper and bi-partite whiskers. The amount of material rejected will vary continuously with the decrease in the volume of the liquid. There is another reason for the variation of the composition along the length of whisker which might happen because of SO_2 evolution during the reduction. In that situation the tie line will be different from oxygen tie line.

In the (liquid + Cu) univariant phase field the removal of oxygen allows the composition of liquid to change and as a result of this copper deposition takes place. Copper formation occurs till a composition is reached which is represented by the tie line intersecting the boundary of (L + Cu) and (L + Cu + Cu_2S) phase fields. From this stage, onwards the removal of oxygen results in the deposition of Cu and Cu_2S together.

In the (Cu + Cu_2O) invariant phase field, the removal of oxygen results in the formation of pure copper and the thermodynamic possibility of the growth of bi-partite whiskers does not exist. It has been realized from the aforementioned thermodynamic principles that the growth mechanism of bi-partite whisker is essentially a solid-liquid mechanism controlled by the gas phase as an oxygen sink.While an attempt to explain the mechanism of whisker growth is made it is also necessary to appreciate

the thermodynamic factors which certainly play a major role in the nucleation and growth process by determining the driving force necessary for the nucleation and subsequent growth. From the available literature it is evident that for whisker nucleation a driving force equivalent to the activity of the material slightly higher than unity is necessary. This condition prevails in the case of the growth of bi-partite and copper whiskers and can be explained on the basis of the Cu-S-O phase diagram. In this phase diagram, the activity of oxygen in any phase field decreases as the composition moves away from the Cu_2O corner. Thus, the activity of oxygen gradually decreases from the (Cu + Cu_2O) edge to (L + Cu) and finally approaches zero at the (Cu + Cu_2S) edge. This means that the driving force for the nucleation of Cu_2S gradually increases resulting the formation of bi-partite whiskers instead of copper whiskers. Representing the oxygen removal by an equilibrium shown below for which the standard Gibbs Free Energy change determines the amount of volume free energy available to create new surface.

$$\{O\}_{Sol} + C\,(s) = CO\,(g) \qquad (7.10)$$

Thus, the volume free energy in this case would be decided by the activity of oxygen either in solution or in the pure solid oxide. Invoking the energy associated with the creation of a surface and related mismatch of phases which gives rise to certain defects eg dislocations explains why a large driving force does not result in the nucleation of whiskers. Frequently, the available volume free energy is distributed amongst all the heterogeneous sites for the initiation of the growth process rather than inserted at one particular site, which leads to whisker growth. It is because the reduction driving force is high that whiskers were not observed when the compositions on the Cu + Cu_2O invariant edge were

reduced. If much smaller reduction potentials are applied it is possible to develop whiskers in this region also.

Applying these principles to (L + Cu) compositions where the oxygen activity is lower than that in the (Cu + Cu_2O) invariant, a limited number of pure copper whiskers are observed because of the presence of copper which must have acted as a nucleation site prior to the reduction step. In this case, whiskers must have nucleated on these sites where only a few dislocations are available. A large number of dislocations would give rise to lateral growth rather than whiskers.

Conditions for the energetics of nucleation of a large number of whiskers seem to be optimum in the (L + Cu + Cu_2S) phase field. A relatively small driving force is available for the nucleation of whiskers because of the small activity of oxygen ie $^{a}Cu_2O$ = 0.15 at 1000^{o}C. From the phase rule it has been appreciated that the precipitation of Cu and Cu_2S commences with the removal of oxygen from the liquid phase. From scanning electron microscopy it has been observed that both bi-partite and pure copper whiskers grew under these conditions, see plate 7.2. These whiskers have grown over a duration of 3 hours. The moment oxygen removal ceases, the precipitation of Cu and Cu_2S also ceases resulting in a cessation in the growth of whiskers. In the (L + Cu_2S) phase field, the driving force is insufficiently small for nucleation of whiskers. The growth of bi-partite whiskers is solely dependent upon the rate of oxygen removal from the system and nucleation on the preferred sites. From the compositions indicated on the ternary diagram, the path of reduction can be determined by drawing tie lines from the oxygen corner through these composition co-ordinates and extrapolating these tie lines to the Cu-Cu_2S edge. As the oxygen is removed from the

system, the composition co-ordinates move away from the oxygen corner. Using mass balance data, the amount of oxygen removed was determined and it was found that in most experiments the reaction was incomplete. On this basis the related phase field was found at the end of the reduction. Excellent agreement was found with the observed related phase field. This fact explains why bi-partite whiskers do not grow when compositions in the (L + Cu) phase field were reduced. The whole process is governed by the rate of reduction. The compositions, during the process of removal of oxygen do not cross the boundary between (L + Cu) and (L + Cu + Cu_2S). The reaction appears to stop well before this boundary is reached. One exception was noticed ie composition 5R in the ternary system which is very close to the boundary of (L + Cu) and (L + Cu + Cu_2S). Reaction with this composition appears to stop at the boundary and further oxygen removal does not occur preventing the growth of whiskers. The kinetic barrier related to the cessation of the reduction of the oxides appears to be the volume of the liquid phase present as this decreases at the same rate as the deposition of Cu or Cu and Cu_2S occur. The mass balance data show that the weight loss was small yet a large deposition of material has taken place which can only be explained on the basis of the Lever Rule.

Mechanistically growth only takes place from energetically favourable sites in a layer like fashion, governed by screw dislocation mechanism. This means the liquid must exist in the vicinity of these favourable sites and hence the supply of material must be maintained during the course of reduction. The time scale over which growth has taken place is unusual for a mechanism based on solid diffusion. The exceptionally fast growth mechanism can only be justified on the basis of precipitation from the liquid

phase. The rate of the growth, this decreases with the rate of removal of oxygen and is independent of any parameter related to solid diffusion mechanism.

b (i) The Discussion of the Results of Whisker Growth During the Heat-Treatment of the Oxide-Sulphide Composite Pellets.

The microstructural evidence obtained from the heat-treatment of oxide-sulphide composites shows that a liquid phase forms during the heat-treatment and drainage takes place around the periphery of the oxide pellet resulting in the generation of copper. From the morphology of the product phase, see plate 7.3 and 7.8, it appears that a gaseous product has evolved during the course of the heat-treatment. The dense layer of porous copper and interfacial cracks support this idea. The liquid phase formed belongs to the Cu-S-O ternary and is rich in sulphur. As the reaction continues, the volume of liquid increases accompanied by a change in composition , when oxygen dissolves in the liquid. It is also worth noting from the equilibrium relationship that the pressure of the gas phase is proportional to the activity of oxygen in the liquid and if this pressure exceeds the atmospheric pressure, the evolution of gas would result with the deposition of copper.

The drainage of a sulphur rich liquid around the periphery of Cu_2O results in copper deposition as the SO_2 pressure becomes several time greater than atmospheric. For this reason no copper coating was observed around the Cu_2O pellet when this pellet was positioned above the sulphide during the heat treatment. At the interface the liquid formed exhibits a concentration gradient of O^{-2} ion and S^{-2} ion between the Cu_2S and Cu_2O surface.

The microstructure also shows that metallic copper is uniformally distributed in the matrix of the oxide pellet irrespective of position during the heat-treatment, whereas copper whiskers are observed on the surface of Cu_2S with a few copper particles in the Cu_2S pellet matrix. These morphological and microstructural changes show that there is a definitive diffusion flux of copper which occurs as a result of S^{-2} ion and O^{-2} dissolution in the liquid phase. The liberation of SO_2 from the melt takes place at a critical value of oxygen dissolution. It can be concluded that the dissolution of anionic species and the migration of cations are inter-related events. Representing the overall process as an electro-chemical process, the following are the reactions:

$$\begin{aligned} Cu_2S &= 2\,Cu^{+1} + S^{-2} + V_M^{+1} + e \quad (a) \\ Cu_2S &= 2\,Cu^{+1} + O^{-2} + V_M^{+1} + e \quad (b) \end{aligned} \qquad (7.12)$$

Also

$$SO_2(g) = 1/2\ S_2(g) + O_2(g). \qquad (7.13)$$

$$\left.\begin{aligned} \tfrac{1}{2}\,S_2(g) &= S^{-2} + V_M + 2\dot{h} \quad a \\ \tfrac{1}{2}\,O_2(g) &= O^{-2} + V_M + 2\dot{h} \quad b \end{aligned}\right\} (7.14)$$

Equation (7.12) represents the electro-chemical mechanism associated with the diffusion of the defect structure and the ionic species whereas equation (7.14) relates the equilibrium between the defect structure and the gas phase.

On this basis it is clear that the equilibrium must exist between the ionic species, defect structure and gas phase.

When dissolution process commences, both Cu_2S and Cu_2O gradually loose their anionic species. Thus, if migration of anionic species takes place towards the Cu_2S-Cu_2O interface to assist dissolution electrochemically cations move in the opposite direction. During the migration of ionic species another event proceeds simultaneously related to the electrochemical equilibrium between the defect structure and the electrons. In the absence of any cationic vacancies the migration of cations is extremely difficult and as a result, in the event of loss of anions from the pellet, cationic species nucleate metal at the solid-liquid interface in the presence of electrons. The nucleation necessitates a condition of relatively high activity. In the presence of cationic vacancies in the lattice cation migration proceeds without nucleation of the metal by a jump mechanism through vacant sites. This means results in the movement of vacancies and anions towards the solid-liquid interface with metallic ions and electrons moving away from this interface. The relative penetration distance of cations in the sulphide and oxide matrix is solely governed by the chemical diffusivity of cations in the two matrices. Thus a chemical potential gradient for cationic species is established which is essentially dependent on the activity of Cu^{+1} ion at the liquid-Cu_2S and liquid-Cu_2O interfaces and it determines the driving force for the transport of cations. From available literature (7.32) data, the chemical diffusivity of Cu in Cu_2S at 440^{o}C and at 100mv in a polycrystal is 7 -8 x 10^{-2} cm^2/sec whereas the chemical diffusivity of Cu in Cu_2O in a single crystal is 3 x 10^{-4} cm^2/sec.

Using the electrochemical mechanism and the related transport steps, conditons for a small degree of supersaturation are derived from the transport of Cu^{+1} ion across the length of the Cu_2S pellet. For the transport of material from the liquid Cu_2S interface to the bulk Cu_2S, the following relationship is developed which represents the physical situation and is dependent on the thermodynamic parameter called the activity coefficient which is high at the liquid - Cu_2S interface.

$$\tilde{D}i = BiRT \left[1 + \frac{d \ln \gamma i}{d \ln Ni} \right] \quad - \quad (7.15)$$

$\tilde{D}i$ = Chemical diffusion coefficient of species 'i'

Bi = Mobility of i^{th} species

γ_i = Activity coefficient of i^{th} species

N_i = Mole fraction of the i^{th} species

T = Temperature in degree Kelvin

R = Gas Constant.

The microstructure of the Cu_2S-liquid interface shows that copper deposition does not take place at the interface see plate 7.3. The reason for Cu nucleation on the surface is evident and the precipitation of copper in the matrix of Cu_2O is explained in terms of the operating transport mechanism. From the microstructure it appears that the cations interacted with electrons resulting in the nucleation of copper a situation which would not have occured if the Cu chemical diffusivity had been high. Thus, the proposed electrochemical mechanism summarises the conditions necessary for the nucleation of whiskers and the related transport mechanisms.

ii) The Growth Mechanisms of Whisker

Once the conditions for nucleation of whiskers are satisfied at energetically favourable sites, growth commences. At these preferred sites, the nuclei grow as a pointed-protruded surface. This particular shape of the nuclei at screw dislocations is energetically preferred and has been verified experimentally. The tip of the protruded surface is energetically the most unstable and has the highest surface free energy. The tip of such whiskers are grooved because the atoms in a surface of radius of curvature 'r' have a higher chemical potential than the atom on a flat surface at the same temperature and pressure. Thus, the tip of a growing whisker is materially unsaturated which also accounts for its relative instability in terms of energy. This relative instability of the tip is related to unsaturated bonds and hence the material is continuously fed at the tip. The unsaturation of material at the tip very closely resembles the unsaturation of material at a moving screw dislocation. Thus, the difference in the chemical potential is given by the Gibbs-Thomson Equation as:

$$\Delta\mu = \frac{\gamma\Omega}{r} + \text{dislocation energy} \qquad (7.16)$$

or $$\Delta\mu = r\,\Omega\,k + \text{dislocation energy}$$

where $\Delta\mu$ = chemical potential difference

γ = surface energy per unit length

k = radius of curvature = $\frac{1}{r}$

r = radius

Ω = volume per atom.

If the radius of curvature 'k' is represented in terms of the rate of change of slope then

$$k = \frac{d^2y/dx^2}{\left[1 - \left(\frac{dy}{dx}\right)^2\right]^{3/2}} \qquad (7.17)$$

In the case when θ is small $dy/dx \ll 1$ and hence

$$k = d^2y/dx^2 \quad \text{and} \quad \Delta\mu = \Omega\gamma \frac{d^2y}{dx^2} \qquad (7.18)$$

It can be seen from the plot shown in fig (7.8) that d^2y/dx^2 is a maximum at $x = 0$. Because γ and Ω are constant hence $\Delta\mu$ is directly proportional to d^2y/dx^2. This is the relationship between diffusional flux and concentration gradient. It is worth remembering that the flux of material is continuously changing at any value of 'x'. Thus, mathematically it is proved that the tip of whisker is energetically the least stable point and during whisker growth process material will be supplied to the tip in order to maintain its stability. This is a necessary and sufficeint condition for the growth of whiskers.

In the past, some workers have suggested that the growth process is essentially assisted by a local increase in the strain energy as a result of the molar volume change. This strain energy is then dissipated by causing the movement of the material out of the surface. Several criticisms arise regarding this mechanism. If whisker growth is dependent on a strain induced mechanism the nature of strain has to be periodic in order to supply the material as the length of whisker changes with time. In the absence of a periodic strain the length of a whisker would not change with time. Also maintaining a periodic strain at one point appears to be very improbable.

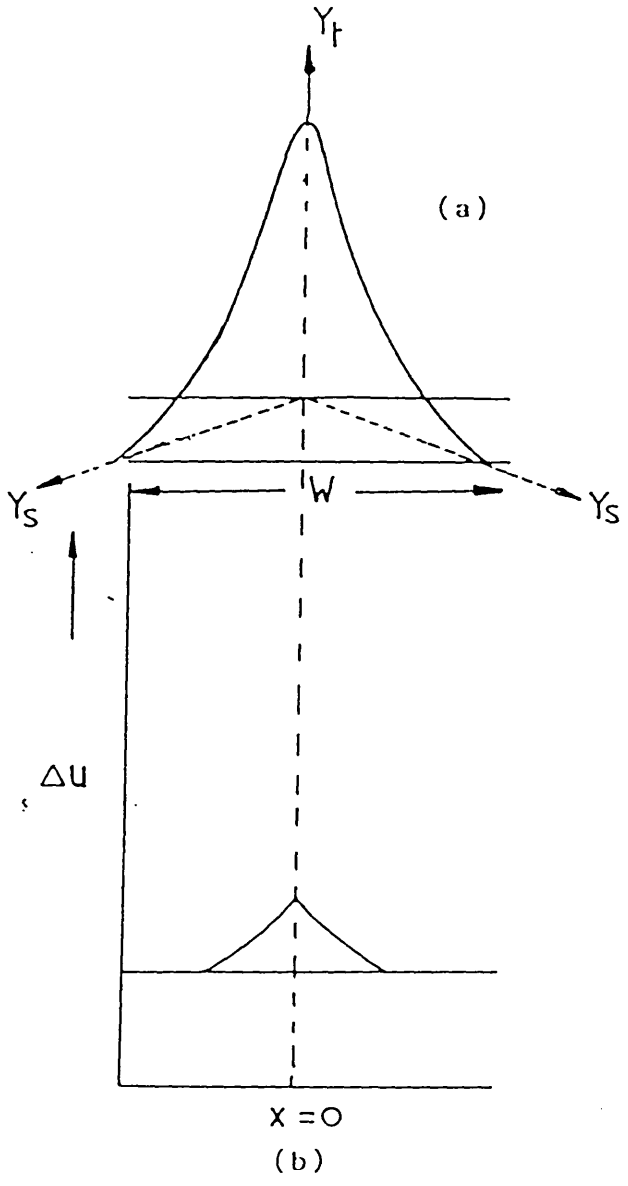


Fig (7.8) Variation of surface energy with distance and its relation with chemical potential. (μ).

Secondly if this mechanism is operative voids due to the absence of material should always be observed and this is not true. Lastly the most important factor is that whiskers are known to be defect free crystals grown in a particular direction. Strain induced growth of this kind would dramatically increase the number of dislocations due to plastic deformation in the whiskers. In contrast the growth process explained on the basis of the Gibbs-Thompson effect does not raise similar objections.

Theories are available in the literature (7.21) which also describes the morphology and diffusion mechanism at different stages of whisker growth. A screw dislocation with a positive burgers vector in the direction of whisker growth will always initiate the generation of a new layer of atoms. In the beginning of the growth process when the width of the root of the whisker is small, surface diffusion is the rate controlling step according to the relationship:

$$D_S = \frac{w}{a_o} \frac{q_s D_v}{P_e} \frac{q_{svap}}{\rho_{vap}} \qquad (7.19)$$

q_s = material transported due to surface diffusion

a_o = lattice parameter w - width

ρ_{vap}, ρ_e density in the vapour phase and in the lattice respectively

D_v = vapour diffusion coefficient

q_{vap} = material transported due to vapour diffusion.

In the present situation, lattice diffusion would play a dominant role in comparison to vapour diffusion as the latter mechanism is only effective if the vapour pressure is reasonably high.With varying 'w' competition remains between lattice and surface diffusion. At large width surface diffusion is probably the dominant mechanism as lattice diffusion is slow under these conditions. By increasing the width, surface diffusion becomes faster but atoms have to travel a longer distance and hence the root of whiskers grows thicker with time at the expense of the length until eventually the longitudinal growth completely ceases. Experimental evidence of the dominance of one mechanism under specific conditions has been proved in a few cases (7.33,7.34). The variation of surface diffusion and the volume diffusion over a range of temperature has been removed by Gjostein, Collins and Shewmon and the data are shown in fig (7.9). The relationship shows that the variation of log D_S with $Tm/_T$ is no longer linear beyond 0.7Tm. At this critical temperature, surface diffusion is a slower process than volume diffusion. The relative slopes of the two different mechanisms can be appreciated by joining the data points at higher temperatures. The graph shows that as the temperature increases the difference between surface and lattice diffusion decreases but contributions are always there due to these two modes at all temperatures.

In the present investigation although no attempt has been made to verify the plane or the direction along which growth of whiskers has taken place, it can be stated that the preferred direction of growth in the case of fcc crystal is (111). In this direction the surface energy is minimum and hence during the growth process the atoms would always try to arrange along a direction in which their overall energy is minimum. The other planes and directions

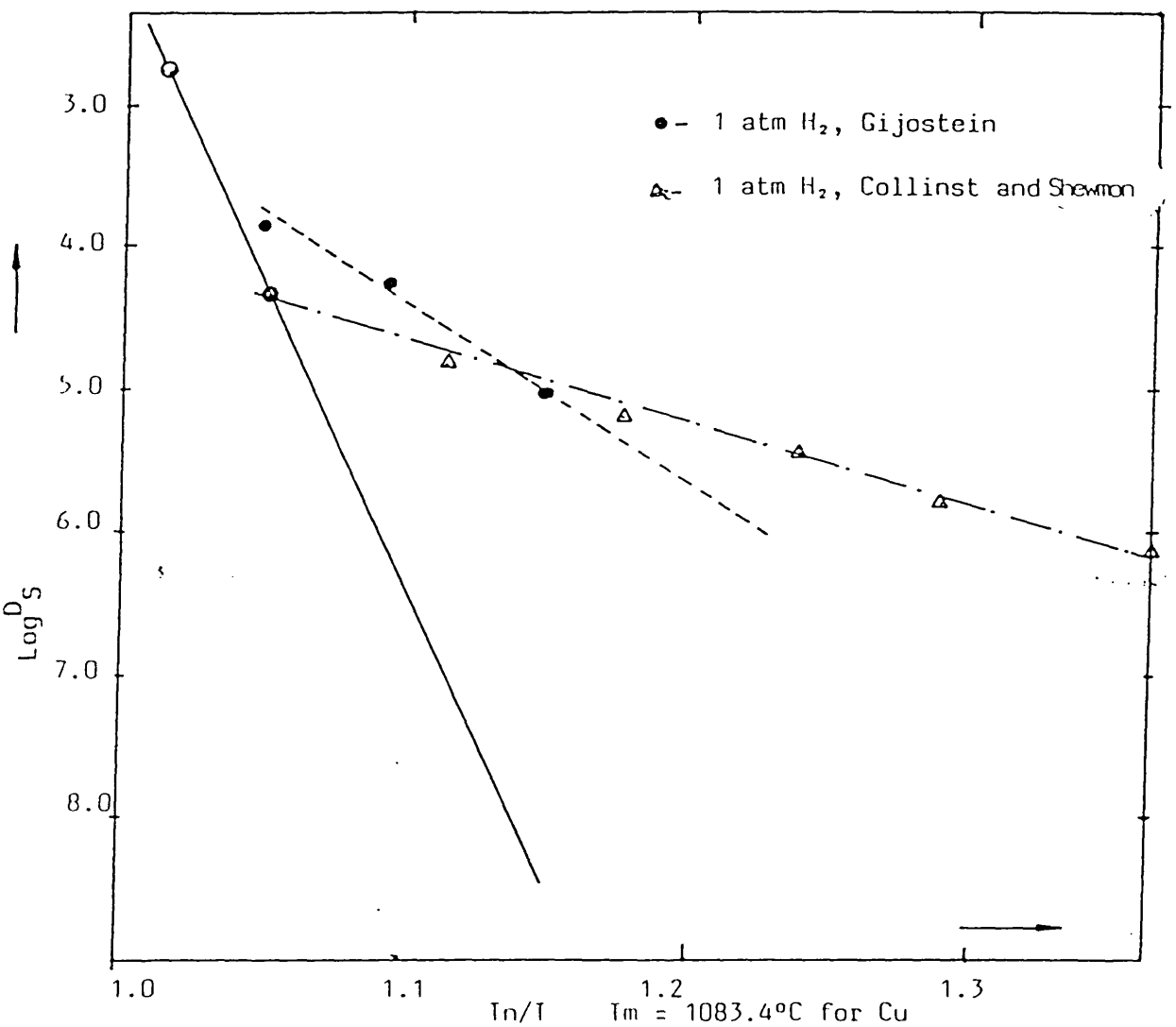


Fig (7.9) Relationship between temperature and surface diffusion in Cu Atm-Hydrogen.

in this system are energetically unstable and materially unsaturated.

(iii) Wagner's Work on Composites and their Interpretation.

Wagner (7.35) designed an experiment with a composite pellet of Cu-Cu_2S, see fig (7.10) and on the periphery of the Cu_2S, Cu_2O powder was smeared. This was then heated in a gentle flow CO_2 at 750°C for 2 hours. The change in dimension of copper core rod was 0.049cm. According to Wagner, the equilibrium prevailing during the heat treatment was

$$Cu_2S(s) + 2Cu_2O(s) = 6Cu + SO_2 \qquad (7.20)$$

for which the value of equilibrium constant k at 750°C is 1.008. In this system, it is evident that the SO_2 partial pressure is extremely small. From the thermodynamic data it can be deduced that if the system is in equilibrium, the nucleation of copper is only possible if SO_2 is immediately removed from the system. Using Cu-Cu_2S and Cu-Cu_2O equilibria the partial pressure of SO_2 has been calculated to be 0.45atm. The possibility of equilibrium between Cu_2O, Cu and the gas phase exists i.e.

$$Cu_2O(s) + CO(g) = 2Cu(s) + CO_2(g) \qquad (7.21)$$

as p_{CO} is extremely small at T = 750°C, K = 9×10^4. Thus, any CO generated in the system would immediately be swept away. The oxidation of Cu_2S by CO_2 at 750°C is thermodynamically impossible as both the equilibrium constant and the partial pressure of CO_2 are small. This condition was chosen carefully by Wagner in order to avoid any other source of nucleation of copper.
A simulation of similar conditions was attempted in this work and the results of experiment no:18 are summarised in Tables (7.4,7.6). The maximum length of whisker

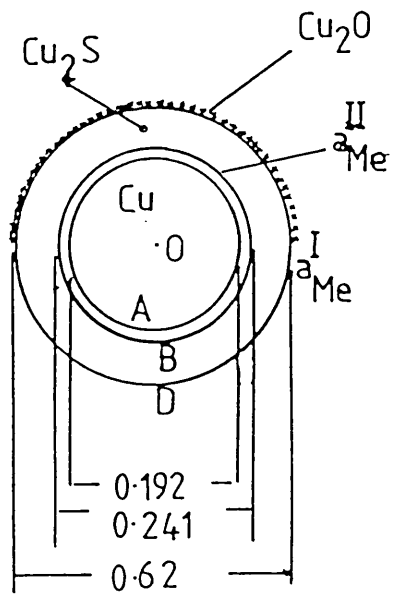


Fig (7.10) Design of pellet in Wagner's experiment.

observed was 5μm on the surface of Cu_2S. Most of the whiskers were observed at the Cu_2S-Cu_2O interface penetrating through the interfacial area. These whiskers were over 150μm long and were densly populated. The growth of copper whiskers was also observed on the peripheral walls of the Cu_2S pellet, see plate (7.9).

From Wagner's observations and this work an attempt has been made to justify that the diffusivity of Cu in Cu_2S is extremely high. Applying Wagner's rate equation:

$$\dot{n}_{Me} = \frac{4A \; C_{Me} \; D^*_{Me}}{r \; f_{Me}} \; \ln \frac{a^I_{Me}}{a^{II}_{Me}} \qquad (7.22).$$

where
- A - area for OB Radius
- C_{Me} - mole/unit volume of metal ions
- r - BO the diffusion path
- D^*_{Me} - intrusic diffusion coefficient.
- $\dot{n}_{Me}$ - rate mole $(area)^{-1}$ sec^{-1}
- f_{Me} - correlation factor = 1.0

we also know that

$$\tilde{D} = \text{Chemical diffusivity} = 3 \frac{D^*_{Me}}{\delta} \qquad (7.23)$$

where 'δ' is the nonstoichiometric factor. Arranging (7.22) and (7.23) we have

$$\tilde{D} = \frac{3}{4} \frac{\dot{n}_{Me} f_{Me}}{C_{Me} \; \delta} \left(\frac{r}{A}\right) \frac{1}{\ln {}^{a^I_{Me}}/_{a^{II}_{Me}}} \qquad (7.24)$$

Substituting the values from Wagner's experimental result, we have:

$$\tilde{D} = 1.096 \times 10^{-3}/\ln \frac{a^{I}_{Me}}{a^{II}_{Me}} \qquad (7.25)$$

which gives $\tilde{D} = 8.36 \times 10^{-3}$ cm^2/sec at 750^{o}C $a^{I}_{Me} = 1.14$ which is much lower then expected from the observations made by Steele (7.32). An enhancement in the value of $\tilde{D}$ can only be obtained if a^{I}_{Me} is small ie the driving force for Cu nucleation is small. Consideration of the equilibrium represented by equation (7.21) shows that $a^{I}_{Me} = 1.004$ which gives $\tilde{D} = 0.273$ cm^2/sec which is in agreement with Steele's measurement on the chemical diffusivity of Cu in Cu_2S. This explains that the equilibrium (7.20) does not govern the transport of the ionic species and hence during the course of reaction, equilibrium between Cu_2O and CO exists. A similar calculation carried out for experiment no:18 with a pellet of 0.25cm in length and 0.635cm in diameter and based on the assumption that all the weight lost was because of oxygen from Cu_2O a value of $\tilde{D} = 0.0385$ cm^2/sec for $a^{I}_{Me} = 1.004$ at 750^{o}C is obtained. The discrepancy in the value of $\tilde{D}$ is about an order of magnitude which can be attributed to the choice of equilibrium excersised to calculate the chemical diffusivity. The weight loss values used for the calculation of $\dot{n}_{Me}$ may be incorrect because both equilibria (7.20) and (7.21) are involved. The evidence for equilibrium (7.21) can be appreciated from the evidence of whisker growth on the Cu_2O composite. From this comparison it is deduced that the equilibrium (7.20) does not prevail in contradiction to Wagner. It is equilibrium (7.21) which is responsible for the fast ionic transport of Cu in Cu_2S.

A similar experiment was also carried out at 1000°C in CO_2 where excessive oxidation of Cu_2S resulted in the formation of copper. These conditions give an extremely high pressure of SO_2 as calculated by the $CO/_{CO_2}$ ratio in equilibrium with Cu at 1000°C. No defined whisker growth was observed in this situation except one very peculiar feature, see plate (7.6b), where striations were observed on the surface of Cu. Similar morphological changes were observed in the surface area of Cu_2S at 750°C. The facets of Cu formed on the surface of Cu_2S was also observed at 750°C see plate (7.6b).

From the graph relating the length of whiskers and the time, it was seen that the growth of whiskers is governed by two mechanisms. The slight deviation from non-linearity in the early stage of growth shows that the rate is apparently governed by a slow surface diffusion mechanism, when the width of whisker is small. The rate increases with increasing width of whiskers but eventually ceases because of the increasing diffusion path. For this reason, the second stage in the growth process is linear; where parabolic relation holds good, see figs(7.7a & 7.7b).

(iv) Whisker Growth During the Reduction of Sulphides.

Whisker growth observed during the reduction of cuprous sulphide with CO indicates that during the course of reduction an oxysulphide liquid has formed whose composition lies in the (l + Cu) phase field. Most of the whiskers grown from the surface of the pellet were pure copper whiskers which confirms the original composition of the liquid phase. The whiskers were not phenomenally long as observed in the case of composites. The faster rate of

reduction of the oxysulphide liquid with CO results in a permanent cessation of the growth process.

Whisker growth was also observed in the case of reduction of sulphide with graphite at 850°C. An identical explanation can be given for this situation except that the number of whiskers observed was significantly smaller than that at 1000°C. The temperature effect indicates that two factors are important. At 850°C, the volume of oxysulphide liquid formed is very small, hence the kinetics of reduction of oxysulphide liquid is slow because of the small area. Secondly, the growth process suffers because of the lower temperature used. No bi-partite whiskers were observed in this situation which indicates that the composition of liquid never enters the phase field $(L+Cu+Cu_2S)$.

The growth observed during the dual heat-treatment of lime-sulphide mixture pellets was mainly of Cu_2S whiskers due to the type of heat-treatment cycle chosen prior to the reduction of the pellet with CO. During the heat-treatment of the pellet at 1000°C a sulphur rich liquid from the $(L + Cu_2S)$ phase field forms which on cooling precipitates Cu_2S and a very small quantity of Cu. For this reason, EDX analysis on the whiskers shows compositions close to pure Cu_2S. These whiskers, shown in plate 7.7 are not formed during the course of reduction. Morphologically they are not similar to whiskers but appear more like irregularly grown crystals from the liquid phase.

(v) The Growth of Faceted Surface and Other Morphologies on the Surface of Cu_2S and Cu:

Depending upon the conditions faceted surface, striations, and surface ripples were observed during the heat-treatment of composite pellets. These topographical changes are shown in plates 7.5 to 7.7 and in plate 7.9. These topographical changes were observed on those areas of the Cu_2S surface where no whisker growth had taken place.From the microscopic

analysis, it appears that the majority of these changes have occured from the liquid phase because in the scanning electron micrographs, there is evidence of a crystal ruptured by a layer of material which appears to have been liquid see plate 7.5. It is rather difficult to comment on the geometrical relationship or the compositions of these facets on the basis of the anisotropy of surface energy of crystallographic planes, but the presence of the liquid on the surface of Cu_2S may explain the diversity of the composition of the crystals and their geometry. This means that bi-partite crystals grow from the surface which is only possible if the liquid composition is in the univariant phase field ie either ($L+Cu_2S$) or ($L+Cu$). Although it is well known that faceting of fcc metals and alloys takes place during heat-treatment under a controlled atmosphere, This kind of faceting developes only one kind of change in the geometry of crystals, whereas in the present situation several geometries have been observed which is rather complex. It seems possible that a gaseous atmosphere containing two surface active elements such as oxygen and sulphur a combination of surface plane anistropy might be demonstrated resulting in many possible geometries. In the case of the heat-treatment of Cu_2S-Cu_2O composites at 750^{o}C in CO_2 atmospheres faceting of copper was observed which was identical to Sundquist's (7.1) observations on fcc metals and alloys, see plate 7.6b. These observations suggest that under oxidising atmospheres faceting of copper takes place and the preferrable planes are (111) and (100), as observed by Sundquist. The ripples and striations on the surface of both Cu and Cu_2S indicate that both crystals also undergo some form of thermal etching in controlled atmospheres. Steps were also observed on the crystal planes and on the rippled surface, but little is known about this.

Although it can be said that these topographical changes are due to anistropy of surface energy and the equilibration of crystallographic planes with the surrounding gas, this needs much more extensive investigation such that the anistropy of surface energy can seperately be investigated under different atmospheric conditions.

****

Chapter 7.

7.1 G.W. Sears - Acta Met vol. 3 1955 pp 361.

7.2 J.W. Cahn - Acta Met vol. 5 1957 pp 169

7.3 J.B. Newkirk and G.W. Sears - Acta Met vol. 3 1955 pp 110

7.4 S.S. Brenner and G.W.Sears - Acta Met vol. 4 1956

7.5 S.S. Brenner - Acta Met vol. 4 1956 pp 62

7.6 Coleman and Sears - Acta Met vol. 5 1957 pp 131

7.7 C. Wagner - The Chipman Conference 1962. MIT Press.

7.8 F.C. Frank - Cross Reference from Oscar Dam. Ph.D Thesis, Imperial College Uni. of London 1982.

7.9 Burton and Cabrera - Cross Reference from Oscar Dam. Ph.D Thesis, Imperial College, Uni. of London, 1982.

7.10 Burton, Cabrera and Frank - Phil. Trans. Roy. Soc. London. Ser.A 1951, vol 243 pp 299-358.

7.11 F.C. Frank - Discussions on Far. Soc. 1949 vol. 5 pp 49-54

7.12 G.W. Sears - Acta Met 1953 vol. 1 pp 57-59
Acta Met. 1955, vol. 3. pp 361-69.

7.13 P.B. Price et al - Acta Met vol. 6 1958 pp 524-31

7.14 R.S. Wagner and W.C. Ellis - TMS AIME vol 233 1965, pp 1053

7.15 G.S. Barker - Cross Ref. Oscar Dam. Ph.D Thesis Imperial College, University of London 1982.

7.16 S.E. Knooce and S.A. Arnold - J.C App. Phy 25 (134) 1954.

7.17 R.M. Fisher et al - Acta Met 2 368 1954.

7.18 Wenzel - Cross Ref. Ph.D Thesis. Oscar Dam Imperial College, University of London 1982.

7.19 V. Finnstrom - Electron Microscopy 1974 vol. 1

7.20 V. Finnstrom - Scan JI of Met. vol. 5 134 1976.

7.21 P.G. Shewmon - Diffusion in Solids. McGraw Hill Publication.

7.22 W.K. Lu - Scan Jl. of Met vol. 2 pp 273, 1973.

7.23 R.E. Cech and T.D. Tiemann - TMS AIME vol. 245 1969, pp 1727

7.24 J.D. Ford and F.A Fahim - Met Trans. 6B 1975 pp 461.

7.25 F. Habashi and R. Dugdale - Met Trans 4B 1973 pp 1865.

7.26 P.M. Prasad and T.R. Mankhand - Trans. Ind. Inst. Met. Vol 32 No. 3 1979, pp 253-85.

7.27 C. Wagner - 'Whiskers' M and B Monograph, London 1972.

7.28 Collins and P.G. Shewmon - Trans AIME 236 (1966) 1354.

7.29 N.A. Gjostein - Surface and Interface. Ed-Burke, Reed and Weiss 1967 pp 271.

7.30 J.W. Martin and R.D. Doherty - Stability of Microstructures Cambridge, Solid State Sci, Series, 1976.

7.31 B.E. Sundquist - Acta Met vol. 12 1964.

7.32 B.C.H. Steele - The Physical Chemistry of Process Metallurgy. The Richardson Conf. IMM 1973.

7.33 N.A. Gjostein - Physico Chemical Measurements in Metal Research. Vol IV Part 2 pp 415 Ed R.Rapp

7.34 Collins and P.G. Shewmon - idid pp 415.

7.35 C. Wagner - Trans AIME.JI of Metals 1952. pp 214.

Chapter 8

Reduction of Nickel Sulphides.

Results and Discussions.

The overall carbothermic reduction reaction in the presence of lime can be written as:-

$$NiS_{(s)} + CaO_{(s)} + C_{(s)} = Ni_{(s)} + CaS_{(s)} + CO_{(g)} \qquad (8.1)$$

$$\Delta G^{o}_{T} = 30\ 050 - 38.44T$$

All the observations using X-ray diffraction analysis are summarized in Table 8.1. The rate of reduction curves were drawn on the basis, of the mass balance carried out using reaction (8.1). From the rate of reduction curves at 800^{o}C to 950^{o}C, it is evident that the extent of reaction is increasing with increasing temperature see fig (8.1). From these rate curves it is evident that several temporary arrests appear and then the reaction recommences. On an average, the initial arrests vary from approximately 1.0 to 2.5 hours duration. It is also worth noting that the rate of reaction is almost identical after each arrest. Although the reaction seems to be incomplete at these temperatures from X-ray diffraction evidence it appears that there is no evidence of the existence of nickel oxide during the course of reaction. This observation is surprising as nickel oxide ought to have formed as a result of the exchange reaction. Identical observations were made with coal where a small amount of graphite was added to assist the production of a pellet on compressing the mixture into a die. The amount of graphite added also compensated for the volatilisation loss from coal (13%). The rate data

collected from the coal reduction shows a similar trend to that observed in the case of graphite.

A greater extent and a faster rate of reaction was observed in the case of coal becasue of its greater reactivity than graphite, see fig (8.2). Once again, the reduction was found to be incomplete with no evidence of any nickel oxide confirmed by X-ray diffraction analysis. One of the most important features of coal reduction is that the rate at any temperature, is faster than that with graphite and the reaction proceeds with a fewer number of temporary arrests.

In order to understand the significance of the arrests during which no weight change was observed on the rate curve a series of experiments were designed. These experiments were carried out with the intention of observing the existence of nickel oxide during the reduction process. The information obtained from these reduction experiments shows that either the nickel oxide (NiO which is the most prevalent) does not exist or it is very unstable due to rapid reduction with carbon or carbon monoxide. From the available literature and from the Ni-S Ellingham diagram it is evident that at higher temperatures nickel sulphide (NiS) decomposes to Ni_3S_2 which melts at about 800^{o}C. In addition there exists a eutectic between Ni and Ni_3S_2 at 637^{o}C.

A few mixtures of NiS and NiO, NiS and CaO, and NiO and CaS were prepared and heat-treated in a flowing stream of argon at 950^{o}C. From the heat-treatment of NiS-NiO mixtures, it is evident that NiO is present at the end of the reaction.

This presence would not be possible if a reaction of the type

$$NiS(s) + 2NiO(s) = 3Ni(s) + SO_2(g) \qquad (8.2)$$

goes to completion.

In the mixtures, it is evident that nickel oxide and nickel sulphide do not react completely. It is also possible that once the liquid sulphide forms in the system, the mechanism of reaction changes. It seems reasonable that nickel oxide might be soluble in the nickel matte and precipitates during cooling. From these mixtures, a maximum amount of 0.5 moles of SO_2 is expected to be generated to give a maximum of 1.5 moles of nickel (see table 1). The existence of pure solid nickel oxide in view of reaction (8.2) and in the presence of the Ni_3S_2 liquid is doubtful. It is evident from the observation that after completion of reaction (8.2) NiO is observed and this is only when there is a solubility of NiO in the matte. The solubility of NiO or 'O' in the matte is governed by the equilibrium given in reaction (8.2) and hence there would be a critical limit of 'O' solubility at and over which SO_2 evolution would be observed but under this value SO_2 evolution would cease. Any oxygen dissolved in the matte would precipitate as NiO during cooling.

The heat-treatments of the reciprocal systems NiO-CaS, and NiS-CaO show that during the process of heat-treatment, nickel is produced. The formation of nickel from these mixtures is evidence in favour of the extent of the exchange reaction during the carbothermic reduction and during the heat-treatment in the absence of any reducing agent. The formation of nickel is related to reactions (8.2) and (8.B3) see Ap. This shows that NiO must have been an intermediary in the process of nickel formation and as soon as it forms, it is consumed by the sulphide. In the other reciprocal system NiO-CaS, it is evident that nickel

has formed as a result of exchange reaction and there is an insignificantly small quantity of the oxide left in proportion to the amount of Ni_3S_2 (as NiS is unstable at high temperatures). The precipitation of NiO has taken place from Ni_3S_2 matte saturated with oxide. It can be explained on the basis of the CaO-CaS-NiS ternary section shown in fig (8.3). From this ternary, it is evident that at 950^{o}C the liquid is in equilibirum with lime saturated with NiS. Since this liquid always lies on the side CaO-A-NiS side, as no CaS is present in the system, it poses a higher activity of NiO in the matte and hence during the cooling of the liquid, NiO precipitation takes place.

The other very significant crystallographic information obtained from the heat-treatment and from the reduction experiments is the relative variation in the'd' spacing of the lime reflexions. From X-ray diffraction analysis it appears after the heat-treatment of NiS-CaO mixture, the lime lattice has become larger which is only possible if a large ion has substituted for smaller ion in the lattice of CaO (a = 4.797^{o}A). The extent of variation of the (311) reflexion as shown in Table 8.2, indicates that there is a dialation in the lattice parameter which is not expected with the replacement of Ca^{+2} ions by Ni^{+2} ions because of the Ca^{+2} ion has a larger ionic radius (0.99^{o}A) than Ni^{+2} (0.69^{o}A). On the other hand, S^{-2} ion has a larger ionic radius than the O^{-2} ion and would result in the dialation of the lattice if NiS is dissolved. From the crystallographic data, it appears that in CaO lattice Ni^{+2} is partially tied up with O^{-2} ion (1.32^{o}A) and partially with S^{-2} ion (1.84^{o}A) as NiS sulphide. Thus the change in the lattice parameter of lime is attributed to the fact that there is a higher S^{-2}/Ni^{+2} ion ratio in the CaO lattice. Thus, it is the $r_{S^{-2}}/r_{O}-2$ ratio which has the greater influence on the change in the lattice parameter rather than the $r_{Ni^{+2}}/r_{Ca^{+2}}$ ratio. The variation

in the 'd' spacing determines the extent of the Ni-S substitution in the CaO lattice and it may indicate the extent of the exchange reaction ocurred. From crystallographic data on the relative variations in the d spacing (hkl) plances of lime, it is probable that the substitution is purely of the type Ni-S not Ni_3S_2 which would create an ionic vacancies in the lattice which would not necessarily conform to a cubic unit cell. In that situation the lattice would be more complex because of vacancy ordering and balance of the cohesive force in the unit cell which would probably distort a cubic unit cell, giving rise to a less symmetric structure.

From the average variations in 'd' spacing of the (311) reflections it has been possible to determine the variation in lattice parameter of CaO with temperature due to Ni-S substitution. The following lattice parameters have been computed at 800^oC d = 4.810A, at 900^oC d = 4.823A and at 950^oC d = 4.821A. What perhaps appears to be an unusual variation with temperature is entirely explainable in terms of eutectic temperature being close to 850^oC. From the heat treatment of reciprocal mixtures (NiS-CaO, NiO-CaS) it is apparent that the plateaux appear on the pct. weight loss versus time curve (see fig 9.4) which is an indication that there is a temporary cessation of SO_2 evolution which is related to nickel deposition. This reflects that the nickel deposition is possible only at any limited P_{SO_2} because the driving force for the nucleation of nickel is related with the factor $\Delta G^o_{Ni} = -RT\ln P''_{SO_2}$. The rate curve for SO_2 evolution in the reciprocal system shows that the rate gradually decreases with time after each plateau which means there is a gradual drop in the oxygen potential of the nickel matte. A similar explanation can be related to the appearance of plateaux in the case of heat-treatment of the NiO: NiS = 1:3 mixture. It can be concluded on the basis of the rate data and from X.R.D. analysis that at the plateau, a steady

state situation for O^{-2} transport is established when the oxygen potential drops in the matte phase. Once the oxygen potential crosses a critical limit, SO_2 or CO evolution recommences.

The respective addition of lime and graphite in the heat-treated mixture of NiS-NiO shows that NiO is unstable in the presence of carbon as confirmed by X.R.D. analysis. In the case of NiS : NiO = 2:1 it is apparent that NiO is present even after the CaO addition. It is evident from the percentage weight loss vs. time curve (fig 8.4) that sufficient time was probably not given for NiO-Ni_3S_2 equilibrium. From the reduction experiments, the slow rate of reduction in the presence of graphite and its relation with the length of the plateau can be appreciated. In this case, a considerable proportion of weight loss is from SO_2 due to Ni_3S_2 and NiO reaction, which would not happen if an active reducing agent like coal is used. Also the farther the extent of the reaction, the longer is the length of the plateau. Therefore, less time is allowed for NiO to react with Ni_3S_2, the lower is the probability of encountering a plateau. In view of this hypothesis, the experiments were conducted with an increased lime to sulphide ratio which would allow an increased surface area for the exchange reaction. As expected a higher extent of reaction was obtained with coal and graphite at 950^{o}C see fig (8.5). Also the rates were faster than those with 1:1 sulphide to lime ratio. Plateaux were once again observed at the same time and at the same extent of reduction, but because of the higher reactivity of coal, the reaction proceeded more quickly. This also means that there is a possibility of generating SO_2 from the sulphide - oxide reaction and the extent of reaction is greater to achieve a steady state

for oxygen build up in the liquid matte. It is also apparent from the nickel-sulphur phase diagram that a liquid phase exists in which metallic nickel can dissolve. The dissolution of metallic nickel in the matte phase would occur until the solubility reaches the phase boundary of the liquid and Ni phase field at which time Ni precipitation would take place. Both these factors appear to affect the length of the plateau in the later stages of reaction. The precipitation of metallic nickel within the Ni_3S_2 phase has been confirmed from JSM 35 scanning microscopy where elemental mapping was carried out, see plates (8.1) and (8.2).

To avoid the problem of the appearance of a plateau, mixtures with increased lime to sulphide, and coal to sulphide ratio were prepared and heated at 950°C. A complete conversion of nickel sulphide to nickel was observed, see fig (8.6) and it was subsequently confirmed by X-ray diffraction analysis. In the case of nickel sulphide reduction at 950°C with CO (NiS : CaO = 1:2) a weight loss higher than theoretical was observed which can be attributed to SO_2 evolution. The initial rate of reduction in the case of CO is slightly faster than coal reduction and in the later stages both coal and CO take almost the same time to undergo completion. From metallographic observations, it was confirmed that increasing the amount of coal, leads to deposition of metal on the coal surface; providing the hypothesis that the existence of a steady state condition related to oxygen is necessary.

From this investigation it is also evident that there is no solid layer of CaS formed around the lime particles, otherwise reaction would have stopped immediately after the initial stage and further reaction would have been only obtained by steady state solid diffusion of S^{-2} and O^{-2}

ions across the product layer. During the course of heat treatment experiments it was discovered that in the matte phase there exists a solubility of CaS and this liquid is probably saturated with CaS. This would always allow the exchange reaction and reduction to continue.

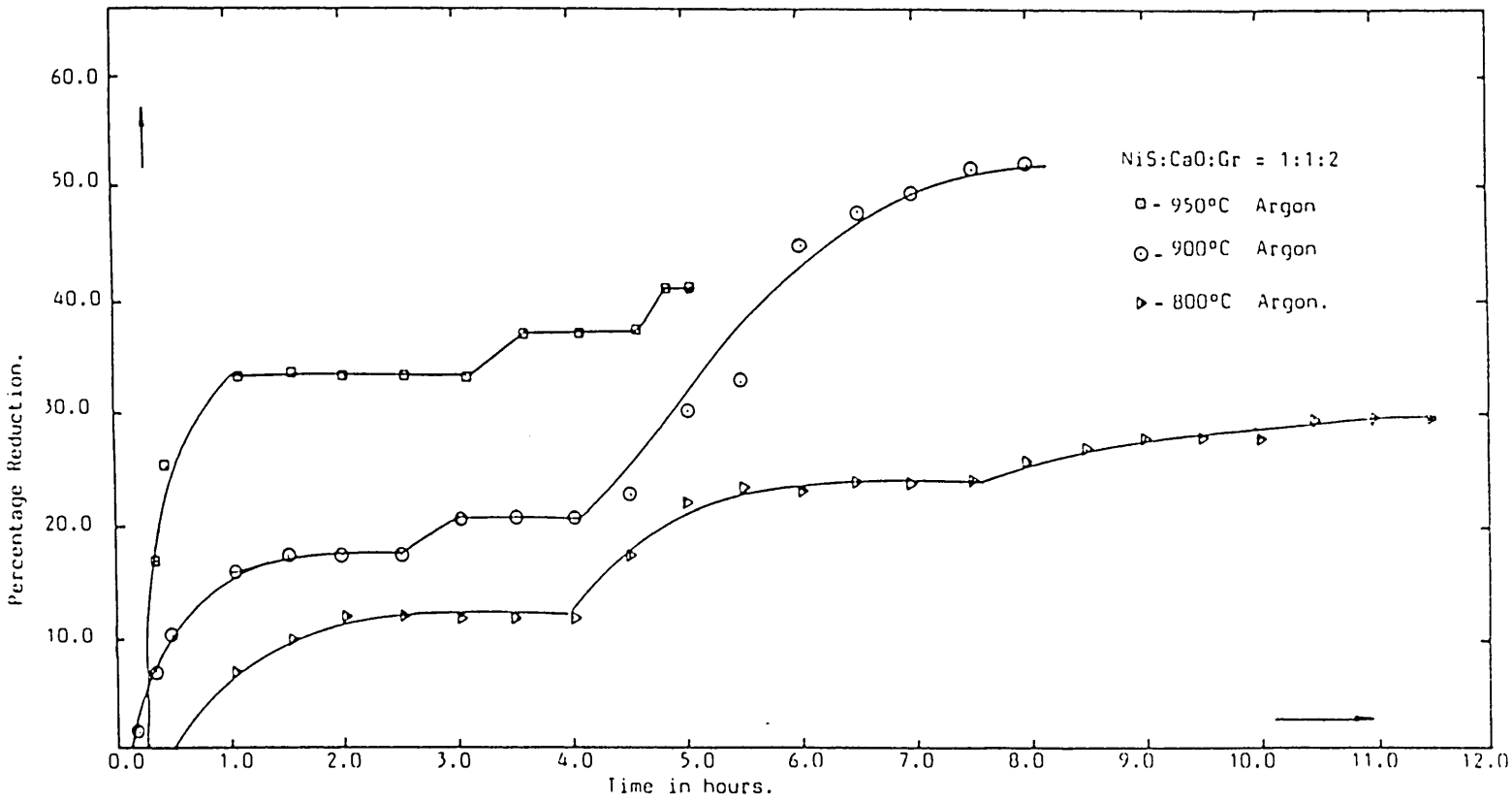


Fig 8.1 Rate of reduction of NiS with graphite in presence of lime.

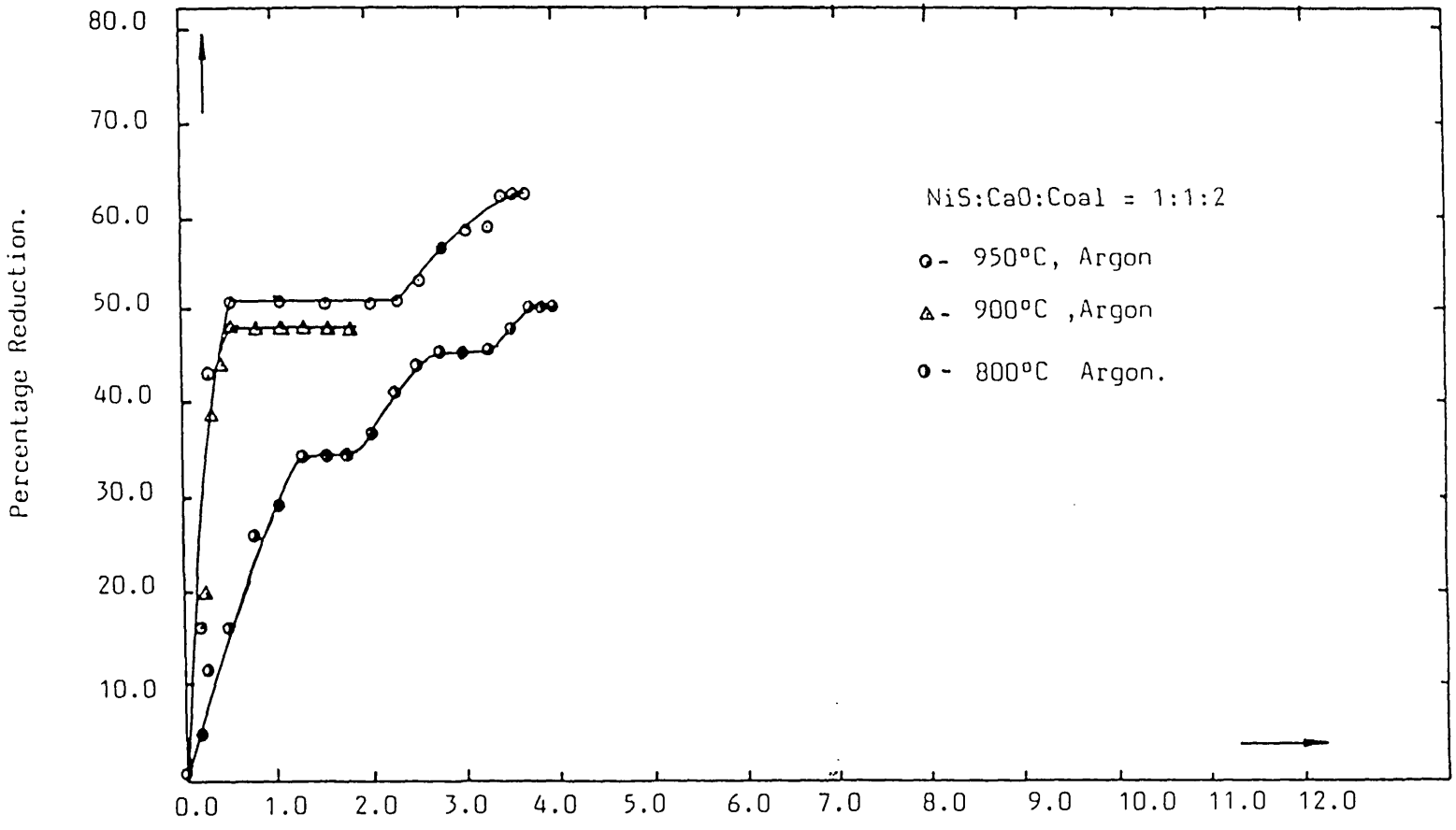


Fig (8.2) Rate of reduction of NiS with coal in presence of lime.

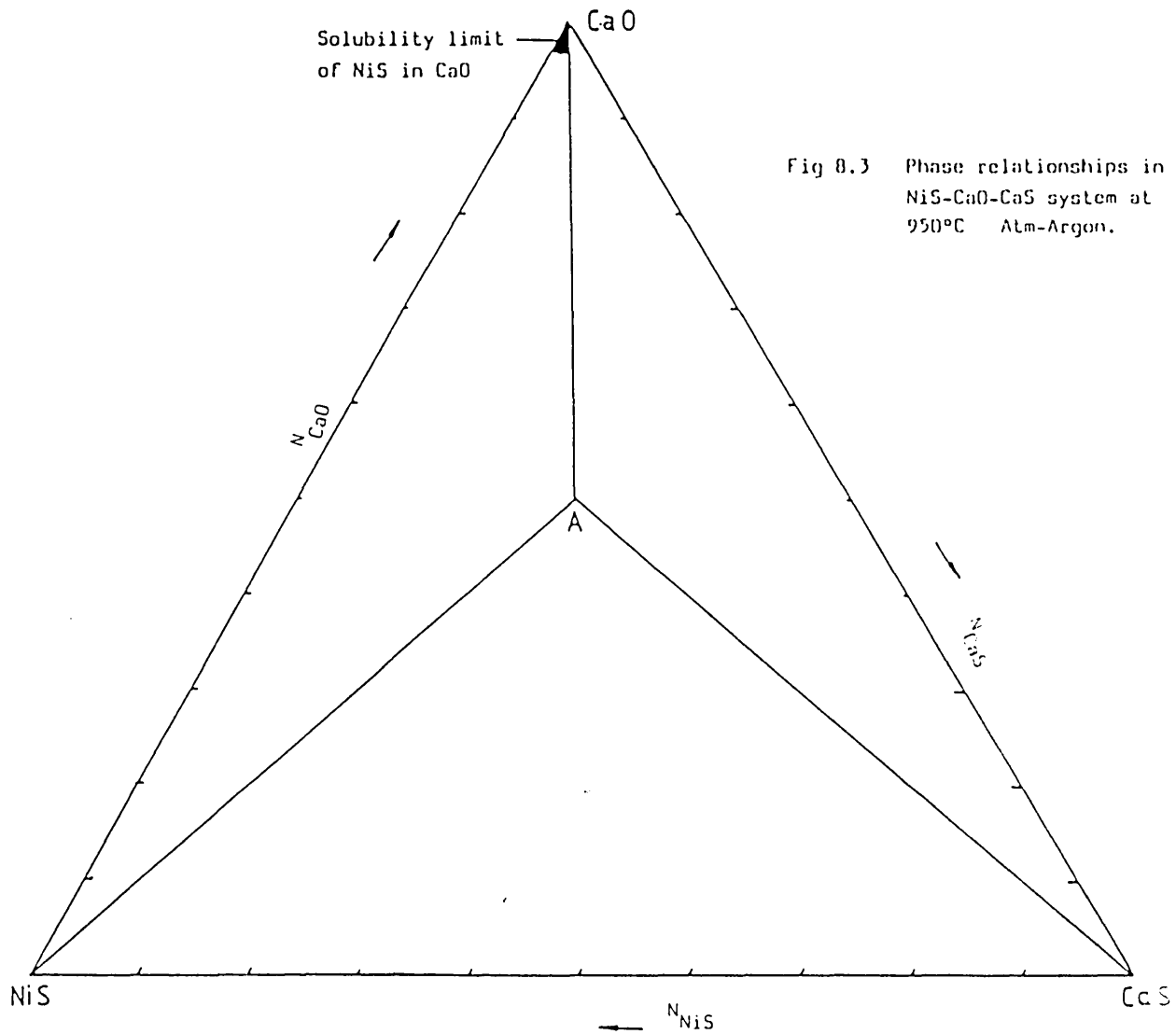


Fig 8.3 Phase relationships in NiS-CaO-CaS system at 950°C Atm-Argon.

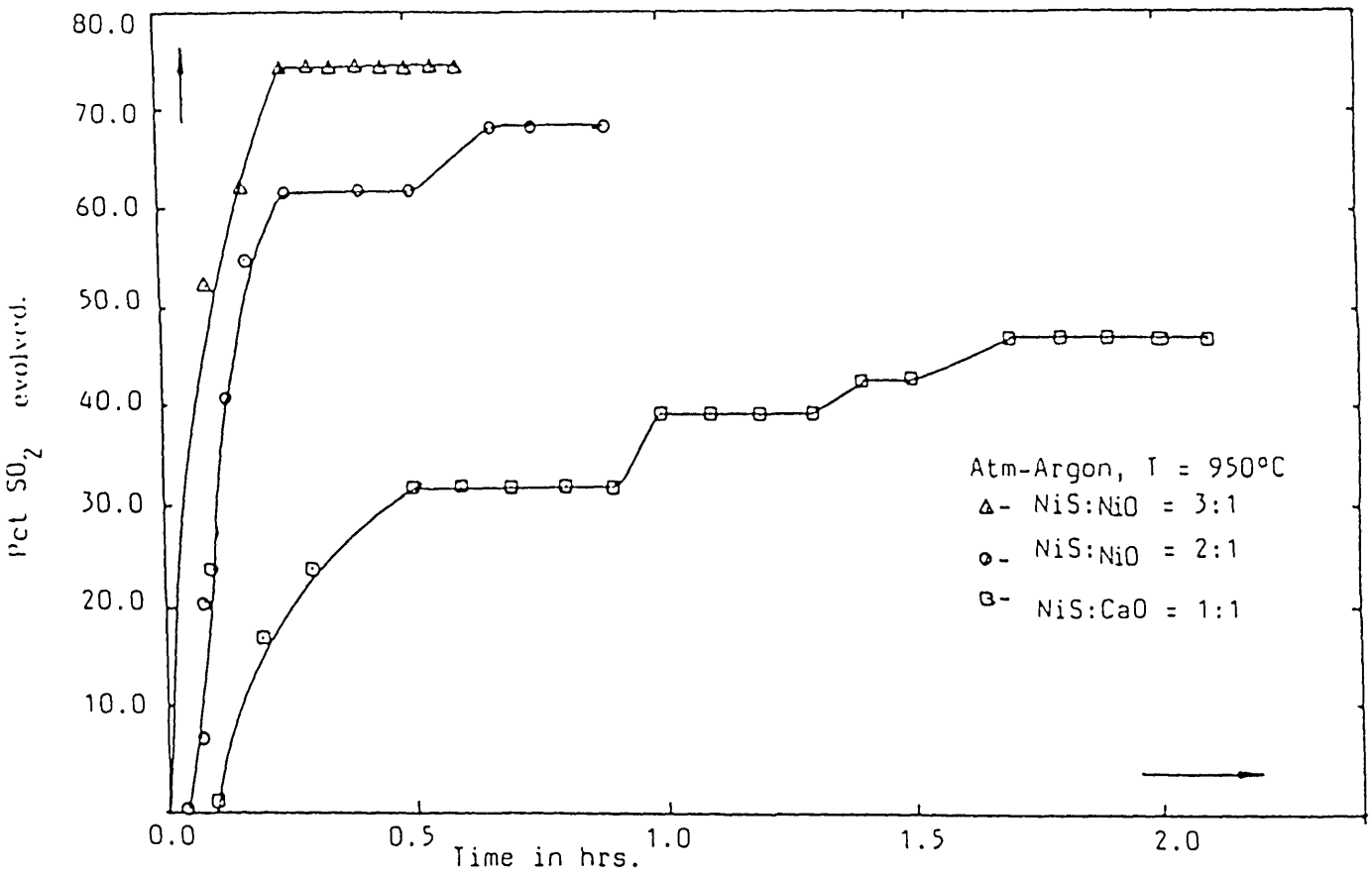


Fig 8.4 Rate of SO_2 evolution during the heat-treatment of NiS in presence of CaO and NiO

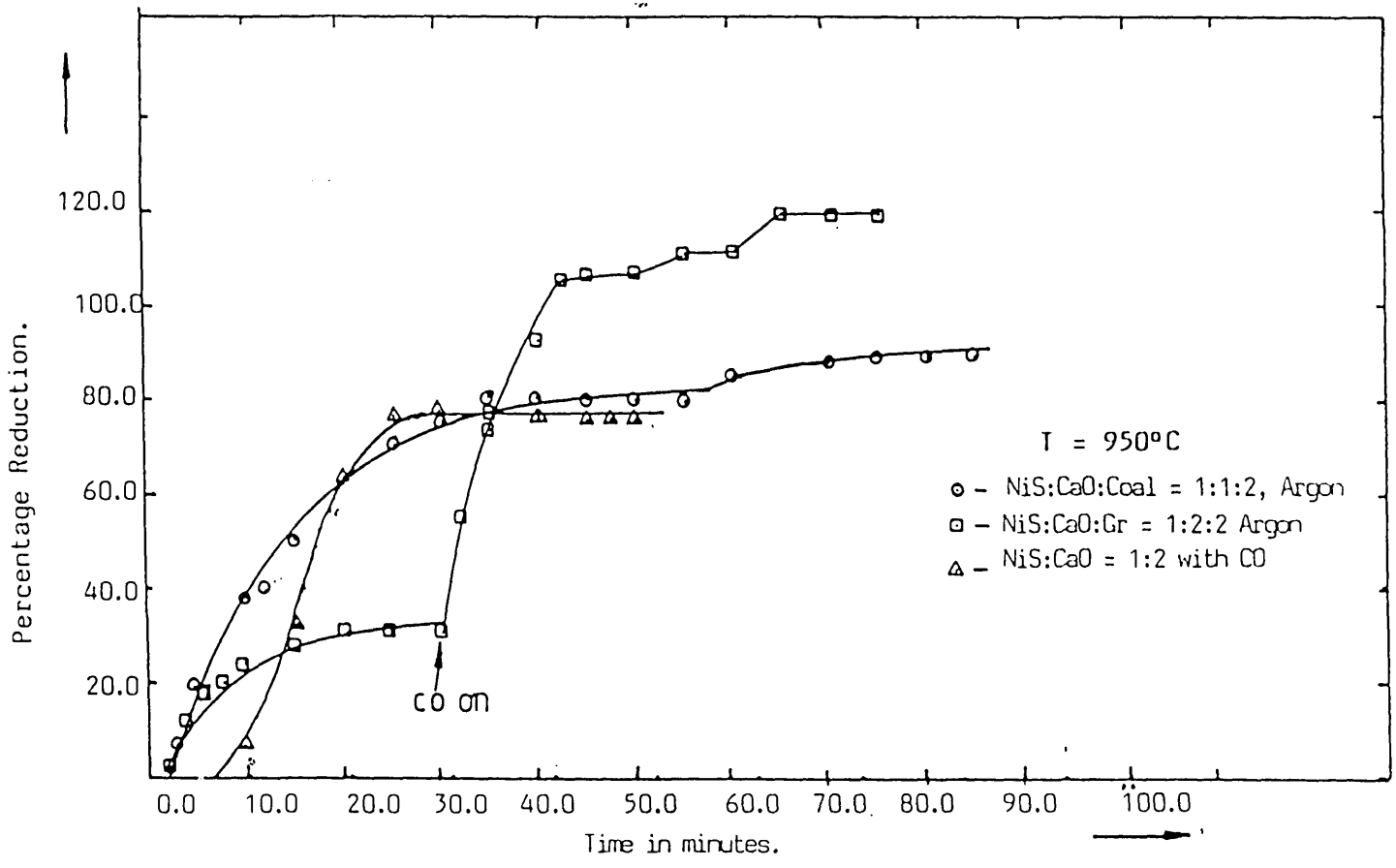


Fig 8.5 Effect of increased lime to NiS ratio on the rate of carbothermic reduction of nickel sulphide at 950°C.

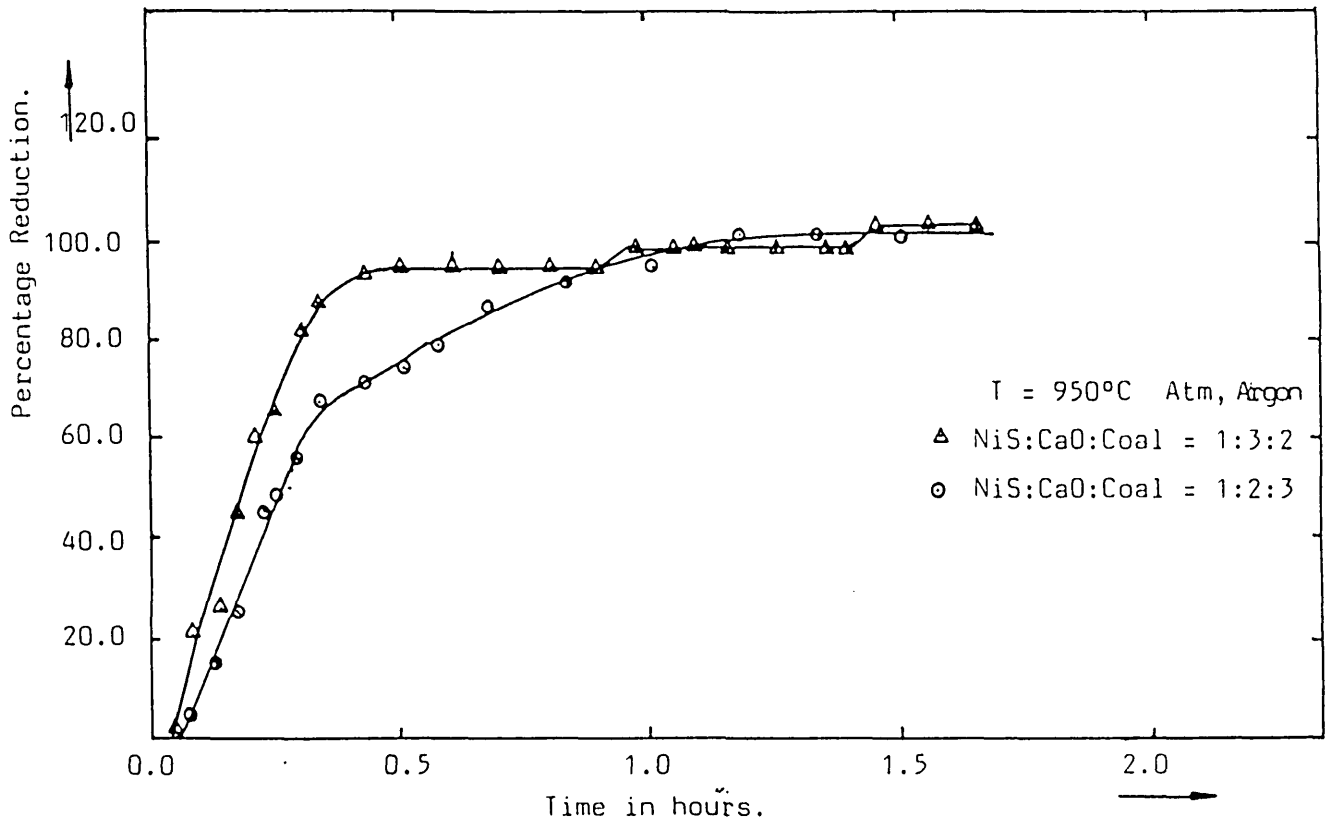
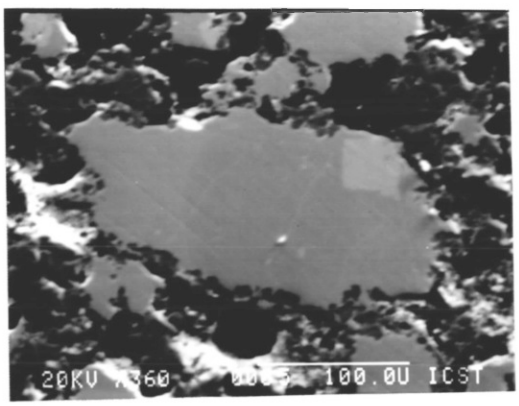
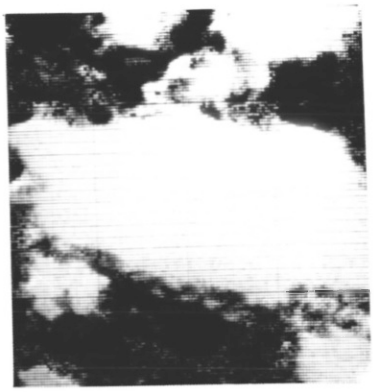


Fig 8.6 Effect of increased coal to NiS and lime to NiS ratio on the rate of reduction of nuckel sulphide at 950°C.

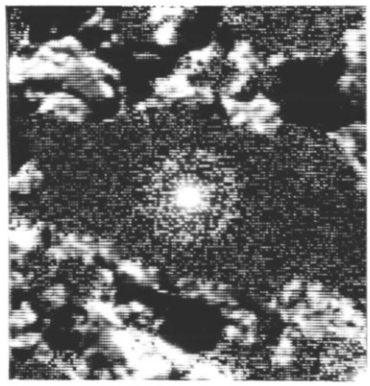
PLATE 8.1



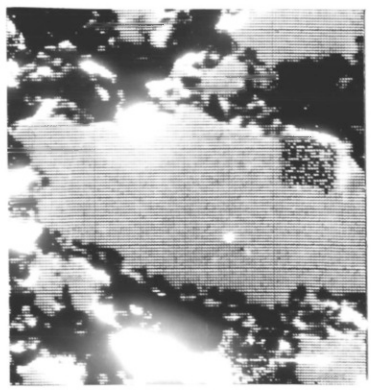
a



b



c



d

Plate 8.1: Energy Dispersive X-ray Analysis of NiS:CaO =1:1 pellet reduced with graphite at 950°C.
a) sample area
b) nickel map
c) calcium map
d) sulphur map.

PLATE 8·2

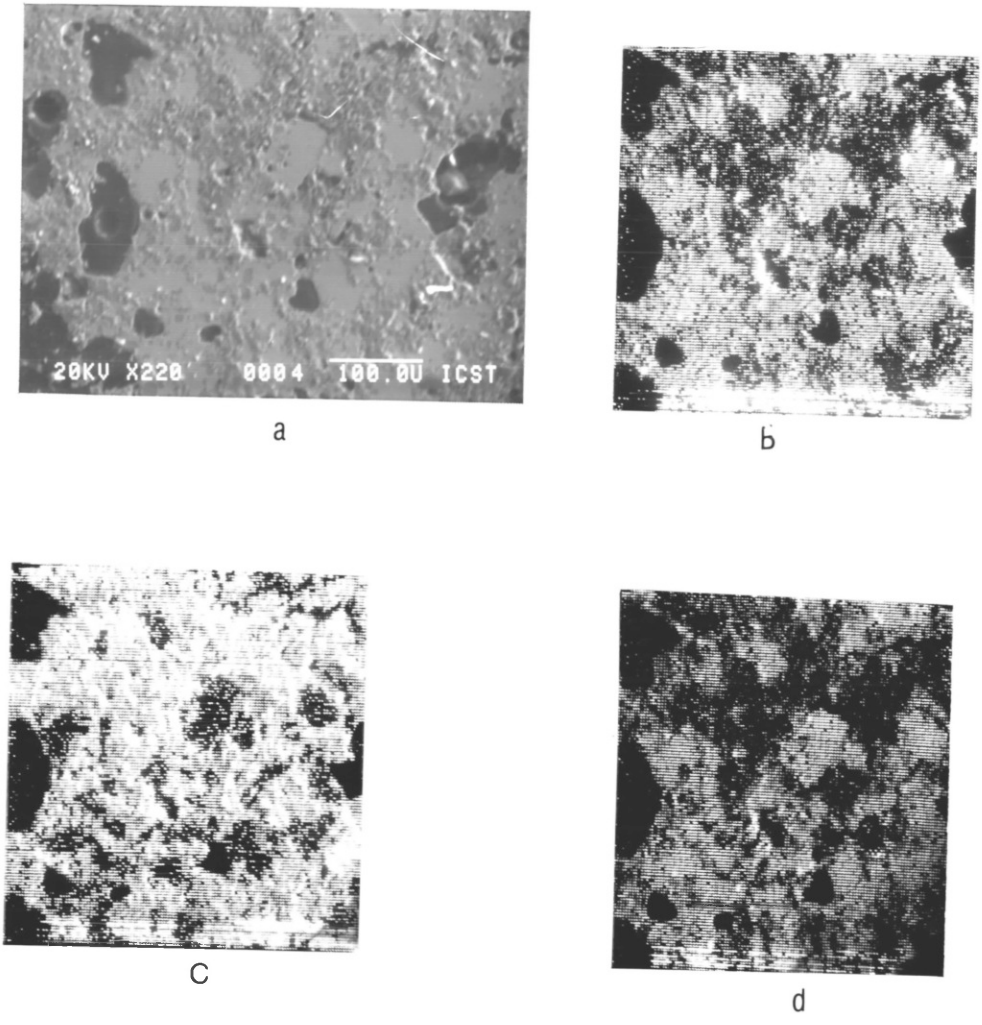


Plate 8.2: Energy Dispersive X-ray Analysis of NiS:CaO =1:1 pellet reduced with coal at 950^{o}C.

a)sample area
b)nickel map
c)calcium map
d)sulphur map.

Summary of the mass balance and X-ray diffraction analysis of the carbothermic reduction of nickel sulphide.

Table 8.1 Summary of Results.

Mixture Composition	T°C	Mass balance % wt loss	% reduction	Atomos.	X.R.D. Analysis Ni_3S_2	CaO	CaS	Ni	Gr	NiO	RUN
NiS:CaO:C = 1:1:2	950	8.58	52.4	Argon	S	M	S	S	W	-	1
NiS:CaO:C = 1:1:2	900	6.41	39.2	Argon	S	S	S	MS	MW	-	2
NiS:CaO:C = 1:1:2	900	6.85	41.84	Argon	S	M	VS	MS	MW	-	2r
NiS:CaO:C = 1:1:2	800	4.75	29.02	Argon	MS	VS	MS	S	MW	-	3
NiS:CaO:C (Coal + Gr) 1:1:2	950	10.19	62.24	Argon	S	M	VS	S	W	-	4
NiS:CaO:C (Coal + Gr) 1:1:2	900	7.87	48.08	Argon	S	MS	VS	S	VW	-	5
NiS:CaO:C (Coal + Gr) = 1:1:2	800	8.25	50.40	Argon	VS	S	VS	MS	VW	-	6

Table 8.1 Contd..

Mixture Composition	T°C	Mass Balance % wt loss	% reduction	Atmos.	X.R.D. Analysis Ni_3S_2	CaO	CaS	Ni	Gr	NiO	RUN.
NiS:NiO = 3:1	950	9.5	68.7	Argon	VS	-	-	S	-	Weak	7
NiS:NiO = 2:1	950	10.88	74.67	Argon	VS	-	-	S	-	Weak	8
NiS:NiO = 3:1 + CaO	950	8.72	26.44	Argon	VS	VS	-	S	-	-	7b
NiS:NiO = 2:1 + CaO	950	9.41	41.98	Argon	S	VS	-	S	-	-	8b
NiS:NiO 3:1 + CaO + Gr	950	8.41	160.8	Argon	M	MS	S	VS	W	-	7c*
NiS:NiO = 2:1 + CaO + Gr	950	9.03	171.6	Argon	MW	M	S	VS	W	-	8c*

Table 8.1 Contd..

Mixture Composition	T°C	Mass Balance %wt loss	% reduction	Atmos.	X.R.D. Analysis. Ni_3S_2	CaO	CaS	Ni	Gr	NiO	RUN.
NiS:CaO = 1:1	950	4.24	43.8	Argon	VS	VS	MW	M	-	-	9
NaS:CaO:C (Coal + Gr) = 1:1:2	950	5.08	31.63	Argon	VS	S	MS	MS	W	-	10
NiS:CaO:Gr = 1:2:2	950	9.13	73.93	Argon	M	VS	S	S	VVW	-	11
NiO:CaS = 1:1	950	11.04	114 .0	Argon	S	VS	S	M	-	VVW	12*
NiS:CaO = 1:1	950	4.64	47.93	Argon	S	VS	M	M	-	-	13
NiS:CaO 1:2	950	8.29	105.2	CO	VVW	S	VS	MS	-	-	14
NiS:CaO (Coal + Gr) = 1:2:2	950	10.9	89.7	Argon	W	S	VS	S	VW	-	15

Table 8.1 Contd.

Mixture Composition	T°C	Mass Balance %wt loss	Mass Balance % reduction	Atmos.	X.R.D. Analysis Ni_3S_2	CaO	CaS	Ni	Gr	NiO	RUN.
NiS:CaO:C (Coal + Gr)	950	12.48	108.9	Argon	W	S	VS	VS	VW	-	16
NiS:CaO = 1:2	950	9.36	118.63	CO	VW	S	VS	MS	-	-	18*
NiS:CaO:C (Coal + Gr) = 1:2:3	950	12.11	105.6	Argon	-	S	VS	VS	-	-	19
NiS:CaO:C (Coal + Gr) 1:3:2	950	10.11	103.5	Argon	-	VS	MS	-	-	-	20

* Drainage of liquid during reduction of heat treatment.

x Weight lost before CO was switched on.

Table 8.2 - Shift in 'd' spacings of the Lime Lines

Run	Mixture Composition	$T^{o}C$	Mass Balance %wt loss	%red uction	Atmos $P_{O_2} = 10^{30}$ atm	$\Delta d^{o}A$ (311)
-	CaO	-	-	-	-	
1	NiS:CaO:C = 1:1:2	950	8.58	52.4	Argon	0.0
2	NiS:CaO:C = 1:1:2	900	6.41	39.2	Argon	-0.9
2rpt	NiS:CaO:C = 1:1:2	900	6.85	41.84	Argon	-0.9
3	NiS:CaO:C = 1:1:2	800	4.75	29.02	Argon	0.0
4	NiS:CaO:C (Coal + Gr) = 1:1:2	950	10.19	62.24	Argon	-0.90
5	NiS:CaO:C (Coal + Gr) = 1:1:2	900	7.87	48.08	Argon	-0.90

Table 8.2 Contd..

Run	Mixture Composition	T°C	Mass Balance %wt loss	%red uction	Atmos. $P_{O_2} = 10^{30}$ atm.	$\Delta d^{o}A$ (311)
6	NiS:CaO:C = 1:1:2	800	8.25	50.40	Argon	-0.40
7	NiS:NiO = 3.1	950	9.5	68.7	Argon	-
8	NiS:NiO = 2:1	950	10.88	74.67	Argon	-
7b	NiS:NiO = 3:1 + CaO	950	9.72	26.44	Argon	-0.90
8b	NiS:NiO = 2:1 + CaO	950	9.41	41.98	Argon	-0.70
7c	NiS:NiO = 3:1 + CaO + Gr	950	8.41	160.8	Argon	-0.70
8c	NiS:NiO = 2:1 + CaO + Gr	950	9.03	171.6	Argon	-0.80
9	NiS:CaO = 1:1	950	4.24	43.8	Argon	-0.80

Table 8.2 Contd..

Run	Mixture Composition	T°C	Mass Balance %wt loss	%red uction	Atmos. $P_{O_2} = 10^{30}$ atm	$\Delta d^{o}A$ (311)
10	NiS:CaO:C (Coal + Gr) = 1:1:2	950	5.08	31.63	Argon	-0.70
11	NiS:CaO:C (Coal + Gr) = 1:2:2	950	9.13	73.93	Argon	-0.8
12	NiO:CaS = 1:1	950	11.04	114.0	Argon	-0.8
13	NiS:CaO = 1:1	950	4.64	47.93	Argon	-0.8
14	NiS:CaO = 1:2	950	8.30	105.2	CO	-0.9
15	NiS:CaO:C (Coal + Gr) = 1:2:2	950	10.9	89.7	Argon	-0.80
16	NiS:CaO = 1:2	950	9.36	118.63	CO	-0.70

Table 8.2 Contd.

Run	Mixture Composition	T°C	Mass Balance %wt loss	%red uction	Atmos P_{O_2} = 10^{30} atm.	$\Delta d^{o}A$ (311)
18	NiS:CaO = 1:2	950	9.36	118.63	CO	-0.70
19	NiS:CaO:C (Coal + Gr) = 1:2:3	950	12.11	105.6	Argon	-0.80
20	NiO:CaO:C (Coal + Gr) = 1:3:2	950		103.5	Argon	-0.80

* There is a slight discrepancy introduced in the measurement of (222) plane because of the following reasons:-

a) Its intensity is very low

b) It appears in the end where films slightly bends during exposure

c) Parallax effect

Table 3.

$T/^{o}C$	$T/^{o}K$	ΔG^{o}_{a}/cal	ΔG^{o}_{b}/cal	ΔG^{o}_{c}/cal	$K_a = \frac{pCO}{atm}$	$Kb = \frac{PCO_2}{pCO}$	$K_c = pH_2O/pH_2$
500	773	-2648	-11214	-8528	5.614	1.488×10^{3}	2.586×10^{2}
600	873	-7098	-11494	-9573	6.001×10^{3}	7.575×10^{2}	2.500×10^{2}
700	973	-11548	11774	-10618	3.941×10^{2}	4.430×10^{2}	2.435×10^{2}
800	1073	-15998	12054	-11663	1.822×10^{3}	2.863×10^{2}	2.382×10^{2}
900	1173	-20448	-12334	-12708	6.491×10^{3}	1.993×10^{2}	$2.340\text{ł}0^{2}$
1000	1273	-24898	-12614	-13753	1.894×10^{4}	1.469×10^{2}	2.305×10^{2}
1100	1373	-29348	-12894	-14798	4.727×10^{4}	1.132×10^{2}	2.275×10^{2}

Appendix 8A Efficiency of reducing agents according to thermodynamics.

Hydrogen gas, coal or graphite and carbon monoxide can all be used as a reducing agent to reduce NiO. Hydgrogen and carbon monoxide are more efficient than solid carbon at low temperatures as indicated by the higher values of their equilibrium constant in the table below. At about $700^{o}C$ carbon is more efficient. Carbon has an additional advantage of producing a reducing agent, CO which accelerates the completion of the reduction.

The reduction of NiO with the above reducing agents can be expressed as follows:-

$$NiO_{(s)} + C_{(s)} = Ni_{(s)} + CO_{(g)} \quad 31\,750 - 44.5T \qquad (a)$$

$$NiO_{(s)} + CO_{(g)} = Ni_{(s)} + CO_{2(g)} \quad - 9050 \quad -2.8T \qquad (b)$$

$$NiO_{(s)} + H_{2(g)} = Ni_{(s)} + H_2O_{(g)} \quad - 450 \quad -10.45T \qquad (c)$$

Appendix 8.B Standard Gibbs Free energy Changes of reactions (in calories per mole).

		ΔG^o
8.(B.1)	$NiS(s) + 2NiO(s) = 3Ni(s) + SO_2(g)$	65 260 - 47.00T
(B.2)	$Ni_3S_2(s) + 4NiO(s) = 7Ni(s) + 2SO_2(g)$	139 800 - 98.59T
(B.3)	$Ni_3S_2(s) + 4/3\ CaO(sO = 3Ni(s) + 4/3\ CaS(s) + 2/3\ SO_2(g)$	-7066- 1707T
(B.4)	$NiS(s) + CaO(s) = NiO(s) + CaS(s)$	-1580 + 5.49T
(B.5)	$NiS(s) + C(gr) = Ni(s) + CO(g)$	31750 - 44.50T
(B.6)	$NiS(s) + CaO(s) = Ni(s) + CaS(s) + CO(g)$	30 170 -39.01T
(B.7)	$NiS(s) + CO(g) = Ni(s) + CO_2(g)$	-9050 - 2.807
(B.8)	$NiS(s) + CaO(s) + CO(g) = Ni(s) + CaS(s) + CO_2(g)$	-10630 + 2.19T

Appendix 8,C

The data for 'd' spacing of lime has been taken from JCPDS Search Manual and on the basis of these 'd' spacings the lattice parameter of lime has been determined which agrees with ASTM card for lime. Contradictingly, the 'd' spacing does not agree with our observation. This is the reason, the lattice parameter has been approximately determined with our observation to note the variation in the lattice parameter during the reduction and the heat treatment process.

Using relationship $a = \frac{\lambda}{2 \sin\theta} \cdot (h^2 + K^2 + l^2)^{\frac{1}{2}}$

$d^{o}A$	hKl
2.778	(111)
2.405	(200)
1.701	(220)
1.451	(311)
1.3901)	(222)

From which a = $4.79^{o}A$.

APPENDIX 1.

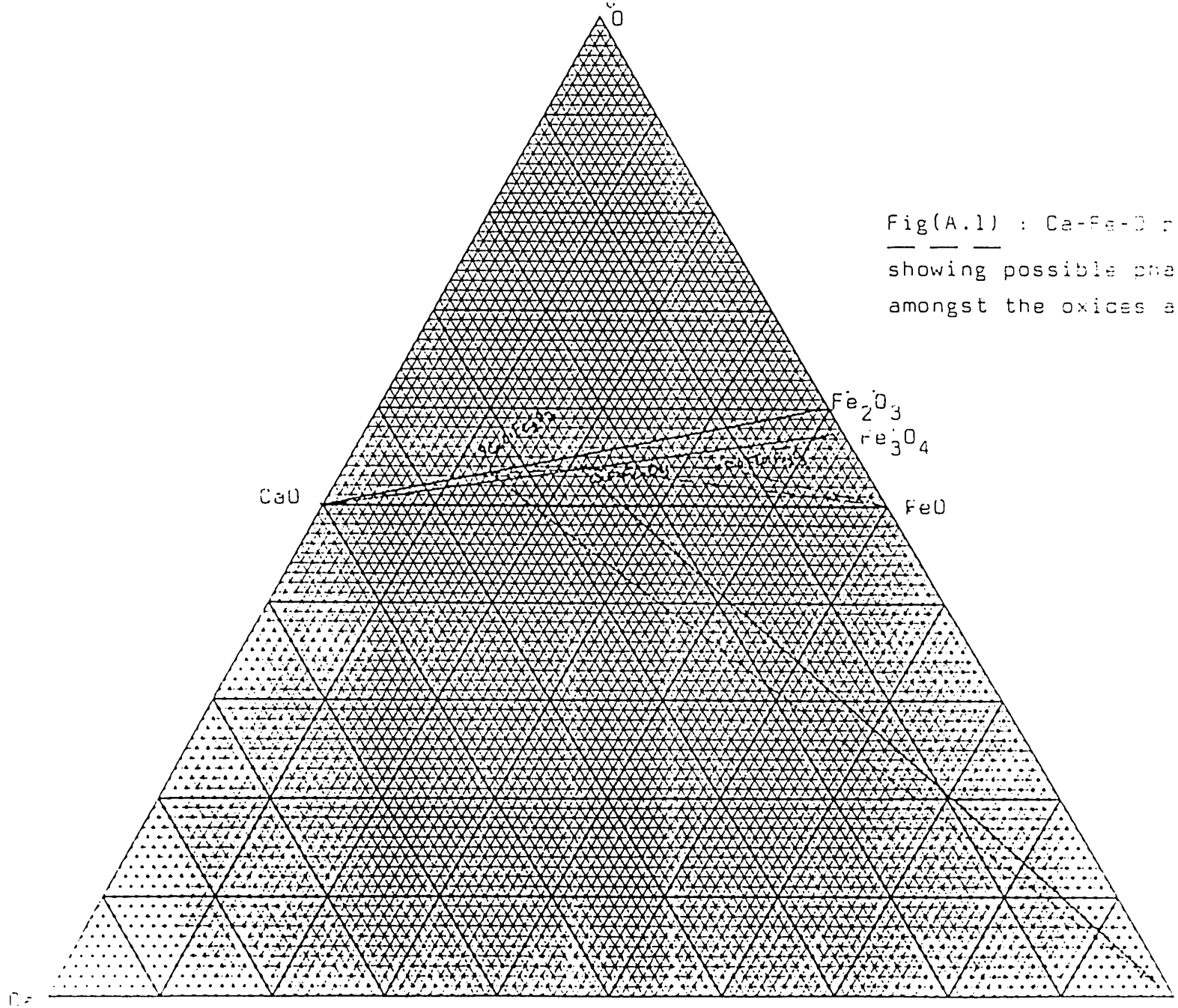
Phase Combinations in Fe-Ca-S-O and Cu-Fe-Ca-S-O Systems.

The phase combinations in the Fe-Ca-S-O system have been investigated in order to determine the path of reaction during the carbothermic reduction of iron sulphides. The phase combinations were investigated making mixtures of the reciprocal systems FeS-CaO and FeO-CaS and heat-treating them in argon atmosphere ($P_{O_2} = 10^{-30}$ atm). The heat treated samples were analysed using the X-ray diffraction technique to characterize the phases formed and to establish any new phase produced. On the basis of the X-ray data and the heat-treatment temperature, it can be broadly said that the results of the present investigation reasonably agree with Tromel's investigation (2.28). From this investigation and from Tromel's investigation it is evident that the iron compounds react much faster than the calcium compounds. It is for these reasons, that a liquid phase was observed for total compositions where the liquid phase is not expected at equilibrium. The higher reactivity of the iron compounds allows such physical changes to occur. In many cases it was extremely difficult to attain equilibrium even after 24 hours heat-treatment. Similar problems appear to have been faced by Tromel because a few of his results indicate phase combinations which are not in equilibrium.

The heat-treated samples were examined by optical microscopy to observe any possible microstructure changes occuring during the heat-treatment. Elemental mapping was carried out using the Energy Dispensive X-ray Technique and these microstructural and compositional variations are shown in plates A(1.1) and A(1.2). On the basis of these investigations, two compounds were found one appears to have composition near to (1.33) CaS.FeO and the other has a composition close to FeS.CaO. The crystallographic

data for 'd' spacing of observed reflexions for the compounds defined as C_I and C_{II} respectively are shown in Table B. The compound C_{II}(FeS.CaO) is probably tetragonal or closely related and C_I is apparently also basically tetragonal but is probably slightly distorted reducing its symmetry. The distortion in the unit cell is almost certainly generated by vacancy ordering in the anionic sublattice. On the FeO rich side of FeO-CaS pseudo binary section, the calcium ferrite, CaO-FeO-Fe_2O_3, forms confirming the observations of Cirilli and Burdese (1,2) and Turkdogan (3). The reason for the stability of this calcium ferrite phase in preference to 2 CaO-Fe_2O_3 which is in equilibrium with iron is explained by a study of the Ca-Fe-O ternary. In the absence of Fe and Fe_3O_4 this calcium ferrite would lie on the tie line forming CaO.Fe_3O_4 and FeO, see fig (A. 1).
The presence of iron in the system stabilizes the C_{II} compound as it controlls the oxygen potential in the system. Appearance of C_I in FeS-CaO was observed on the CaO rich side and is only possible at higher oxygen potential.

A quinary compound in Cu-Fe-Ca-S-O system was also discovered and it exists probably in equilibrium with compound C_{II} and CaS. The crystal structure of this compound appears to be very similar to bornite and is stabilized by the compound C_{II} in the quinary system. The crystallographic data for this compound is also shown in Table B together with the data for bornite mineral. The chemical formula for this compound is not known because of lack of information on the crystal structure or analysis.



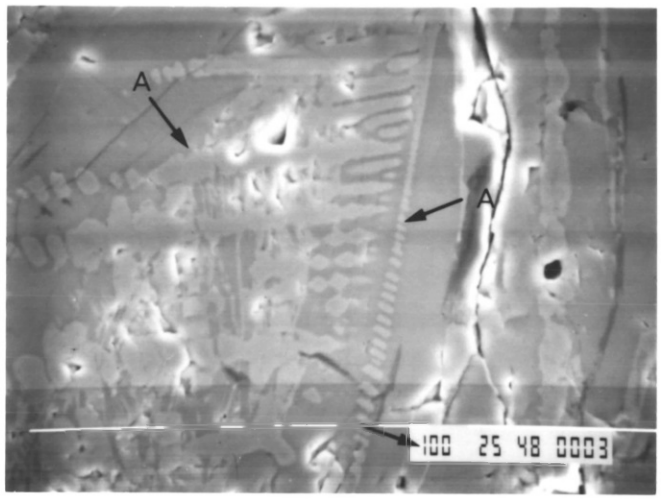
Fig(A.1) : Ca-Fe-O phase diagram showing possible phase relations amongst the oxides and the ferrites.

REFERENCES.

1. V. Cirilli and A. Burdese. La Metallurgia Italiana, No. 8-9, 1952 pp.371.
2. A. Burdese La Metallurgia Italiana, No. 8-9, 1952 pp.343.
3. E.T. Turkdogan. Trans AIME Vol. 221, 1961, pp.546

PLATE A1.1

a



A: PRO-EUTECTIC PHASE

b

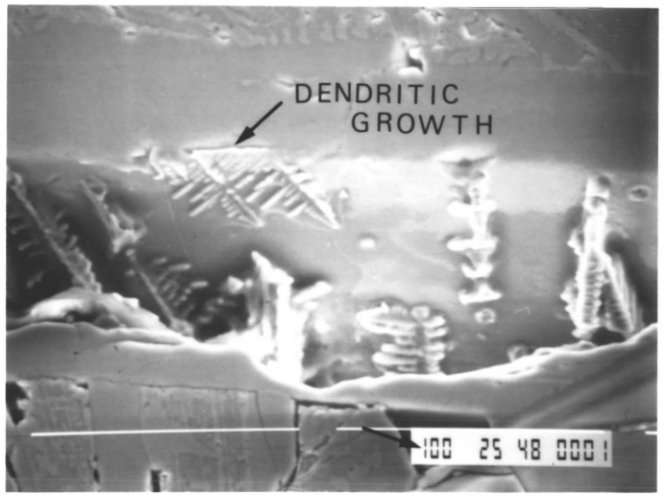


Plate A1.1 Scanning electron micrograph of heat treated FeO:CaS = 2:1 mixture in argon at 1000°C

(a) Formation of proeutectic phase

(b) Dendritic growth during the course of solidification

PLATE A1.2

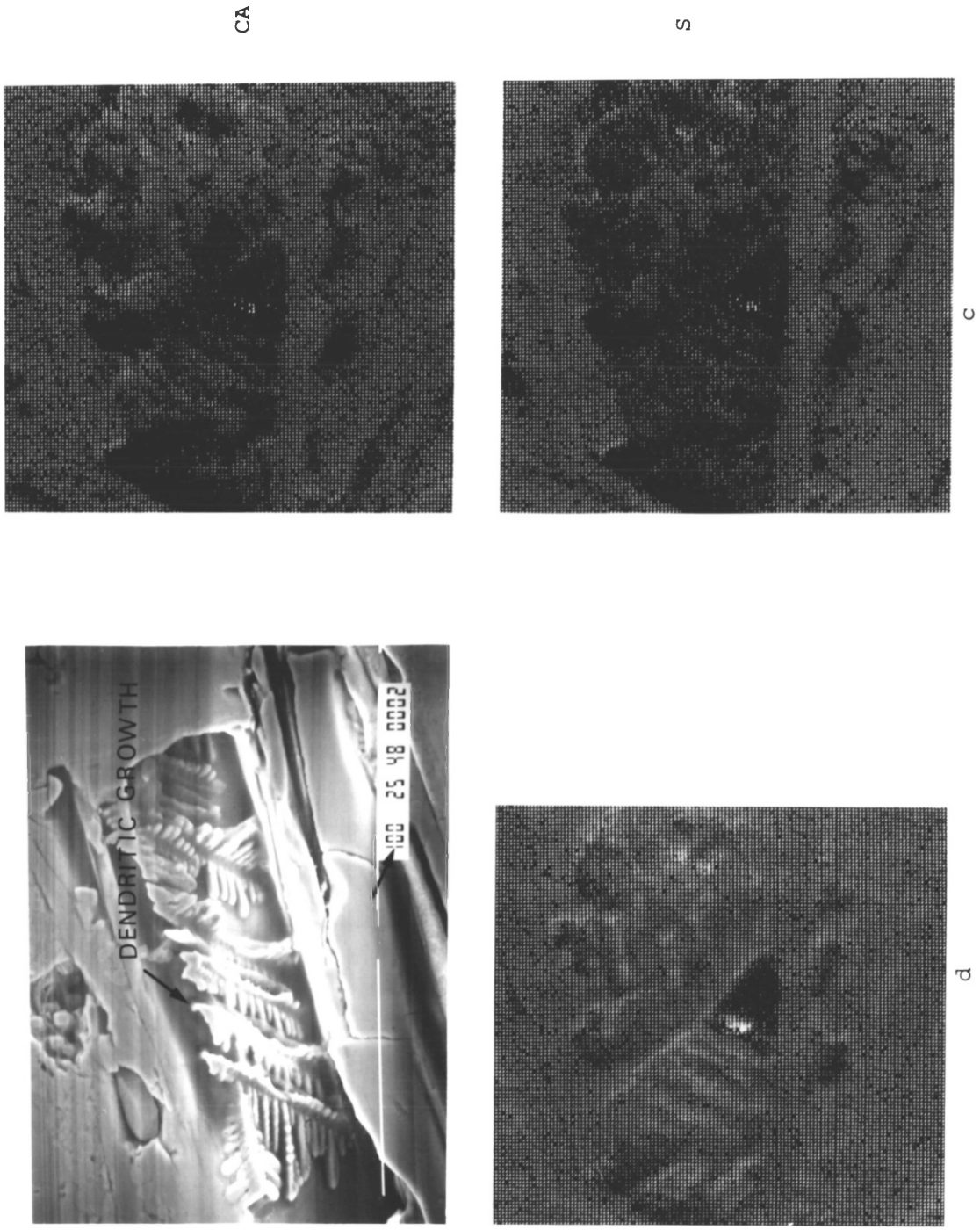


Plate A1.2 EDX elemental analysis and scanning electron micrograph of FeO:CaS = 2.5:1 mixture heat treated in argon atmosphere at 1000°C.

(a) Scanning micrograph of dendrites growing from the liquid phase

(b) 'Ca' distribution (c) 'S' distribution

(d) 'Fe' distribution

Table A: Phase Cominations in Fe-Ca-S-O System.

Mixture Composition	Temperature	pct wt loss	Physical Condition of Pellet	Atmosphere $p_{O_2}=10^{-30}$	CaO	FeS	CaS	FeO	CaO.FeS	CaS.FeO	CaO	Fe	Fe_2O_3	Fe_3O_4
FeS:CaO=1:1	900°C	0.627	100 pct liq.	Argon	WM	W	VS	-	MS	WM	-	-	-	-
FeS(+Fe):CaO = 1:1	950°C	0.413	70 pct liq	Argon	-	VVW	M	-	VS	VVW	-	W	-	-
FeS:CaO = 1:2	900°C	0.981	30 pct liq	Argon	M	VVW	VS	-	MS	VW	-	-	-	-
FeS(+Fe):CaO = 1:2	950°C	0.538	50 pct liq	Argon	MS	VVW	VS	-	S	VW	-	M	-	-
FeO(+Fe):CaS = 1:1	800°C	0.548	Solid	Argon	-	-	S	WM	M	VS	-	M	-	-
FeO:CaS = 1:1	800°C	1.348	Solid	Argon	-	VVW	MS	M	W	VS	-	-	-	-
FeO:CaS = 1:1	900°C	0.418	Solid	Argon	-	-	M	-	S	VS	-	-	-	-
FeO:CaS = 1:1	950°C	0.238	Solid	Argon	-	-	M	-	S	VS	-	-	-	-
*FeO(+Fe):CaS = 1:1	1000°C	0.265	Liquid	Argon	-	-	VS	VW	-	VS	-	M	-	-
FeO:CaS = 1:1	1000°C	0.295	Liquid	Argon	-	-	VS	VW	W	VS	-	-	-	-
FeO:CaS = 1:1	965°C	0.106	Solid	Argon	-	-	M	VVW	S	VS	-	-	-	-
			Liquid		-	-	MS	W	VW	VS	-	-	-	-

Table Contd..

Mixture Composition	Temperature	pct wt loss	Physical Condition of Pellet	Atmosphere $p_{O_2} = 10^{-30}$	CaO	FeS	CaS	FeO	CaO.FeS	CaS.FeO	CaO	Fe	Fe_2O_3	Fe_3O_4
FeO:CaS = 52:48	800°C	0.129	Solid	Argon	-	-	MS	VVW	WM	VS	-	VW	-	-
FeO:CaS = 52:48	900°C	0.129	Solid	Argon	VVW	VW	M	-	S	VS	-	VW	-	-
FeO:CaS = 52:48	950°C	0.102	Solid	Argon	-	-	-	-	VS	VS	-	VVW	-	-
			Liquid		VVW	VW	MS	-	MS	VS	-	W	-	-
FeO:CaS = 52:48	1000°C	0.102	Liquid	Argon	VVW	W	S	W	-	VS	-	W	-	-
FeO:CaS = 56:44	800°C	0.100	Solid	Argon	-	-	S	S	W	VS	-	VW	-	-
*FeO:CaS = = 56.44	1000°C	0.383	Liquid	Argon	-	-	S	WM	-	VS	-	VW	-	-
*FeO:CaS = 2:1	900°C	5.41	Liquid + Solid	Argon	-	-	-	WM	W	VS	WM	-	-	-
*FeO:CaS = 2:5:1	900°C	3.45	Liquid + Solid	Argon	-	-	-	WM	W	MS	S	-	-	-
*FeO:CaS = 2:1	1000°C	5.11	20 pct Liquid	Argon	-	-	VVW	S	Med	VS	WM	-	-	-
*FeO:CaS = 2:5:1	1000°C	0.595	Solid	Argon	-	-	VVW	VS	-	VS	-	-	-	-
			Liquid		-	-	-	W	-	VS	-	-	-	-
FeO:CaS = 74:26	800°C	0.588	Solid	Argon	-	-	VVW	MS	-	VS	-	-	-	-
*FeO:CaS = 74:26	1000°C	1.42	Liquid	Argon	-	-	-	MS	-	VS	-	-	-	-
FeO:CaS = 1:2	800°C	0.978	Solid	Argon	-	-	VS	S	WM	S	-	-	-	-
*FeO:CaS = 1:2	1000°C	1.01	(L + S)	Argon	-	-	VS	W	Med	MS	-	-	-	-

* Preheat-treatment first at 800°C

\+ Drainage of Liquid.

Table B: Crystallographic data for compounds in quarternary (Fe-S-Ca-O) and quinary (Cu-Fe-S-Ca-O) systems.

	(1.33 CaS.FeO(1-x)FeO(C_I)		FeS.CaO (C_{II})		Quinary Compound.	
	d^oA	Relative Int.	d^oA	Relative Int.	d^oA	Relative Int.
1	7.45	VW	5.70	W	15.0	W
2	4.80	VVW	3.25	W	5.20	VW
3	4.39	W	3.10	S	4.95	W
4	3.88	VVW	2.82	M	3.45	VW
5	3.75	VVW	2.46	VS	3.12	W
6	3.68	VVW	2.09	VW	2.70	S
7	3.59	VVW	2.08	VW	2.66	VS
8	3.44	W	1.94	WM	2.54	WM
9	3.05	W	1.88	S	2.37	M
10	2.93	W	1.82	VW	2.18	MS
11	2.79	S	1.74	VW	2.14	W
12	2.755	WM	1.635	S	1.94	W
13	2.70	VW	1.558	S	1.92	VW
14	2.655	M	1.54	VW	1.91	MS
15	2.60	VW	1.49	VW	1.90	W
16	2.35	VS	1.48	VW	1.83	WM
17	2.18	WM	1.465	VW	1.78	WM
18	1.96	VS			1.67	W
19	1.585	WM			1.55	MS
20	1.51	MS			1.535	M
21	1.395	MS			1.405	WM

The symbols used in the text are:-

VS - Very Strong M - Medium VW - Very Weak
MS - Medium Strong WM - Weak Medium VVW - Very Very Weak
S - Strong W - Weak.

BORNITE Mineral X-ray Diffraction Pattern:-

Crystall Structure:- Tetragonal $a_o = 10.94$

$c_o = 21.88$ $C/_a = 2.0$

Reference - 14-323 JSPDS Powder DIffraction File.

d^oA	I/I
4.08	10
3.64	5
3.48	40
3.18	60
3.01	5
2.80	20
2.74	50
2.63	5
2.50	40
2.13	20
2.11	5
1.937	100
1.850F	10
1.652	30
1.584	10
1.534	10
1.474	5
1.427	20
1.370	20

APPENDIX 2

A mixture of cuprous sulphide with $CaSO_4$ was prepared in the ratio of 1:3 and was heat-treated in a flowing stream of argon at 1000^{o}C. The chemical equilibrium prevailing under these conditions is represented by the following equation:

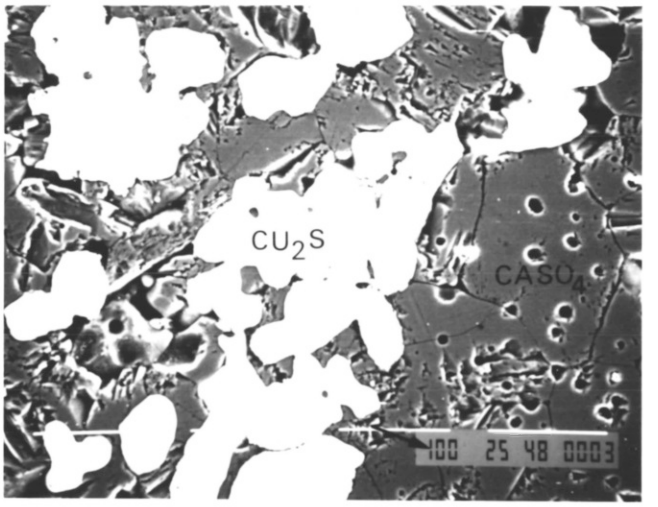
$$Cu_2S(s) + 2CaSO_4(s) = 2Cu(s) + 2CaO(s) + 3SO_2(g)$$

$$\Delta G^{o}T = 165800 - 107.63T$$

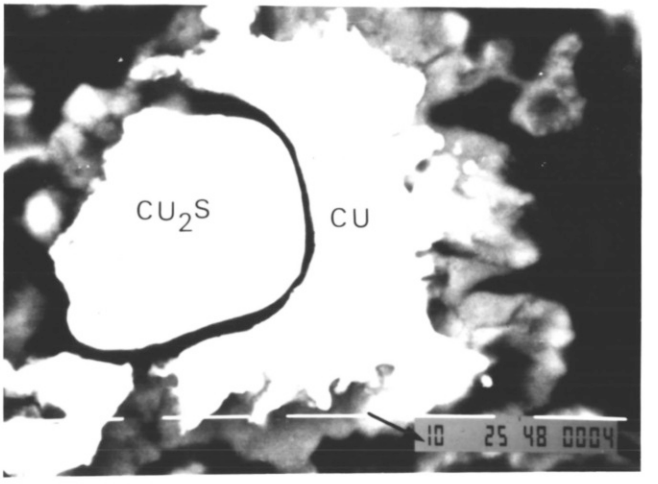
At T = 1273^{o}K, $^{p}SO_2$ = 0.0225 atm, for unit activities of all the condensed phases. The microstructure of the heat-treated pellet shows evidence of copper formed at the interface of $CaSO_4$ and Cu_2S. The morphological information obtained from the microstructure shows that both Cu_2S and Cu might have been liquid at the operating temperature, see plate A(2.1). Since the melting point of Cu_2S is 1130^{o}C this observation indicates that the reaction might have progressed through a some other liquid phase. The system needs to be investigated thoroughly in conjunction with the related phases present.

****

PLATE A2.1



a



b

Plate A2.1 Calcination of $CaSO_4$ in presence of Cu_2S at 1000°C in argon atmosphere.

(a) Liquid Cu_2S in the form of oxygen rich matte in the matrix of $CaSO_4$

(b) Copper grown as a result of calcination

CONCLUSIONS

1) The carbothermic reduction of metal sulphides has been investigated in order to explore the possibility of a single step metal production process without producing sulphur dioxide gas. The results of carbothermic reduction of metal sulphides shows that metals of over 99.0 pct purity can be produced within a reasonable short time(e.g. within 20 minutes for 100 pct metallization was observed in the case of CuS, $Cu_{2-x}S$ and $Fe_{1-x}S$ with coal, MS:CaO:Coal=1:2:2) The present investigation proves the feasibility of such a process industrially. The most suitable way of producing metal is probably a counter current moving bed reactor. The optimum conditions for the process can be achieved by operating under the right temperature and composition,so that a large quantity of liquid phase does not form which would hamper the operation. Of special significance is the extension of this work to complex sulphide ores where a satisfactory one stage process would be most welcome.

2)The calcination of calcium sulphate was investigated to appreciate the problems encountered during the slow reduction step of metal sulphides(CuS, $Cu_{2-x}S$) in the presence of lime. This investigation also shows that the calcium sulphate is a potential desulphurizing agent and can be used in the process.

3)The investigation on the growth of bi-partite whiskers,show that bi-partite whiskers can be grown from an invariant phase field by applying suitable thermodynamic conditions. Similar techniques to produce bi-partite whiskers could be of great importance in a number of fields especially of new electronic and eletrical materials.